POLYMER SILICATE AND MAGNETIC POLYMER NANOCOMPOSITES: PROCESSING AND CHARACTERIZATION

By

AJIT BHASKAR

A THESIS PRESENTED TO THE GRADUATE SCHOOL
OF THE UNIVERSITY OF FLORIDA IN PARTIAL FULFILLMENT
OF THE REQUIREMENTS FOR THE DEGREE OF
MASTER OF SCIENCE

UNIVERSITY OF FLORIDA

2003

This document is dedicated to Professor Beatty, my parents and my sister.

ACKNOWLEDGMENTS

First of all, I would like to express my heartfelt gratitude to Professor Beatty, my committee chair and mentor. He not only taught me the fundamentals of polymers, but also provided me financial support, and showed me the meaning of the word “research.”

I would like to thank my committee members Professor Abbas A Zaman and Professor Hassan El-Shall for their invaluable guidance and support.

I would also like to thank Professor Beatty’s graduate students Nathan Tortorella, Woo-Hyuk Jung and Xiaosang Huang, not only for helping me with my research but also for making research a pleasant and memorable experience.

I am also very thankful to my parents and younger sister who have encouraged me for all these years.

Finally I would like to thank all the funding agencies.

TABLE OF CONTENTS

page

LIST OF TABLES

LIST OF FIGURES

Figure page

Abstract of Thesis Presented to the Graduate School
of the University of Florida in Partial Fulfillment of the
Requirements for the Degree of Master of Science

POLYMER-SILICATE AND MAGNETIC POLYMER NANOCOMPOSITES:
PROCESSING AND CHARACTERIZATION

By

Ajit Bhaskar

August 2003

Chair: Charles L Beatty
Major Department: Materials Science and Engineering

The research can be categorized with respect to the fillers used, namely clay and ferrite magnetic nanoparticles. Polymer layered silicate nanocomposites (PLSNs) are nanocomposites of polymers and clays.

One of the investigations carried out was regarding the amount of compatibilizer necessary to get the optimum adhesion between the hydrophobic polymer and the hydrophilic clay. The matrix used was polypropylene (PP) and the clay used was an organically modified montmorillonite. It was found that beyond a certain concentration of the compatibilizer, the mechanical properties deteriorated. This was explained on the basis of the ways in which the compatibilizer, a maleic anhydride grafted polypropylene, influenced the nanocomposites.

In another work, the impact properties of the nanocomposites processed above were attempted to be improved using different elastomeric species and using different processing protocols. It was observed that a low molecular weight oligomeric elastomer

produced the best results. It was also found that the sequence of addition of elastomer affected the mechanical and impact properties.

Nanocomposites of PMMA and Laponite were prepared for enhanced abrasion and wear resistance, for window-based applications. However, the major challenge was to preserve the optical clarity of PMMA, a key emotive property that makes it a commodity plastic. A recent technique called nano-indentation was employed for assessing the hardness of these materials.

Nanocomposites of polymers using magnetic nanoparticles offer an interesting research avenue. Nanocomposites using Polycarbonate (PC) and Ni-Zn based ferrite nanoparticles were prepared. They were found to be clear with a brown tinge, and were characterized for different properties. It was found that the melt viscosities of these nanocomposites were significantly lower than the pure polymer. This was explained on the basis of the different phases added to PC.

Most of the processing for the research was carried out using a reactive twin-screw extruder, which simulates continuous, mass-production operations to a considerable extent. An insight into the microstructure was obtained using various techniques such as differential scanning calorimetry, X-Ray diffraction, transmission electron microscopy, and nanoindentation. Mechanical properties were evaluated using tensile tests and Izod impact testing. The results obtained from these analytical tools were interpreted and a coherent explanation of different phenomena occurring on a macroscopic as well as microscopic level was attempted.

CHAPTER 1
INTRODUCTION

My research focuses on polymer nanocomposites. Nanocomposites of polymers with different fillers were processed and characterized. The entire research can be classified based on the nature of filler employed, namely clay and ferrite nanoparticles. Figure 1.1 shows a schematic describing the same.

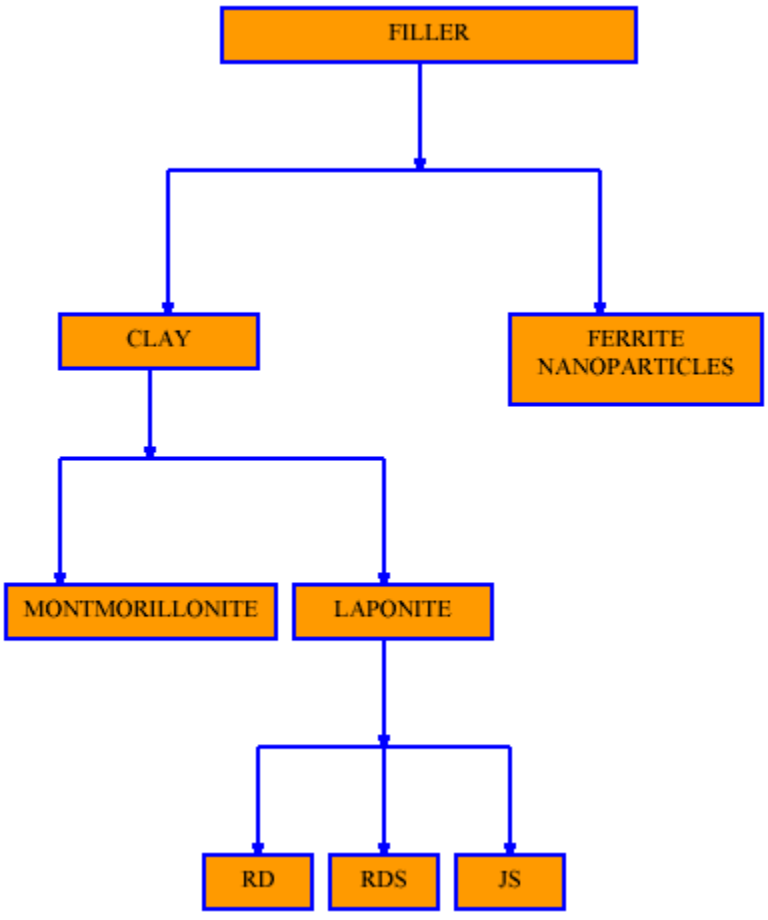

Figure 1.1. Classification of research areas on the basis of filler employed.

Two different clays were used, montmorillonite and laponite. Chapters 2 and 3 describe research on polypropylene/montmorillonite nanocomposites. Chapter 4 deals with Poly (methyl methacrylate)/laponite nanocomposites. Finally, Chapter 5 describes Polycarbonate/ferrite nanocomposites. Chapter 6 discusses suggestions for future research. Here, many ideas and concepts from earlier research have been attempted to be applied to different avenues having different applications. The following section gives a summary of each of these chapters.

1.1 Polymer Nanocomposites

1.1.1 Effect of Compatibilizer Concentration on the Mechanical Properties of Polypropylene-Montmorillonite Nanocomposites

One of the objectives of this research was to demonstrate that addition of clay to a polymeric matrix not only enhanced the properties of the pristine polymer, but it could also achieve the same with small loadings. This could be attributed to the large surface to mass ratio when compared to traditional fillers used for polymeric composites. However, the major difficulty in preparing these nanocomposites was exfoliation of clay. Exfoliation is one of the terms used to determine the extent of dispersion of clay in the polymer matrix. The clay used for this work was montmorillonite, a smectite clay. The clay structure comprised of tetrahedral layers of silica sandwiching octahedral layers of alumina. On a whole, the structure looked like nearly parallel layers of silica held by alumina *pillars*. Figure 1.2 shows the structure of montmorillonite clay.

When these galleries (i.e, the clay interlayers) are split far apart by the application of high temperature and shear force generated due to the molten polymer and the extruder in which it is processed, this type of dispersion is called exfoliation.

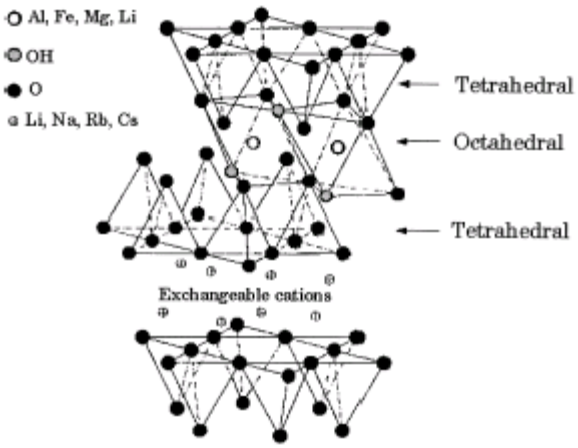

Figure 1.2. Structure of montmorillonite clay.

Other type of clay platelet separation possible is intercalation. Figure 1.3 shows the different types of clay platelet separations. Several publications involving polymer clay nanocomposites have been published with polar polymers (such as Nylon 6, Nylon 6,6, Polyurethane) as the matrix material. In this work, a non-polar polymer, namely polypropylene was chosen.

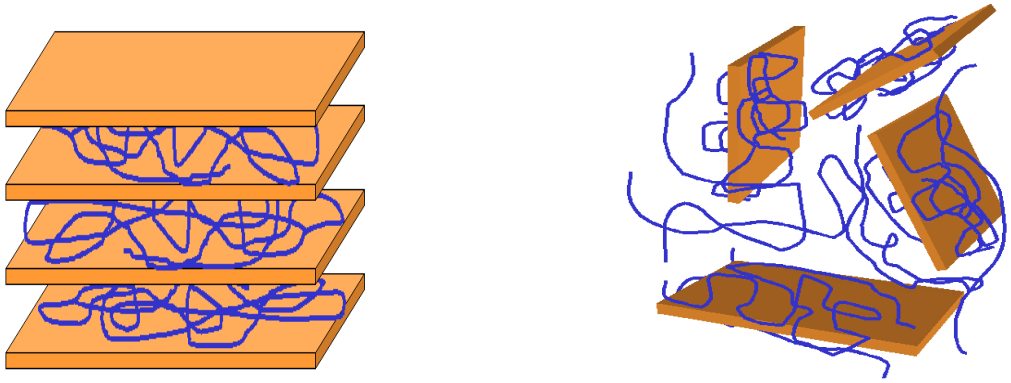

Figure 1.3. Different types of clay platelet dispersion by diffusion of polymer chains.

This is because PP is an inexpensive commercial plastic used for a variety of applications. Besides, it is difficult for the clay to bond to a non-polar polymer, which can be attributed to the hydrophilic nature of the clay and organophilic nature of the matrix.

So, the clay used in this study was organically modified. However, it was found that the use of a compatibilizer between the polymer and the clay yielded better mechanical properties. The compatibilizer used in this work was a maleic anhydride modified polypropylene. It was also found out that when no compatibilizer was added, the mechanical properties were inferior in comparison to the pure polymer. Thus it could be deduced that in spite of the clay being modified to behave in an organophilic manner, the use of a compatibilizer was necessary. To acquire an in depth insight into the effect of the compatibilizer, its concentration in the nanocomposite was varied. It was observed that after a certain percentage of the compatibilizer, the mechanical properties started to degrade. It was concluded that compatibilizers were necessary components for good dispersion of clay, but beyond a certain concentration, they had deleterious effects on the mechanical properties of the nanocomposite.

1.1.2 Improving Impact Properties of Polypropylene/Clay Nanocomposites

Several publications show property enhancement in polymers upon the addition of clay, but most of the publications do not address impact properties in detail. Hence, a study was done in order to investigate the impact behavior of polymer clay nanocomposites and schemes for improving their impact properties were proposed.

In one scheme, a functionalized elastomer was added before and after processing the polymer clay nanocomposite in two different processing protocols.

In another scheme, an oligomeric, end functionalized elastomer was melt blended with the compatibilizer, and the resulting modified compatibilizer was then used for processing the nanocomposite.

It was found that the second scheme produced better mechanical properties. Thus, it was speculated that oligomeric elastomer was able to penetrate into the clay galleries

more easily and because of functional groups present; it could also bond well to create a more stable composite with respect to interfacial behavior. In addition, other mechanical properties of the nanocomposite were not sacrificed significantly.

The functionalization of the polymeric elastomer used was carried out in a reactive twin-screw extruder, so this work was a combination of nanotechnology and reactive extrusion. The functionalizing agent used was glycidyl methacrylate.

1.1.3 PMMA/Laponite Nanocomposites

This research was focused on making wear/abrasion resistant PMMA for superior windows based applications. The clay used here was Laponite JS, a synthetic clay, which already existed as nanoparticles when dispersed in water. These particles were disc-shaped. Two different loadings of clay were chosen, namely 2-wt % and 5-wt %. The surface hardness was characterized using nanoindentation technique. It was found that the addition of clay significantly reduced the penetration of the probe and hence, these nanocomposites exhibited increased hardness. However, it was also observed that only the 2-wt % nanocomposite exhibited optical clarity close to pure PMMA. The nanocomposite containing 5-wt % clay was translucent.

1.1.4 Polycarbonate-Ferrite Nanocomposites

The aim of this research was to obtain magnetic nanocomposite materials. Nano-sized ferrite particles prepared at the Department of Materials Science and Engineering, University of Florida with help from Junyeon Hwang (working for Professor Darryl P. Butt). These particles were prepared using a co-precipitation method, with carefully controlled parameters such as temperature and pH.

The synthesized particles were dispersed in a polymer matrix. The matrix material chosen was polycarbonate (PC). This is a transparent polymer, and is completely

amorphous. The ferrites were first coated with a low molecular weight PVA (Poly Vinyl Alcohol). The ferrites are known to bond with alcoholic groups by means of silanol reaction. After coating the ferrites with PVA, these were dispersed in molten polycarbonate. The resulting material was still optically clear, with a brown tinge to it. With respect to mechanical behavior, the nanocomposite was more brittle than the virgin polymer, and exhibited a higher tensile modulus than pure PC. Characterization using a SQUID magnetometer showed that the nanocomposite was magnetic in nature.

1.1.5 Future Research

Several concepts applied in the above research may be extended to other avenues as well. Few of these include polymer/clay modified cement. It is suggested that this approach may produce cement with good tensile properties. Another area is that of glass fibers. Recycling of glass fibers is one of the interests. It is possible that by imparting appropriate chemical treatment to the waste, ground fiberglass, they could be used again with resins such as unsaturated polyesters, epoxy, etc. Impact modified glass fibers is another area of interest. It is again possible that by giving the appropriate chemical treatment, glass fibers when introduced into resins yield composites with better impact properties without significant loss in tensile properties.

1.2 A Word on Processing and Characterization of Nanocomposites

The equipment used for processing the nanocomposites by melt blending was a 30mm APV reactive twin-screw extruder, with a co-rotating intermeshing configuration of the screws. The length to diameter ratio (also addressed as l/d) was 40. The extruder had eight temperature zones, including feed and die zones.

Characterization of nanocomposites prepared was performed using the following techniques:

1. Tensile testing: Helps in comparing the tensile behavior of different materials and their tensile moduli. This test also tells us about the relative stiffness of different materials.

2. X-Ray Diffraction: The shift in diffraction peaks shows the extent of exfoliation or intercalation that has taken place. This also helps in getting an overall picture of intercalation/exfoliation in bulk.

3. Transmission Electron Microscopy (TEM): Is very effective in studying a local region of the nanocomposite for exfoliation. The greater the number of individual platelets that could be counted in a TEM micrograph, greater the extent of intercalation/exfoliation.

4. Nanoindentation: A very novel and useful tool for probing hardness of nanocomposite materials, especially at the surface. Its details are described later in appropriate sections.

5. Izod Impact Testing: It gives the impact strength of a material. Here, a swinging hammer is made to impact a specimen and the energy lost by the hammer upon impact is a measure of the impact strength of the material.

6. Differential Scanning Calorimetry: This technique is used to evaluate the behavior of a material upon heating. Different transitions such as melting, glass transition and crystallization behavior can be studied with this technique.

CHAPTER 2
EFFECT OF COMPATIBILIZER CONCENTRATION ON MECHANICAL PROPERTIES OF POLYPROPYLENE/MONTMORILLONITE NANOCOMPOSITES

2.1 Introduction

A nanocomposite is defined as a material in which the dispersing phase has at least one of its dimensions in the order of nano (10^{-9}) meters.

Polymer clay nanocomposites are a class of hybrid materials in which clays having a layered silicate structure are dispersed into a polymeric matrix. The spacing between these layers is of the order of few (2-3) nanometers prior to dispersion of polymer. Hence the hybrid is called a polymer clay *nanocomposite* [1-6].

The use of clays instead of traditional fillers is being encouraged for numerous reasons. First and foremost, due to high surface to mass ratio of clays, the same amount of property enhancement may be achieved with lesser quantity of clay than traditional fillers such as glass fibers. This is because increased surface/mass ratio means greater area available for adhesion. Thus, tremendous savings may be made with respect to weight of the end product. This may also make processing easier. Further, research at Toyota motor company has shown that for nylon-6/montmorillonite clay nanocomposites, at a loading of only 4.2 wt% clay, the modulus doubled, the tensile strength increased by more than 50%, and the heat distortion temperature increased by 80 ^{o}C compared to the pure polymer [7-8]. Researchers also demonstrated that organoclays exfoliated in nylon 6 matrix and greatly improved the dimensional stability, the barrier properties and even flame retardance [9-11].

However, the clay nanolayers are not easily dispersed in polymers due to their preferred face-to-face stacking tactoids. Dispersion of tactoids is further hindered by the fact that clays are hydrophilic in nature, and are therefore, incompatible with majority of polymers that are primarily hydrophobic. Hence, these clays are surface-modified (usually with an organic ammonium salt) in order to enhance compatibility between the matrix polymer and the clay. Such clays are termed as *organoclays*. This concept has been extended into various polymer systems including polyamides [12-17], epoxies [18-29], polyurethanes [30-38], polypropylene [39-62], polyesters [63-66]**,** polystyrene [67-81], polyethylene [82], elastomers [83-87] and polysiloxanes [88] among others. Many liquid crystalline polymers have also been explored [89-92].

For true nanocomposites, the clay nanolayers must be uniformly dispersed (exfoliated) in the polymer matrix, as opposed to being aggregated (intercalated) into clusters of layers [1]. Figure 2.1 shows this. Dispersion and distribution of the filler is achieved when the hydrodynamic separation forces of the polymer melt overcome the agglomerating forces between the clay interlayers [12]. The exfoliation of clay in a polymer optimizes the number of reinforcing elements for carrying the applied load and deflecting cracks. The coupling between tremendous surface area of the clay (~760 m^2/g) and the polymer matrix facilitates stress transfer to the reinforcement phase, allowing for such tensile improvements. High aspect ratio nanolayers also provide properties that are not possible for larger-scaled composites.

The impermeable clay layers pose a tortuous pathway for a permeant to traverse the nanocomposite. Figure 2.2 demonstrates the same.

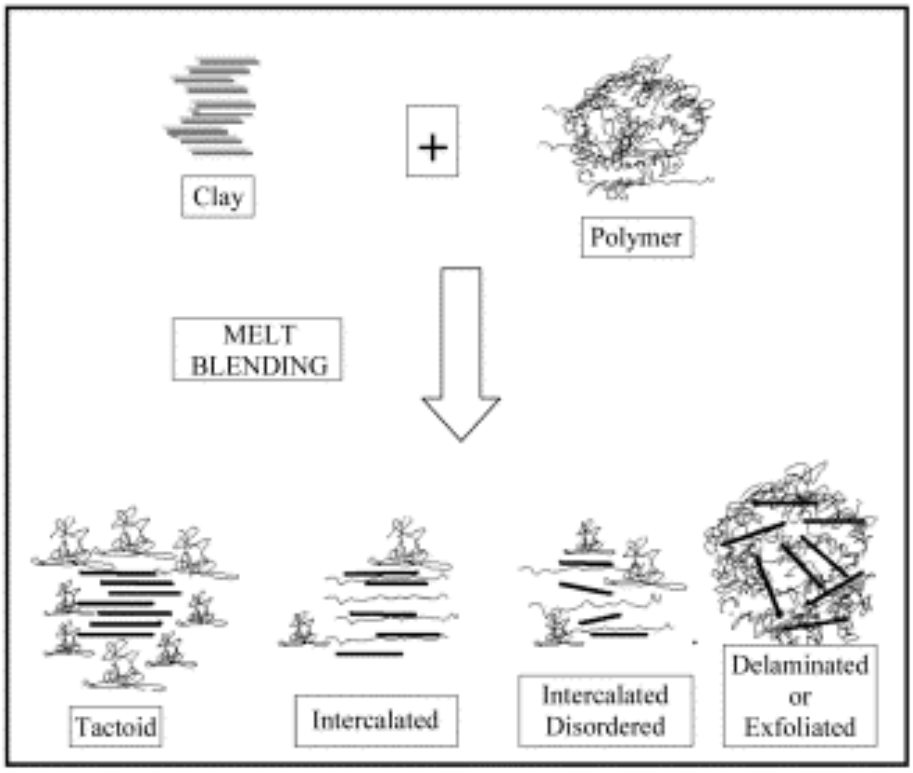

Figure 2.1. Schematic illustrations of (A) a conventional; (B) an intercalated; (C) an ordered exfoliated; and (D) a disordered exfoliated polymer clay nanocomposite. The clay interlayer spacing is fixed in an intercalated nanocomposite. On the other hand, in an exfoliated nanocomposite, the average gallery height is determined by clay silicate loading. The difference between ordered and disordered exfoliated nanocomposites is that the former can be detected by X-ray diffraction and the latter is X-ray amorphous.

The enhanced barrier characteristics, chemical resistance, reduced solvent uptake and flame retardance of polymer clay nanocomposites all benefit from the hindered diffusion pathways through the nanocomposite. The replacement of inorganic cations by organic onium ions on the gallery surfaces of smectite clays not only serves to match the clay surface polarity with the polarity of the polymer, but it also expands the clay galleries. Depending on the charge density of clay and the onium ion surfactant, different arrangements of the onium ions are possible. In general, longer the surfactant chain length, and the higher the charge density of the clay, further apart the clay layers will be forced.

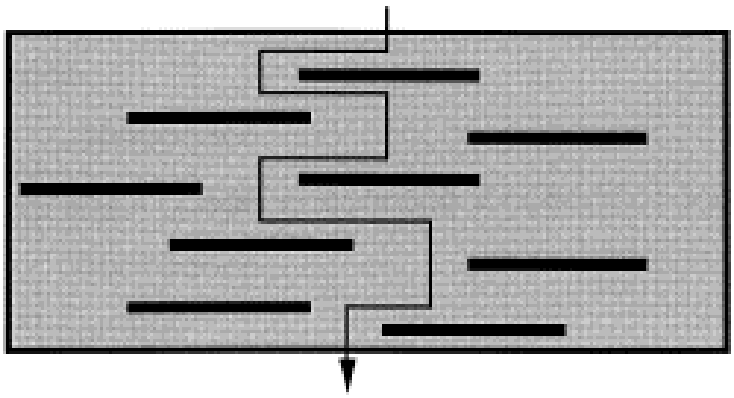

Figure 2.2. A model for the torturous zigzag diffusion path in an exfoliated polymer clay nanocomposite when used as a gas barrier.

This is expected since both of these parameters contribute to increasing the volume occupied by the intragallery surfactant [1, 93]. Depending on the charge density of the clay, the onium ions may lie parallel to the clay surface as a monolayer, a lateral bilayer, a pseudo-trimolecular layer, or an inclined paraffin structure. At very high charge densities, large surfactant ions can adopt lipid bilayer orientations in the clay galleries. Figure 2.3 shows this. Polymer clay nanocomposites are being used in under the hood applications in automotive industry [1, 94].

2.2 Polypropylene Clay Nanocomposites

Polypropylene is a thermoplastic polymer, and is one of the most widely used polymers in the industry. It is inexpensive and is relatively easier to recycle and offers versatility in terms is properties and applications. The introduction of traditional fillers into PP requires special processing technologies involving prepreg preparation and fiber impregnation [39, 95-96].

This is the reason special emphasis is being laid on PP/clay nano-hybrids. These can be synthesized using a relatively easier approach of melt blending.

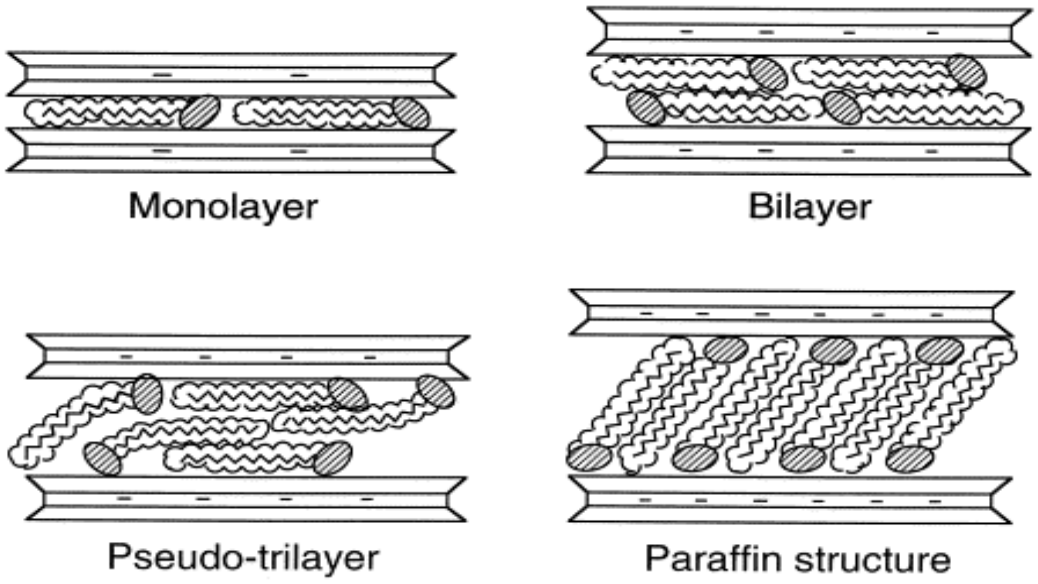

Figure 2.3. Orientations of alkyl ammonium ions in the galleries of layered silicates with different layer charge densities.

Researchers at Toyota and other laboratories [1, 46, 61, 97, 98, 99] have reported that it is possible to prepare PP–clay hybrids by simple melt mixing of three components, i.e., PP, maleic anhydride-modified polypropylene oligomers (PP-MA), and clay intercalated with alkyl ammonium ions [51, 61, 97, 100-101]. Some of the common approaches adopted for preparing PP/Clay nanocomposites (PPCNs) are:

1. The clay is first blended with polar oligomeric species. Strong interactions result between the polar groups on the oligomeric species and the oxygen based groups on the clay. Examples of polar oligomers are maleic anhydride grafted PP and certain alcohol based oligomers. This system is then blended with PP for increasing the gallery spacing in the clay.

2. The clay is dispersed in a solvent, followed by the addition of a monomer. Then the monomer is polymerized to prepare a system compatible with PP. This clay-polymer hybrid is then blended with PP.

From a processing perspective of nanocomposites, many methods have been reported. These include melt intercalation [12-14, 39-49, 51-58, 70, 80], solution blending [69, 74, 78] and in-situ polymerization [67, 71-73, 75, 77,79, 81].

2.3 Research Objectives and Strategy

In this research, the nanocomposites were prepared by combining the two above mentioned approaches. The clay was dispersed in a solvent. The low molecular weight compatibilizer was blended with PP instead of clay. The dispersed clay was then blended with the modified PP blend to give a nanocomposite.

An attempt was made for studying the effects of the compatibilizer concentration on mechanical properties of PPCNs. Primary emphasis was laid on tensile properties. This is because the tensile properties are a very important criterion for materials selection for most of the applications. It has been reported in literature that using method #1 listed in the previous section for preparing PPCNs, a compatibilizer to clay ratio of 3:1 worked best.

Kato et al. have observed that the density of the compatibilizer, a maleic anhydride modified PP, had a remarkable effect on the final morphology of the nanocomposite [61]. However, in their work, the authors did not make comments about the mechanical and thermal properties of the nanocomposites. Thus, it was shown that the ratio of 3:1 was best from an exfoliation/intercalation point of view.

D. Garcia Lopez et al. [59] have also observed a similar ratio. However, it was seen from their work that the increase in tensile strength was not very significant.

Hence, an attempt was made to study in depth, the role of the compatibilizer and the effect of its concentration on various mechanical properties of the nanocomposite.

2.4 Materials

Montell (now Basell) supplied PP used for this research. The grade was Profax 6523. This was an extrusion grade plastic. Table 2.1 shows some of its properties.

Table2.1. Properties of Polypropylene (Basell Profax 6523) used for the research.

PROPERTY	VALUE	TEST METHOD
PHYSICAL		
Specific Gravity	0.9	ASTM D792
Melt Flow Rate (230 °C)	4.00 g/10 min	ASTM D1238
MECHANICAL		
Tensile Strength @ Yield	4900 psi	ASTM D638
Tensile Elongation @ Yield	12 %	ASTM D638
Flexural Modulus (Procedure A)	1% Secant: 200000 psi	ASTM D790
Notched Izod Impact (73 °F)	0.7 ft-lb/in	ASTM D256
Rockwell Hardness (R-Scale)	86	ASTM D785
THERMAL		
DTUL @66psi – Unannealed	199 ^{o}F	ASTM D648

Nanocor supplied the clay used for this study. The name of the product was Nanomer® I.34TCN. It was specifically designed for extrusion compounding. Table 2.2 enlists some of its properties. However, it is worth mentioning that this clay was not designed for moisture barrier applications [102].

Table 2.2. Physical properties of Nanomer® I.34 TCN.

PROPERTY	VALUE
Appearance	White Powder
Mean Dry Particle Size (Microns)	16-22
+ 325 Mesh Residue (%)	0.1
Specific Gravity	2.0
Moisture (%)	3.0
Bulk Density (gms/cc)	0.30-0.36
Purity (%)	98.5

The agent used for dispersing the clay was Xylene, supplied by Fisher Scientific. Eastman Chemical Company supplied the compatibilizer used for the research under the trade name Epolene® G-3003. Table 2.3 describes some of its properties.

Table 2.3. Properties of Epolene® G-3003.

PROPERTY	VALUE
Ring & Ball Softening Point , ºC	158
Penetration Hardness	<1
Density @ 25 ºC	0.912
Acid Number	8
Viscosity, cP (mPa•s) @ 190 ºC	60,000
Melt Index @ 190 ºC	12.7
Color (Gardner)	25
Molecular Weight	27,200

Epolene® is a maleic anhydride grafted PP. It has a much lower molecular weight and consequently a lower softening point than PP. Thus, its chains exhibit greater mobility. Figure 2.4 shows the structure of a maleic anhydride group.

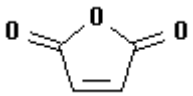

Figure 2.4. A Maleic anhydride group.

2.5 Processing

The nanocomposites were processed by melt compounding using a 30 mm APV co-rotating twin crew extruder, with 8-zone temperature settings ranging from 200 °C (feed zone) to 234 °C (die zone). The screw length to diameter ratio (L/D) was 40. Figures 2.5 shows a schematic representation of the extruder.

Figure 2.6 shows the processing in the form of a block diagram. The Zenith pump is generally used for introducing the reactive species. However, upon preparing the clay dispersion, it was feared that the same might plug the pump. Hence, it was not used. The clay dispersion was introduced at the feed zone.

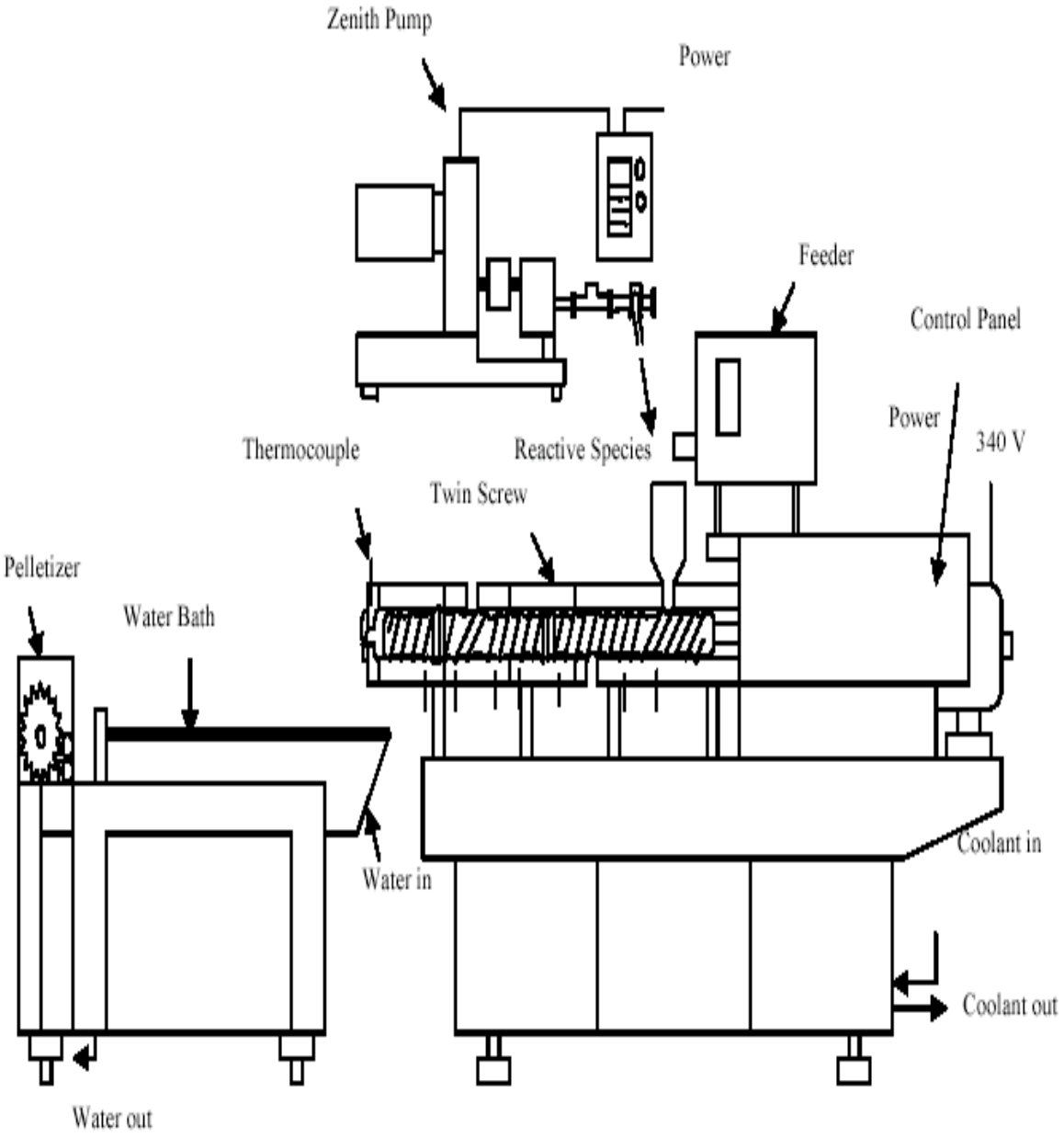

Figure 2.5. Schematic of reactive twin-screw extruder.

Table 2.4 shows the temperature profile along the different zones of the extruder. PP and Epolene were dried in an air-circulating oven prior to any melt compounding operation. The temperature was 80 ^{o}C. Drying was done to ensure removal of moisture. This was particularly important for Epolene, which had polar groups associated with it.

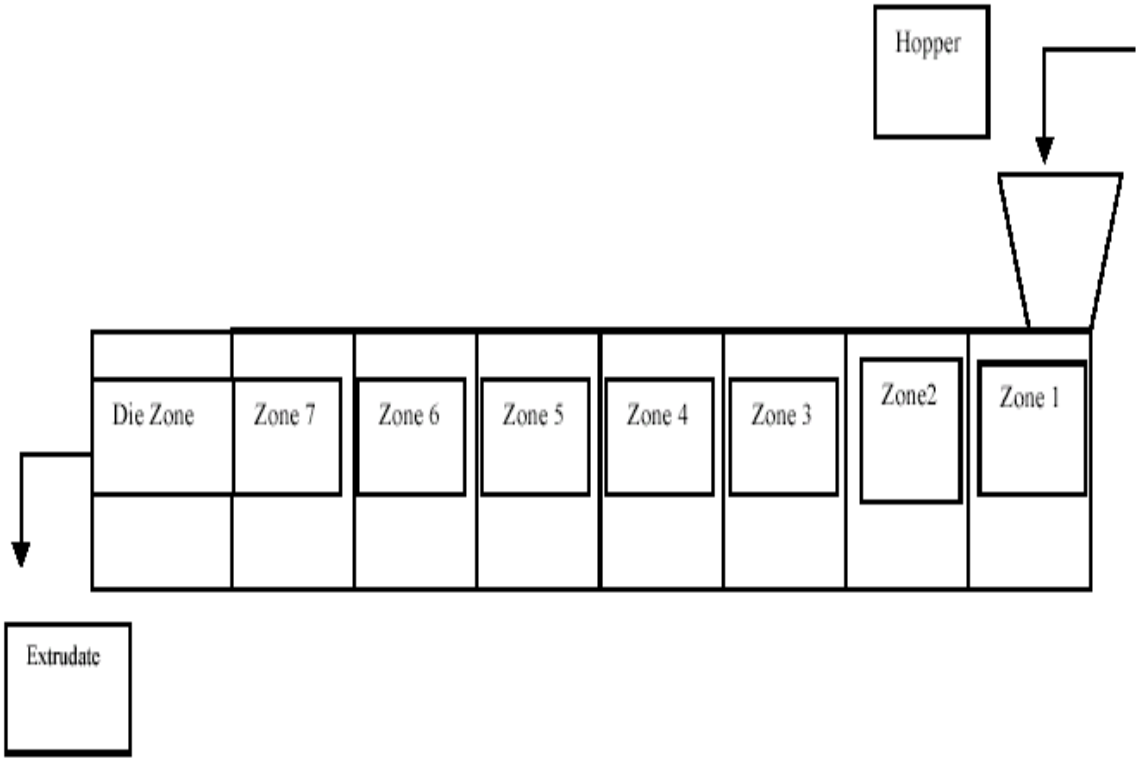

Figure 2.6. Block diagram of the extruder showing different zones.

The preparation of the sample containing 90-wt % PP, 5-wt % Epolene and 5-wt % clay is described. Nanocomposites with other compatibilizer concentrations were prepared in a similar fashion.

Table 2.4. Different temperature Zones of the twin screw extruder.

Zone	Temperature (^{o}C)
Zone 1 (Feed Zone)	200
Zone 2	204
Zone 3	208
Zone 4	214
Zone 5	218
Zone 6	223
Zone 7	227
Zone 8 (Die Zone)	234

PP was blended with Epolene in the weight ratio 90:5 in the extruder. The extruded strands were received in a flowing water bath, which formed a part of the extruder. These

strands were pelletized and dried for 24 hrs. in a vacuum oven at 95 ^{o}C. These pellets were melt-compounded with the clay.

The clay was dispersed in xylene (clay: xylene used was approximately 1:5 by weight). The dispersion was magnetically stirred for 10 minutes prior to addition to pellets at the feed zone of the extruder. The resulting strands were received in a flowing water bath, pelletized and vacuum dried for 24 hours under conditions described above. Table 2.5 summarizes the compositions (by weight, dry basis) of different nanocomposites thus prepared.

A sample without any compatibilizer was also prepared in order to demonstrate the effect and necessity of Epolene®. Pure PP was also run through the extruder under identical conditions in order to ensure uniform thermal history for all the materials compared for different properties.

Table 2.5. Designation of different PPCNs. All compositions are in weight%.

SAMPLE DESIGNATION	% POLYPROPYLENE	% EPOLENE	% CLAY
PP/Clay (95:5)	95	0	5
PP/EP/Clay (90:5:5)	90	5	5
PP/EP/Clay (85.5:9.5: 5)	85.5	9.5	5
PP/EP/Clay (76:19:5)	76	19	5
PP/EP/Clay (47.5:47.5:5)	47.5	47.5	5

2.6 Characterization

Polymer characterization is considered to be a separate discipline of study in the field of polymers. It involves the investigation of the microstructure-property relationships of a polymeric material. Examination of microscopic details of the structure in order to understand the morphology, measurement of mechanical and thermal properties are all part of the characterization process. The following analytical tools were employed for characterizing the PPCNs:

- Tensile Testing
- X-Ray Diffraction
- Differential Scanning Calorimetry
- Transmission Electron Microscopy

2.6.1 Specimen Preparation

Specimens for all the above mentioned techniques were prepared by compression molding. Compression molding is a process in which a polymer is made to take the shape of a mold by pressing it between two heated plates. The heat melts the polymer (if semi-crystalline) or takes the polymer chains well above the glass transition temperature (if amorphous). The machine used for compression molding was a Carver, model C-81000-141 press. Figure 2.7 shows the details of the press. Figure 2.8 shows the details of the compression molding process, and the placement of the mold containing polymer pellets between two metal plates.

In order to prepare the specimens, the press was first heated to 420 ^{o}F. The mold used was square in shape, with dimensions of 70 mm X 70 mm X 0.8 mm. The mold was placed on a metal plate covered with Teflon® coated aluminum foil. The mold was then filled with dried pellets. This plate with mold and the pellets was placed on the bottom plate of the press. Another Teflon® coated aluminum foil covered metal plate was placed on top of the mold bearing plate, to give a sandwiched assembly.

The bottom plate of the press was raised until the assembly just touched the top plate of the press. The pellets were then allowed to convert into a liquid state by heat transfer from the press. This took about 5-6 minutes. After that the pressure of the system was raised to 10, 000 psi. Initially, due to resistance offered by the liquid polymer as well relatively incomplete conversion to liquid, the pressure dropped below 10,000 psi. Under these circumstances, it was necessary again to raise the pressure to 10,000 psi.

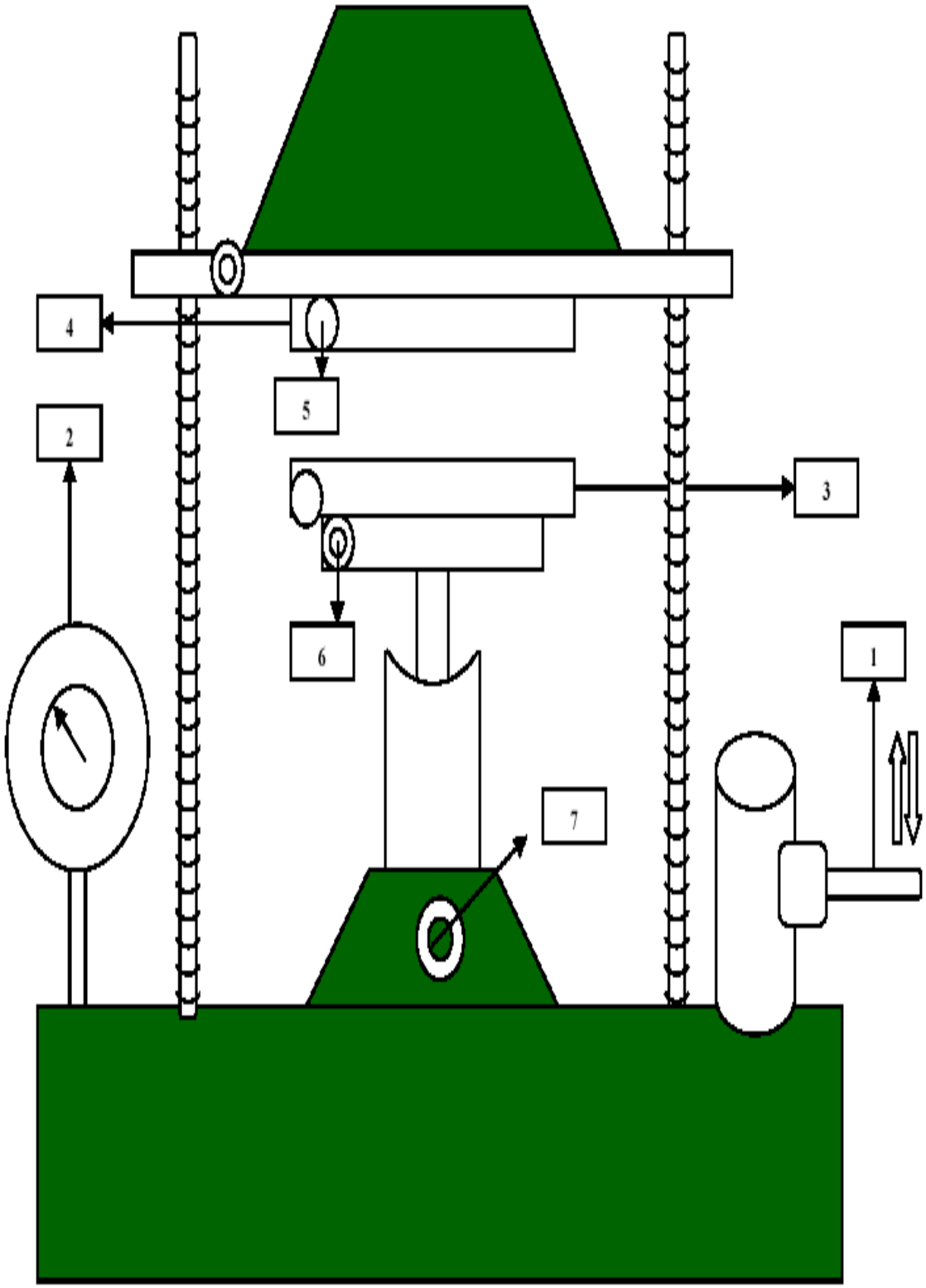

Figure 2.7. Schematic diagram of Carver compression molding press.

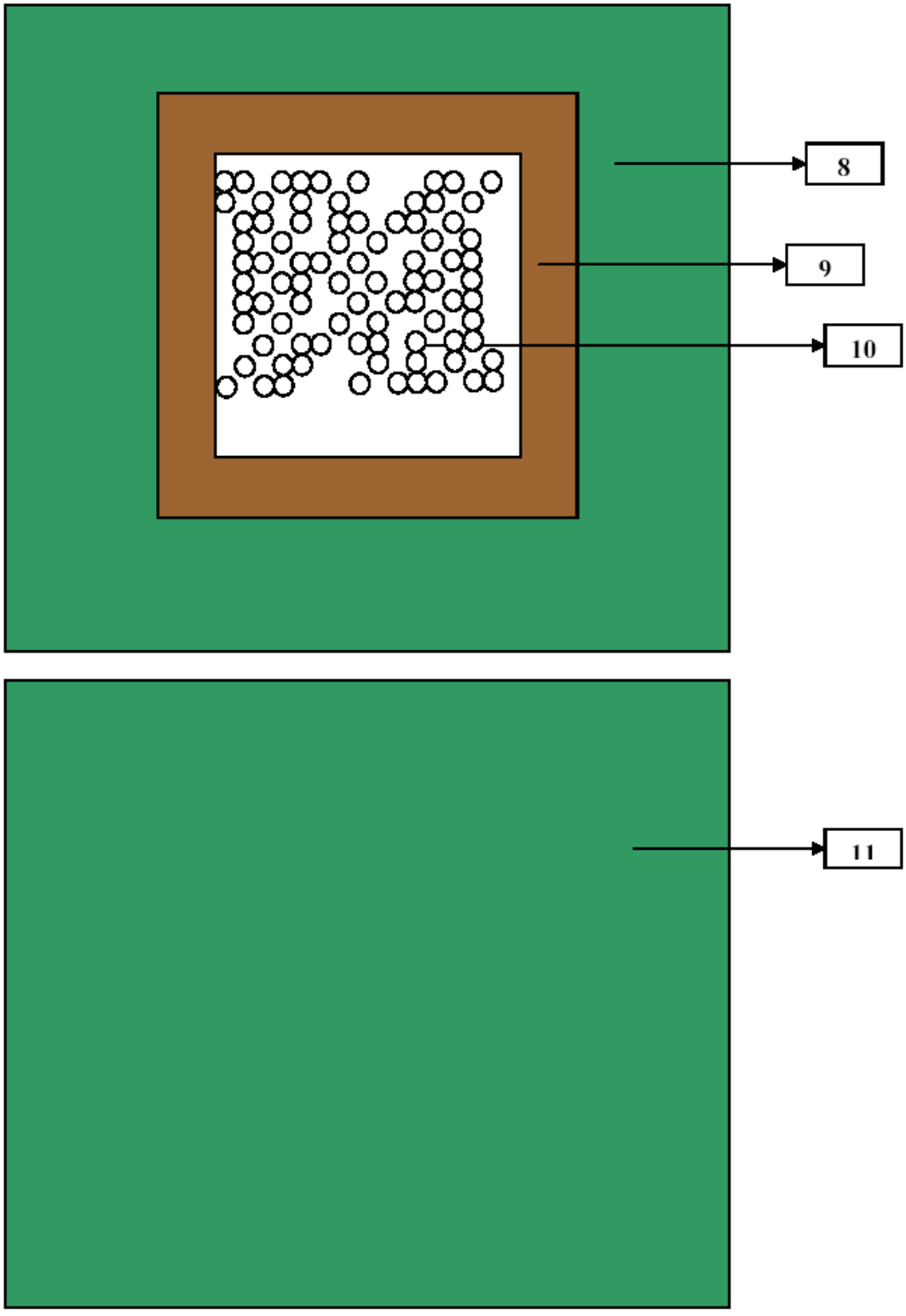

Figure 2.8. Placement of mold between two metal plates covered with Teflon® coated aluminum foil.

INDEX:

1. Lever for raising bottom plate
2. Pressure gauge
3. Bottom plate
4. Top plate
5. Temperature dial
6. Temperature controller
7. Pressure release screw
8. Metal plate “a” covered with Teflon® coated aluminum foil
9. Mold
10. Pellets
11. Metal plate “b” covered with Teflon® coated aluminum foil.

This was repeated until the pressure attained a steady value of 10,000 psi. The pressure could be measured using a gauge attached to the press.

A pressure of 10, 000 psi. on the gauge corresponded to 9302 psi. on the sample. This was calculated using the formula:

$$Ps \times As = Pg \times Ag \qquad \text{(Equation 2.1)}$$

Where, Ps = Pressure on the sample

As = Cross sectional area of the sample

Pg = Gauge pressure

Ag = Cross sectional area of the piston of the press.

As = 4900 mm^2

Ag = 3.14. $(3^2)/4$

Pg = 10, 000 psi.

After the gauge pressure became steady at 10, 000 psi., the mold was allowed to rest at the above mentioned temperature and pressure for 10 minutes. After that, the heat supply to the press was turned off. Immediately after this, the pressure-release screw was turned. The hot plate assembly containing the mold between the two metal plates was

removed and was immersed in a cold-water reservoir and kept for 3 minutes. Then, the entire assembly was flipped over and was immersed in the reservoir for 3 more minutes. After the mold cooled down to ambient temperature, the solidified sheet was then taken out of the mold. Sheets were prepared in this way for pure PP, and the various nanocomposites.

These sheets served as specimens for all the characterization techniques.

2.6.2 Tensile Testing

The aim of tensile testing was to evaluate the mechanical response of the materials to a known strain or deformation rate. This gives a plot of stress versus strain from which a wealth of information may be obtained such as the brittle or ductile behavior, tensile modulus or an indication of stiffness of the material, tensile strength etc.

The instrument used for performing tensile testing was an EnduraTEC ELF 3200 Series machine. The main parts of the system were:

- The linear motor assembly: Had a patented high-bandwidth, low-distortion actuator from Bose Corporation.
- Testing Chamber: Had facilities for introducing hot air, for increasing temperature as well as introducing liquid nitrogen. A bulb for viewing the test in case liquid nitrogen made the chamber cloudy was also provided. The door had a transparent section for viewing testing while in progress. There were two sets of grips. The bottom grip was stationary and was connected to the load cell. The upper grip was mobile and its motion was regulated by the Wintest® software, and ultimately, the linear motor.
- Temperature Control: With the help of the software, temperature could be varied between –50 ^{o}C to 150 ^{o}C.
- Controller box, which acted as an interface between the computer and the machine itself.

Figure 2.9 shows the front view of the machine. Figure 2.10 describes the testing chamber. Figure 2.11 provides a rough description of the temperature controlling unit and

the emergency stop button. Figure 2.12 shows the control unit. None of the parts were hydraulic, so maintenance was quite easy. It should be noted that the test was displacement controlled, i.e., the specimen was pulled by a pre-determined amount with each step of testing. The corresponding load exerted on the sample for pulling was recorded.

The testing procedure can be described in steps as follows:

- The machine and the software were turned on.
- The specimen for tensile testing was a rectangular strip, which was cut from the compression-molded sheet using a penknife. Its width and thickness were measured using a micrometer.
- The specimen was placed between the grips and the grips were tightened. Over-tightening of the grips was avoided, especially for brittle materials, in order to avoid failure at grips.
- The linear motor was turned on using the “locals” button in the software.
- Load and displacement associated with the grips were tared. After that, the distance between the ends of the grips was measured. This was the gauge length. This value was usually 27 mm.
- The system was first tuned for a square wave of certain amplitude. The purpose of tuning was to make the command given to the machine by the software and the output generated by the machine match as closely as possible. Adjusting the PID control parameters during the time when the square wave was acting on the system did the required tuning.
- The tuning was double checked by re-tuning the system with a sinusoidal waveform.
- The waveform was set to “ramp”. This was the waveform used for tensile testing. Strain rate could be set according to requirements, by typing the value in the appropriate box.
- File names for saving the test data were specified using the data acquisition menu. This menu also allowed deciding the rate of scanning, number of scans and time between the scans for acquiring data.

- The machine stopped automatically after the specimen failed. In case the specimen did not fail, the machine stopped acquiring data beyond a critical extension of the specimen. This value was 7.082 mm.

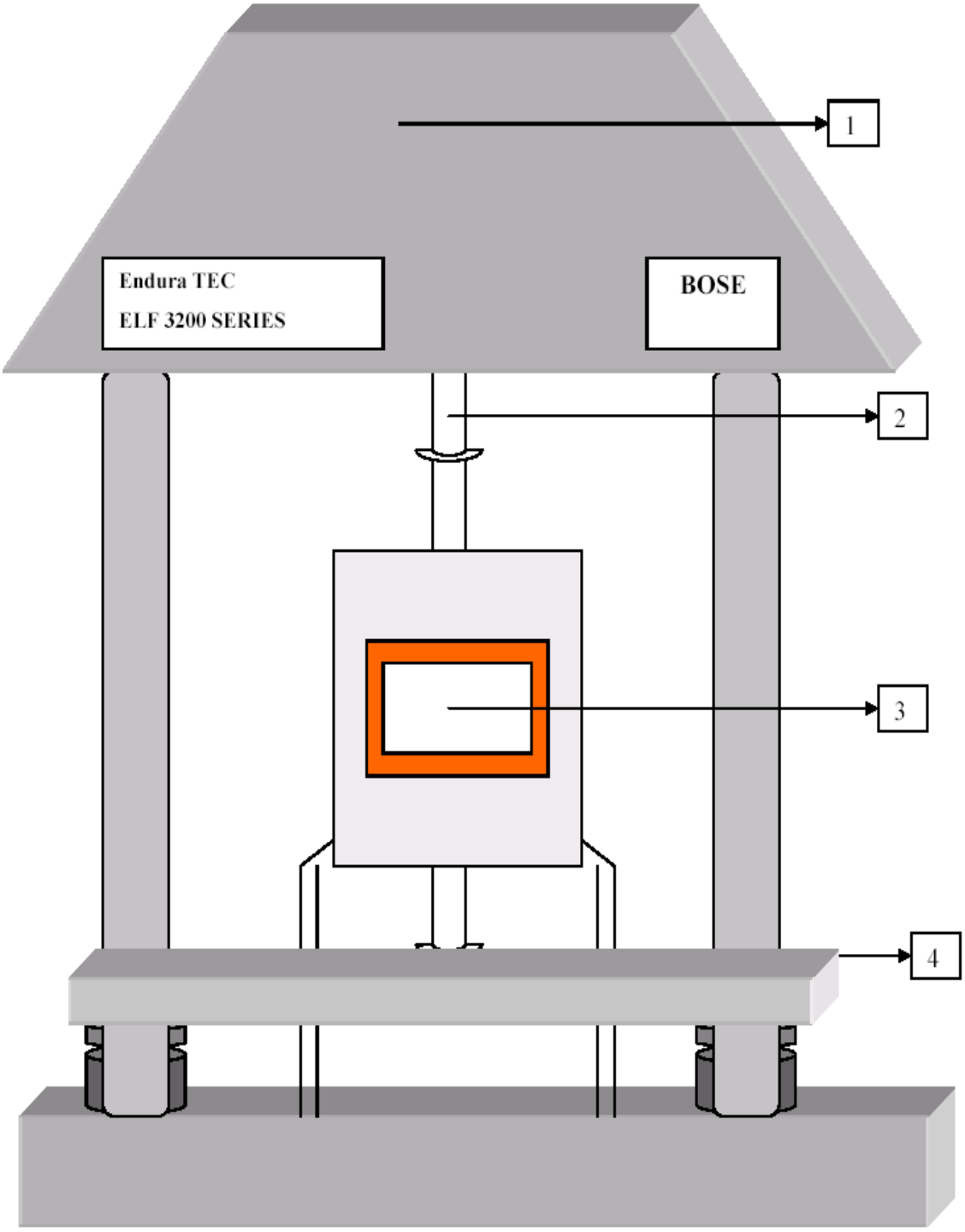

Figure 2.9. The EnduraTEC ELF 3200 series machine.

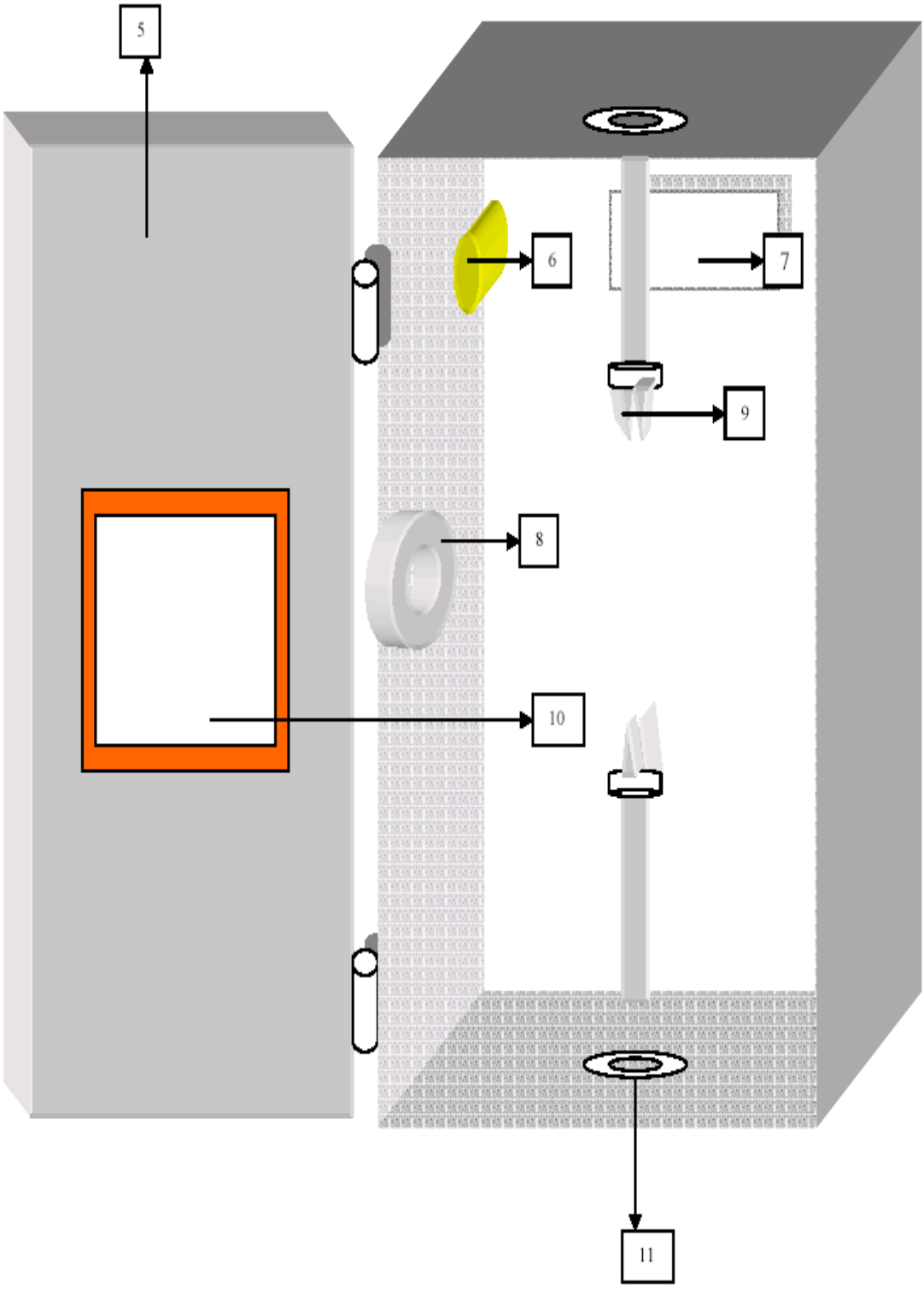

Figure 2.10. Specimen testing chamber.

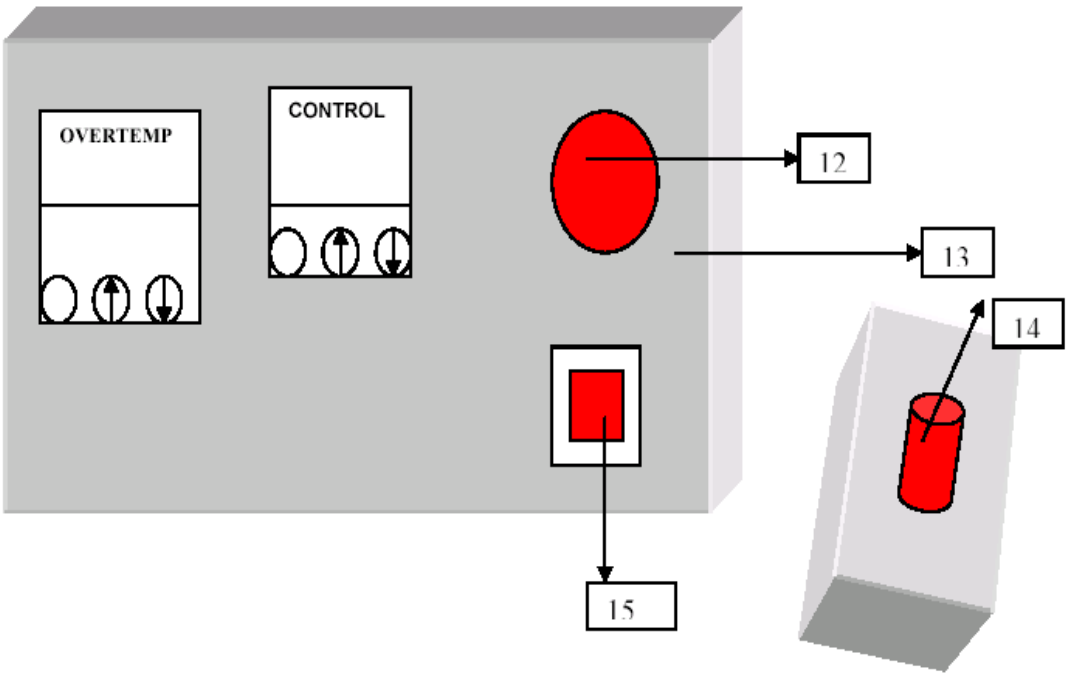

Figure 2.11. Temperature control box and emergency stop buttons.

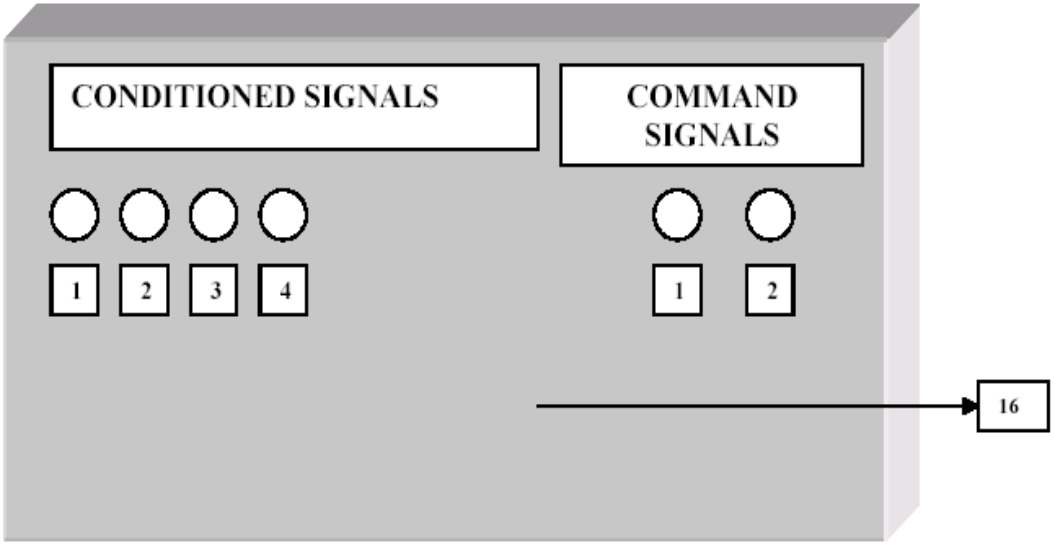

Figure 2.12. Control unit. This acts as an interface between the computer and software.

INDEX:

1) Linear motor assembly
2) Connection between linear motor assembly and grips
3) Testing chamber
4) Load cell
5) Door
6) Bulb
7) Liquid nitrogen inlet
8) Hot air blowing unit
9) Grip
10) Transparent portion of door for viewing testing
11) To load cell
12) Air flow warning button
13) Temperature control box
14) Emergency stop button
15) Heat enable button
16) Control unit (acts as an interface between the computer and the machine).

The tensile testing data was obtained as a text file inforce versus displacement form. Knowing the width and thickness of the specimen, cross-sectional area of the specimen could be calculated using the formula:

$$Area = Width \times Thickness \qquad \text{(Equation 2.2)}$$

The stress on the sample could be calculated by using the formula:

$$Stress = Force \div Area \qquad \text{(Equation 2.3)}$$

Now, engineering strain is given by the formula:

$$\varepsilon = \Delta l \div lo \qquad \text{(Equation 2.4)}$$

The displacement obtained from the testing data was Δl. l_0, the initial separation between the grips (usually 27 mm) was already known. So strain could be calculated. Knowing stress and strain, stress versus strain curves could be plotted.

temperature of testing was For the purpose of tensile testing, typical specimen width was between 4-5 mm and the thickness was between 0.6 to 0.9 mm. The strain rate used was 0.1 mm/sec. The 29 ^{o}C. 2-3 specimens were tested for each material.

The scatter for modulus and tensile strength values were found to lie between 4-10 %. Figure 2.13 shows the stress strain plots for various materials. Figure 2.14 shows the variation of tensile modulus with compatibilizer concentration.

The modulus values were obtained by calculating the slopes of the linear regions of the stress strain curves. Figure 2.15 shows the variation of tensile strength with compatibilizer concentration. Table 2.6 lists the tensile moduli and tensile strengths of PP and PPCNs. Representative data points generated by the Wintest® software are provided in Appendix A.

2.6.3 X-Ray Diffraction

When a beam of electron interacts with an atom, some of the incident electrons have sufficient energy to knock out an inner shell electron of that atom. As a result, an electron from one of the outer shells jumps in.

In doing so, energy has to be emitted. Emitting X-rays can do this. These X-rays are characteristic of every atom and give information specifically about it. This is because each atom has its own excitation energies for its electron shells. Figure 2.16 illustrates the principles of XRD. When X-rays impinge on a crystalline material, atomic planes diffract them.

The objective of performing XRD was to explore the possibility of any intercalation or exfoliation in the layered silicates due to possible penetration by the polymer into the clay layers.

This is usually determined by the shifts in low angle peaks for the clay.

According to Bragg's law:

$$N\lambda = 2d\sin\theta \qquad \text{(Equation 2.5)}$$

Where N = order of diffraction

λ = wavelength of X-rays used

d = interplanar spacing and

θ = semi-angle of diffraction.

So, as the semi angle varies, the d spacing between the clay layers also varies. If the polymer is successful in penetrating the clay layers, then the d spacing of the clay layers increases, thereby reducing the angle corresponding to the peak observed. Bragg's law quantifies this. Here, N, the order of diffraction is assumed to be one.

X-Ray diffraction analysis was performed using a Philips APD 3720 instrument, using a Cu-K_α X-Ray source (Wavelength = 1.54 Å). The range of angles scanned was 0-18 degrees. Reflective mode was used and the experiment was carried out at 15 ^oC.

Table 2.6. Tensile moduli and tensile strengths of PP and PPCNs. Strain rate = 0.01 mm/sec., temperature of testing = 29 ^oC.

MATERIAL	TENSILE MODULUS N/mm^2	TENSILE STRENGTH N/mm^2
PP	1000	22.49
PP/Clay 95:5	968	18.9
PP/EP/Clay 90:5:5	2480	22.02
PP/EP/Clay 85.5:9.5:5	2891	23.6
PP/EP/Clay 76:19:5	1411	20.1
PP/EP/Clay 47.5:47.5:5	1144	18.9

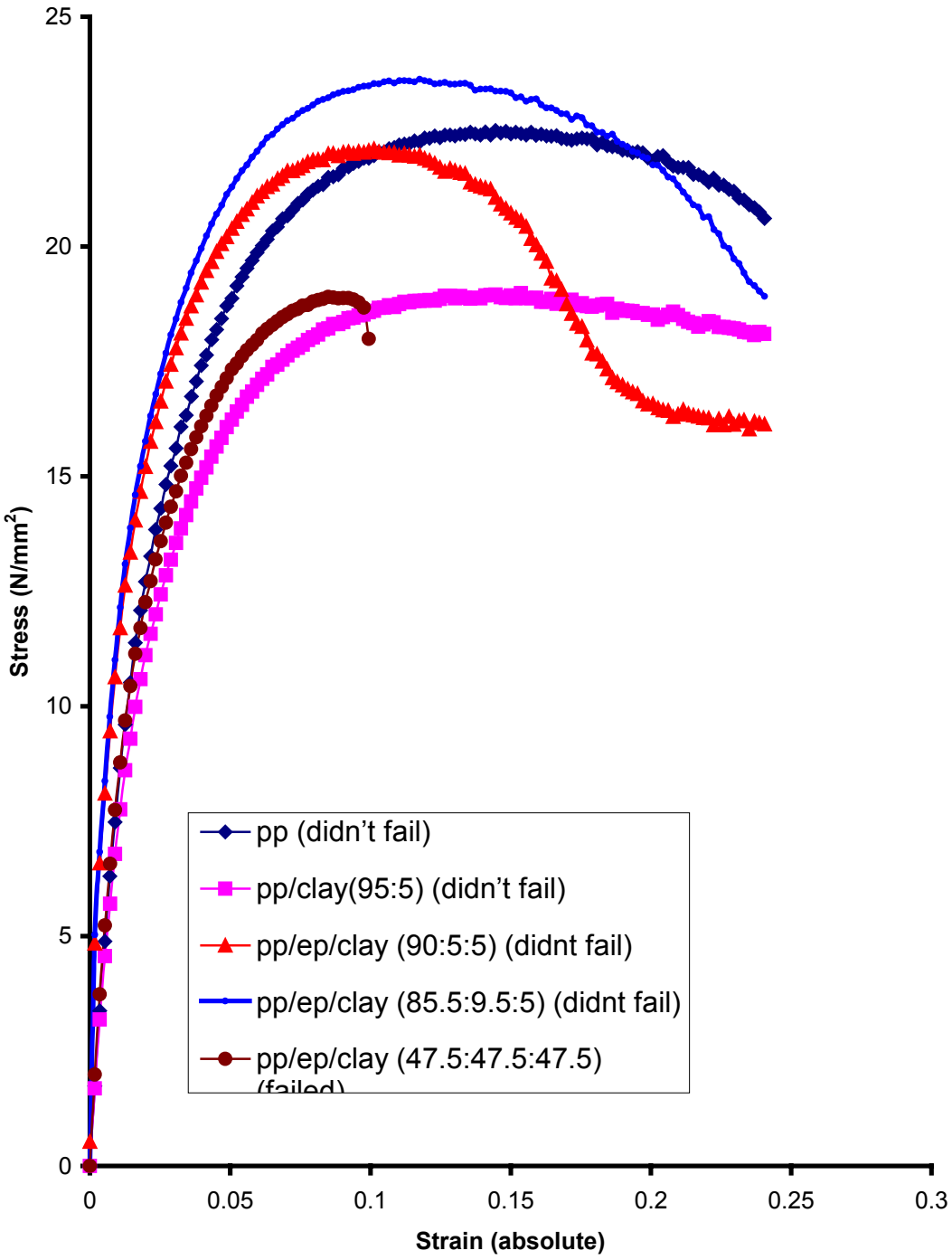

Figure 2.13. Stress versus strain plots for different PPCNs. Strain rate = 0.01 mm/sec., temperature of testing = 29 ^{o}C.

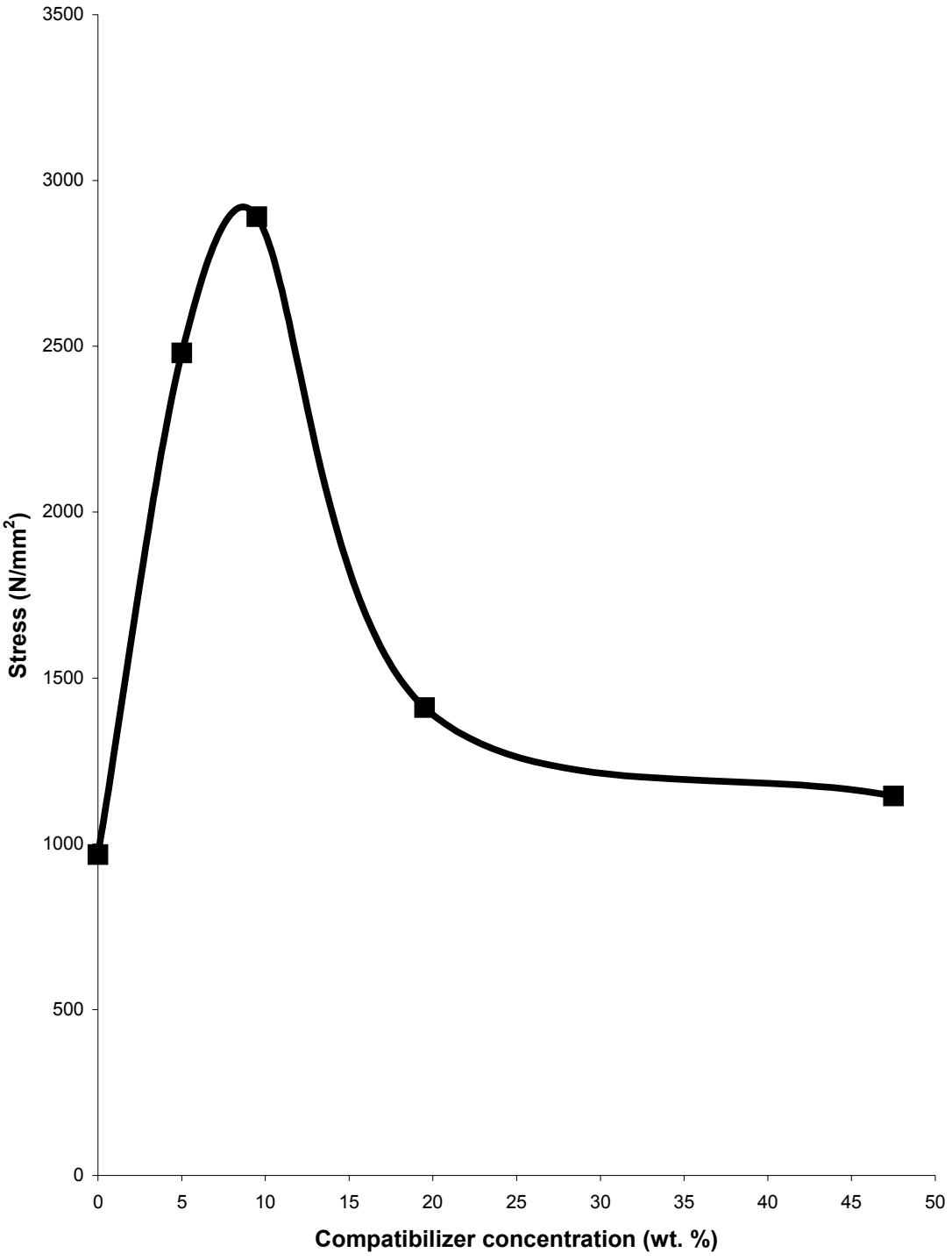

Figure 2.14. Dependence of tensile modulus on compatibilizer concentration. Strain rate = 0.01 mm/sec., temperature of testing = 29 ^{o}C.

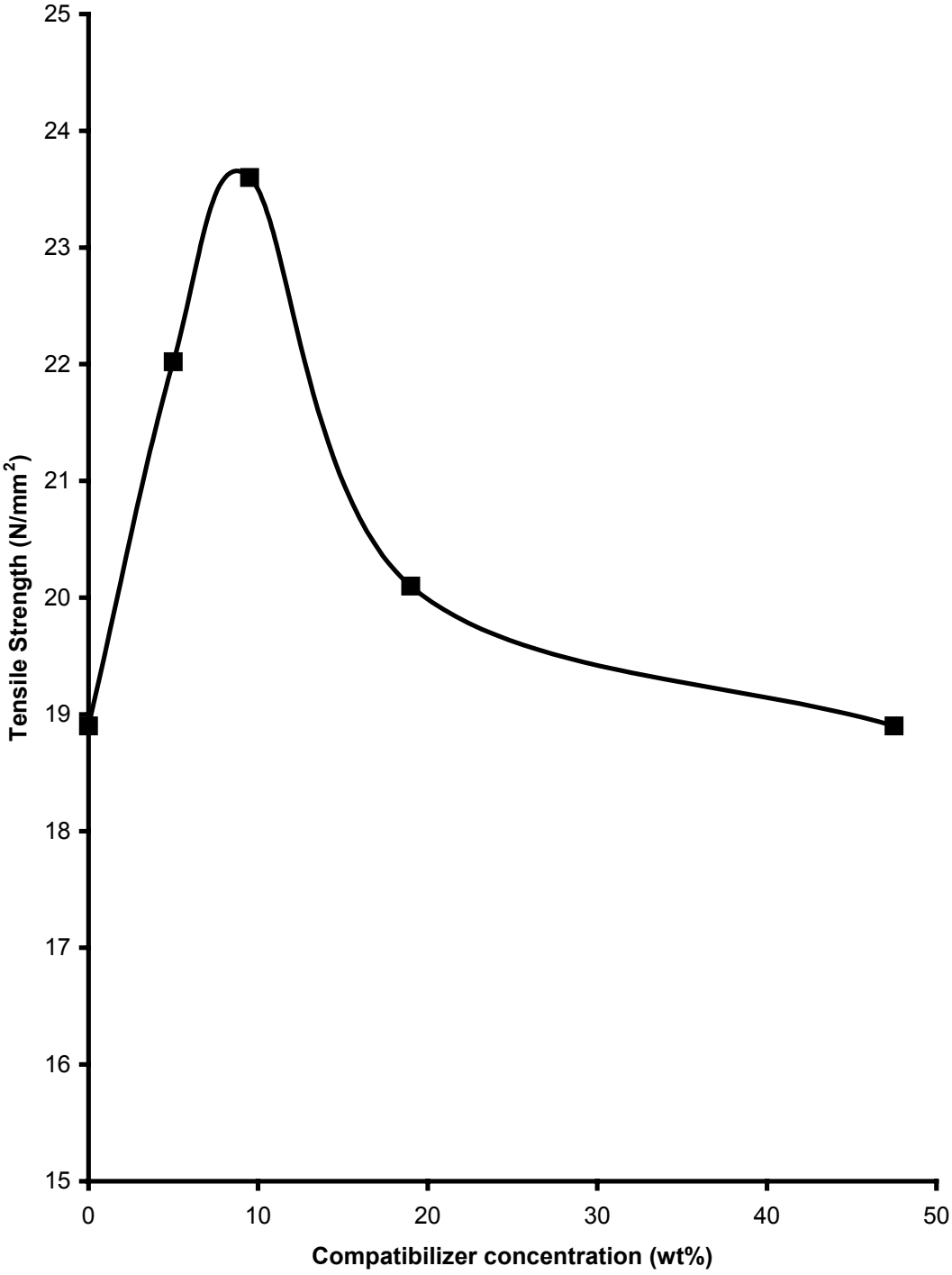

Figure 2.15. Dependence of tensile strength on compatibilizer concentration**.** Strain rate = 0.01 mm/sec., temperature of testing = 29 ^{o}C.

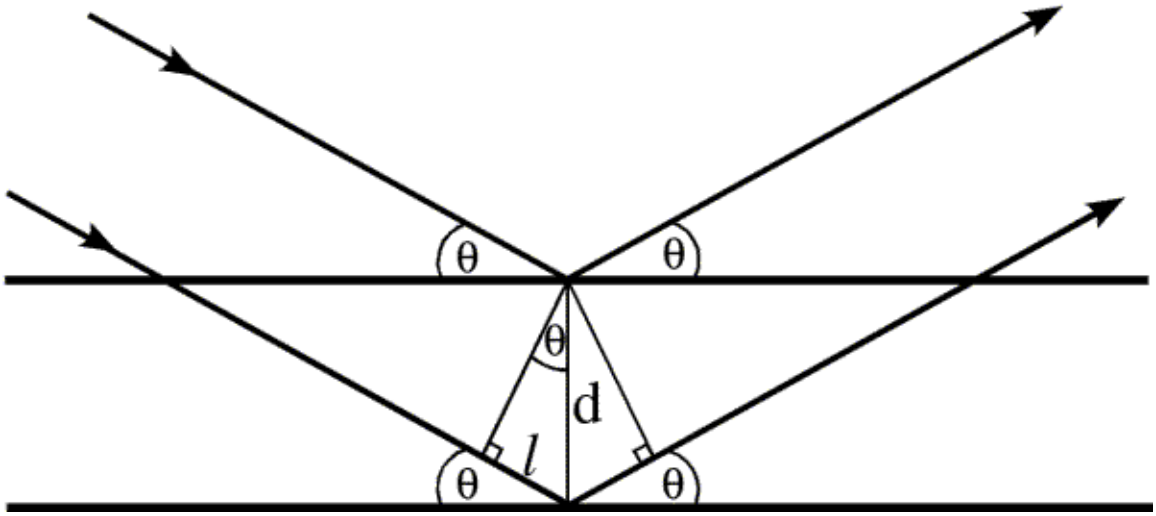

Figure 2.16. Fundamentals of X-ray Diffraction. Here, l= path difference, d= interplanar spacing and θ = semi-angle of diffraction.

The following stepwise procedure was followed:

- A 1 cm^2 square was cut from the compression molded sheet of the sample, on which XRD analysis was to be done.
- This square was mounted on a glass slide using double-sided scotch tape.
- A dummy, with the same height as the sample, was mounted on the slide to go into the sample holder. Usually, the dummy was made out of cut pieces of glass slides and cover slips, which were then fastened together with double-sided tape. The purpose of the dummy was to ensure uniform level throughout the glass slide.
- The specimen was loaded on the spring clip with the glass slide extending towards the user.
- The slide was pushed back completely.
- The door was placed with its contact down.
- Depressing “Blk Start” button on X-ray checked water.
- 20 seconds were given for the “operate” light to turn on.
- The voltage was set to 40 kV.
- The current was set to 20 mA.
- The kV was reset to 40 kV.

- The shutter control was turned to ∞.
- Pressing the appropriate button opened shutter.
- On the software, using the APD menu and the sub menus within, system preparation and system parameters were defined.
- Under the "Identify" menu, program name, scan parameters and data collection parameters were set.
- F1 key was pressed to start testing.
- The instrument was shut down upon completion of test.

Figure 2.17 shows the entire XRD pattern for each material. Figure 2.18 shows the low angle region of the XRD patterns shown in Figure 2.17.

2.6.4 Differential Scanning Calorimetry (DSC)

This characterization technique is used to study the response of a polymer to thermal energy, or in other words, the behavior of a polymer is studied when it is heated [103]. Information regarding thermal transitions of polymers, such as melting, crystallization, and glass transition could be obtained. The basic set up of any DSC instrument consists of two symmetrically placed pans in a silver chamber.

This chamber is heavily insulated from the atmosphere so that temperature can be controlled from the heaters and liquid nitrogen alone. Two pans are placed on each side of the chamber. One of them is blank, i.e., has nothing, whereas the other has the polymer sample in it. The amount of sample required ranges from 8-15 mg. After the pans have been placed, the chamber is closed and is taken to a starting temperature, from which it is started to heat. This starting point depends on the temperatures at which thermal transitions take place for the polymer. For example, if polypropylene, with a glass transition temperature between –10 ^{o}C to 0 ^{o}C, is being used, the starting temperature should be about –50 ^{o}C in order to cover the entire Tg transition. It is to be kept in mind

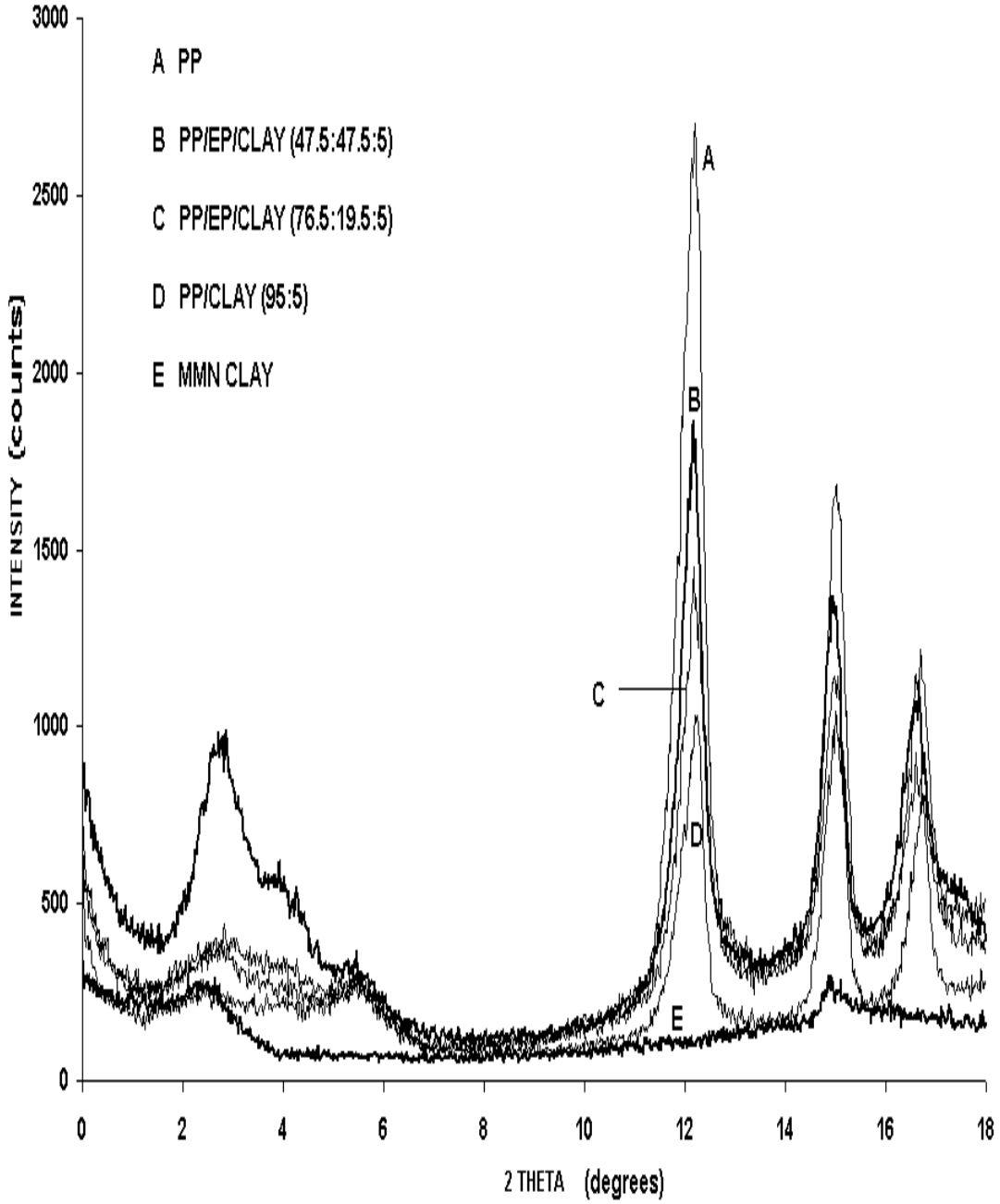

Figure 2.17. Complete XRD patterns for PP and PPCNs in reflective mode, at 15 ^{o}C.

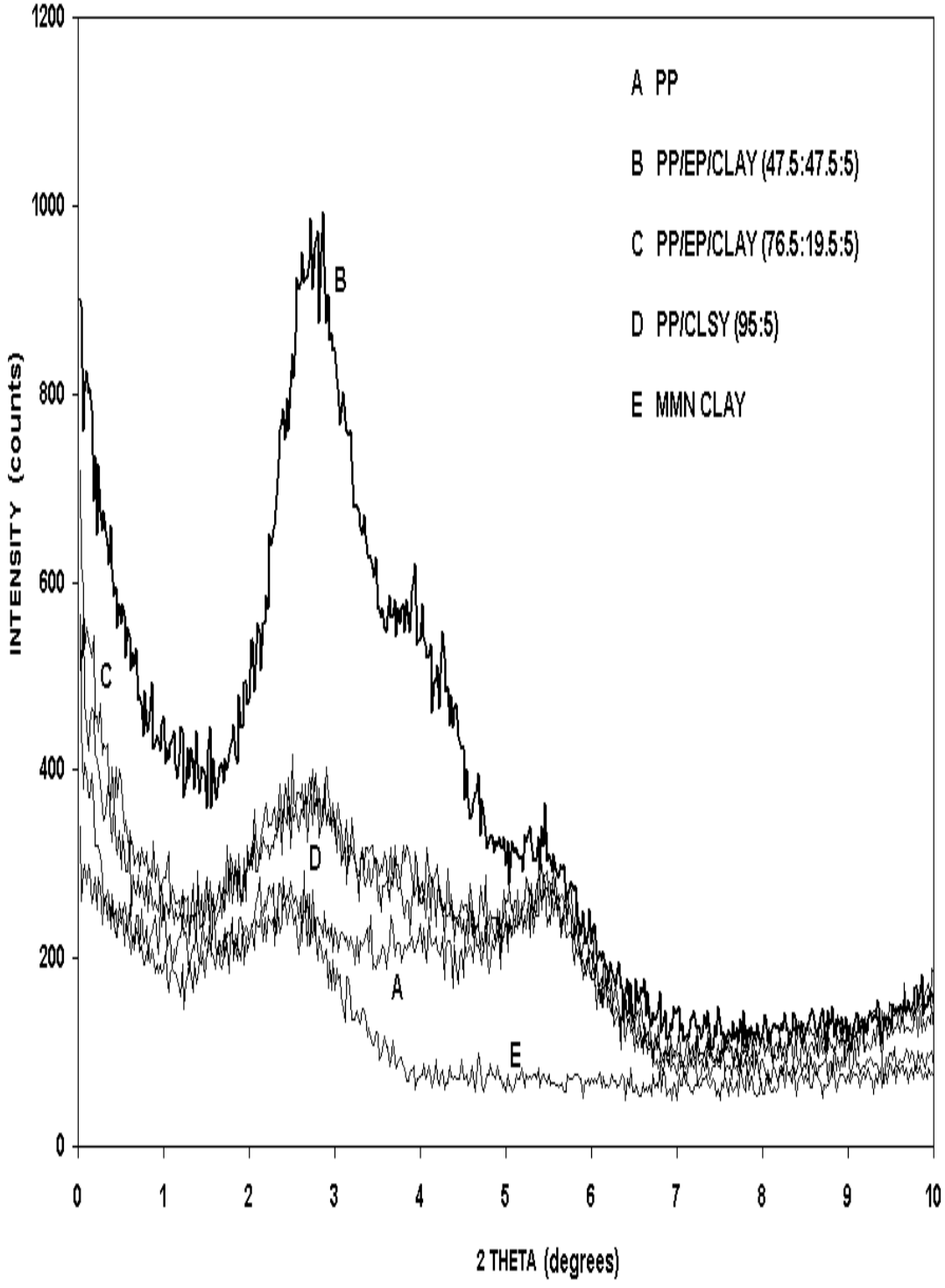

Figure 2.18. Lower angle region of XRD patterns for PP and PPCNs in reflective mode, at 15 ^{o}C.

that a polymer generally does not undergo transitions at a well-defined temperature, but it does so over a range of temperatures. After taking the polymer to the starting point, it is heated. As mentioned earlier, one of the pans is blank while the other has extra material in it, which is the polymer. Hence, heat requirements would be different for the two sides of the chamber. It is this difference in heat versus temperature that we plot in order to study the thermal transitions. Specific heat versus temperature can also be plotted. Specific heat can be obtained by dividing the heat supplied by the temperature difference resulting from the supply of heat. Thus specific heat is nothing but the amount of heat required to produce a certain temperature difference, and this obviously depends on the characteristics of the material. Figure 2.19 shows Tg transition on a DSC thermogram.

The Figure shows that the polymer is absorbing heat and this results in a dip. For measuring glass transition temperatures, there are different procedures, one of which is to take the average of the starting point and end point of the transition. After glass transition, the polymer chains have a lot of mobility. They try to get themselves ordered. Finally when they get ordered after acquiring sufficient energy, they give off heat. This corresponds to the crystallization transition. Figure 2.20 shows this. This peak can help distinguishing between a crystalline and an amorphous system. Amorphous polymers do not show this peak.

If the polymer is heated beyond its crystallization temperature, eventually a stage is reached when the temperature of the polymer does not rise until heat is absorbed. This stage is called melting. In other words, crystallization is “undone”. Now, the furnace has to supply additional heat because the polymer is absorbing heat, and the furnace to keep

the temperature of the chamber rising at a constant rate as well. This results in a large dip. Figure 2.21 shows the melting transition on a DSC thermogram.

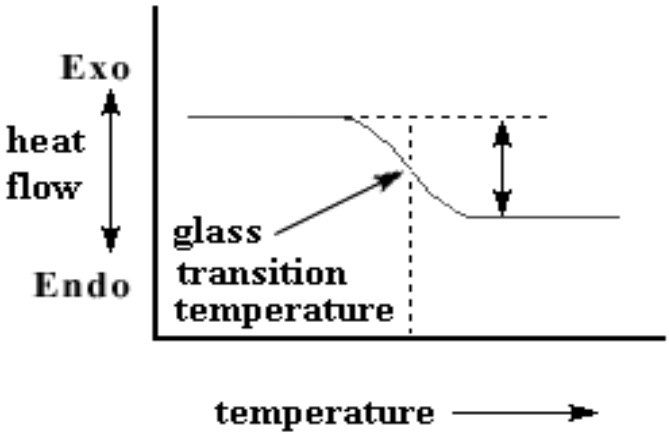

Figure 2.19. Glass transition on a DSC thermogram.

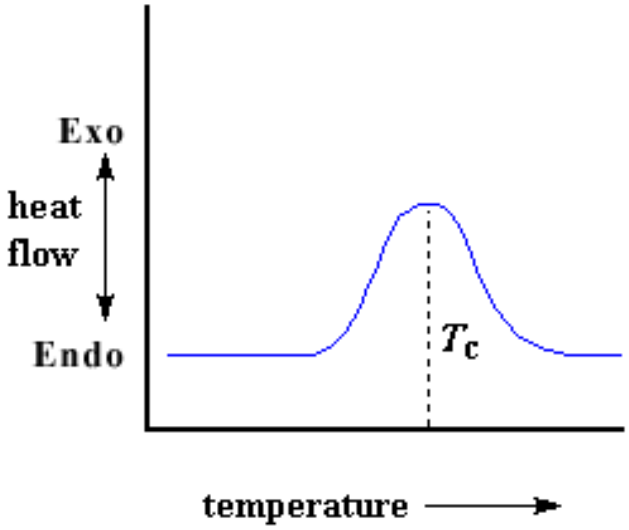

Figure 2.20. Crystallization transition on a DSC thermogram.

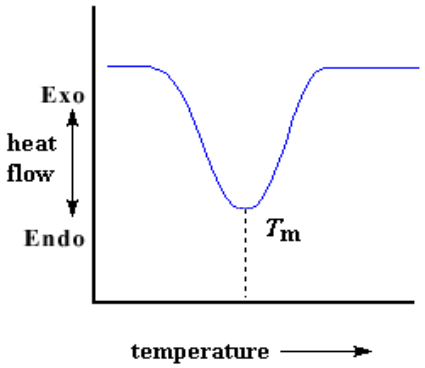

Figure 2.21. Melting transition on a DSC thermogram.

The heat of melting can be obtained by measuring the area of the corresponding peak. One very important information that can be obtained from a DSC plot, often called a *thermogram* is % crystallinity of the sample. Knowing the total heat of melting H_m and the total heat of crystallization H_c, $H_m - H_c$ gives the heat released by the crystals in the polymer chains that were present before the sample was heated. Dividing this by the specific heat of melting, the grams of polymer that was crystalline before heating the sample can be obtained. So, dividing this number by total mass of the sample and then multiplying by 100 would yield % crystallinity.

DSC for this research was performed using a ThermoHaake DSC 220C model instrument, whose basic make-up is just as described above. However, the procedure had a minor difference. The instrument had to be calibrated first. This was done by doing a blank run with alumina in the reference pan and blank in the sample pan. This was followed by the actual experimental run with alumina in the reference pan and polymer in the sample pan. Crimped pans were used for placing the samples. Heating rate used was 10 ^{o} C/min, whereas the samples were cooled at 50 ^{o}C / min. The starting temperature was – 50 ^{o}C and the maximum temperature to which the samples were heated was 250 ^{o}C. Two cycles were performed. This was to ensure that during the first cycle, any

thermal history effects due to processing would be removed. Figure 2.22 shows the entire heating thermogram.

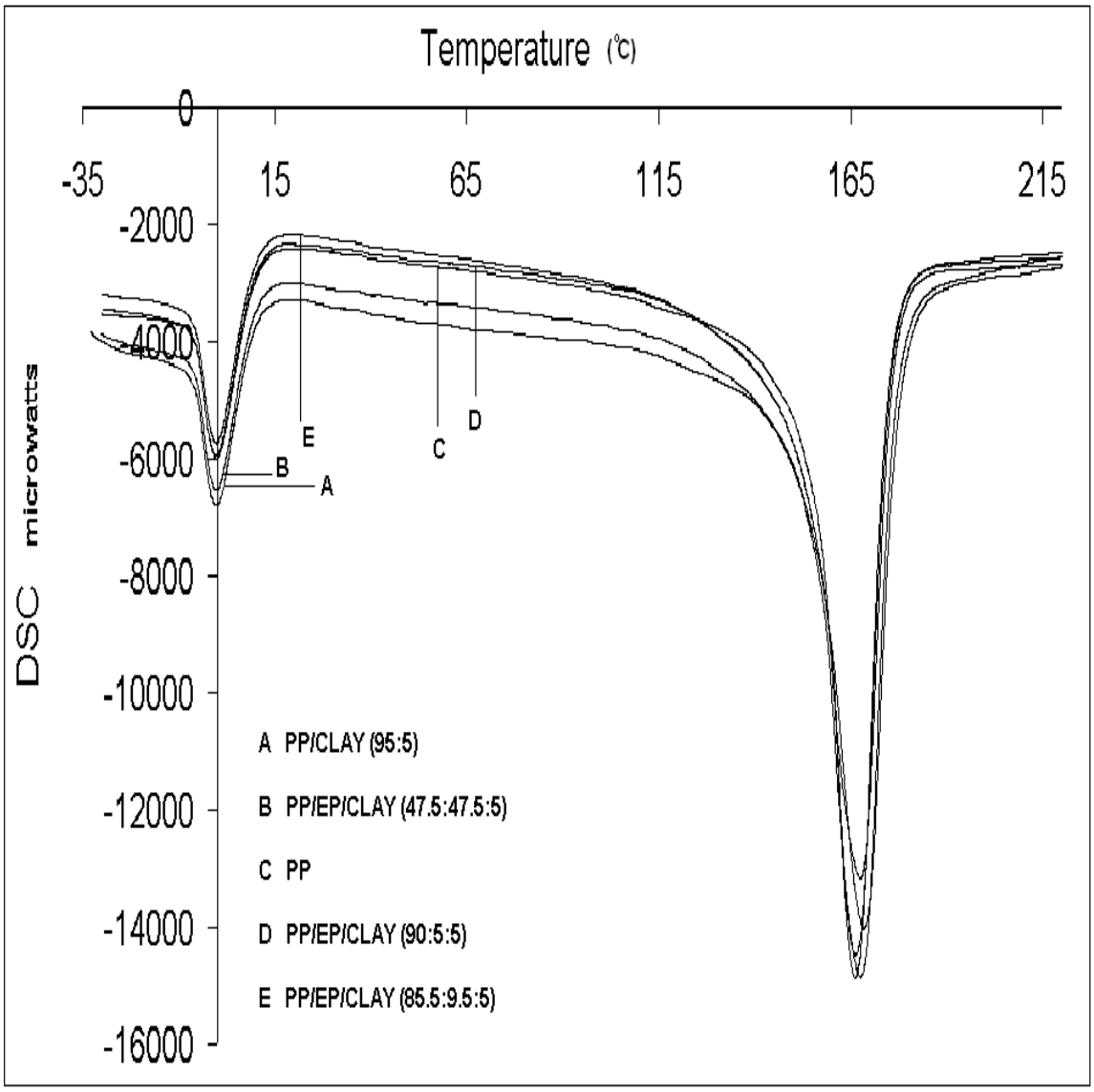

Figure 2.22. DSC heating thermograms for PP and PPCNs. Heating rate = 10 ^{o}C/minute.

Figure 2.23 shows the Tg region of the heating thermogram for the sake of clarity. Figure 2.24 shows the melting region alone for the same reason. Figure 2.25 shows the cooling thermogram and the crystallization peaks.

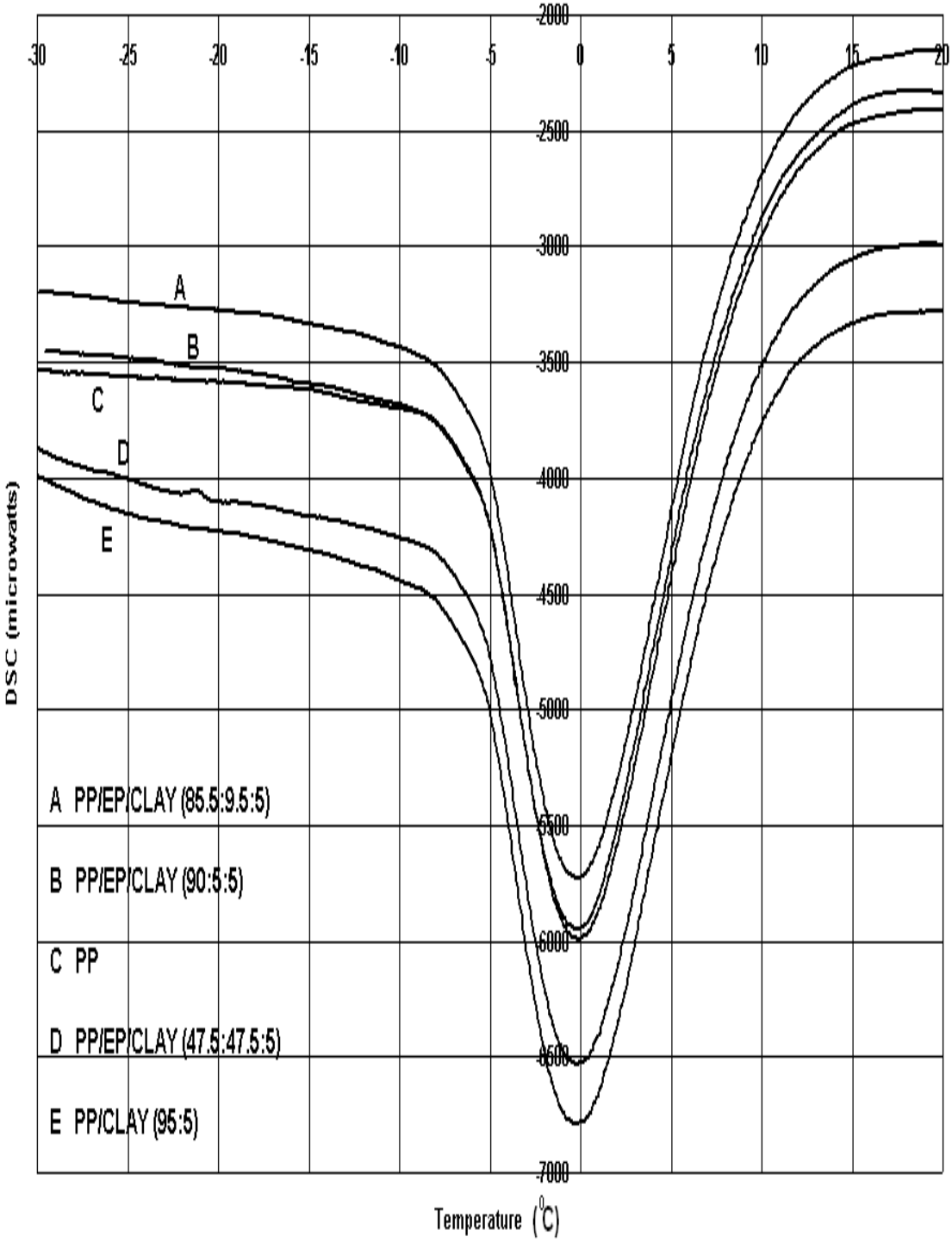

Figure 2.23. Tg region of DSC heating thermograms for PP and PPCNs. Heating rate = 10 ^{o}C/minute.

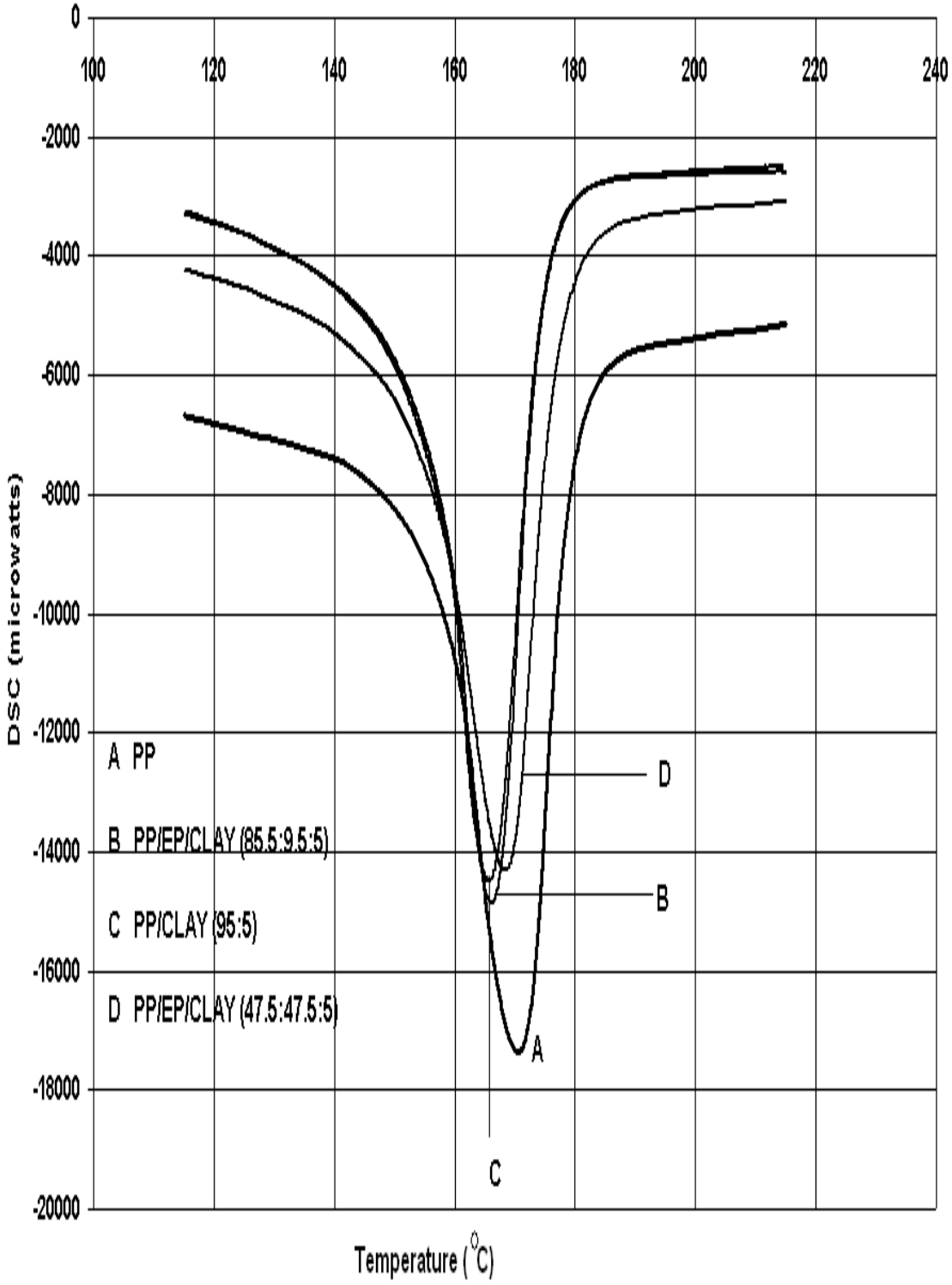

Figure 2.24. Tm transition for PP and PPCNs obtained from DSC heating thermogram. Heating rate = 10 ^{o} C/minute.

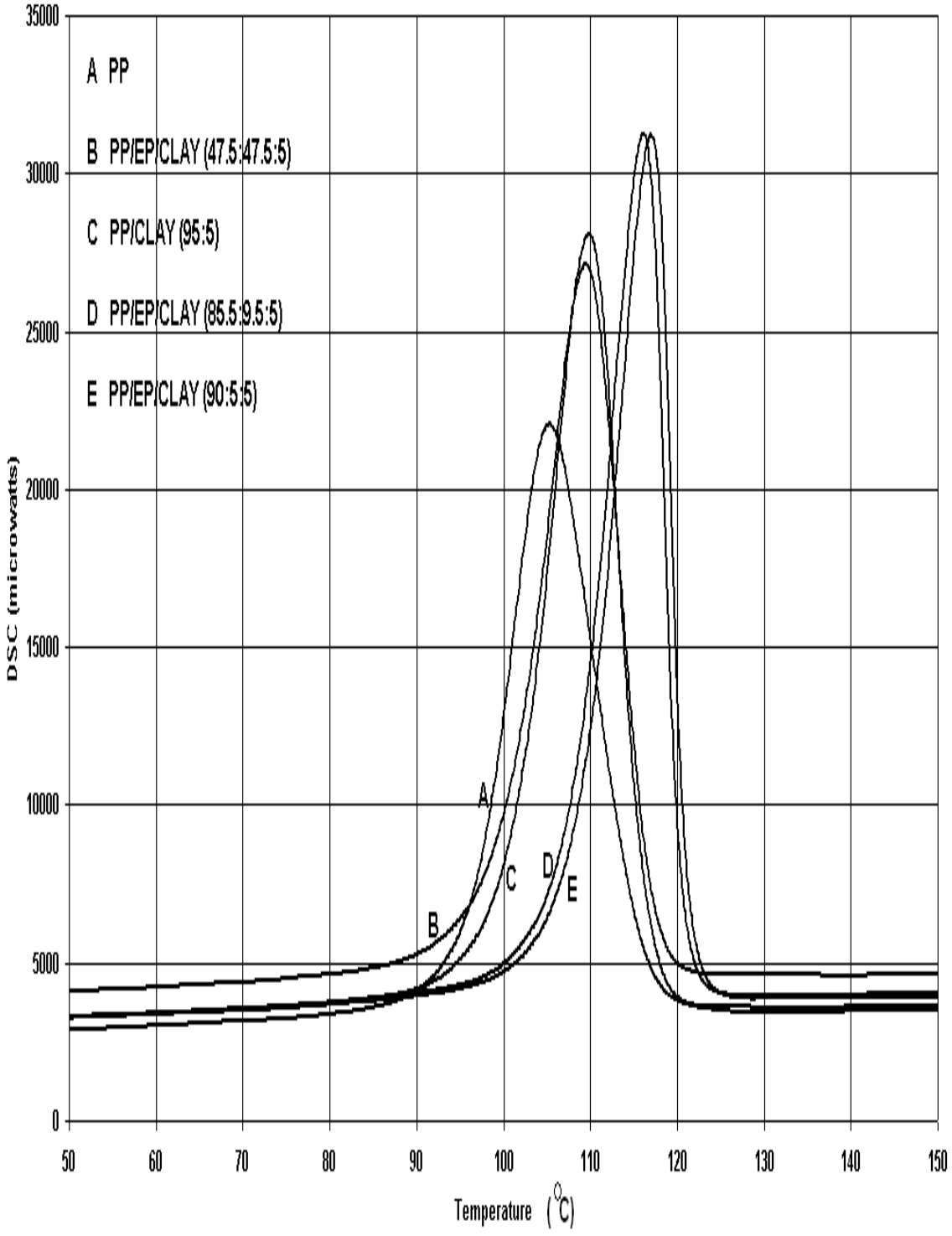

Figure 2.25. DSC cooling thermograms for PP and PPCNs. Cooling rate = 50 ^{o}C/minute.

2.6.5 Transmission Electron Microscopy (TEM)

TEM is an extremely valuable tool for characterizing polymer/clay nanocomposites. This is because with this technique, the clay galleries dispersed in the polymer can be actually *seen*. Greater the number of individual platelets that can be counted on a TEM micrograph, better the dispersion of the clay.

However, TEM demands a very careful preparation of specimens. Polymers are charged when bombarded with electrons. So, polymer specimens are coated with carbon or gold/palladium coatings.

Fundamentally, a TEM makes use of electron optics. A high-energy beam of electrons is directed towards a thin specimen (usually 100 nm thin slices). The electrons that are transmitted through the specimen are collected on a screen and these give information about the microstructure of the material. The TEM consists of an electron gun. This could be either thermionic or a field emission gun. The filament however, is mostly made of tungsten, and is V-shaped. LaB_6 filaments can also be used, but they are quite expensive. Other components of the TEM are condenser lens assembly, specimen stage, objective lens assembly and the recording system. A very high quality vacuum should be maintained at all times in order to make maximum use of the electrons emitted by the gun.

The contrast obtained in a TEM image is atomic contrast. In our case, polymers have elements like carbon, hydrogen and oxygen, whereas the clay has silicon, aluminum etc., that have a higher atomic number. Thus, they scatter more and transmit fewer electrons. So, they appear dark in the micrograph.

For preparing specimens for TEM, a few thin slices were cut from the compression-molded sheet of the material. These were embedded in a two-part epoxy

resin in a mold, and were cured in a vacuum oven at 40 ^{o}C. Next, 100 nm thin slices were cut using an Ultracut microtoming machine**.** It was found that the polymer embedded in epoxy was hard enough to be cut with a diamond knife without being cooled with liquid nitrogen (referred to as ultracryomicrotomy). The slices were obtained in a small pool of water that was present in a specially designed area surrounding the diamond knife. These were picked up using hair tipped brushes and were mounted on copper grids. Carbon coating of slices followed this. It is worthwhile mentioning that sample preparation can introduce voids in the specimen. Figure 2.22 shows this [104].

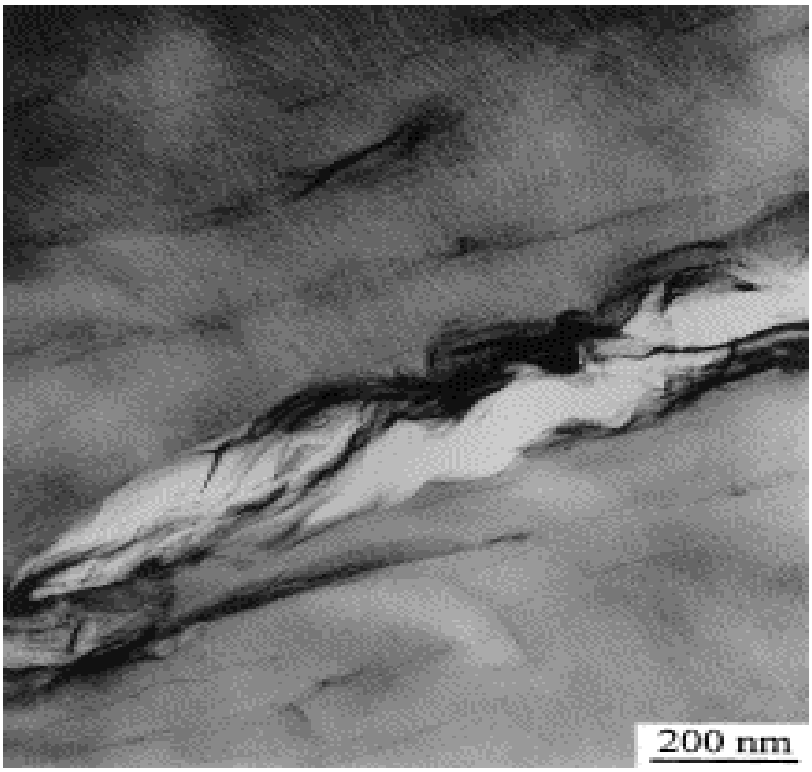

Figure 2.26. Void formation between the folded silicate layers during the microtoming of the bulk nanocomposite.

The prepared specimens were viewed under a JEOL 2010F TEM. Figure 2.24 shows TEM images for PP/Clay (95:5). Figure 2.25 shows TEM images for PP/EP/Clay (85.5:9.5:5). Figure 2.26 shows TEM images for PP/EP/Clay (47.5:47.5:5).

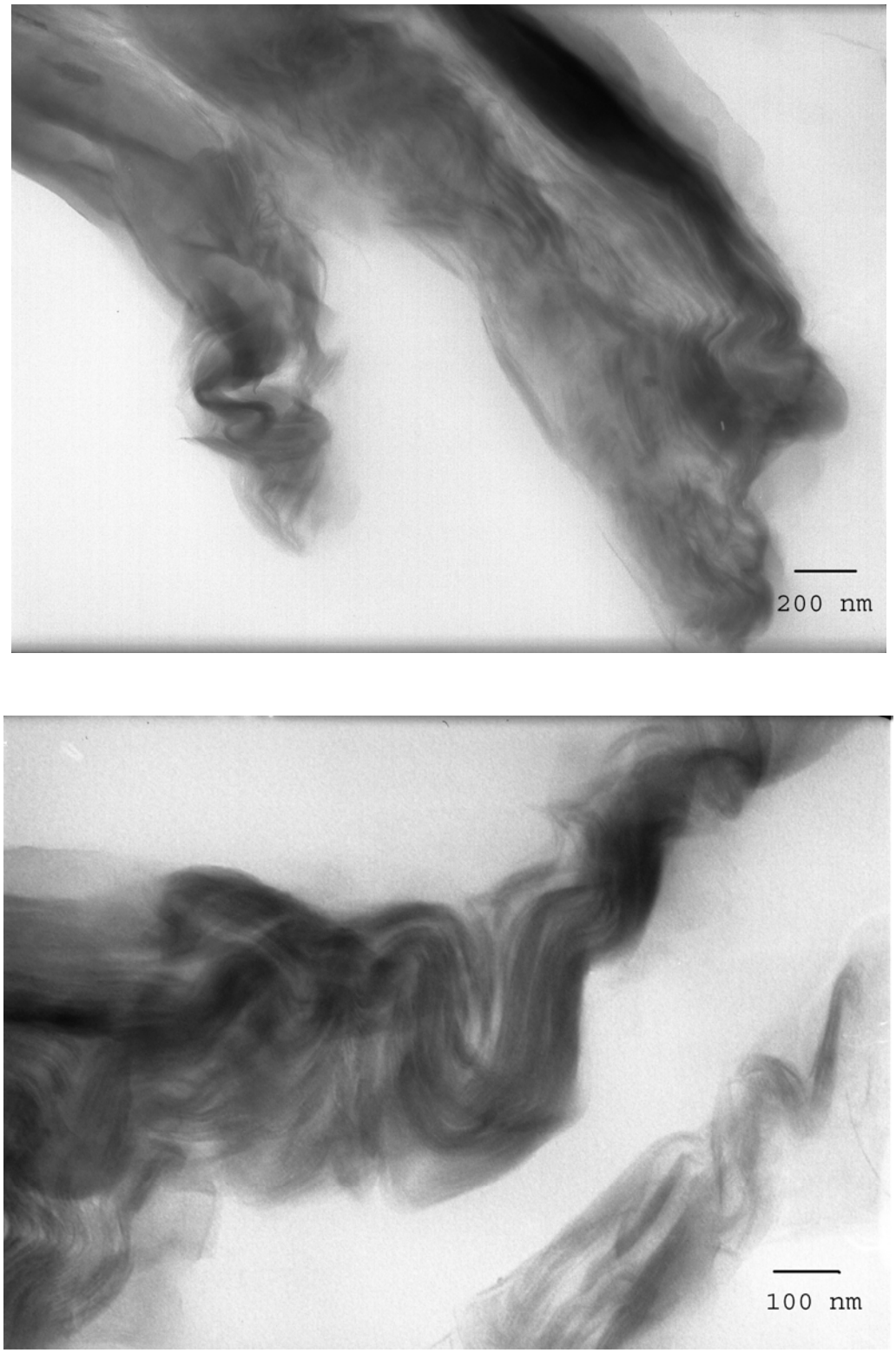

Figure 2.27. TEM micrographs of PP/CLAY (95:5).

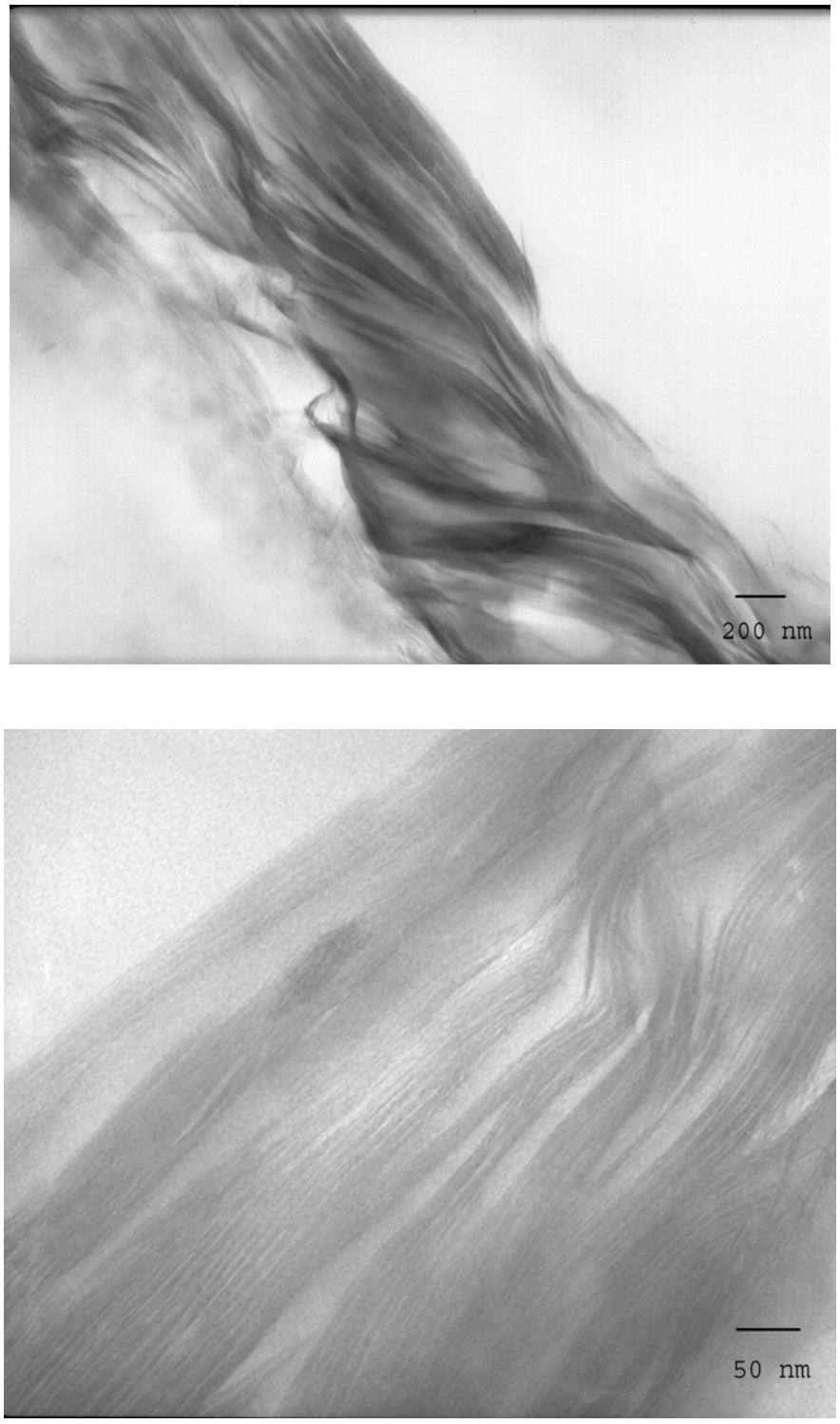

Figure 2.28. TEM micrographs of PP/EP/CLAY (85.5:9.5:5).

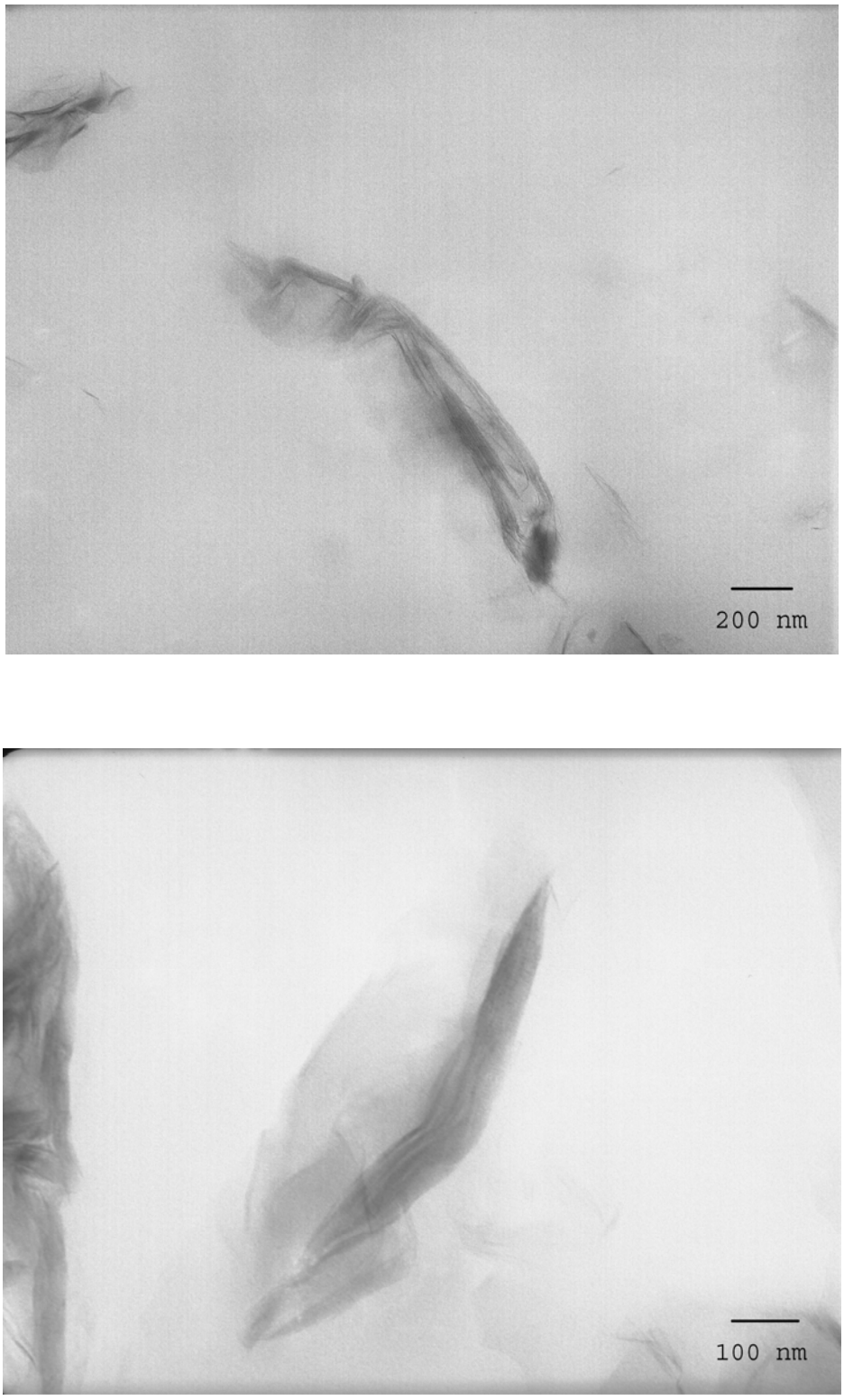

Figure 2.29. TEM micrographs of PP/EP/CLAY (85.5:9.5:5).

2.7 Discussion of Results

In this section, the results obtained in the form of various plots, tables and curves from different characterization techniques are discussed and their implications are elaborated.

2.7.1 Tensile Testing

It is evident from Figure 2.13 that with the addition of clay and compatibilizer, the tensile properties showed remarkable improvement. Both modulus and tensile strength for the materials designated PP/EP/CLAY (90:5:5) and PP/EP/CLAY (85.5:9.5:5) were much better than pure PP. However, the same were inferior for PP/Clay (95:5). This material did not have any compatibilizer. This showed the necessity for adding Epolene. Table 2.6 shows the variation in modulus and tensile strength with variation in compatibilizer concentration. Figure 2.14 conveys the same pictorially. It was seen that for PP/EP/CLAY (90:5:5), the modulus was 148% greater than pure polypropylene, whereas for PP/EP/CLAY (85.5:9.5:5), the increase was 189.1%. This means that for these materials, the tensile moduli were more than two times that of pure PP.

Figure 2.15 shows the dependence of tensile strength on compatibilizer concentration. The trend observed is similar to that with tensile modulus. An interesting feature to note regarding the trends shown by Figure 2.14 and Figure 2.15 was that the properties reached a maximum at a certain compatibilizer concentration and then leveled off after showing a decreasing trend. However, the weight % of clay in all these materials was constant, which was 5%. A possible hypothesis was proposed for such a behavior.

Two additional components were added to PP. First was a low molecular weight compatibilizer, whose molecular weight was significantly lower than PP. The other material was clay, which acts as reinforcing agent. It was seen from Figure 2.13 that

when no compatibilizer was present (i.e., for PP/CLAY (95:5)), the material still exhibited ductile behavior. This is because the clay has been modified organically to exhibit some compatibility with hydrophobic polymeric systems. However, the extent of clay dispersion and distribution was not adequate at this stage to optimize the number of load bearing clay platelets per unit volume. Hence, the modulus and tensile strength were lower than PP.

When some compatibilizer was added (i.e., PP/EP/CLAY (90:5:5)), it was seen that the modulus showed tremendous improvement, and the tensile strength increased as well. However, the increase in tensile strength was not proportionate to the increase in tensile modulus. This is because the introduction of clay tends to make PP brittle. However, at higher stress and strain values, the small, low molecular weight compatibilizer chains tend to flow more easily than PP. In other words, the clay increases the tensile modulus, but the compatibilizer tends to bring it down. Hence, there is a certain amount of compatibilizer that can be added for a given amount of clay (to be added with PP) in order to get the optimum mechanical properties.

So, the addition of a low molecular material may adversely affect the tensile properties. But on the other hand, the compatibilizer may also increase the spacing between the clay galleries, thereby increasing the effective surface area available for bonding. This could mean enhanced adhesion between the polymer matrix and the clay. This could lead to better mechanical properties. This is supported by TEM images, which are discussed in a later section. So there are two effects of the compatibilizer on the system:

- Being a low molecular component, it tends to have detrimental effects on the mechanical properties of the nanocomposite.

- It tends to increase the spacing between the clay platelets. This tends to enhance the mechanical properties.

Now, as the percentage of compatibilizer was increased beyond 5 wt% (i.e., PP/EP/CLAY (85.5:9.5:5)), it was seen that the tensile properties improve further. The modulus and tensile strength were enhanced even further. Thus, we see that factor (a) is still prevalent over factor (b).

Upon increasing the concentration of the compatibilizer further (i.e., PP/EP/CLAY (76:19:5)), a drastic drop in both modulus and tensile strength was observed. This showed that the low molecular factor associated with Epolene® overcame its reinforcing capability by increasing the clay interlayer spacing. When the concentration of Epolene® was increased to 47.5 % by weight, the tensile properties not only got worse, but also the material failed when subjected to tensile testing. This was not observed with any other material, including pure PP. This indicated the there was excessive low molecular weight Epolene® present, and its effect on tensile properties by increment of clay interlayer spacing was certainly overcame by its own mechanically weak character. This material not only failed but it also did so in a brittle fashion. This is possibly due to presence of excessive low molecular weight component, as well many load bearing clay platelets per unit volume, which also tend to make the nanocomposite brittle.

2.7.2 X-Ray Diffraction

Figure 2.17 shows the entire range of angles covered, which is between 0 to 18 ^{o}, while Figure 2.18 shows the low angle region of the same plot. It is known that pure clay has a diffraction peak, which corresponds to Si 001 plane, between 2 to 4 degrees. It can be seen from the plots that some intercalation has taken place, but the shift in the peaks is not very significant. XRD gives an overall view of the extent of clay dispersion. For

actually *seeing* the clay dispersion on a local scale, TEM is employed, and its results are discussed in a later section.

2.7.3 DSC

The DSC heating thermogram is shown in Figure 2.22. It is noteworthy that the abscissa of the plot is heat supplied by the instrument, which is directly proportional to specific heat. Since it is hard to distinguish between individual thermograms, Tg and Tm regions are shown separately in Figure 2.23 and Figure 2.24 respectively. From Figure 2.23, it is seen that there is not a significant shift in the Tg transition for the nanocomposites. However, it can be said that at glass transition, the heat requirement for PP/CLAY (95:5) is the least. This could be because the clay has a lower specific heat capacity than the pure polymer, and hence, the heat capacity of the composite decreases. Upon adding Epolene® (90:5:5), the heat capacity is slightly increased. However, the heat capacity of Epolene® is lower than PP. Hence, some chain confinement has possibly taken place. The addition of Epolene facilitates the penetration of PP chains into clay galleries as well as bonding between the clay and the matrix PP, thereby increasing the heat requirement for Tg. Increment in thermal requirement is observed for PP/EP/Clay (85.5:9.5:5) also, for the same reason. Both the nanocomposites also show a slightly higher Tg than PP. But the heat capacity of the system PP/EP/Clay (47.5:47.5:5) is found to be lower than PP. This could be because the low molecular weight (and hence lower energy required to move the chains) factor associated with Epolene has overcome its ability to aid chain intercalation. Also, the weight fraction of PP has decreased drastically in this nanocomposite.

From Figure 2.24, it is seen that there are considerable shifts in Tm values. The Tm of PP is 171.4 ^{o}C. The Tm of PP/Clay (95:5) is 166.5 ^{o}C, about 5 ^{o}C lower than PP. This

could be because the clay may be acting as a nucleating agent. So, there are numerous sites for heterogeneous nucleation per unit volume of the material. As a result, unlike PP, where there are fewer, but larger crystals, in the nanocomposite, there are numerous, but smaller crystals. The Tm values for all the nanocomposites are lower than PP, due to the possible explanation provided above.

Figure 2.23 shows the cooling thermogram. Here also, the abscissa of the plot is heat supplied by the instrument. The large peaks between ca. 100 ^{o}C and ca. 150 ^{o}C represent crystallization phenomena. The most striking feature of the plot is the significant shift in the Tc (crystallization temperature) for the nanocomposites, ranging from about 4-12 degrees. This means that crystallization phenomenon begins much earlier for the nanocomposites. This also indicates that the clay might be acting as a nucleating agent. It is also seen from the figure that crystallization begins earliest for PP/EP/CLAY (90:5:5), which is very close to the onset of crystallization of PP/EP/CLAY (85.5:9.5:5). However, for the material PP/EP/CLAY (47.5.47.5:5), crystallization temperature is lower than the other nanocomposites. This is an interesting result. This is because PP/EP/CLAY (47.5.47.5:5) is expected to disperse the clay best and hence, the number of nucleating sites available per unit volume of the material is expected to be the highest for this material. Then why does the onset of crystallization occur much later than PP/EP/CLAY (85.5:9.5:5)? In a work by Potzgay et al. [105] the authors have proposed that crystallization is actually caused by those clay-platelets that are least separated by the penetration of polymer chains. This could explain the results obtained in this research. It offers an explanation for the earlier crystallization of PP/EP/CLAY (90:5:5) than PP/EP/CLAY (85.5:9.5:5), and also that the crystallization temperature of PP/EP/CLAY

(47.5:475:5) is the least among the nanocomposites containing Epolene, because Epolene facilitates increase in clay-interlayer spacing. However, PP/Clay (95:5) does not follow this trend. This is possibly due to excessive stacked tactoids with virtually no polymer are present. So the number of nucleation sites per unit volume is drastically lower than the other nanocomposites. In summary, the following things should be kept in mind, while addressing crystallization behavior of nanocomposites:

- Epolene is more compatible with clay than PP and plays an important role at the PP/Clay interface.
- Epolene melts and crystallizes at temperatures much lower than PP.
- The molecular weight of Epolene is much lower than PP, so it exhibits higher mobility than PP at any temperature above its glass transition.
- Increase in Epolene concentration means more liquid material at elevated temperatures, but also better dispersion of clay in the polymeric matrix.

These reasons also help to explain as to why be the crystallization temperature of PP/CLAY (95:5) greater than PP/EP/CLAY (47.5:47.5:5), besides the explanation provided by Potzgay et al.

2.7.4 TEM

TEM micrographs shown in Figures 2.25 through 2.27 enable us to view to dispersion of clay on a local scale. It can be seen that clay is poorly dispersed in PP/CLAY (95:5) (Figure 2.25). There are quite big and distinct stacks of platelets in this material. The marker for the image taken at 10 kX gives a rough estimate of the size of these domains. The domains are approximately 2-3 microns large. The image taken at a higher magnification, 100 kX, shows that there is a significant amount of tactoids formation with little or no penetration by the polymer. This is evident from the big dark region that can be seen in the image. This can be explained by the fact that the

organophilic polymer is still not very compatible with the clay, which is even though modified with organic substances. However, there are numerous platelets that are expanded by the penetration of polymer chains. In other words there is some intercalation. For PP/EP/Clay (85.5:19:5) (Figure 2.26), we observe that the dispersion is much better than PP/CLAY (95:5), and that the stacks of platelets that contain very less polymer are smaller and fewer.

For PP/CLAY (47.5:47.5:5) (Figure 2.27), we see that the dispersion is even better. Even at low magnifications, such as 30 kX, the size of the stacked tactoids does not exceed ~ 600 nm, as seen from the image.

It should be noted however, that these images do not represent the entire sample, with respect to dispersion and distribution of the clay. But the images prove a fundamental concept, which is the necessity of a compatibilizer for enhanced dispersion and distribution of clay platelets.

2.8 Conclusions

The following can be concluded from the following research:

- Compatibilizers are necessary ingredients for enhanced dispersion and adhesion of silicates in organophilic polymer systems, especially with non-polar polymers such as PP.
- Better dispersion and distribution of clay platelets gave rise to better mechanical properties of nanocomposites. This was explained by the increase in number of load bearing clay platelets per unit volume of the material and also the uniformity of distribution of the platelets.
- However, when added beyond a certain concentration, the compatibilizer had deleterious effects on the mechanical properties of the nanocomposites.
- Addition of compatibilizer, besides affecting the extent of clay dispersion and mechanical properties, also influenced the thermal behavior of the nanocomposites.
- Compatibilizer also played a role in crystallization of the nanocomposites.

CHAPTER 3
IMPACT MODIFICATION OF POLYPROPYLENE/MONTMORILONITE CLAY NANOCOMPOSITES

3.1 Introduction

Numerous papers have been published on polymer/clay nanocomposites, but very few address one of the key issues associated with them, which is their impact properties. In spite of the fact that tensile modulus, tensile strength, barrier properties etc. show a significant increase upon the addition of clay, the impact properties remain either close to the original polymer matrix or they are inferior.

The aim of the present work was to investigate and improve the impact properties of polymer/montmorillonite clay nanocomposites. The proposed strategy was to add elastomeric species. This has been a proven technique for improving the impact properties of many materials. Other objectives were:

3. To study the effects of introducing the elastomer on the extent of intercalation/exfoliation of the clay.
4. The effect of introducing the elastomer on other properties such as tensile properties and thermal behavior.
5. To determine the effects of method of preparation of the rubber modified polymer clay nanocomposite on the above mentioned aspects.

If we succeed in improving the impact properties on these novel class of materials, without sacrificing other assets ot these materials, then polymer clay nanocomposites would be more *complete materials* with respect to improved properties in a balanced fashion that could be used for a variety of applications.

Figure 3.1 [12] shows a typical trend in the Izod impact strength of montmorillonite-modified polymer, which was Nylon-6 in this case. It was observed that the pure polymer was superior in comparison to the nanocomposites.

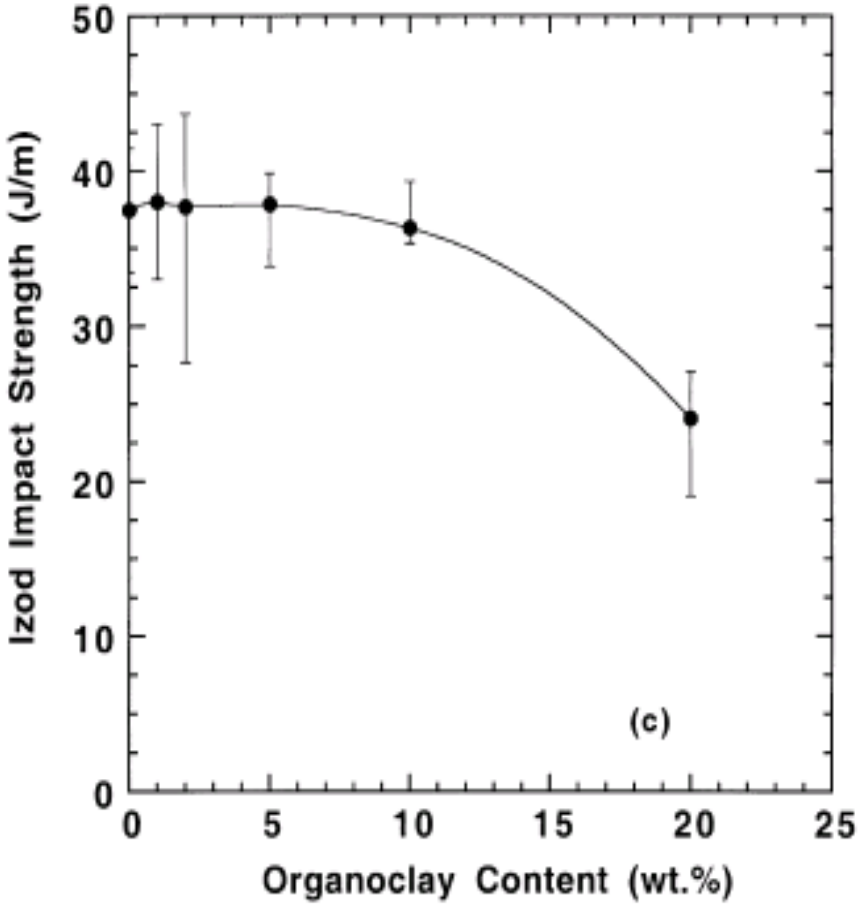

Figure 3.1. Notched Izod impact strength of nylon 6 and 95/05 composites as a function of clay loading.

This is because the large surface area of the clay provides greater space for the polymeric matrix to adhere to it, but at the same time, it also increases the possibility of formation of regions where the polymer does not adhere to the surface of the clay. This could result in microvoids. These really impair the impact properties.

This is because they act as stress concentrators and initiators for crack formation. Further, it is also believed that addition of clay also alters local chain dynamics [15].

Michler and coworkers [106] suggested that depending on their orientation with respect to the axis of tension, a role could be attributed to the silicate layers with respect to formation of micro voids. They showed that intercalated morphology showed more cavitation than the exfoliated morphology.

Thus, morphological considerations are of great importance in addressing the impact properties of polymer clay nanocomposites. In spite of the fact that the inorganic clays are modified with many additives such alkyl ammonium chloride, that also facilitate improved adhesion between the filler and the matrix, the impact properties do not show significant increase. In fact, in many cases, deterioration has been observed [14, 39, 43, 47, 60,107].

As stated earlier, it has been shown that intercalated polymer clay nanocomposites tend to show extensive cavitation. Figure 3.2 [15] shows this. In this work, it was revealed that at room temperature, the polyamide/clay nanocomposite was quite fragile.

Further, the volume strain evolution upon drawing revealed that pristine polymer deformed with little volume variation, whereas the nanocomposite showed cavitation. These observations corroborated the above mentioned reason for describing the stagnant or deteriorating nature of the impact properties.

The impact modification of polymer/clay nanocomposites calls for a slightly different approach than for traditional fiber reinforced composites. This is because the way in which the nanocomposite is formed is different. The clay has a layered structure, with the distance between the layers being a few nanometers in size. The polymer chains have to penetrate into these galleries and increase the separation. This also disperses and distributes the clay platelets uniformly throughout the matrix.

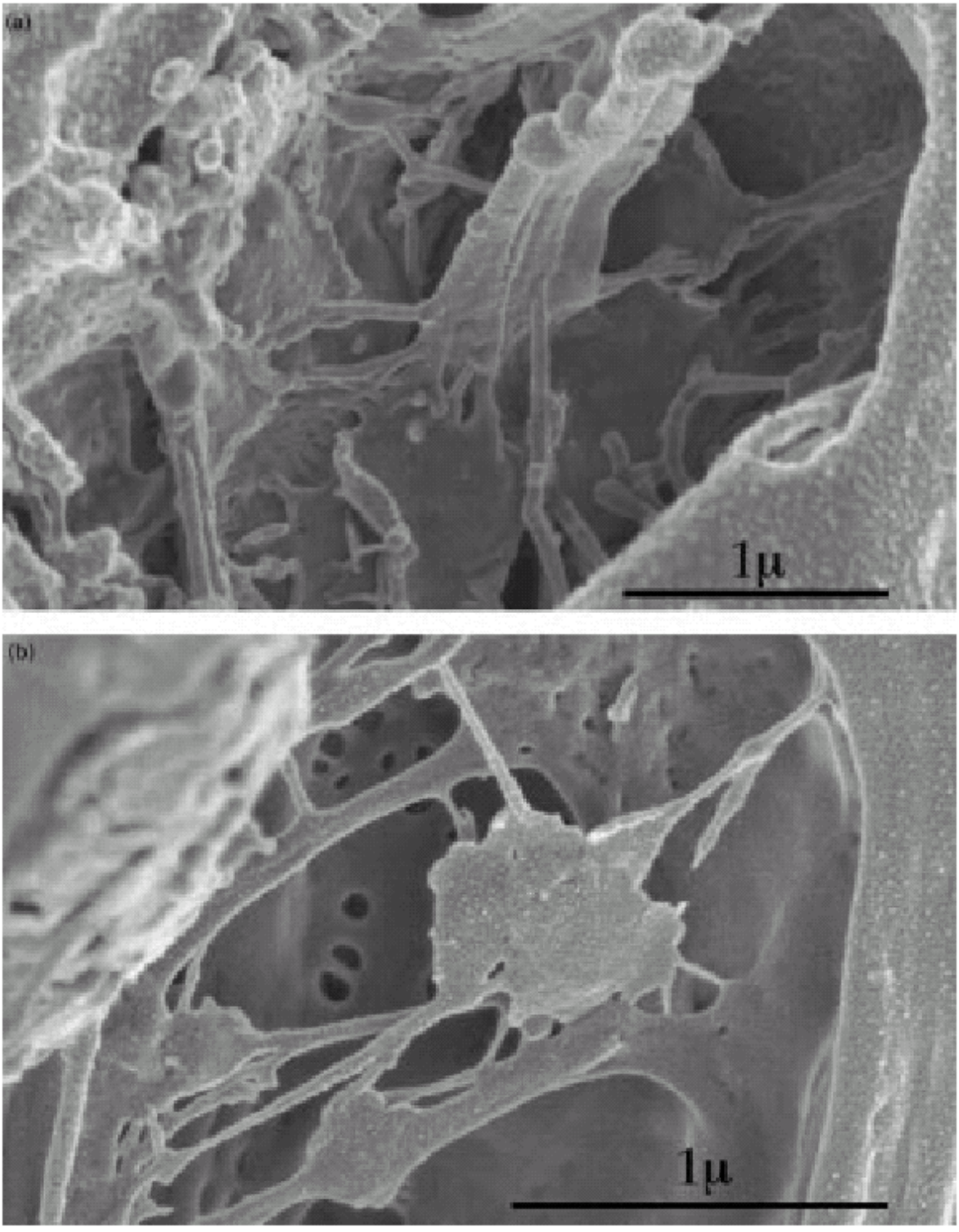

Figure 3.2. SEM observation: (a) Cavitated nanocomposite; (b) Fibrillated nanocomposite and polymer/clay interaction.

In doing so, they also have to bond to the surface of the clay platelets. On the other hand, there is no such penetration of polymer chains in case of traditional fiber reinforced composites.

Cho et al. reported that for a given loading of clay, the Izod impact strength increased with increasing temperature. But still, the pure polymer showed better impact properties at any given temperature than the montmorillonite-modified nanocomposites [12]. Figure 3.3 [12] shows this.

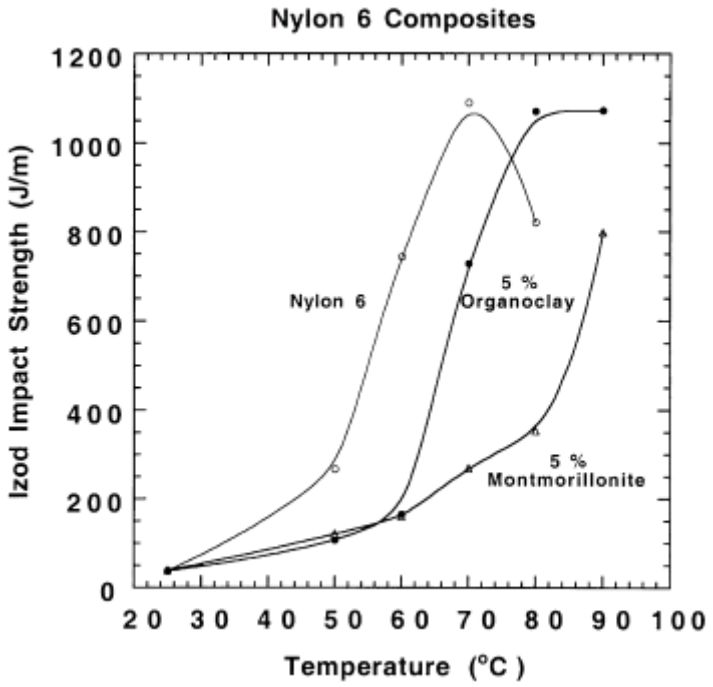

Figure 3.3. Notched Izod impact strength of nylon 6 and 95/05 composites as a function of temperature.

The rationale of Cho et al. was the following:

Upon increasing the temperature, the softness of the material is increased, and so are the motions between the polymer chains. This indicates that the volume occupied by the voids decreases and hence, impact properties improve. However, increased

temperature has adverse effects on other properties such as storage modulus and tensile strength, which are very important engineering properties for material selection.

So, it is seen that improving the impact properties of polymer clay nanocomposites is not an easy task. It is however, envisioned that there are certain strategies, which will be discussed in the next section, that could possibly overcome this problem.

3.2 Research Strategies

Blending or reactive blending with elastomeric materials seemed to be an interesting possibility. This was because imparting rubbery domains would greatly enhance energy dissipation during fracture. Figure 3.4 illustrates this.

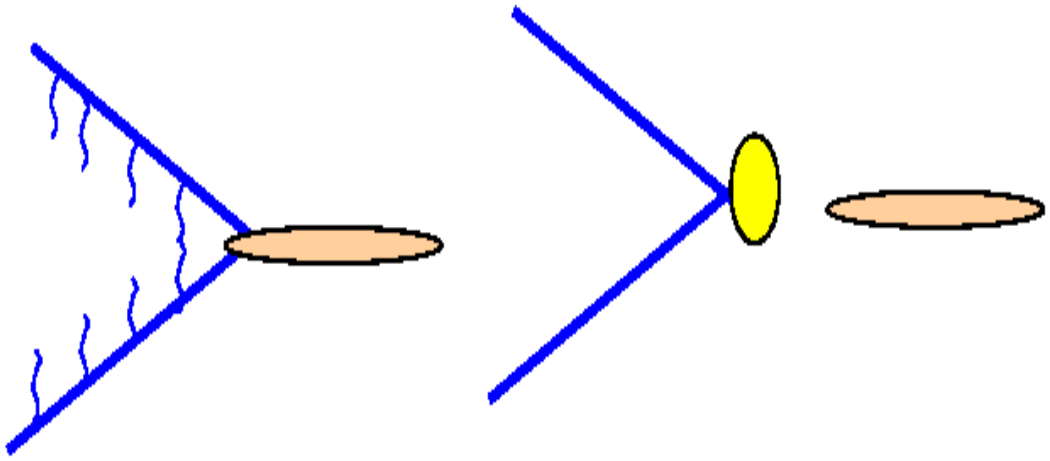

Figure 3.4. Effect of addition of elastomer on craze crack structure. (a) Propagating crack along the matrix material, along with craze fibrils. (b) Propagating crack in a material with rubbery domains. Here, the rubbery domains absorb the energy due to their extremely large size of plastic zone so that fracture process is retarded. Also there is little crazing upon introducing elastomers. Elastomers undergo tearing phenomena due to their large plastic zone.

This method for improving the impact properties of a wide variety of materials has been employed since 1960s [110-117], and is being used till date [118-124].

However, due to dearth of publications regarding rubber toughening of polymer clay nanocomposites, nothing definite could be stated about the outcomes of this method

prior to performing experiments. But the organically modified clays were not as hydrophilic as glass fibers were. So the issues related to compatibilization of the interface between the matrix polymer, clay and the elastomer were alleviated to a considerable extent. This was corroborated by the fact that elastomers being liquids at room temperature possessed better wetting characteristics. However, it is well known that the elastomers also tend to reduce the tensile modulus because of their liquid like behavior. Figure 3.5 illustrates this.

Hence, attempts were made towards improving the impact properties of the nanocomposites, without sacrificing the tensile properties significantly.

3.3 Materials

Montell (now Basell) supplied PP used for this study. Table 3.1 enlists its properties. The compatibilizer used was Epolene® G-3003, supplied by Eastman Chemical Company. Table 3.2 lists some of its properties.

The clay used for this study was Nanomer® I.34TCN, supplied by Nanocor Inc. Table 3.3 describes some of its properties.

Two different elastomers were used for this research. DuPont– Dow Elastomers supplied the first, a polyolefin elastomer, under the trade name Engage® (grade 8842). Table 3.4 shows some of its properties.

The other elastomer was an oligomeric polybutadiene whose ends are functionalized with epoxy and hydroxyl groups. Aldrich chemicals supplied this. Table 3.5 shows some of its properties.

Sigma Aldrich supplied Glycidyl methacrylate used for this research. Table 3.6 enlists some of its properties.

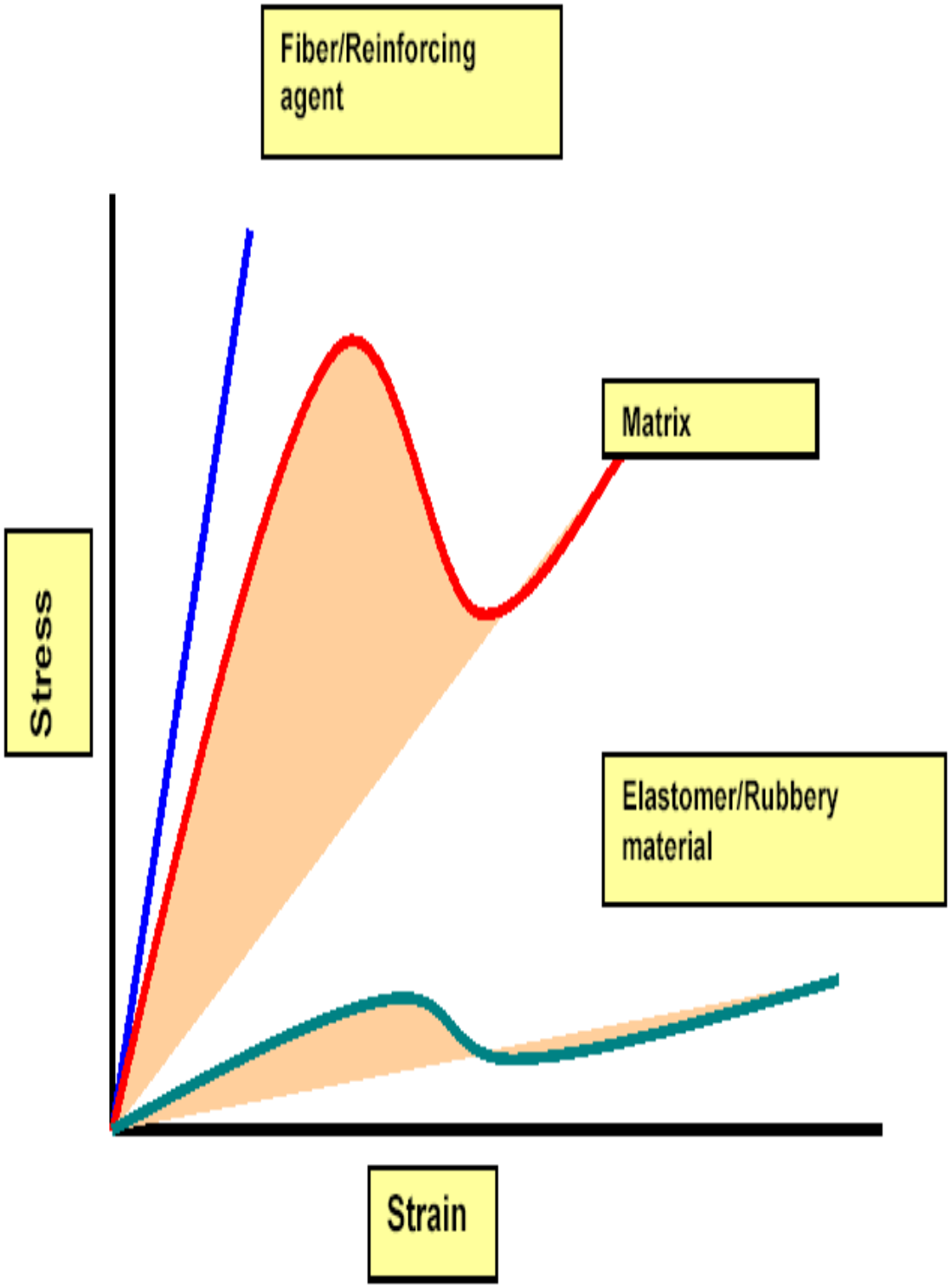

Figure 3.5. Stress strain curves for different types of materials.

Table 3.1. Properties of Basell Profax 6523 Polypropylene used for the research.

PROPERTY	VALUE	TEST METHOD
PHYSICAL		
Specific Gravity	0.9	ASTM D792
Melt Flow Rate (230 °C)	4.00 g/10 min	ASTM D1238
MECHANICAL		
Tensile Strength @ Yield	4900 psi	ASTM D638
Tensile Elongation @ Yield	12 %	ASTM D638
Flexural Modulus (Procedure A)	1% Secant: 200000 psi	ASTM D790
Notched Izod Impact (73 °F)	0.7 ft-lb/in	ASTM D256
Rockwell Hardness (R-Scale)	86	ASTM D785
THERMAL		
DTUL @66psi – Unannealed	199 ^{o}F	ASTM D648

Table 3.2. Properties of Epolene® G-3003.

PROPERTY	VALUE
Ring & Ball Softening Point (ºC)	158[h]
Penetration Hardness	<1
Density @ 25 ºC	0.912
Acid Number	8
Viscosity, cP (mPa•s) @ 190 ºC	60,000
Melt Index @ 190ºC	12.7
Color (Gardner)	25
Molecular Weight	27,200
Manufacturer	Eastman Chemical Company

Table 3.3. Physical properties of Nanomer® I.34 TCN.

PROPERTY	VALUE
Appearance	White Powder
Mean Dry Particle Size (Microns)	16-22
+ 325 Mesh Residue (%)	0.1
Specific Gravity	2.0
Moisture (%)	3.0
Bulk Density (gms/cc)	0.30-0.36
Purity (% min)	98.5
Manufacturer	Nanocor

Table 3.4. Properties of Engage® 8842.

PROPERTY	VALUE
Co monomer Content (wt%) by ^{13}C NMR/FTIR	45
Density (g/cm^3), ASTM D-792	0.857
Mooney Viscosity ASTM D-1646 ML at 121 °C	26
Melt Index (dg/min) ASTM D-1238 190 °C, 2.16kg	1.0
Durometer Hardness, Shore A ASTM D-2240	50
DSC Melting Peak (°C) Rate 10 °C/min	33
Ultimate Tensile Strength, MPa ASTM D-638, 508 mm/min	2.1
Ultimate Elongation (%) ASTM D-638, 508 mm/min	975
Manufacturer	DuPont Dow Elastomers.

Table 3.5. Properties of oligomeric, epoxy and hydroxyl end functionalized polybutadiene.

PROPERTY	VALUE
M_n	1,300
M_w	2,600
Microstructure	55% 1,4-trans; 15% 1,4-cis; vinyl 30%
Viscosity	250 poise
Fp	>230 °F
Density	1.01 g/mL
Manufacturer	Aldrich Chemicals.

Table 3.6. Properties of Glycidyl methacrylate

PROPERTY	VALUE
Molecular Formula	$C_7 H_{10} O_3$
Weight % epichlorohydrin	0.2%
Weight % R-glycidol	~ 1
Boiling point	189 °C/760 mm Hg
Freezing point	169 °F
Density	1.042 g/mL
Structural formula	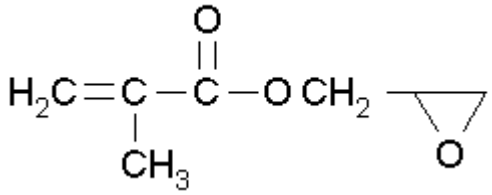
Manufacturer	Aldrich Chemicals.

3.4 Processing

The main equipment used for processing the nanocomposites was a 30mm APV co-rotating reactive twin-screw extruder. This extruder had eight temperature zones from feed zone to die zone. Hence, the processing temperature ranged from 200 °C (feed zone) to 234 °C (die zone). The screw L/D was 40. PP and Epolene® pellets were dried in an air-circulating oven at 80 °C for 24 hrs.

Different processing protocols were employed. The following protocol was used in preparing the functionalized oligomer impact-modified polymer nanocomposite.

This was labeled as protocol A. First, the compatibilizer (Epolene®) and end-functionalized oligomeric elastomer were blended together in a batch mixer (150 ^{o}C, for 2 hours) in the weight ratio of (4.75: 0.25). The elastomer was dissolved in xylene. Figure 3.6 shows the details of this operation.

This product was designated as Comp/F-olig. The resulting product was crushed and dried for 24 hours in an air-circulating oven at 80 °C.

Next, PP and Comp/F-olig, mixed in the weight ratio (90:5) were blended in the twin-screw extruder. The resulting strands were pelletized and dried for 30 hours under conditions described above. Subsequently, the PP+Comp/F-olig pellets were melt-compounded with 5-wt % clay.

To ensure good mixing, the clay was also dispersed in xylene, before being added to the molten PP/Comp/F-Olig mixture at the feed zone along the screw channel. The resulting strands were pelletized and dried as described above. This product was designated as PP/Comp/F-Olig /Clay. The feed rate of PP, PP/Comp and other blends described earlier was 40 grams/min., whereas the feed rate of clay was 2 grams/min. In order to verify that the characteristics of the compounded materials were not significantly influenced by the sequence of the preparation, two other impact-modified nanocomposites were prepared. The polymeric elastomer was used for this purpose. For the first sample, designated PP/Comp/F-POE/Clay, protocol B was used.

Here, the polyolefin elastomer (POE) was first functionalized with Glycidyl methacrylate (GMA) in the reactive twin-screw extruder. Next, PP and Epolene® were blended in the extruder in the weight ratio 90:4.75. The functionalized elastomer was then added to the PP/Compatibilizer blend in the weight ratio of 94.75:0.25. Finally, clay (dispersed in xylene) was added to the above blend. Xylene: clay used was 5:1 by weight. The weight ratio of PP, Epolene®, polyolefin elastomer and Clay now became 90:4.75:0.25:5.

For the second sample, designated PP/Comp/Clay/F-POE, protocol C was employed.

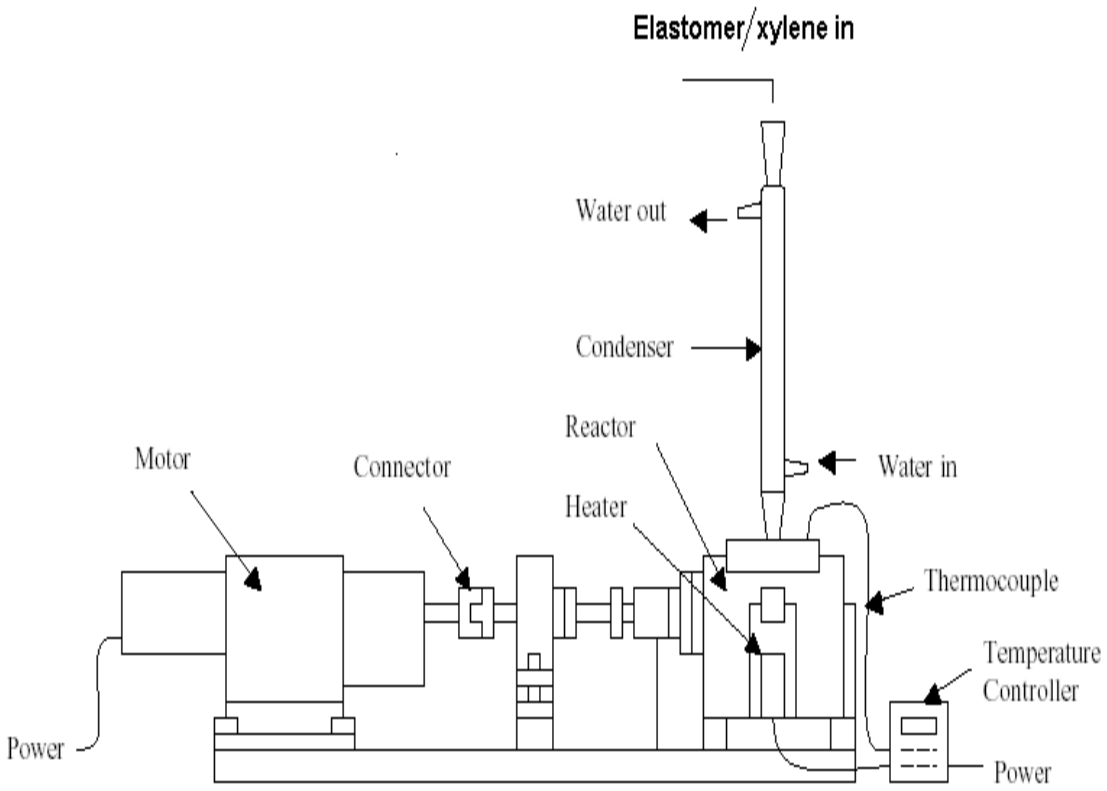

Figure 3.6. Schematic representation showing mixing of Epolene® with oligomeric polybutadiene.

Here, the sequence from functionalized POE and clay was reversed, that is, the clay was added to PP/Compatibilizer mixture before the functionalized POE. The weight percentage of each component remained the same. The reference material used for comparing the properties of the impact-modified nanocomposites was PP/Comp/Clay (90:5:5).

Table 3.7 summarizes the designations of different nanocomposites and their method of preparation. Table 3.8 summarizes the weight percentage of different components in various nanocomposites processed. Figure 3.7 shows the operation in the form of a block diagram.

3.5 Characterization

The following characterization are used to obtain an understanding of the structure property relationships in the nanocomposites processed:

- Tensile testing
- X-Ray Diffraction
- Izod impact testing
- Differential Scanning Calorimetry
- Transmission electron microscopy

Table 3.7. Preparation of Impact modified nanocomposites.

MATERIAL	METHOD OF PREPARATION
PP/EP/F-OLIG /CLAY (PROTOCOL A)	Epolene is blended with functionalized oligomeric polybutadiene (95% Epolene and 5% F-olig – PB by weight). The matrix is prepared by taking 90 parts of pure PP and 5 parts of (epolene+f-oligomeric PB). 95 parts of this matrix are added to 5 parts of clay (by weight). Hence in 100 parts of the nanocomposite, there is 90 % PP, 4.75%Epolene, 0.25% F-olig PB, 5% clay.
PP/EP/F-POE/CLAY (PROTOCOL B)	PP is blended with Epolene. F-POE is added to this. Thus the matrix material is prepared, which is PP/Epolene/F-POE. To this, clay is added to make the nanocomposite.
PP/EP/CLAY/F-POE (PROTOCOL C)	The nanocomposite is prepared first by blending PP, Epolene and clay. F-POE is then added to this nanocomposite.
PP/EP/CLAY (90:5:5) (REFERENCE MATERIAL)	90 parts of PP (by weight) are blended with 5 parts of Epolene. 5 parts by wt. of the montmorillonite clay is added to make the nanocomposite.

Table 3.8. Percent composition of different nanocomposites by weight (dry basis).

SAMPLE DESIGNATION	WT. % PP	WT. % EPOLENE	WT. % CLAY	WT. % POE	WT. % F-OLIGOMER
PP/COMP/CLAY	90	5	5	0	0
PP/COMP/F/OLIG/CLAY	90	4.75	5	0	0.25
PP/COMP/CLAY/F-POE	90	4.75	5	0.25	0
PP/COMP/F-POE/CLAY	90	4.75	5	0.25	0

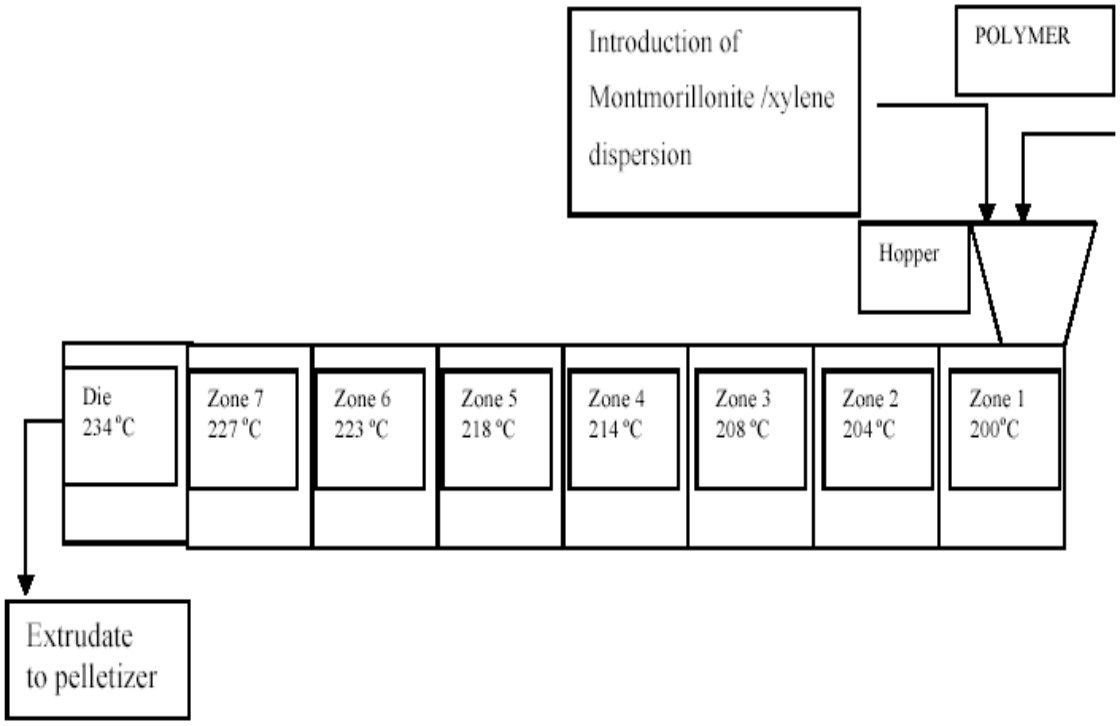

Figure 3.7. Synthesis of impact modified nanocomposites using a reactive twin-screw extruder.

3.5.1 Specimen Preparation

Specimens for the listed techniques were prepared using compression molding. The temperature used was 205 ^{o}C, and the pressure used was 10, 000 psi. Sheets were prepared for pure PP, and the nanocomposites.

In order to prepare the specimens, the press was first heated to 420 ^{o}F. The mold used was square in shape, with dimensions of 70 mm X 70 mm X 0.8 mm. The mold was placed on a metal plate covered with Teflon® coated aluminum foil. The mold was then

filled with dried pellets. This plate with mold and the pellets was placed on the bottom plate of the press. Another Teflon® coated aluminum foil covered metal plate was placed on top of the mold bearing plate, to give a sandwiched assembly. The bottom plate of the press was raised until the assembly just touched the top plate of the press. The pellets were then allowed to convert into a liquid state by heat transfer from the press. This took about 5-6 minutes. After that the pressure of the system was raised to 10, 000 psi. Initially, due to resistance offered by the liquid polymer as well relatively incomplete conversion to liquid, the pressure dropped below 10,000 psi. Under these circumstances, it was necessary again to raise the pressure to 10,000 psi. This was repeated until the pressure attained a steady value of 10,000 psi. The pressure could be measured using a gauge attached to the press. A pressure of 10, 000 psi. on the gauge corresponded to 9302 psi. on the sample. This was calculated using the formula:

$$Ps \times As = Pg \times Ag \qquad \text{(Equation 3.1)}$$

Where, Ps = Pressure on the sample

As = Cross sectional area of the sample

Pg = Gauge pressure

Ag = Cross sectional area of the piston of the press.

As = 70 X 70 mm2

Ag = 3.14 X (32)/4

Pg = 10, 000 psi.

After the gauge pressure became steady at 10, 000 psi., the mold was allowed to rest at the abovementioned temperature and pressure for 10 minutes. After that, the heat supply to the press was turned off. Immediately after this, the pressure-release screw was

turned. The hot plate assembly containing the mold between the two metal plates was removed and was immersed in a cold-water reservoir and kept for 3 minutes. Then, the entire assembly was flipped over and was replaced in the reservoir for 3 more minutes. After the mold cooled down, the solidified sheet was then taken out of the mold. Sheets were prepared in this way for pure PP, and the various nanocomposites.

These sheets served as specimens for all the characterization techniques.

3.5.2 Tensile Testing

The aim of performing tensile testing was to evaluate the mechanical response of the materials to a known strain or deformation rate. This gives us a plot of stress versus strain from which we can obtain a wealth of information such as the brittle or ductile behavior, tensile modulus or an indication of stiffness of the material, tensile strength etc. Tensile testing was carried out using an EnduraTEC ELF 3200 series machine. It consisted of the following components:

- The linear motor assembly: Had a patented high-bandwidth, low-distortion actuator from Bose Corporation.
- Testing Chamber: Had facilities for introducing hot air, for increasing temperature as well as introducing liquid nitrogen. A bulb for viewing the test in case liquid nitrogen made the chamber cloudy was also provided. The door had a transparent section for enabling to view testing while in progress. There were two sets of grips. The bottom grip was stationary and was connected to the load cell. The upper grip was mobile and its motion was regulated by the Wintest® software, and ultimately, the linear motor.
- Temperature Control: With the help of the software, temperature could be varied between –50 ^{o}C to 150 ^{o}C.
- Controller box, that acts as an interface between the computer and the machine itself.

Strain rate used was 0.01 mm/sec and temperature of testing was 28 ^{o}C. Figure 3.8 presents the results obtained from tensile testing.

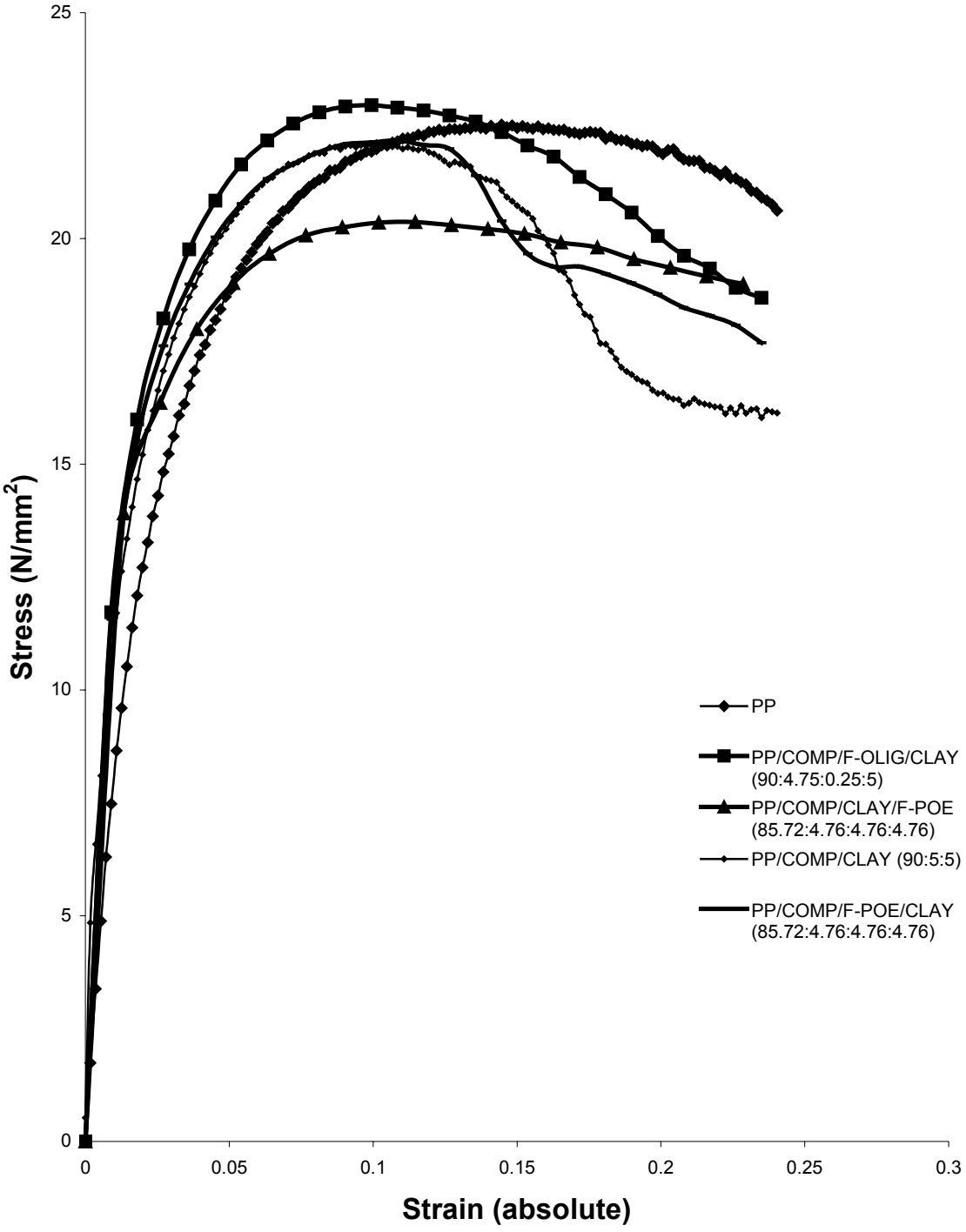

Figure 3.8. Tensile behavior of PP and impact modified PP/Clay nanocomposites at 0.01 mm/sec., 28 ^{o}C.

Table 3.9. Tensile properties of PP and impact modified PPCNs.

MATERIAL	MODULUS (N/mm^2)	TENSILE STRSNGTH N/mm^2
PP	949.25	22.3
PP/COMP/CLAY (90:5:5)	1892.1	21.68
PP/COMP/CLAY/F-POE	1023.1	19.89
PP/COMP/F-POE/CLAY	1185.3	21.7
PP/COMP/CLAY/F-OLIG	1307.6	22.67

3.5.3 X-Ray Diffraction

The objective of performing XRD was to explore the possibility of any intercalation or exfoliation in the layered silicates due to possible penetration by the polymer into the clay layers. This is usually determined by the shifts in low angle peaks for the clay. This is because according to Bragg's law:

$$d = n\lambda/(2d\sin\theta) \qquad \text{(Equation 3.2)}$$

d = interplanar spacing,

n = order of diffraction

λ = wavelength of X-Ray source, and

θ = semi-angle of diffraction

So, as the semi angle varies, the d spacing between the clay layers varies. If the polymer is successful in penetrating the clay layers, then the d spacing of the clay layers increases, thereby reducing the angle corresponding to the peak observed.

XRD was performed using a Philips APD 3720 instrument using a Cu-K_α X-Ray source (Wavelength = 1.54 Å). The range of angles swept was 0-75 degrees. Reflective

mode was used and temperature was 15 ^{o}C. Figure 3.9 and Figure 3.10 present the results obtained from XRD.

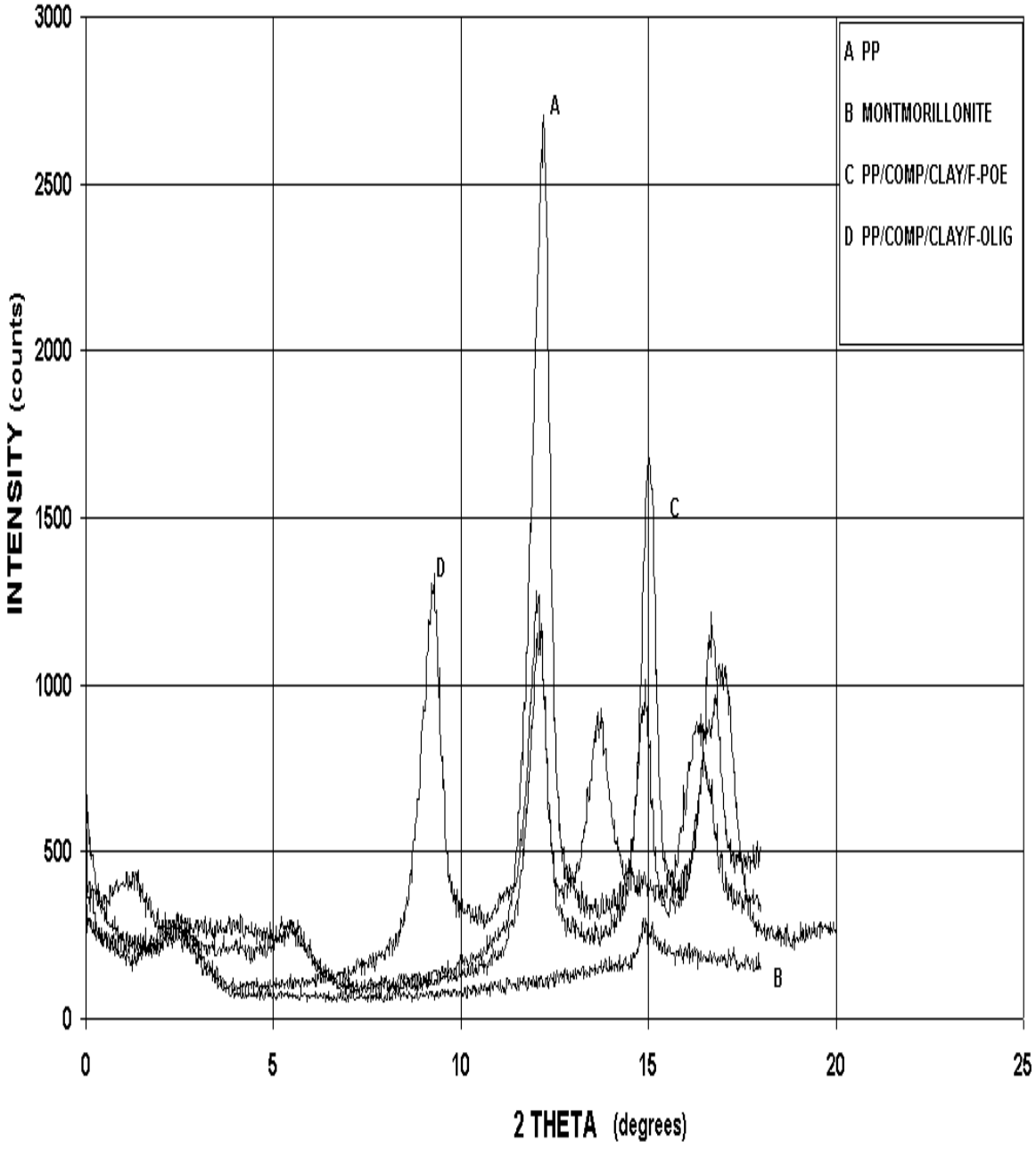

Figure 3.9. XRD patterns for PP and impact modified PP clay nanocomposites in reflective mode, at 15 ^{o}C.

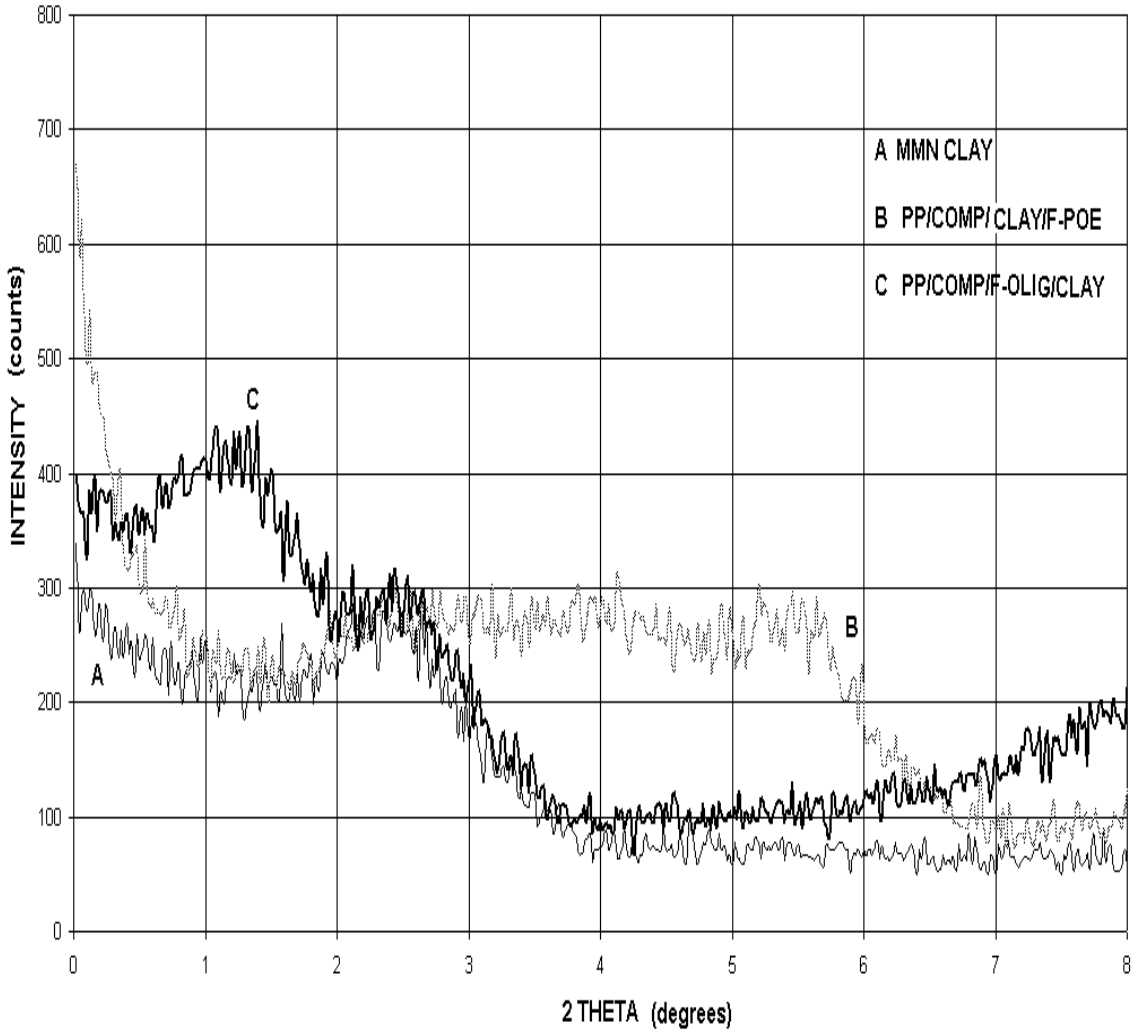

Figure 3.10. Low angle region of XRD plot shown in figure 3.9 in reflective mode, at 15 ^{o}C.

3.5.4 Izod Impact Testing

In this method to determine impact strength, a metallic pendulum swings on its track and strikes a notched, cantilevered plastic sample. The energy lost (required to break the sample) as the pendulum continues on its path is measured from the distance of its follow through. Figure 3.11 shows the instrument. Impact testing was carried using a TMI #41869 model machine.

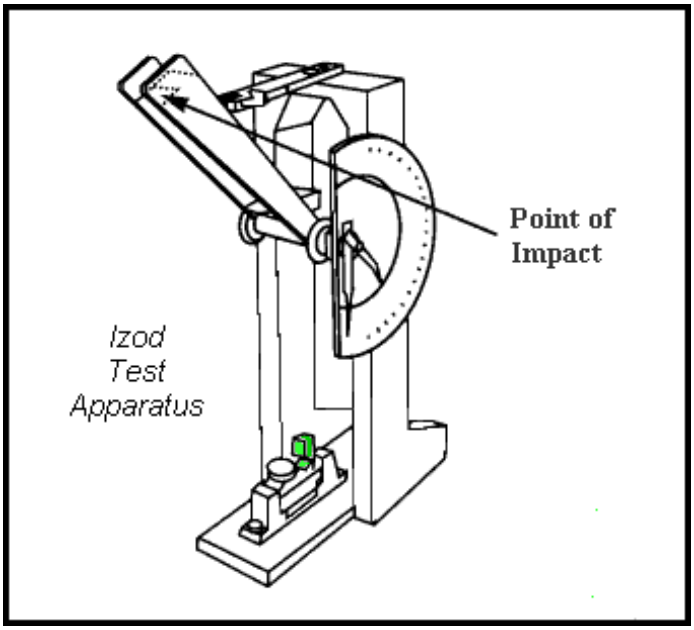

Figure 3.11. Izod impact testing apparatus.

In this research while making impact testing bars as per as ASTM D-256, formation of air bubbles could not be avoided, even after repeated trials. Hence, impact testing was carried out with a specimen that had lesser thickness and width than the prescribed standard. For the same reason, it could not be notched as well. Hence, the impact testing was performed in the un-notched mode. Table 3.10 summarizes the results obtained.

Table 3.10. Impact strengths of impact modified PP/clay nanocomposites at 25 ^{o}C.

MATERIAL	IMPACT STRENGTH IN ft. lb / sq. in
PP	15.91
PP/COMP/CLAY	14.85
PP/COMP/CLAY/F-POE	16.98
PP/COMP/CLAY/F-OLIG	26.52

3.5.5 Differential Scanning Calorimetry

DSC describes the behavior of a material when subjected to heat at a controlled rate. This enables us to determine different transitions associated with the polymer such as glass transition, melting transition, besides crystallization behavior etc.

DSC on the samples was performed using a ThermoHaake DSC 220 C model instrument. Heating rate used was 10 ^{o}C/minute, while cooling rate was 50 ^{o}C/min. Two sweeps of this thermal treatment were performed.

The output of the instrument is a plot between heat supplied in microwatts versus temperature. The heat supplied is directly proportional to the specific heat of the material being tested. Figure 3.12 shows the heating thermogram. Figures 3.13 and 3.14 show the Tg and Tm transitions separately for the purpose of clarity. Figure 3.15 shows the cooling thermogram.

3.5.6 Transmission Electron Microscopy

TEM images usually complement XRD data and also enable us to see details at a nanometer scale. However, it should be noted that this technique gives image of a very small section of the material.

Transmission electron microscopy was performed on PP/COMP/F-POE/CLAY using a JEOL 2010 Field emission TEM instrument. For PP/COMP/F-OLIG/CLAY, a JEOL 200 CX instrument was used. It has a tungsten based thermionic gun. Figure 3.16 shows the TEM image for the oligomer-modified nanocomposite. Figures 3.17 and Figure 3.18 present the TEM images for polyolefin-modified elastomer. Use of two different instruments for the samples may result in difficulty in comparing the details with respect to intercalation of clay platelets.

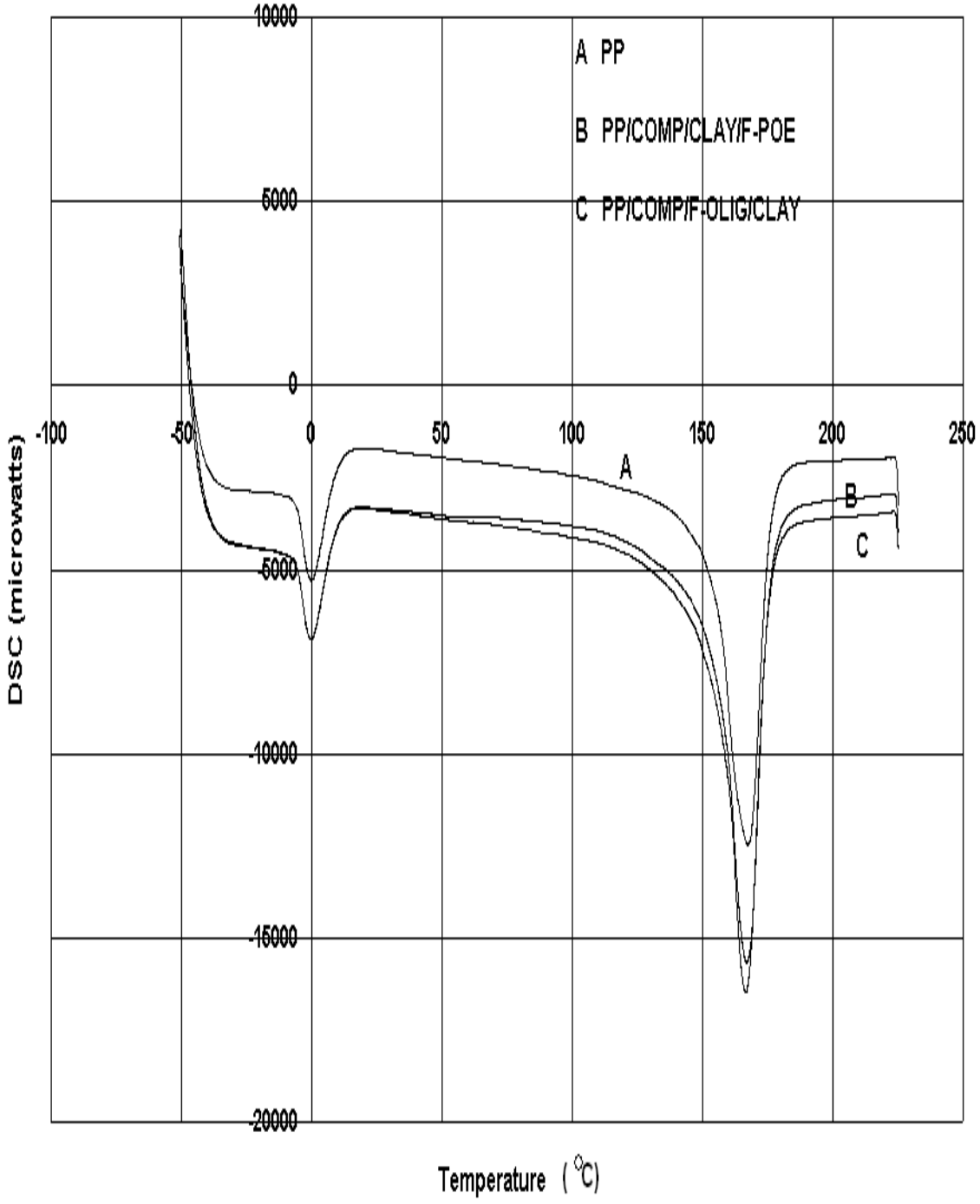

Figure 3.12. DSC heating thermogram for PP and impact modified PP/clay nanocomposites. Heating rate = 10 ^{o}C/min., cooling rate = 50 ^{o}C/min.

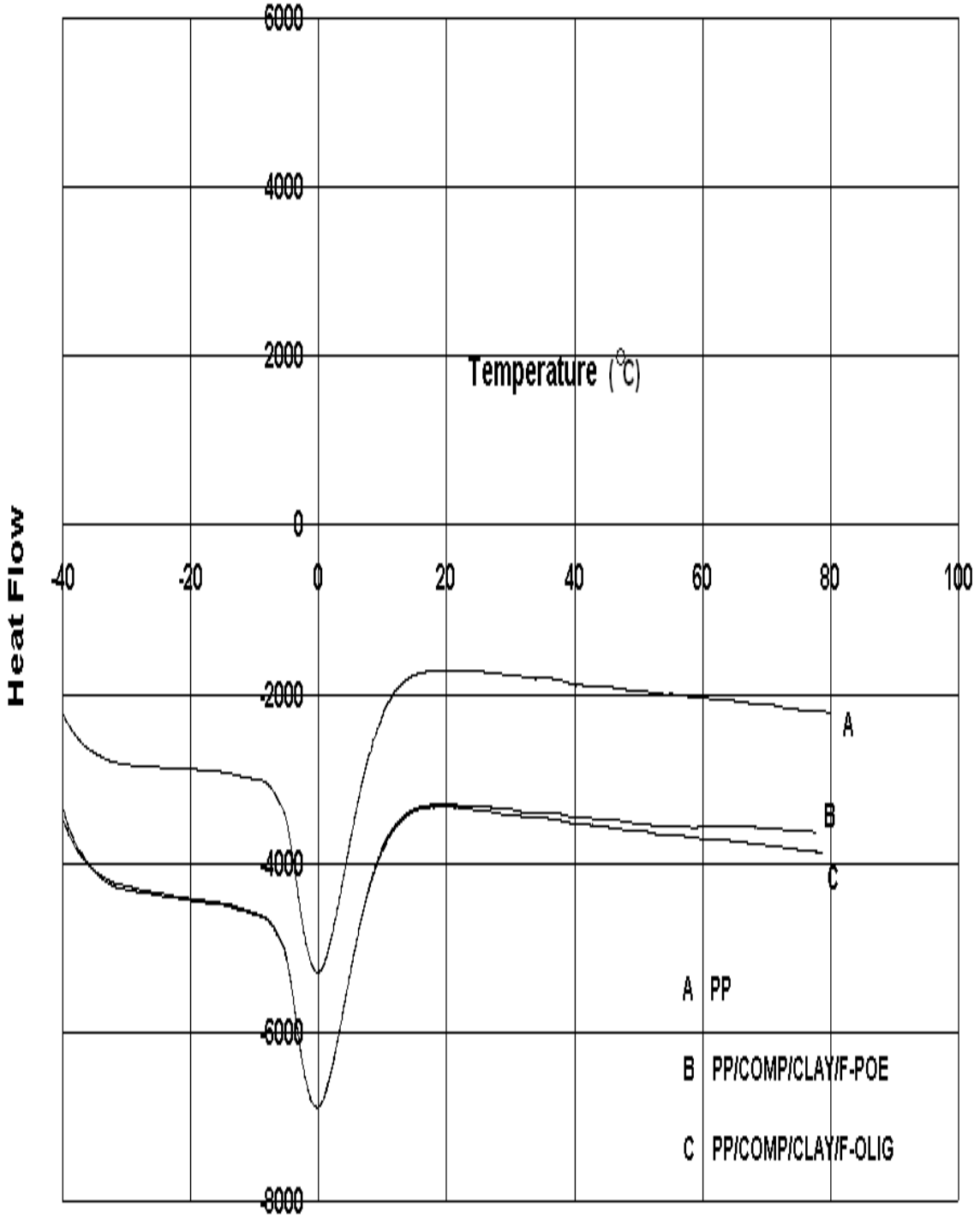

Figure 3.13.Tg region of DSC heating thermograms presented in Figure 3.12. Heating rate = 10 ^{o}C/min., cooling rate = 50 ^{o}C/min.

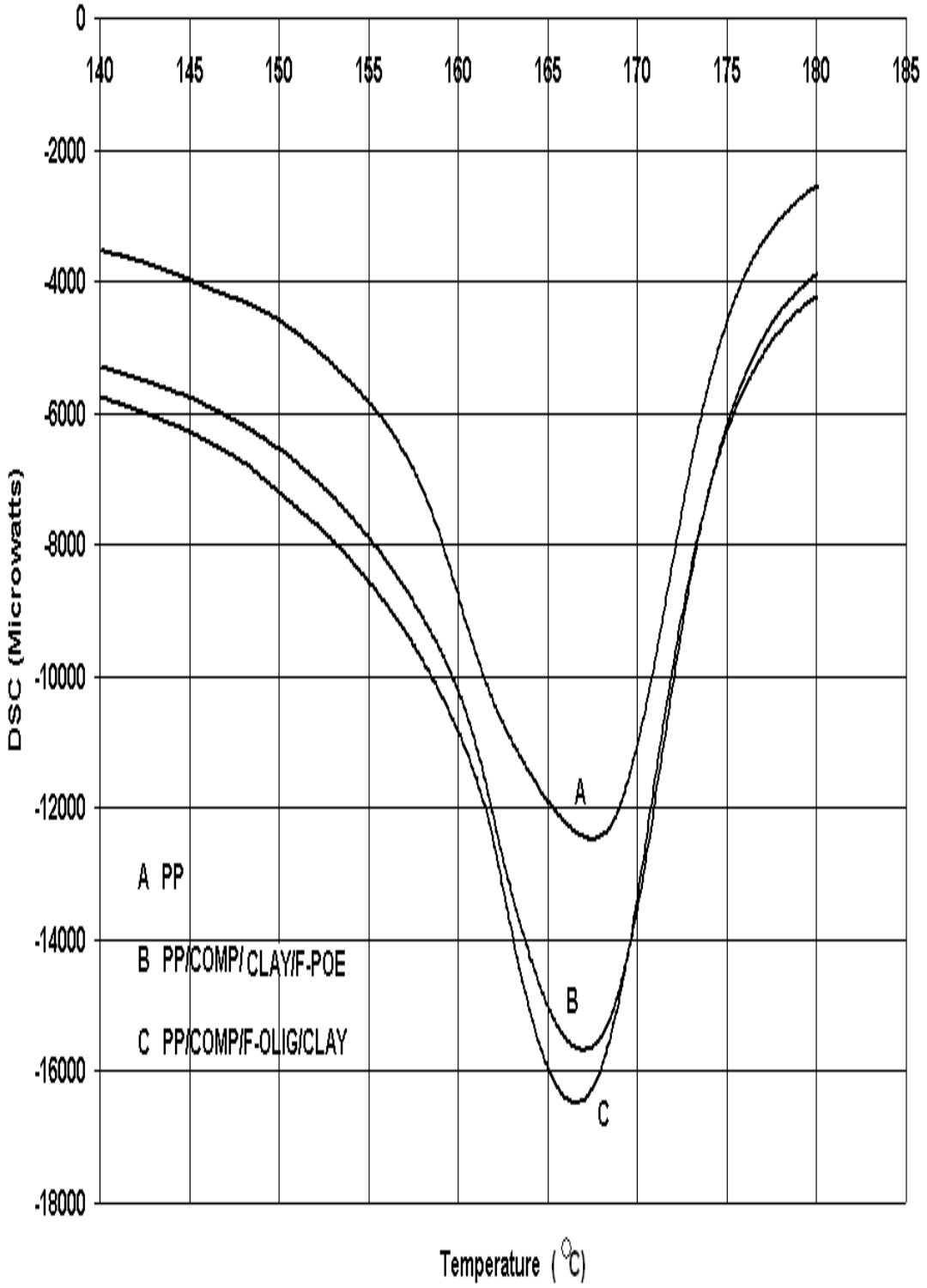

Figure 3.14. Tm region of DSC heating thermograms presented in Figure 3.12. Heating rate = 10 ^{o}C/min., cooling rate = 50 ^{o}C/min.

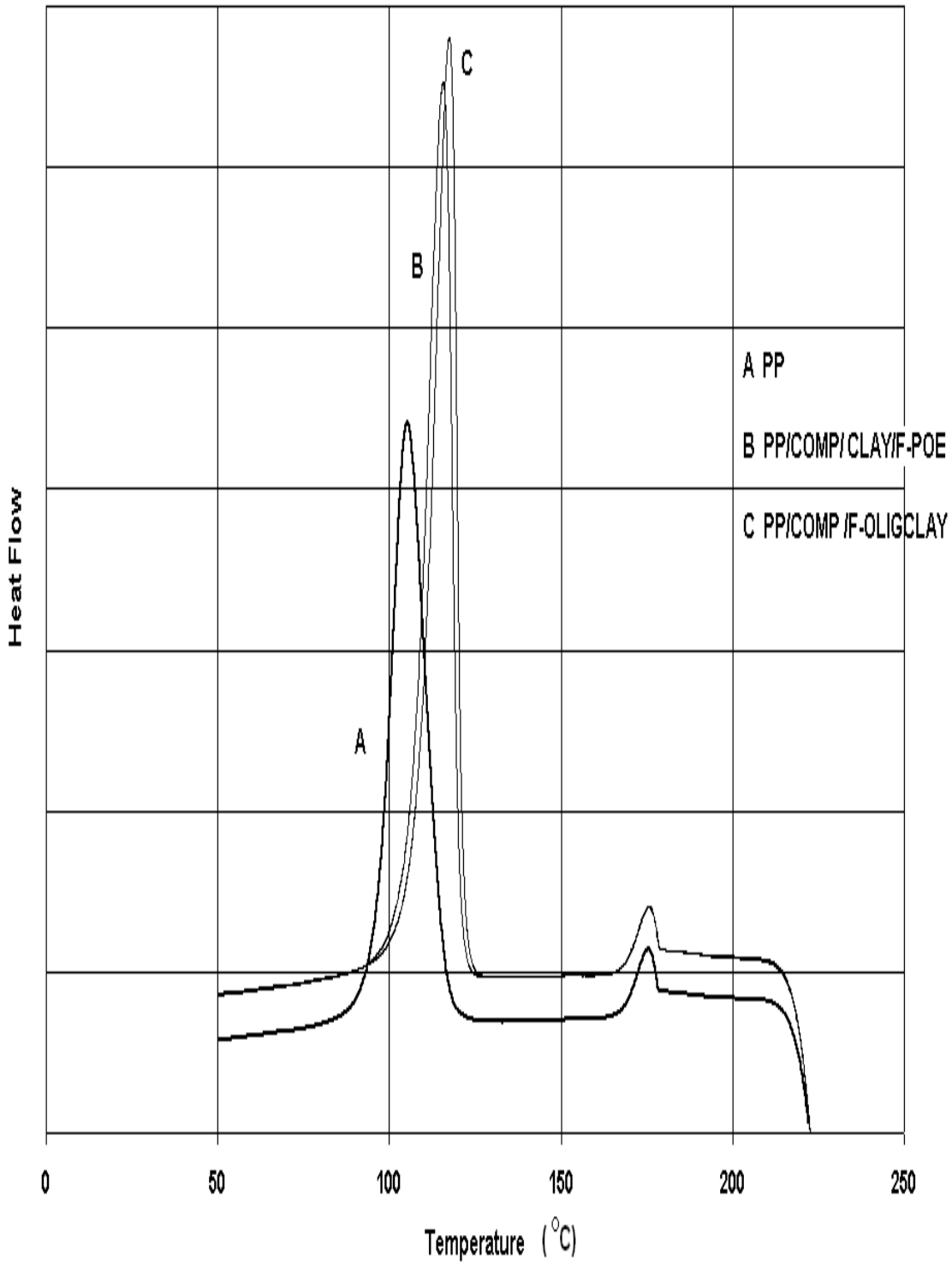

Figure 3.15. DSC cooling thermogram for PP and impact modified PP/clay nanocomposites. Heating rate = 10 ^{o}C/min., cooling rate = 50 ^{o}C/min.

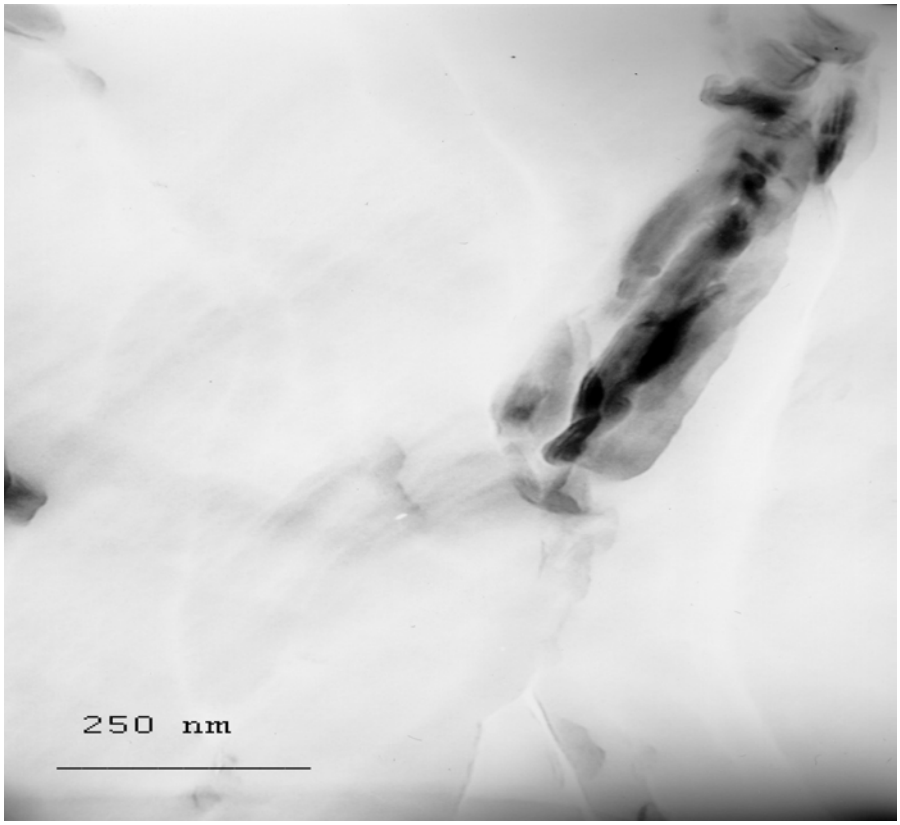

Figure 3.16. TEM micrograph of PP/COMP/F-OLIG/CLAY.

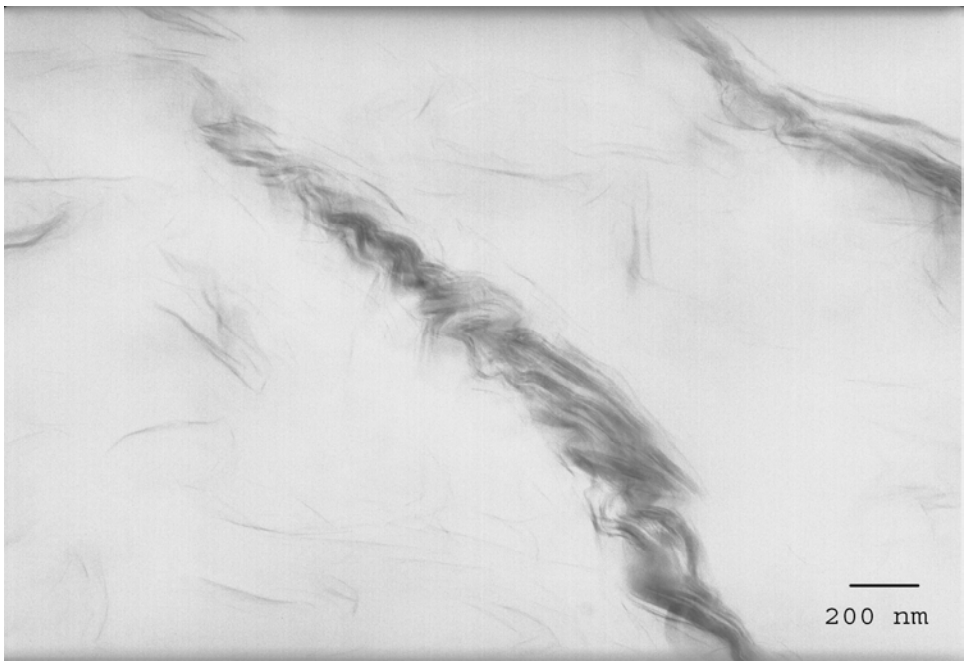

Figure 3.17. TEM micrographs of PP/COMP/F-POE/CLAY

Figure 3.18. TEM micrographs of PP/COMP/F-POE/CLAY at a higher magnification..

3.6 Discussion of Results

Having employed different characterization techniques for analyzing the mechanical behavior and microstructure of the impact modified nanocomposites, it is essential that the results obtained from these be analyzed and interpreted appropriately in order to explain different phenomena occurring in these materials. This section deals with the same.

3.6.1 Tensile Testing

From Figure 3.8 it is evident that the nanocomposite labeled PP/Comp/Clay/F-olig shows the highest tensile strength. Its modulus is higher than PP as well as any other nanocomposite prepared by any other impact modification route employed during processing. It is also clear that the sequence of addition of elastomers, i.e., prior and after the addition of clay also has a significant influence on the tensile behavior. It can be

concluded from Table 3.9 that between PP/Comp/Clay/F-POE and PP/Comp/F-POE/Clay, the nanocomposite in which the elastomer has been added prior to addition of clay shows better tensile modulus, tensile strength as well as impact strength. It is also noteworthy that for the oligomeric impact modification route, the elastomer was added prior to the addition of clay. So, the tensile testing results indicate that the addition of elastomr prior to the addition of clay gives better mechanical properties. The tensile modulus of all the impact-modified nanocomposites is however, lower than PP/Comp/Clay (90:5:5). The modulus of PP/Comp/Clay/F-Olig is about 31% lower than PP/Comp/Clay (90:5:5), but is still about 37% higher than pure PP. This can be explained on the basis of fundamental tensile behavior of elastomers. Elastomers have very low glass transitions (usually much below 0 ^{o}C), so at room temperature, they are liquids, so they exhibit liquid like flow upon subject to tensile stress. This means that for a small deforming force, they exhibit much larger extensions, than regular solids. As a result, the overall tensile modulus (an indication of "solid" like behavior") is reduced.

3.6.2 X-Ray Diffraction

It can be inferred from figure 3.9 and figure 3.10 that the use of oligomeric elastomer in much more effective than using a polymeric elastomer, with respect to intercalation. It is seen that the clay spacing for this case has increased significantly, as the $Si_{d=001}$ peak at ca 2.4 ^{o} has shifted to ca 1.2 ^{o}. The interlayer spacing corresponding to these angles, can be calculated by using Bragg's law:

$$N\lambda = 2d\sin\theta \qquad \text{(Equation 3.3)}$$

, where N = order of diffraction

λ = wavelength of X-Ray

d = interplanar spacing, and

θ = semi-angle of diffraction.

Here, wavelength used = 1.4 Å.

N = 1.

So, for $\theta = 1.2^{o}$,

d = 33.4 Å.

For $\theta = 0.6^{o}$,

d = 66.8 Å.

Hence, it can be concluded that the interlayer spacing has increased by 100%. So, a lot of surface area of clay is now available to the polymer for bonding. This also serves as an explanation for the high tensile strength of oligomer-modified nanocomposite.

This is not observed for the polymeric elastomer modification of PP/clay nanocomposite. This could be because of the smaller size of the oligomeric chains and hence greater mobility. So, these chains are likely to penetrate the galleries of the clay better than the polyolefin elastomer and therefore, aid chain intercalation better. Figure 3.19 illustrates this concept.

3.6.3 Differential Scanning Calorimetry

The DSC heating thermograms (Figures 3.12 through 3.15) do not show significant changes in Tg for any of the impact-modified nanocomposites. A possible explanation for this behavior is that the elastomer chains might have preferentially penetrated into the clay galleries, and spread them apart. Added to this is the low molecular weight of the polyolefin elastomer compared to PP and also the oligomeric nature of the end functionalized elastomer. The heat requirement for Tg transition is greatest for PP. This is expected because the clay has a lower specific heat than PP and so does Epolene, due to its low molecular weight.

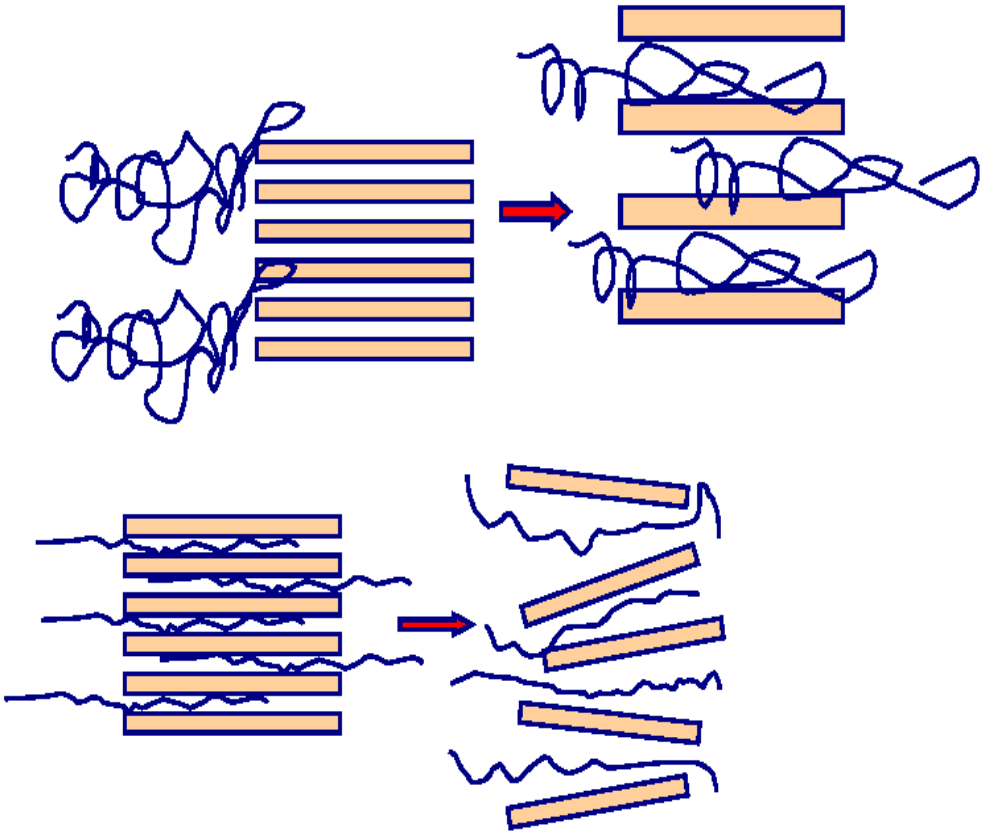

Figure 3.19. Schematic showing that oligomeric elastomers may be more effective in aiding chain intercalation than polymeric elastomers.

The cooling thermogram (Figure 3.15) shows some interesting details. The most striking feature of the plot is the significant shift in the Tc (crystallization temperature) for the nanocomposites, ranging from about 4-12 degrees. This means that crystallization phenomenon begins much earlier for the nanocomposites. This indicates that the clay might be acting as a nucleating agent. It is also seen that the oligomer-modified nanocomposite shows highest % crystallinity on a relative scale. This may be explained by the fact that these were able to penetrate the clay galleries more effectively, so that now, there are more nucleation sites per unit volume of the material. This is corroborated by the enhanced tensile strength of the oligomer-modified nanocomposite.

The fact that the polymeric elastomer modified nanocomposite also shows enhanced crystallinity indicates that there is some penetration of these molecules inside the clay galleries. But this is certainly less than its oligomer-modified counterpart, as indicated by XRD data.

3.6.4 Izod Impact Testing

From Table 3.10, it is seen that the oligomeric route for impact modification works the best. Even though the tests were not conducted in accordance with ASTM standards, it was ensured that each material was tested in the same way. Specimen preparation, placement of specimen on the test apparatus, etc. were kept the same. The impact strength of the oligomer-modified nanocomposite is about 78% greater than the unmodified nanocomposite and 67% greater than pure polypropylene. This is a significant improvement in the impact strength of PP, which is otherwise known for its poor impact properties.

This behavior may be once again explained by the smaller molecular size of the oligomeric impact modifier, which can penetrate into the clay intergalleries more easily than the polymeric impact modifier, due to increased mobility. The smaller size of molecules account for enhanced mobility and hence, aids better in chain intercalation. Another possibility is bonding between Epolene and oligomeric elastomer. It is possible that the oligomeric elastomer chains are grafted onto Epolene chains by reaction with the maleic groups. It is also possible that the other free end of the graft could bond with the clay. This is because the oligomer has greater mobility. This could mean enhanced adhesion, and consequently higher impact strength.

Tensile testing results (Figure 3.8) indicated that the oligomer-modified nanocomposite occupied the highest area under the stress-strain curve. This could also mean highest fracture toughness.

3.6.5 TEM

TEM images for both routes of impact modification show significant amount of intercalation. However, a good comparison cannot be drawn due to difference in the instruments used for taking the images. However, as seen from the results of other characterization techniques, the oligomeric, end functionalized elastomer is able to penetrate into the galleries more effectively.

3.7 Conclusions

From this research, we can draw the following conclusions:

- Impact modification of polypropylene clay nanocomposites could be done by the addition of functionalized elastomeric species.
- The sequence of addition of addition of elastomer had a significant effect on the mechanical behavior of the resulting nanocomposites.
- It was observed that if the elastomer was added prior to addition of clay, the mechanical properties of the resulting nanocomposites were better than if the elastomer was added after the addition of clay.
- Impact modification of the nanocomposite involved some sacrifice of tensile properties. However, this was seen to be the least in case of oligomer-modified nanocomposite
- The addition of elastomer also altered the crystallization behavior of the nanocomposites. The impact-modified nanocomposites showed enhanced crystallinity.

CHAPTER 4
PMMA / LAPONITE NANOCOMPOSITES

4.1 Introduction

Poly (methyl methacrylate) or PMMA is a transparent polymer. It is used in several applications such as windows, paints, intra-ocular lenses, bone cement, lubricating oils and hydraulic fluids. The polymer is transparent due to its amorphous character (atactic PMMA). PMMA is used in windows, because its optical clarity is not adversely affected by increasing thickness, as the case is with silica based inorganic glasses. Figure 4.1 shows the structural formula of atactic PMMA.

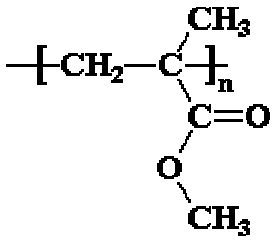

Figure 4.1. Structural formula of atactic PMMA.

4.2 Research Objectives and Strategy

The aim of the research was to enhance the hardness, and abrasion resistance of PMMA, for window based applications. However, in doing so, the optical clarity of PMMA had to be preserved. This is because it is this key emotive property that makes PMMA based products a valuable commodity.

The method chosen for the improvement of hardness and abrasion resistance was the formation of a nanocomposite with clay. Montmorillonite, the clay used for earlier

research is not a good choice for this research. This is because the mean particle size of montmorillonite is of the order of several microns. Further, the light absorbing chromophores due to the presence of iron oxide in montmorillonite pose additional difficulties in preparing optically clear nanocomposites.

Hence, it was proposed that synthetic clay be used. Several authors have reported the preparation and characterization of PMMA/Montmorillonite Clay nanocomposites [125-127]. Hwu et al. have reported a method in which both polymer and clay were dissolved separately and then mixed together [128]. Lee et al. reported a method based on emulsion polymerization with clay [129]. These papers discussed different approaches for synthesizing PMMA/montmorillonite clay nanocomposites such as solution dispersion of clay in MMA followed by polymerization, melt blending etc. However, most of them did not address a key issue associated with PMMA/montmorillonite Clay nanocomposites, which was the transparency or the optical clarity of the nanocomposites. Publications regarding PMMA/montmorillonite Clay nanocomposites did not address the use of synthetic clays as an alternative. So an attempt was made here to enhance the wear/abrasion properties of PMMA and yet keeping it transparent, by forming a nanocomposite with synthetic clay.

4.3 Materials

The clay used for the research was Laponite. Laponite is an entirely synthetic product. It is synthesized by treating salts of sodium, lithium and magnesium with sodium silicate under controlled conditions. Milling is done to carry out size reduction of the resulting product. Figure 4.2 shows the layered structure of clay. In the layered structure, there are six magnesium ions sandwiched between two rows of four silicon atoms.

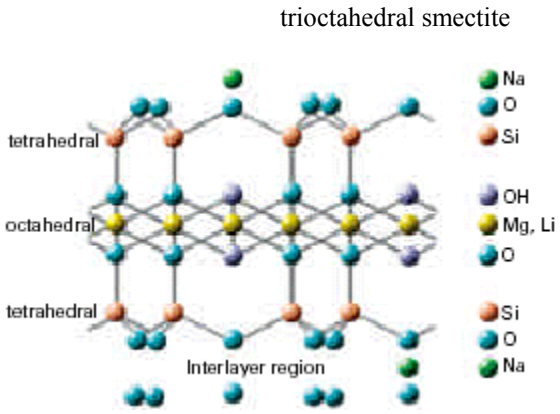

Figure 4.2. Layered structure of Laponite.

The magnesium ions are octahedral in shape and the silicon atoms are tetrahedral in shape. This gives a positive forty-four units of charge. Twenty oxygen atoms and four hydroxyl groups balance this. When dispersed in water, the particles exhibit a disc like shape, with a diameter or 25 nm and a thickness of 0.92 nm. Figure 4.3 shows this. Southern Clay Company supplies Laponite clays under different trade names.

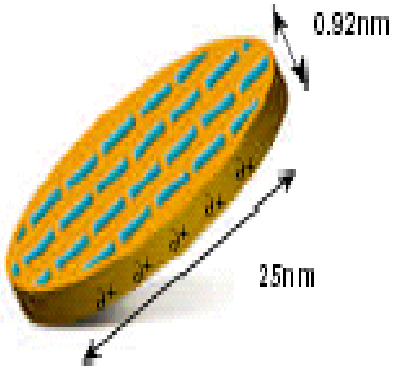

Figure 4.3. Idealized, average shape of laponite particles when dispersed in water.

Laponite has been used for a wide variety of applications such as catalyst components [130-131], biological applications [132-133], electrodes [134], as well as with polymers [135-139].

Three different clays, supplied by Southern Clay Company were examined, namely Laponite RD, Laponite JS and Laponite RDS. The clay used for this research was

Laponite JS. This was a fluorosilicate-modified laponite. Table 4.1 lists its chemical composition. Table 4.2 shows some of its properties.

Table 4.1. Chemical composition of Laponites.

MATERIAL	COMPOSITION (DRY BASIS), WT %		
	JS	RD	RDS
SiO_2	50.2%	59.5%	54.5%
MgO	22.2%	27.5%	26.0%
Li_2O	1.2%	0.8%	0.8%
Na_2 O	7.5%	2.8%	5.6%
P_2O_5	5.4%		4.4%
F	4.8%		

The reason for using JS was that it was the only variety that did not form a thick gel when dispersed in water. Other varieties of Laponite did so, thereby posing processing problems, as far as melt processing was concerned. It is worth mentioning that even though other varieties formed thick gels, they could still be used for modifying PMMA, but with processing difficulties [140].

A significant advantage of using Laponite is that it does not have any chromophores. This is because the synthetic clay is thoroughly purified.

Atoglas, under the trade name Plexiglass, supplied the PMMA for this research. The product name was V-825. Table 4.3 lists some of its properties. A compatibilizer material such as Epolene® for PP clay nanocomposites because PMMA being a polar polymer was expected to show interactions with clay.

Table 4.2. Physical properties of Laponites.

PROPERTY	JS	RD	RDS
Appearance	Free flowing white powder	Free flowing white powder	Free flowing white powder
Bulk Density	950 kg/m^3	1000 kg/m^3	1000 kg/m^3
Surface Area	300 m^2/g	370 m^2/g	330 m^2/g
Loss on ignition	8.7%	8.2%	8.0%
PH (2% suspension)	10	9.8	9.7
Storage	Hygroscopic, should be stored under dry conditions.	Hygroscopic and should be stored under dry conditions.	Hygroscopic and should be stored under dry conditions.

4.4 Processing

In order to obtain a good dispersion of Laponite JS in water, it is important to adjust the pH of the dispersion. This is because the clay has a net negative charge associated with it.

So, by maintaining a pH of about 10 using 1 M NaOH solution, the sodium ions are drawn towards the crystal surface of the clay due to electrostatic attraction.

But the osmotic pressure from the water present in bulk pulls them away. So, equilibrium is established in which an electrical double layer is formed. So, when two particles approach each other, they are repelled due to similar charge. Hence, the particles remain dispersed. PMMA pellets were dried for about 30 hours in an air-circulating oven at about 80 ^{o}C prior to melt blending. The clay was dispersed in water, to which 2 drops of 1 M NaOH solution were added.

Table 4.3. Properties of PMMA.

PROPERTY	VALUE	TEST METHOD
PHYSICAL		
Melt flow rate (230 ^{o}C / 3.8 kg)	3.7 g/10 min.	ASTM D1238
Specific Gravity	1.19	ASTM D792
Water Absorption (24 hr. immersion)	0.3% weight gain	ASTM D570
MECHANICAL		
Tensile Strength @ Maximum	10200 psi	ASTM D638
Tensile Elongation @ Break	6 %	ASTM D638
Tensile Modulus	450000 psi	ASTM D638
Flexural Modulus	450000 psi	ASTM D790
Notched Izod (73 °F/23 °C)	0.3 ft-lb/in notch	ASTM D256
Rockwell Hardness	93 M	ASTM D785
THERMAL		
HDT (455 kPa; annealed)	221 ^{o}F	ASTM D648
Thermal Conductivity	1.3 BTU/hr*ft^2 *F/in	ASTM C177
OPTICAL		
Refractive Index (ND @ 73 °F)	1.49	ASTM D542

However, all mass balance was carried out on a dry basis. Melt processing of the nanocomposites was carried out in a 30mm APV co-rotating reactive twin-screw extruder. This extruder had eight temperature zones from feed to die (including the die zone). The screw L/D was 40. The temperature range used for processing the nanocomposites was 190 ^{o}C to 225 ^{o}C. Figure 4.4 shows the operation in greater detail.

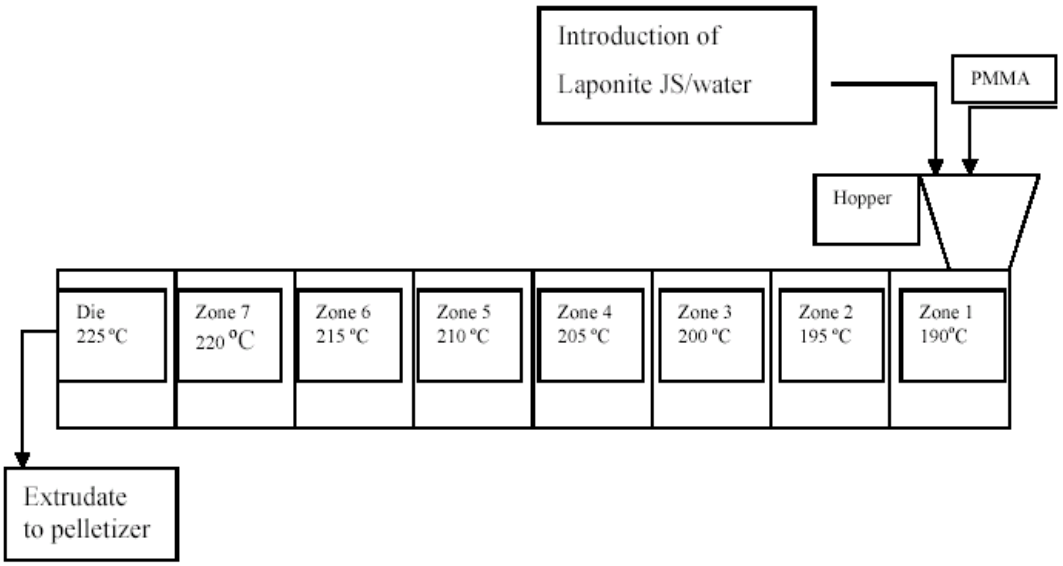

Figure 4.4. Synthesis of PMMA/Laponite JS nanocomposites using a reactive twin-screw extruder.

The clay, dispersed in water/NaOH was placed in an ultrasonicator (Mettler Electronics, 105-120 V, 2 Amperes, 50-60 Hz ultrasonicator) for about 20 minutes, prior to adding it to the polymer. This dispersion was fed to the molten polymer at the feed zone of the extruder. The resulting strands that came out of the die zone were collected in a flowing water bath. Then they were pelletized, and the pellets were dried in an air-circulating oven at about 80 ^{o}C. Nanocomposites containing 2 wt% and 5 wt% of the clay were prepared in the way described above. Pure PMMA was also ran through the extruder under identical conditions of processing in order to keep the thermal history of each material same.

4.5 Characterization

The following analytical tools were employed in order to measure various properties as well as for obtaining an insight into the microstructure of the processed nanocomposites:

- Tensile Testing
- X-Ray Diffraction
- Differential Scanning Calorimetry
- Transmission Electron Microscopy
- Nano-indentation

4.5.1 Sample preparation

Samples for the listed techniques were prepared using compression molding. Compression molding is a process in which a polymer is made to take the shape of a mold by pressing it between two heated plates. The heat melts the polymer (if semi-crystalline) or takes the polymer chains well above the glass transition temperature (if amorphous). The press used for compression molding was a Carver, model C-81000-141 press.

In order to prepare the samples, the press was first heated to 450 ^{o}F. The mold used was square in shape, with dimensions of 70 mm X 70 mm X 0.8 mm. The mold was placed on a metal plate covered with Teflon® coated aluminum foil. The mold was then filled with dried pellets. This plate with mold and the pellets was placed on the bottom plate of the press. Another Teflon® coated aluminum foil covered metal plate was placed on top of the mold bearing plate, to give a sandwiched assembly.

The bottom plate of the press was raised until the assembly just touched the top plate of the press. The pellets were then allowed to convert into a liquid state by heat transfer from the press. This took about 5-6 minutes. After that the pressure of the system was raised to 10, 000 psi. Initially, due to resistance offered by the liquid polymer as well relatively incomplete conversion to liquid, the pressure dropped below 10,000 psi.

Under these circumstances, it was necessary again to raise the pressure to 10,000 psi. This was repeated until the pressure attained a steady value of 10,000 psi. The

pressure could be measured using a gauge attached to the press. A pressure of 10, 000 psi. on the gauge corresponded to 9302 psi. on the sample. This was calculated using the formula:

$$Ps \times As = Pg \times Ag \qquad \text{(Equation 4.1)}$$

Where, Ps = Pressure on the sample

As = Cross sectional area of the sample

Pg = Gauge pressure

Ag = Cross sectional area of the piston of the press.

As $= 4900\ mm^2$

Ag $= 3.14. (3^2)/4$

Pg = 10, 000 psi.

After the gauge pressure became steady at 10, 000 psi., the mold was allowed to rest at the abovementioned temperature and pressure for 10 minutes. After that, the heat supply to the press was turned off. The mold was allowed to cool to ambient temperature. The mold containing the solidified sheet was taken out.

These sheets served as specimens for all the characterization techniques.

4.5.2 Tensile Testing

The aim of performing tensile testing was to evaluate the mechanical response of the materials to a known strain or deformation rate. This gives us a plot of stress versus strain from which we can obtain a wealth of information such as the brittle or ductile behavior, tensile modulus or an indication of stiffness of the material, tensile strength etc. Tensile testing was carried out using an EnduraTEC ELF 3200 series machine. It consisted of the following components:

- The linear motor assembly: Had a patented high-bandwidth, low-distortion actuator from Bose Corporation.

- Testing Chamber: Had facilities for introducing hot air, for increasing temperature as well as introducing liquid nitrogen. A bulb for viewing the test in case liquid nitrogen makes the chamber cloudy was also provided. The door had a transparent section for enabling to view testing while in progress. There were two sets of grips. The bottom grip was stationary and was connected to the load cell. The upper grip was mobile and its motion was regulated by the Wintest® software, and ultimately, the linear motor.

- Temperature Control: With the help of the software, temperature could be varied between –50 ^{o}C to 150 ^{o}C.

- Controller box that acted as an interface between the computer and the machine itself.

The strain rate used was 0.05 mm/sec. and the testing temperature was 28 ^{o}C.

Tensile testing data could be obtained for PMMA and PMMA/2 wt% Laponite nanocomposite only. The nanocomposite containing 5-wt % clay was too brittle. Consequently, strips could not be cut, without introducing cracks or notches. Thus, the material was rendered unfit for testing. Figures 4.5 and 4.6 show the results obtained from tensile testing.

4.5.3 X-Ray Diffraction

The objective of performing XRD was to explore the possibility of any intercalation or exfoliation in the layered silicates due to possible penetration by the polymer into the clay layers. This is usually determined by the shifts in low angle peaks for the clay. This is because according to Bragg's law:

$$n\lambda = 2d\sin\theta \qquad \text{(Equation 4.2)}$$

d = interplanar spacing,

n = order of diffraction

λ = wavelength of X-Ray source, and

θ = semi-angle of diffraction

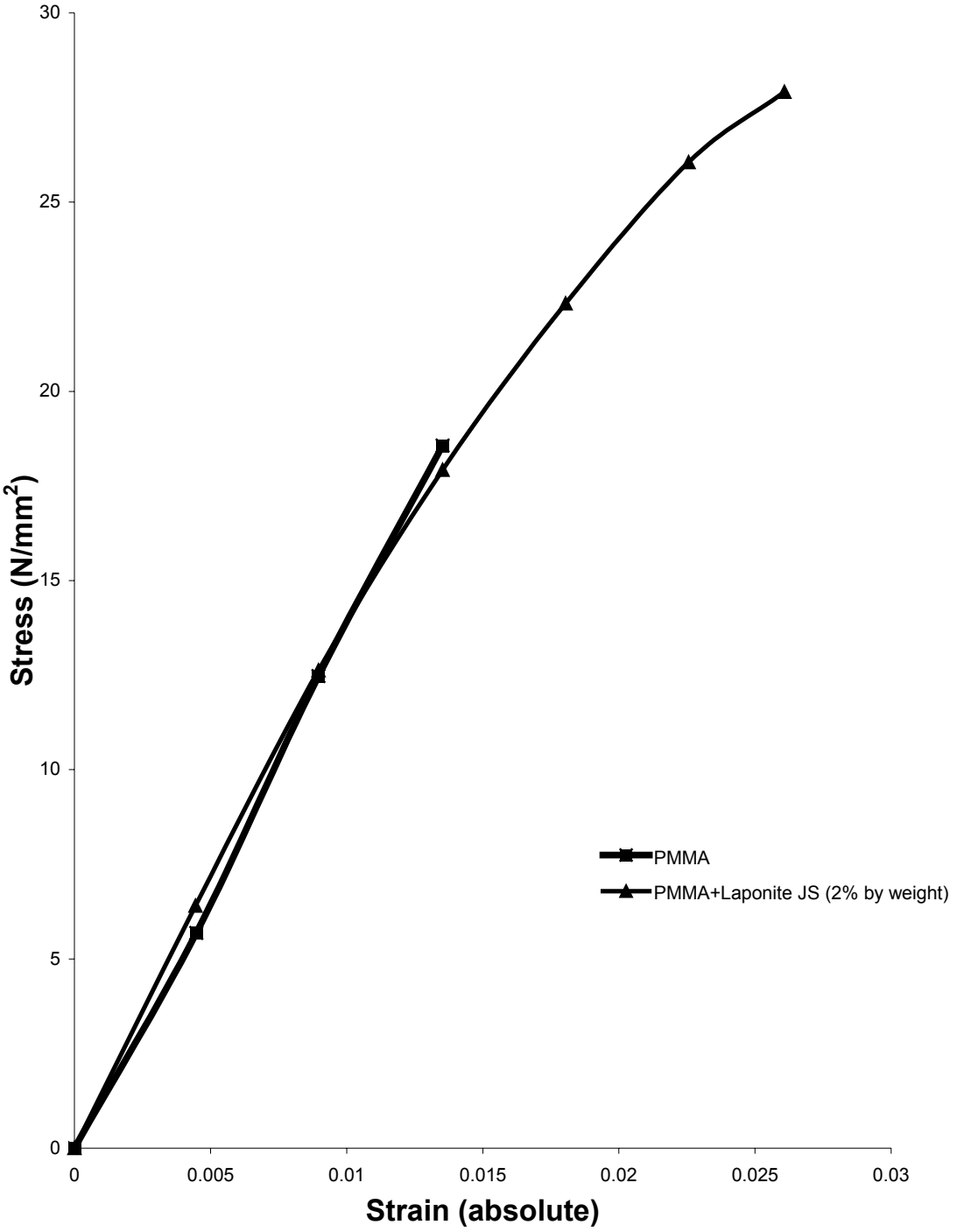

Figure 4.5. Tensile testing results for PMMA and PMMA + 2 wt % Laponite JS at 0.05 mm/sec, 28 ^{o}C. All samples tested showed failure.

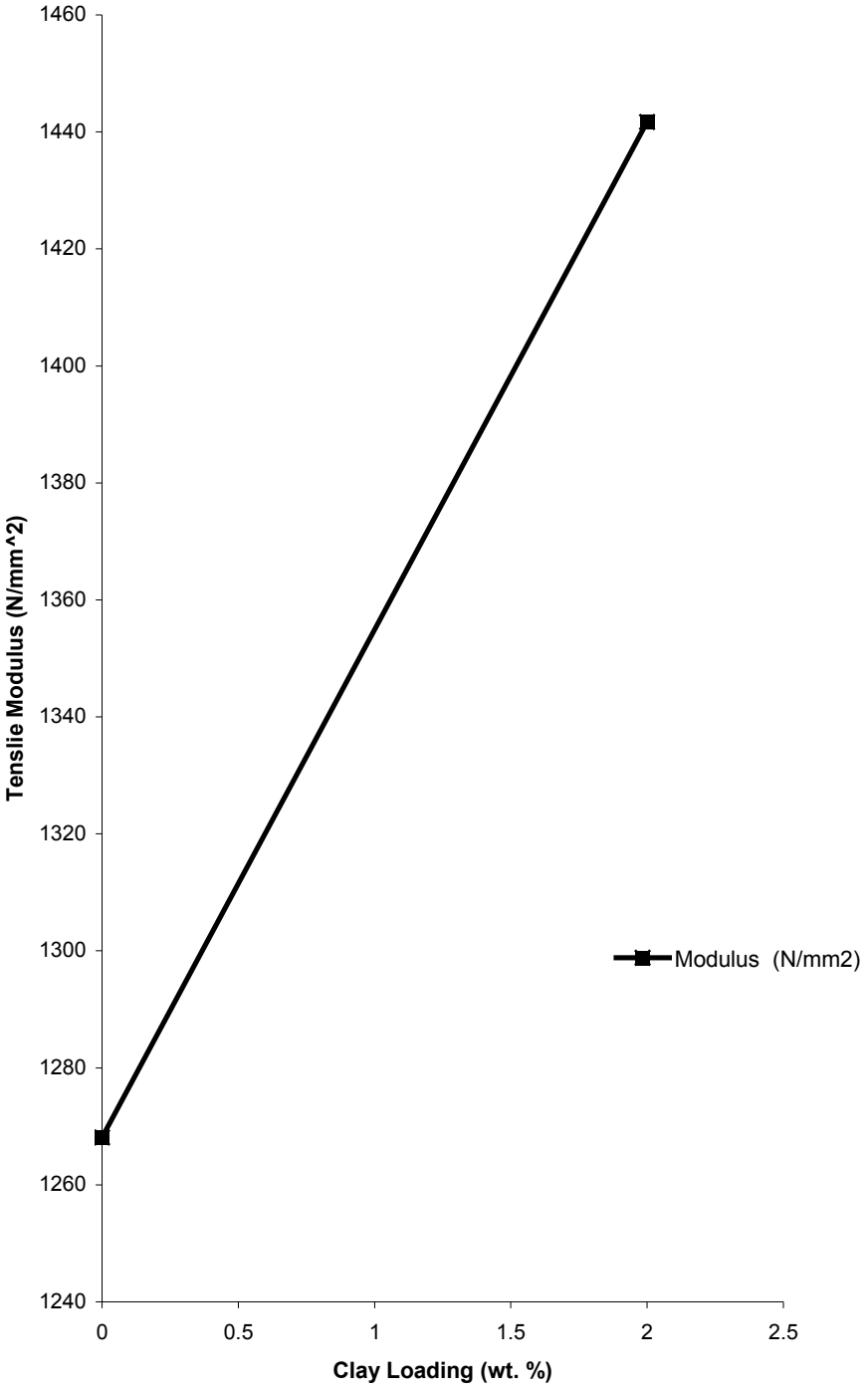

Figure 4.6. Dependence of tensile modulus on clay loading. Modulus values were obtained from linear region of the curves in Figure 4.5. Strain rate = 0.05 mm/sec, temperature = 28 ^{o}C.

So, as the semi angle varies, the d spacing between the clay layers varies. If the polymer is successful in penetrating the clay layers, then the d spacing of the clay layers increases, thereby reducing the angle corresponding to the peak observed.

XRD was performed using a Philips APD 3720 instrument. This uses a Cu-K_α X-ray source (Wavelength = 1.54 Å). The range of angles swept was 0-75 degrees. Reflective mode was used and temperature was 15 ^oC. Figure 4.7 presents the results obtained from XRD.

4.5.4 Differential Scanning Calorimetry (DSC)

DSC describes the behavior of a material when subjected to heat at a controlled rate. This enables us to determine different transitions associated with the polymer such as glass transition, melting transition, besides crystallization behavior etc. DSC on the samples was performed using a ThermoHaake DSC 220 C model instrument. Heating rate used was 10 ^oC/minute, while cooling rate was 50 ^oC/min.

Two sweeps of this thermal treatment were performed. Figure 4.8 shows the DSC thermograms. Note that in this case, procurement of cooling thermograms is not necessary, because atactic PMMA being an amorphous polymer does not crystallize. The output from the instrument is the heat supplied in microwatts versus temperature. The heat supplied by the instrument is directly proportional to the specific heat of the material.

4.5.5 Transmission Electron Microscopy (TEM)

TEM complements XRD by observing a very small section of the material for the possibility of intercalation or exfoliation. It can also provide information on dispersion of particles. It however, supplies information on a very local scale. However, it is a valuable tool because it enables us to *see* the polymer and the clay on a nanometer scale.

Transmission electron microscopy was performed on the nanocomposites using a JEOL 2010 field emission TEM instrument. Figures 4.9 through 4.14 show the TEM images.

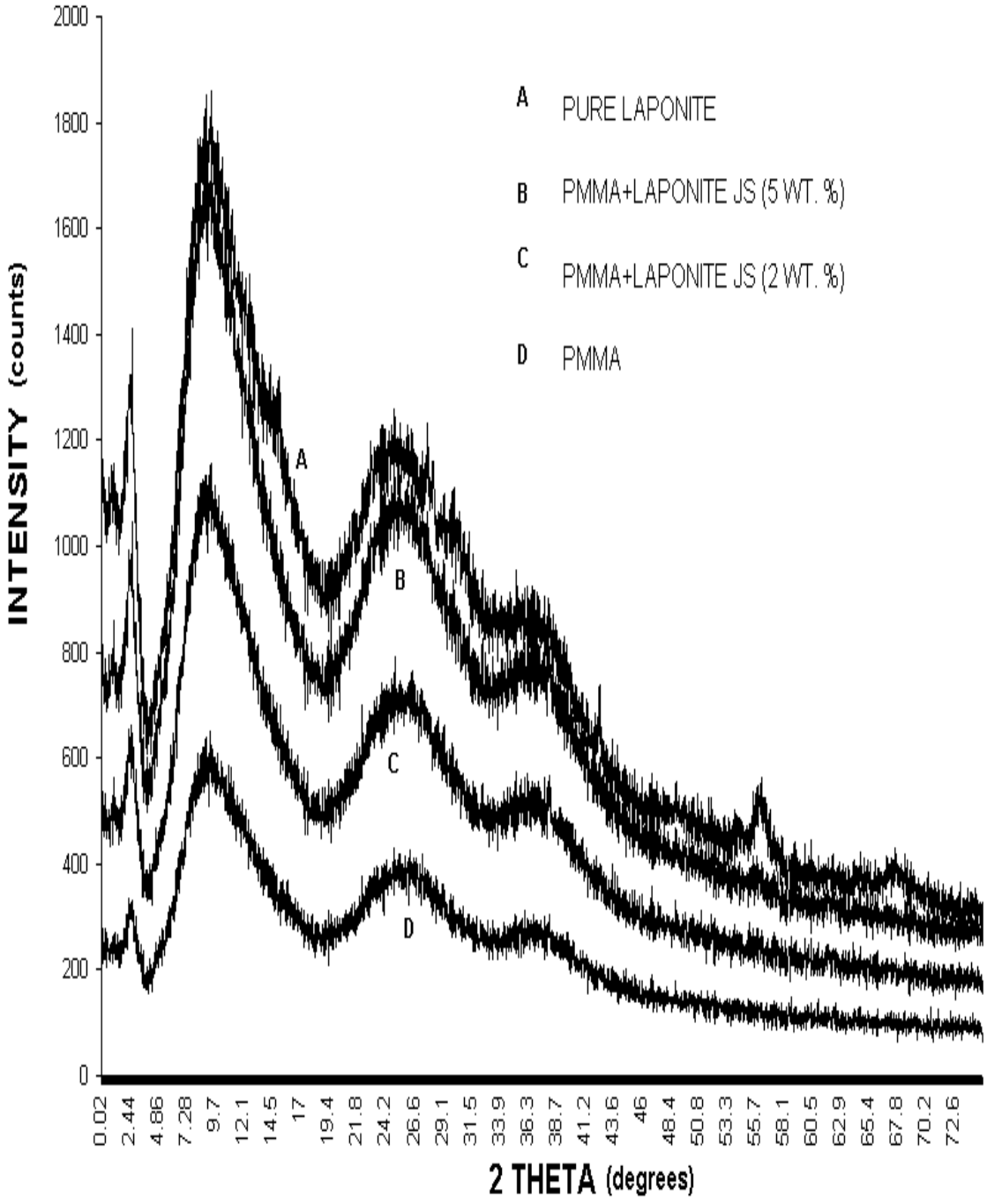

Figure 4.7. XRD patterns (reflective mode) for PMMA and PMMA/Laponite nanocomposites. Reflective mode, temperature = 15 ^{o}C.

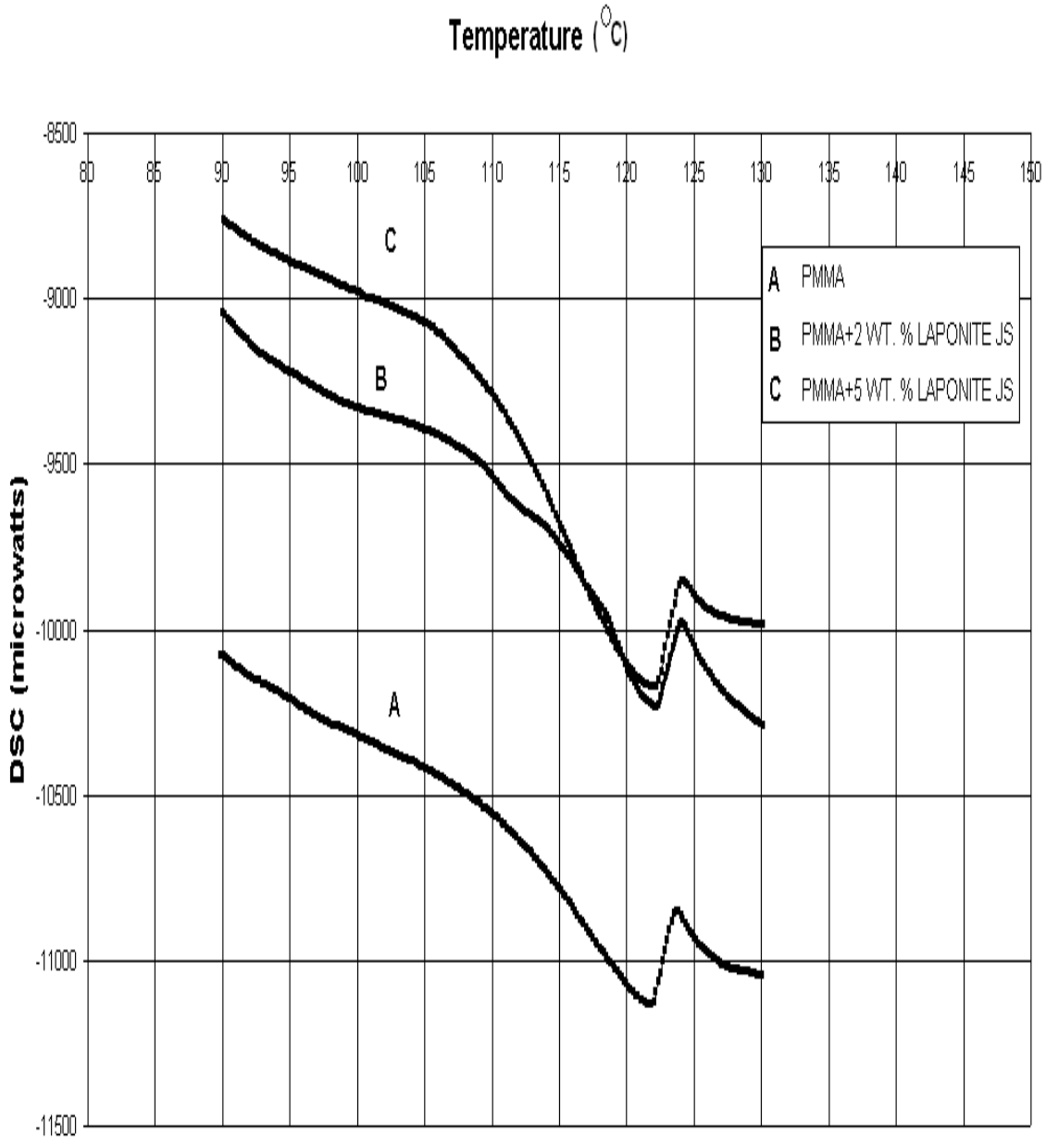

Figure 4.8. DSC thermograms for PMMA and PMMA/Laponite JS nanocomposites. Heating rate = 10 °C/min., cooling rate = 50 °C/min.

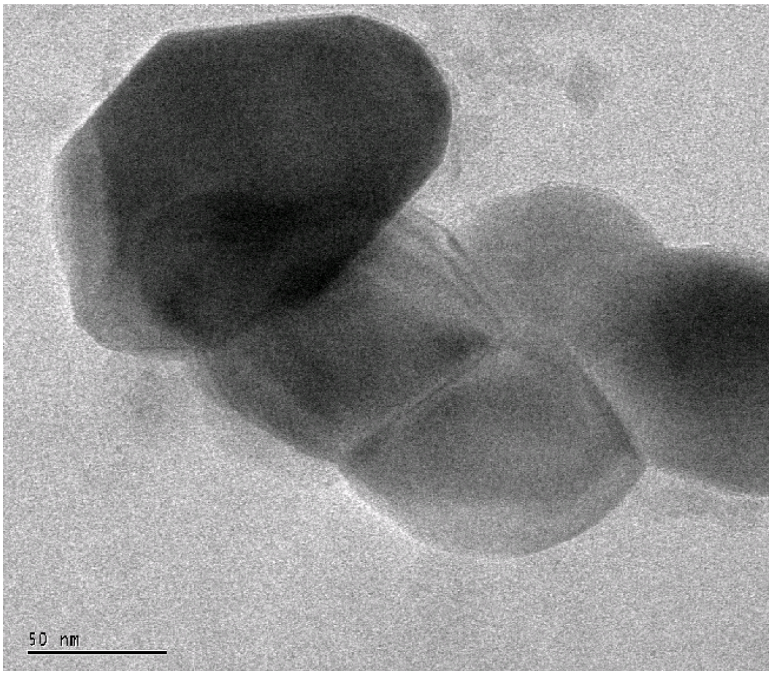

Figure 4.9. TEM micrograph of PMMA/2 wt % Laponite JS at 60 kX.

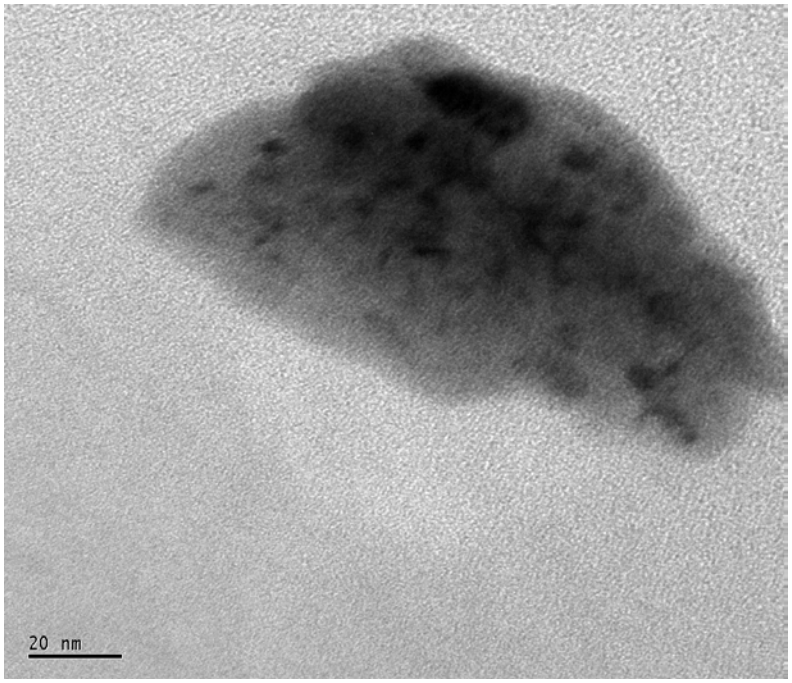

Figure 4.10. TEM micrograph of PMMA/2 wt % Laponite JS at 100 kX.

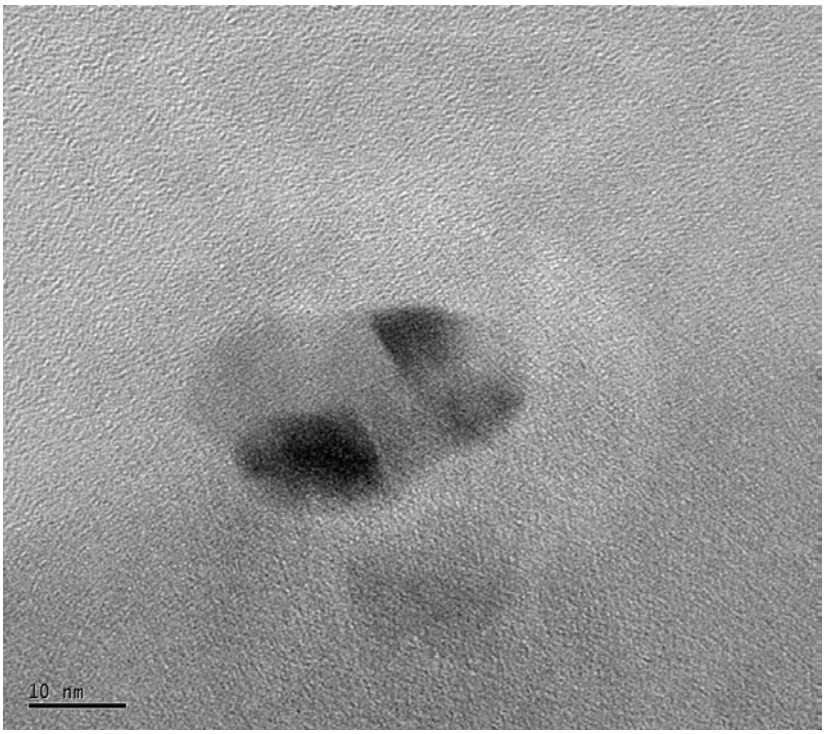

Figure 4.11. TEM micrograph of PMMA/2 wt % Laponite JS at 200 kX.

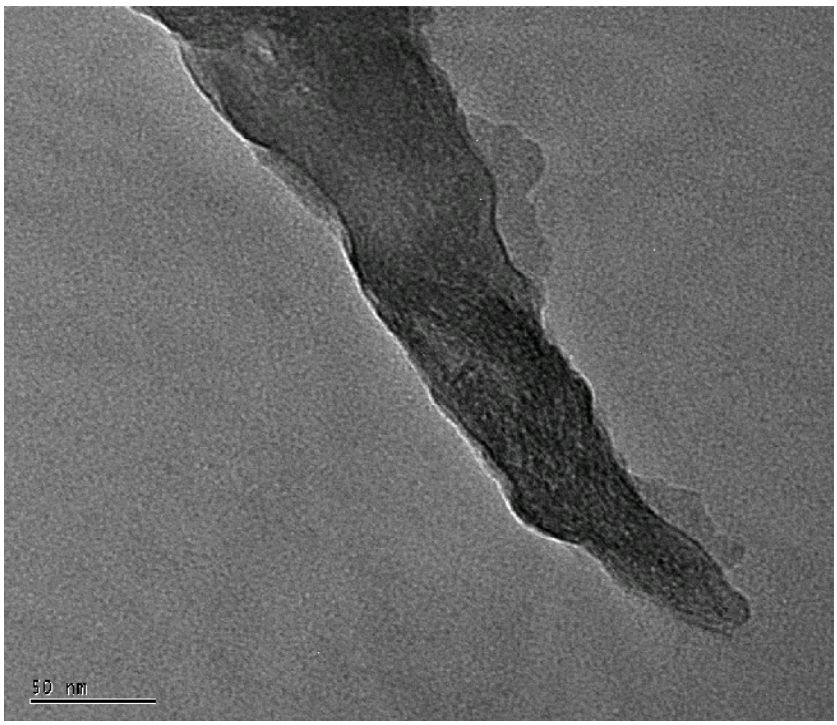

Figure 4.12. TEM micrograph of PMMA/5 wt % Laponite JS at 50 kX.

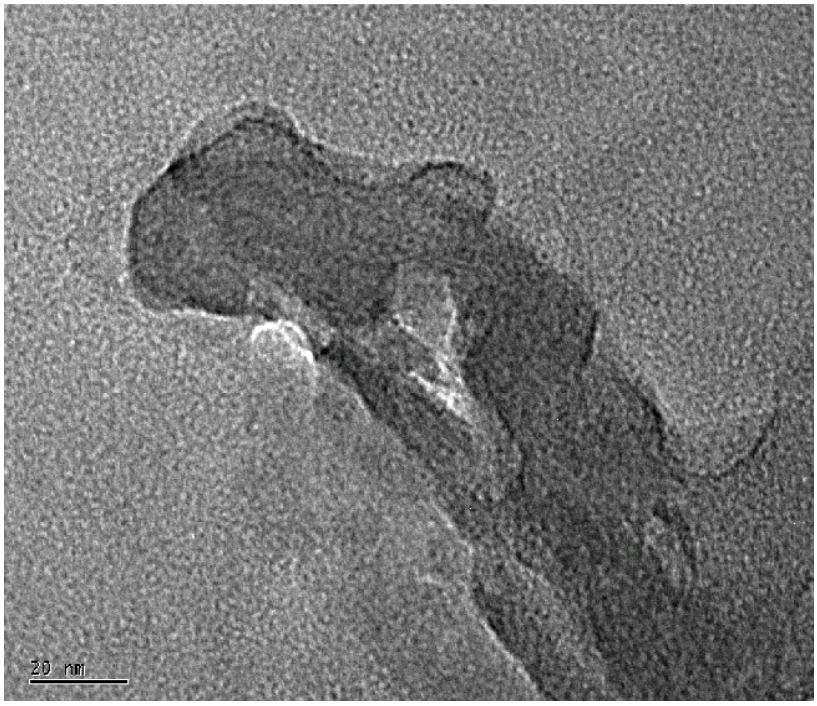

Figure 4.13. TEM micrograph of PMMA/5 wt % Laponite JS at 100 kX.

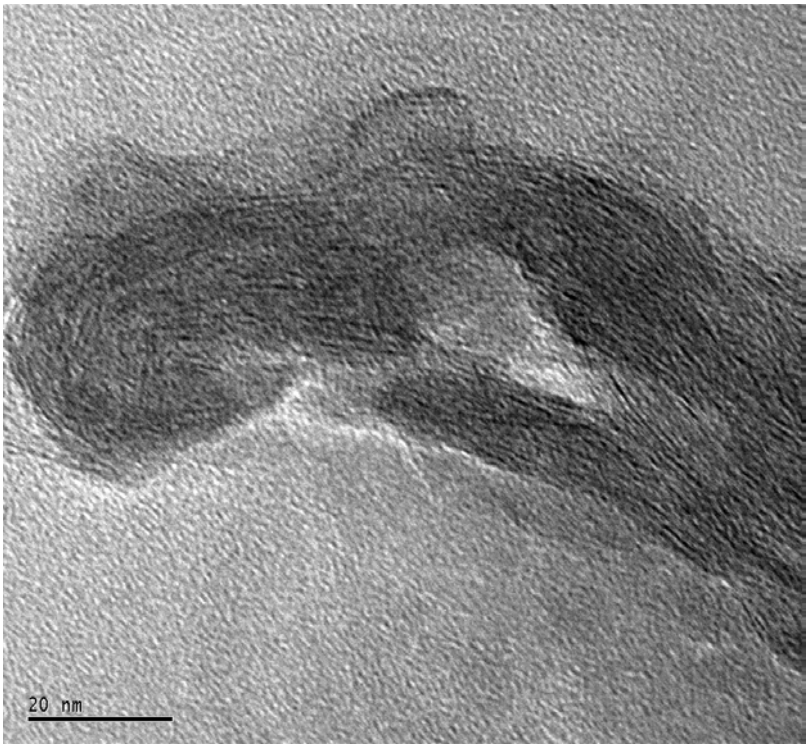

Figure 4.14. TEM micrograph of PMMA/5 wt % Laponite JS at 150 kX.

4.5.6 Nanoindentation

Nanoindenting is a relatively new method for characterization of materials' mechanical properties on a very small scale. Features less than 100 nm across and thin films less than 5 nm thickness can be evaluated [141-152]. Test methods include indentation for comparative and qualitative hardness measurements. The instrument used for performing nanoindentation characterization was a Hysitron Inc. Micro Nanoindentor.

The maximum and minimum load force that could be applied were approximately 5 mN and 5 μN, respectively, with a force resolution of 100 nN. A three-sided, pyramid-shaped diamond probe tip was used for indenting the sample.

For indenting, the probe was forced into the surface at 100 nN/sec. and to a selected maximum force. The test consisted of a loading and a de-loading cycle, yielding a force-displacement curve for each cycle.

For preparing specimens, a triangular section of the material from the compression-molded sheet was cut using a penknife. This was mounted on a circular specimen mount, made out of glass using a two-part epoxy mixture. The specimen adhered firmly to the mount upon setting of epoxy.

The instrument was first calibrated with a standard quartz sample prior to testing the specimens. Four different loads, namely 250, 500, 1000 and 5000 micronewtons were employed. Nanoindentation was done at six different points per sample to ensure consistency in results. Figures 4.15 through 4.18 show representative results. Table 4.4 summarizes the results for every specimen, and includes maximum displacement, force applied and rate of application of force.

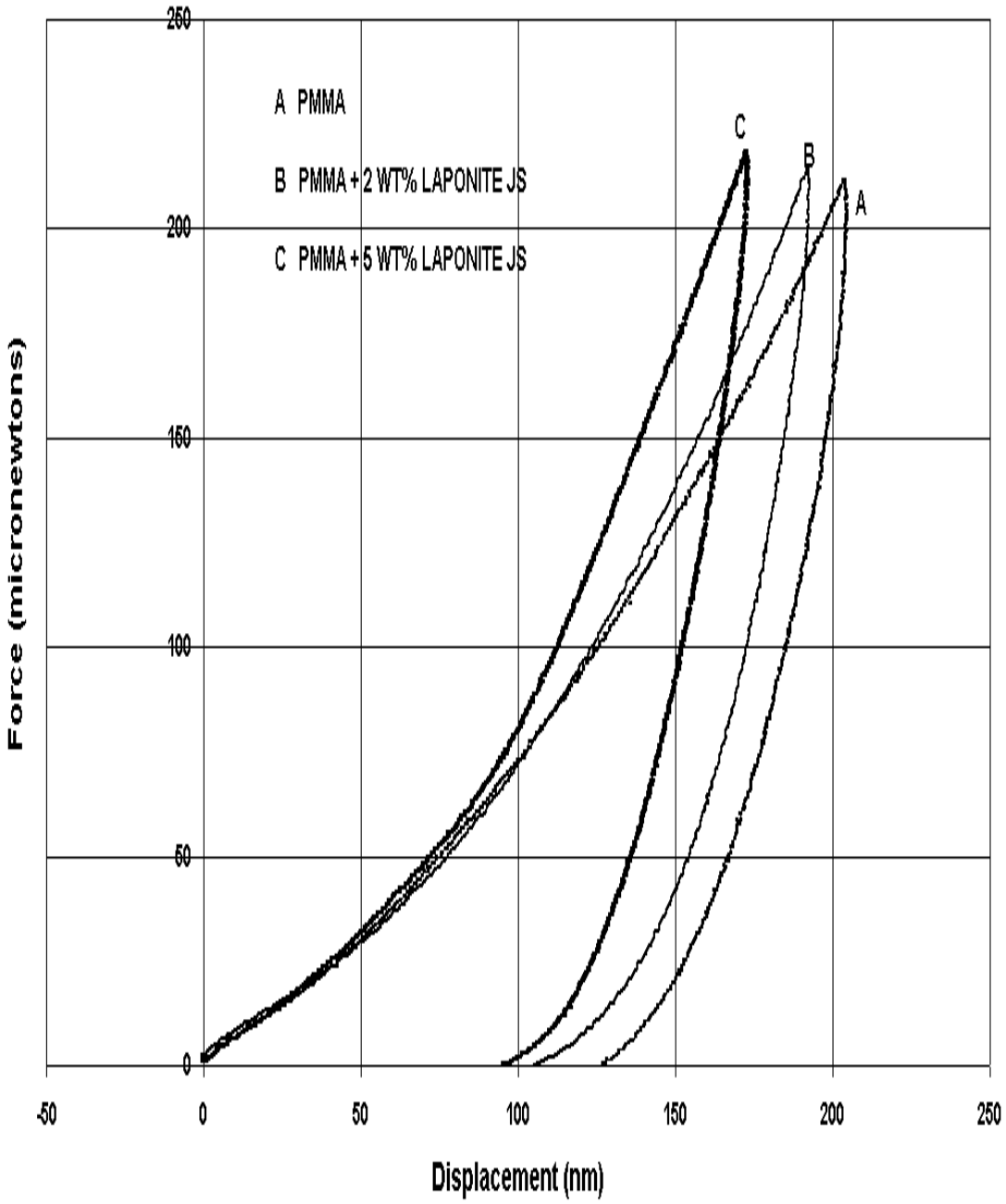

Figure 4.15. Nanoindentation results for PMMA and PMMA/Laponite JS nanocomposites at 250 μN. Force was applied at 100 nN/sec.

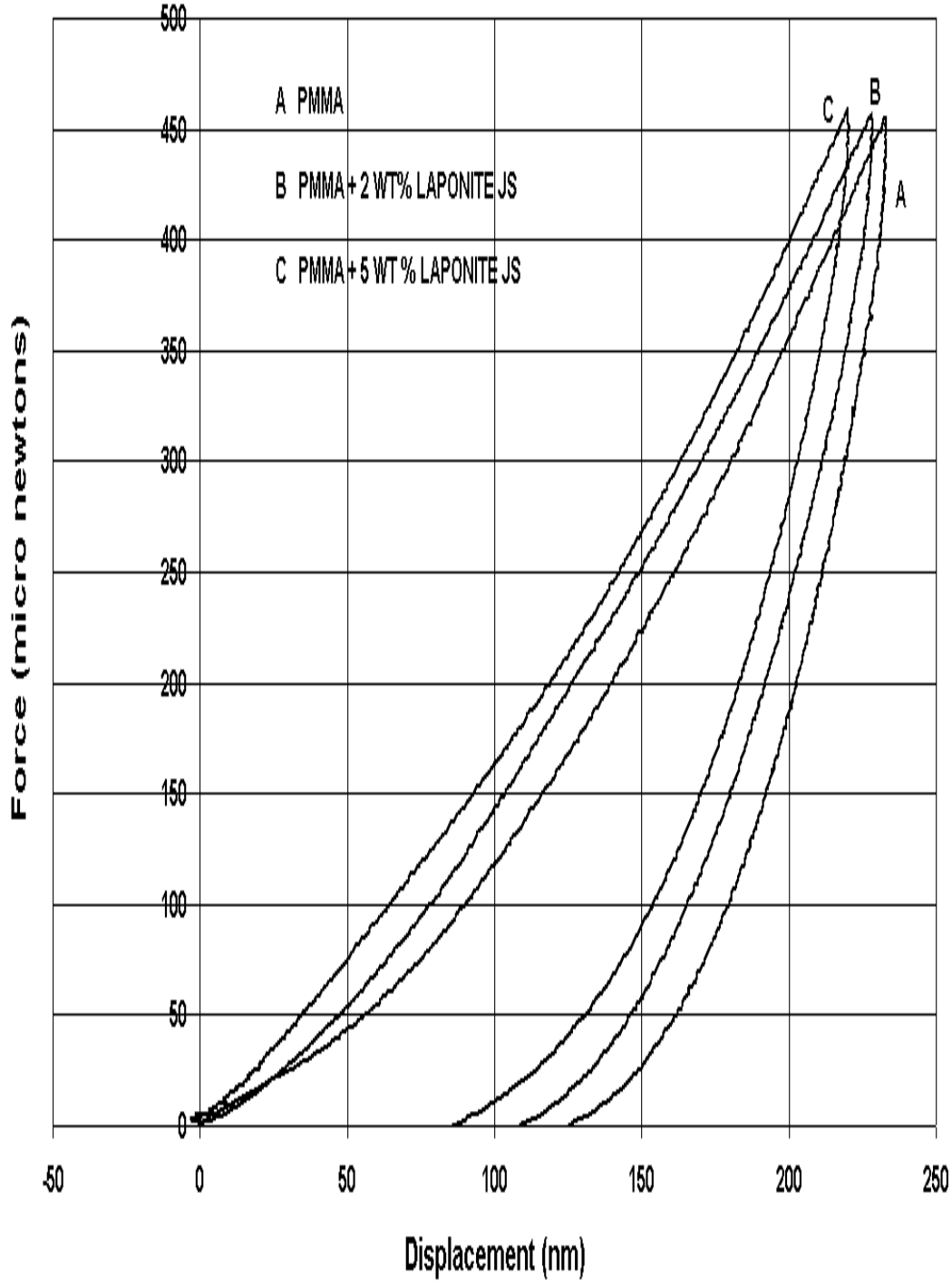

Figure 4.16. Nanoindentation results for PMMA and PMMA/Laponite JS nanocomposites at 500 μN. Force was applied at 100 nN/sec.

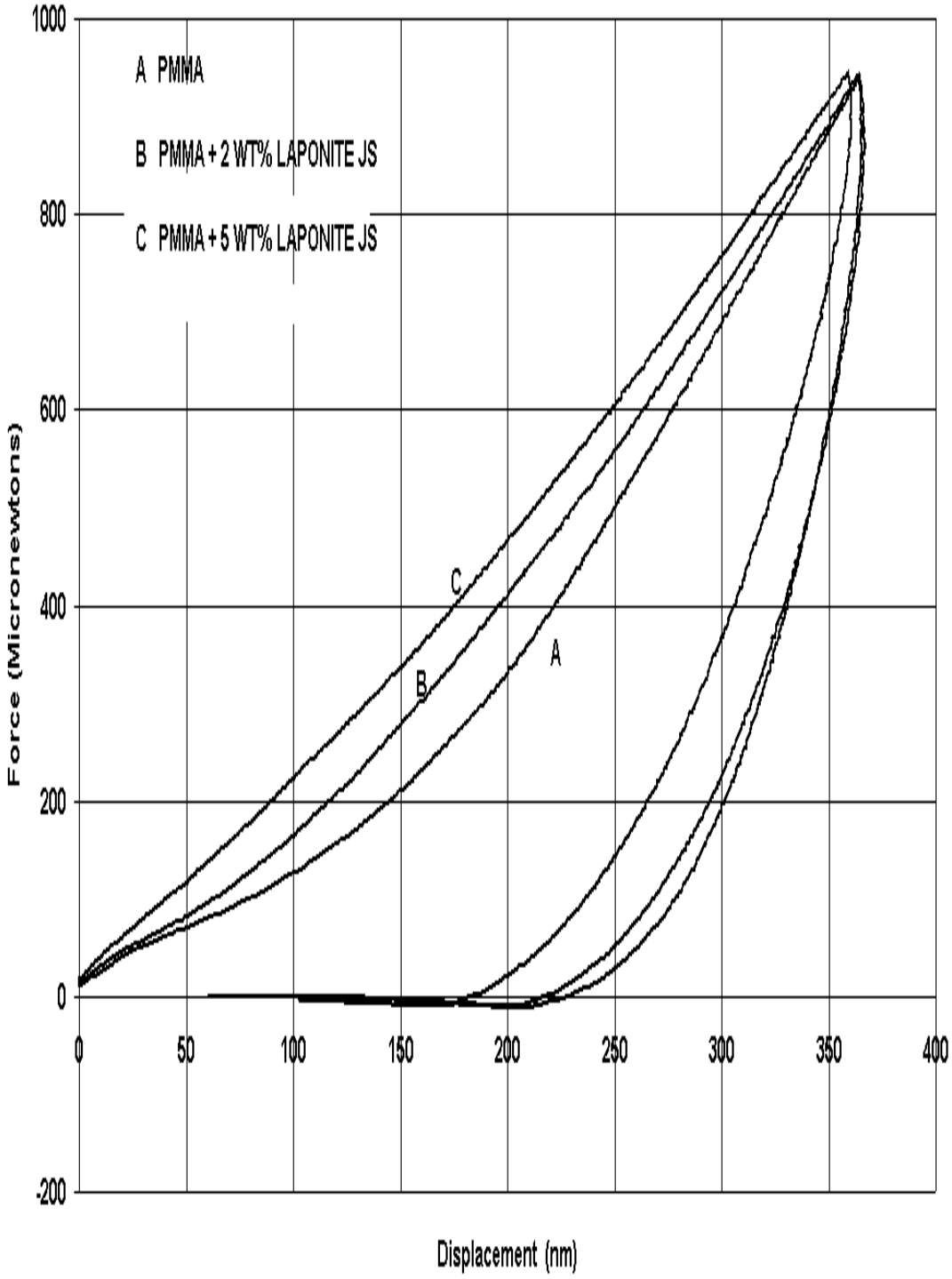

Figure 4.17. Nanoindentation results for PMMA and PMMA/Laponite JS nanocomposites at 1000 μN. Force was applied at 100 nN/sec.

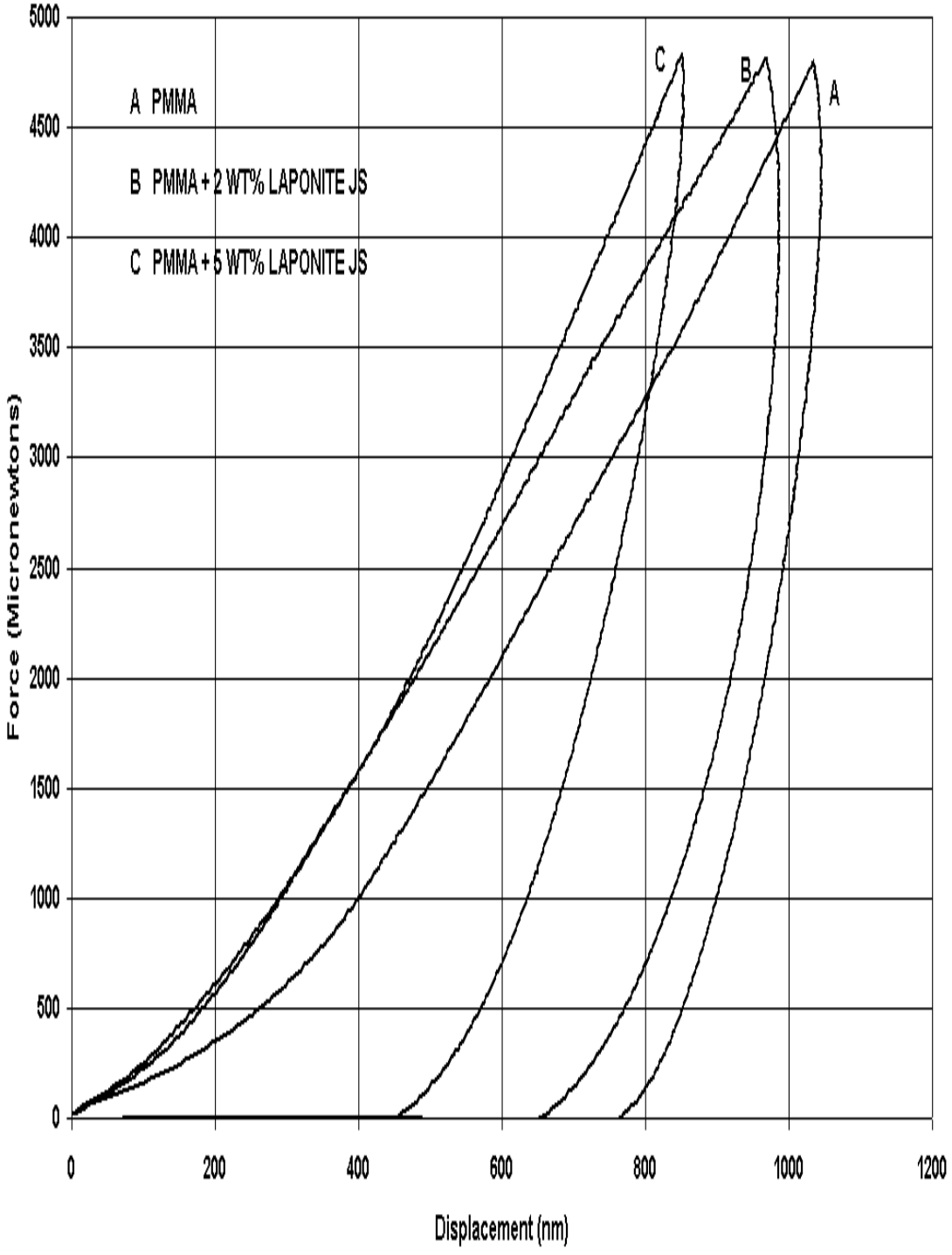

Figure 4.18. Nanoindentation results for PMMA and PMMA/Laponite JS nanocomposites at 5000 μN. Force was applied at 100 nN/sec.

Table 4.4. Nanoindentation results showing force and peak displacements for each specimen tested. Force was applied at 100nN/sec.

FORCE (μN)	DISPLACEMENT (nm)																	
	PMMA						PMMA + 2 WT % LAPONITE JS						PMMA + 5 WT % LAPONITE JS					
	1	2	3	4	5	6	1	2	3	4	5	6	1	2	3	4	5	6
250	175	205	187	196	189	182	154	160	145	161	142	163	132	126	139	141	144	118
500	240	237	239	249	251	255	210	220	218	221	207	219	184	192	200	181	188	190
1000	356	380	375	366	358	371	324	336	318	323	311	339	288	279	274	293	280	276
5000	998	967	972	991	983	973	720	754	731	742	716	725	567	589	580	577	560	581

4.6 Discussion of Results

Having characterized the materials for different properties and microstructure, it is now important to interpret the results in order to obtain an understanding of different phenomena taking place.

4.6.1 Tensile Testing

From figure 4.5, it is evident that the nanocomposite containing 2 wt% clay has a greater tensile strength. In fact, its tensile strength is 47.3% greater than pure PMMA. The variation of modulus is amplified in Figure 4.6. We see that the modulus of the 2 wt% Laponite JS nanocomposite has increased from 1265 N/mm^2 to 1440 N/mm^2, an increase of 13.83%. This could be attributed to the addition of clay. Also, PMMA being a polar polymer tends to exhibit stronger interactions (e.g. polar interactions) with clays than non-polar polymers such as PP.

The increase in modulus and tensile strength indicated a greater area under the stress-strain curve, which means greater energy to failure, which could possibly convert to higher fracture toughness also. This was indeed one of the goals of the research.

4.6.2 X-Ray Diffraction

Figure 4.7 shows the entire XRD pattern for each material, including pure clay. Being a silicate based material; this also exhibits a low angle peak like montmorillonite. We can also see that there are two high angle peaks for Laponite JS; at ca 56 degrees and ca 68 degrees. From Bragg's law,

We have $d = n \lambda / (2 \sin \theta)$.

Assuming n=1, i.e., first order diffraction,

$d = \lambda / (2 \sin \theta)$.

Here, $\lambda = 1.54$ Å.

$2\theta = 56$ degrees.

So, d = 1.64 Å.

Similarly, d-spacing corresponding to the peak at 68 degrees is 1.37 Å.

It is possible that these d-spacings correspond to the lattice spacings of the crystalline unit cells.

These high angle peaks disappear in the nanocomposites. This could be possibly because of interactions between clay and the polymer. There is not much evidence indicating intercalation or exfoliation. So a concrete explanation could not be provided with the data available. Evidence for interactions between clay and polymer are also furnished by TEM images, besides tensile testing, which are discussed in a later section. However, it should be noted here that in this case, our main aim is to disperse and distribute the nano-size discs uniformly into PMMA. Intercalation or exfoliation due to penetration by polymer chains into clay layers would be an added advantage.

4.6.3 DSC

DSC thermograms presented in Figure 4.8 do not show a significant shift in Tg. The Tg of the 2 wt% nanocomposite is 1 ^{o}C greater than PMMA, while that of 5 wt % nanocomposite is about 2 ^{o}C greater than PMMA. This is again because in this case, unlike montmorillonite, our primary objective is not to exfoliate or intercalate the clay with the polymer, but to uniformly disperse the clay nanoparticles. So there is not much chain confinement effect, which would result form the penetration of polymer chains into clay layers, due to addition of clay. The slight in Tg is possibly due to bonding between PMMA and laponite.

The heat requirements for transition increase as we add clay to the polymer. However, the increase is only 15%. Many reasons are possible. Firstly, clay particles tend

to retain moisture. The specific heat of water is 1 cal/g- ^{o}C, whereas Cp values for PMMA and clay are 0.32 cal/g- ^{o}C and 0.27 cal/g- ^{o}C respectively. So, the Cp of water is more than 3 times that of PMMA. So even low moisture content increases the heat requirement for the transition significantly. Further, as stated earlier, the heat supplied by the instrument is directly proportional to the Cp of the material being tested. Secondly, the polymer could be interacting with the clay, through polar interactions. This is supported by the slightly higher Tg values of the nanocomposites.

4.6.4 TEM

TEM micrographs are shown in figures 4.9 through 4.14. For the nanocomposite containing 2-wt% clay, we see that even at low magnifications (50 kX), there are domains formed by the aggregation of clay particles. But the particles appear to be separate and not in the form of stacks. This indicates significant dispersion of particles in PMMA matrix. This is of course, facilitated by shearing inside the extruder. At higher magnifications, namely 100 kX and 200 kX, we can observe many gray regions. The regions that appear dark (or black on a relative scale) represent clay, which are composed of higher atomic weight elements. On the other hand, the light background represents primarily the polymer. The marker for 100-kX image indicates that the domain size is approximately 80 nm, which corresponds to three laponite particles juxtaposed. The surrounding region entirely consists of polymer. This is good dispersion, considering the fact that we have used melt compounding. The image obtained at 200 kX shows that just one clay particle is being viewed. As evident from the figure, there is a gray region that separates the two dark regions. This could possibly be due to interactions between polymer and the clay, thereby breaking the 25 nm disks into smaller units. This could

however, be a localized case since XRD does not show any evidence of intercalation or exfoliation.

TEM images for the 5 wt % clay nanocomposite show that the domains or agglomerates are much bigger than those found in 2 wt % clay nanocomposite. There is also some stacking of the particles over one other, which was not observed for its lower wt% counterpart. This accounts for the fact that upon visual examination, the 2 wt % clay nanocomposite was almost as clear as PMMA, whereas the 5 wt % clay nanocomposite was translucent. The domain size of 2 wt % PMMA/Laponite JS nanohybrid was around 75 –100 nm, still less than the smallest size discernible to unaided human eyes, which is about 200 nm. An interesting feature of Figure 4.14 is the presence of ridge-like lines. The spacing between these lines is approximately 2-3 nm, while their lateral dimensions are of the order of 25-30 nm. These are possibly due to a stack of clay particles being viewed sideways from the TEM.

Using a slightly higher boiling dispersing agent than water could do an improvement in dispersion. Water boils at 100 ^{o}C, whereas the processing temperatures exceed 150 ^{o}C easily. So, when the clay-dispersion is introduced at the feed zone, the water boils off quickly, leading to agglomeration of particles. Using a higher boiling solvent might ensure that the dispersion stays as a fluid for a longer time inside the extruder.

4.6.5 Nanoindentation

Nanoindentation results shown in Figures 4.15 through 4.18 are in the form of force versus displacement curves. It is necessary to understand what these plots indicate. Firstly, there are two parts for each curve: the ascending part, or the loading region, and then the descending or the de-loading region.

Consider the force versus displacement plot for 250 μN (Figure 4.15). Upon drawing a horizontal line from 150 micronewtons, marking the points where this line intersected the loading region for each material, and dropping perpendiculars from each of these points, displacement for each material could be obtained. This is nothing but the depth of penetration caused by the tip. Figure 4.19 demonstrates the same.

Now, lesser the depth of penetration for a given force, greater is the resistance offered by the material to the penetration of the tip, and consequently, harder that material is. From Figure 4.19 we see that for 150 μN, the displacement for PMMA is about 170 nm, whereas it is 160 nm for PMMA + 2 wt % clay and 140 nm for PMMA + 5 wt% clay.

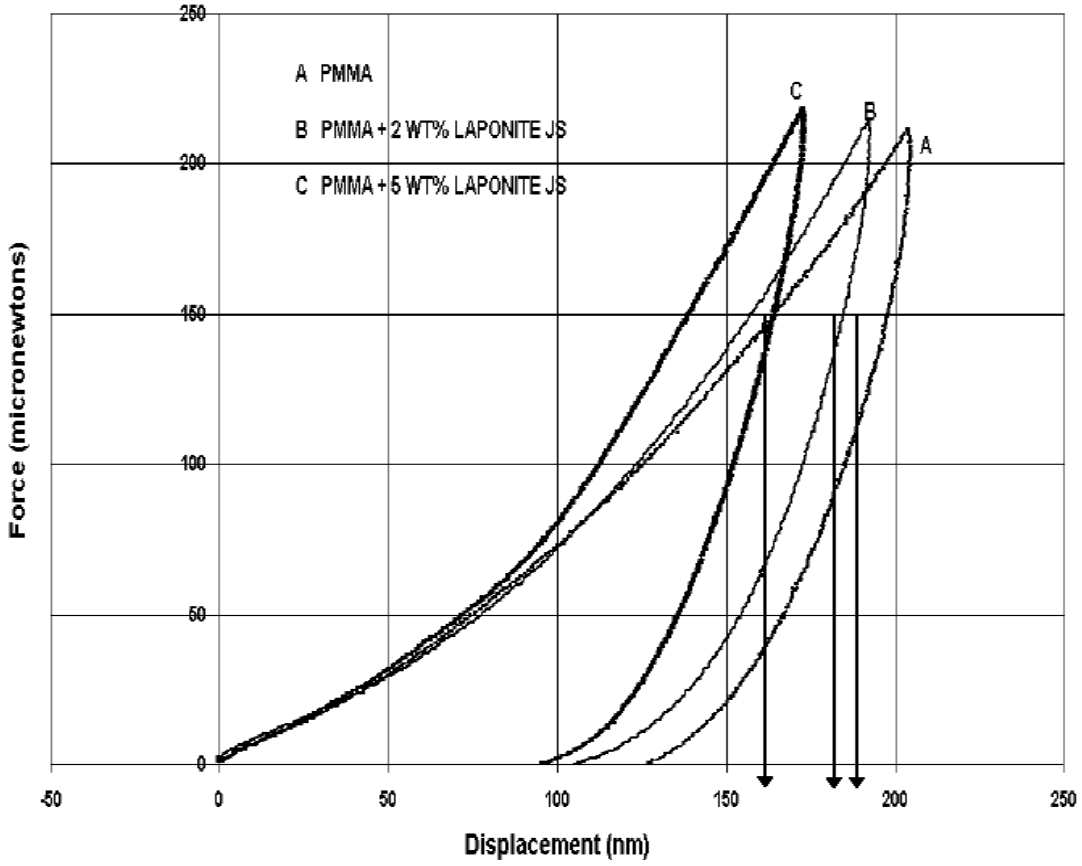

Figure 4.19. Interpretation of nanoindentation data.

Thus, it can be said that the 5 wt% clay nanocomposite is the hardest material out of the three. This is quite expected, since it has maximum amount of clay. Figure 4.20 shows a plot of load versus peak displacement in order to make the interpretation easier.

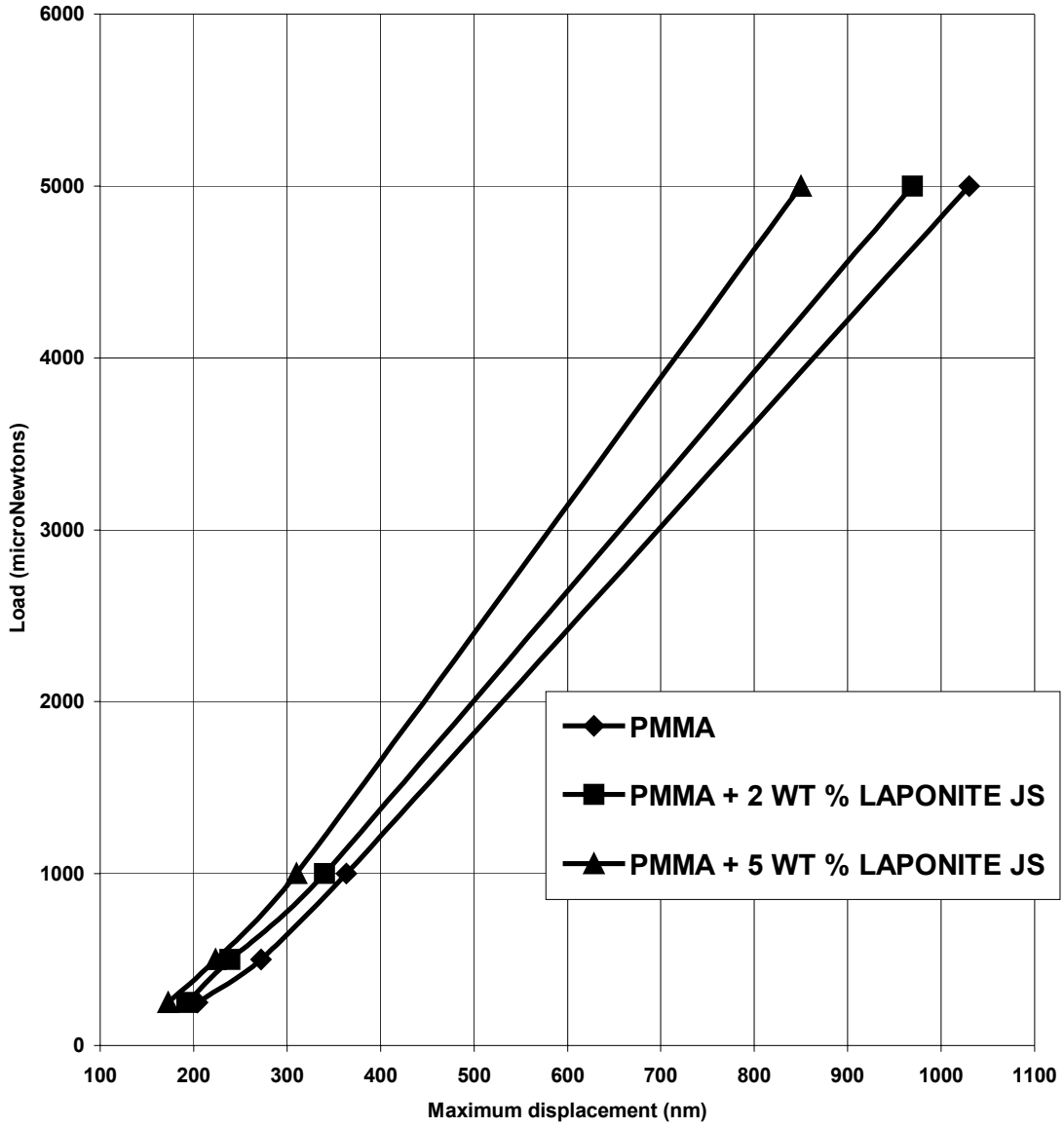

Figure 4.20. Load versus maximum distance penetrated by the tip. The curves show that the nanocomposite containing 5-wt % clay is the hardest material. Force was applied at 100 nN/sec.

From Figure 4.20 it can be seen that the curve for the 5 wt % clay nanocomposite shows least displacement for a given indenting force, suggesting that it is the hardest material. This is, however, a qualitative measure. Table 4.4 shows the peak displacement and force values for different materials at six different indents for each material tested.

4.7 Conclusions

The following can be concluded about the research:

- Nanocomposites of PMMA and synthetic Laponite JS were prepared with 2 and 5 wt% loadings of clay, and were characterized for different properties.
- The 2 wt% nanocomposite looked almost as transparent as PMMA, where as its 5 wt% counterpart appeared translucent. This was explained on the basis of domain sizes of clay particles that aggregated. TEM images help elucidating the same.
- The nanocomposite showed superior mechanical properties, both in terms of modulus and tensile strength. It also showed increased hardness. This was explained on the basis of addition of clay.
- The primary goal of the research, i.e., obtaining optically clear PMMA with enhanced hardness and abrasion resistance was met with some success. These properties were evaluated using nanoindentation technique, which showed significant increase in hardness upon the addition of clay.
- It is suggested that the dispersion of the clay could be improved by the use of a higher boiling dispersing agent.

CHAPTER 5
POLYCARBONATE-FERITE MAGNETIC NANOCOMPOSITES

5.1 Introduction

Polycarbonate (PC) is an engineering plastic. It is a transparent polymer, known for its toughness and excellent optical properties. PC gets its name from the carbonate group that is present in its backbone. Bisphenol A and phosgene chemistry is used for producing high molecular weight PC. Figure 5.1 shows the structure of PC.

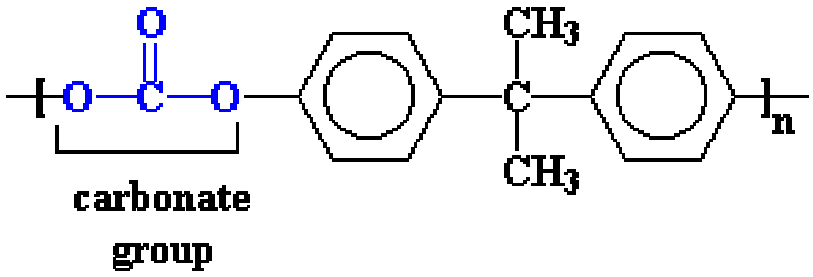

Figure 5.1. Structure of Polycarbonate.

PC is used for making shatterproof windows, lightweight eyeglass and lenses. Besides, blends of PC with ABS (Acrylonitrile Butadiene Styrene terpolymer) find extensive use in a variety of appliances. PC can be made as a thermoplastic or as a thermoset, depending on the chemistry used.

5.2 Research Objectives and Strategy

Cellular phones have become an integral part of our day-to-day lives. They have made communication very easy and have become quite affordable. The use and production of cellular phones have skyrocketed within the last decade, with many technologies focusing on making these cellular phones lighter in weight and smaller in

size. However, the fact remains that the component that accounts for most of their mass is the antenna. This is because it is metallic in nature. Metals have a higher density than polymers. The function of the antenna is to pick up different electromagnetic signals that enable communication. Therefore, it is an indispensable component of a cell phone. However, most of the other components are made out of plastics. For example, the housing is quite often made out of PC/ABS blend. The circuit board is made of epoxy resin. Hence, if we could make the plastic housing magnetic enough to pick up the signals that are normally received by the antenna, tremendous savings in weight of these cell phones could be made.

The objective of this research was therefore, to disperse nano-size, magnetic ferrite particles into a polymeric matrix. The matrix material chosen for this research was PC. This is because it is a transparent polymer, and is also a key plastic used in making the housings. Further, the optical clarity of the resulting nanocomposite serves as a guide for determining the extent of dispersion of these nanoparticles. Poly (Vinyl Alcohol) (PVA) used for this research was supplied by Aldrich Chemicals and had a molecular weight of about 13,000 – 23,000and it was 87-89% hydrolyzed. The role of PVA is expected to be similar to that of a compatibilizer. It can interact with both ferrites and PC, due to its polar character. Figure. 5.5 shows the interactions envisioned between PC, PVA and ferrites

5.3 Materials

GE Plastics supplied the PC required for the research, under the trade name Lexan®. The name of the product was 123R. Table 5.1 lists some of its properties.

Table 5.1. Properties of Lexan.

PROPERTY	VALUE	UNIT	METHOD
MECHANICAL			
Tensile Stress, yield	9000	psi	ASTM D 638
Tensile Stress, break	9500	psi	ASTM D 638
Flex Stress, yield	13500	psi	ASTM D 790
Hardness, Rockwell M	70	-	ASTM D 785
Taber Abrasion, CS-17, 1 kg	10	MG/1000cy	ASTM D 1044
Izod Impact, notched, 73 ^{o}F	13.0	ft-lb/in	ASTM D 256
THERMAL			
Vicat Softening Temp, Rate B	310	^{o}F	ASTM D 1525
HDT	280	^{o}F	ASTM D 648
Thermal Conductivity	0.19	W/m- ^{o}C	ASTM C 177
PHYSICAL			
Specific Gravity, solid	1.20	-	ASTM D 792
Water Absorption, 24 hours @ 73 ^{o}F	0.150	%	ASTM D 570
Melt Flow Rate, 300C/1.2 kgf	17.5	g/10 min	ASTM D 1238
OPTICAL AND ELECTRICAL			
Light Transmission, 0.100"	88.0	%	ASTM D 1003
Haze, 0.100"	1.0	%	ASTM D 1003
Refractive Index	1.586	-	ASTM D 542
Dielectric Strength, in air, 125 mils	380	V/MIL	ASTM D 149
Dielectric Constant, 1 MHz	2.96	-	ASTM D 150

The nano size ferrite particles for this research were synthesized at the Department of Materials Science and Engineering, University of Florida. Several methods have been reported for synthesis of nanoparticles, such as sol-gel processing [153-154], irradiation [155-156], hydrothermal synthesis [157-158], co precipitation [159-161], aerogel techniques [162-163], mechanical methods [164-165], as well as other techniques [166-172].

The ferrite nano particles for this research were prepared by using a co-precipitation method. The starting materials were:

$Fe(NO_3)_3.9H2O$ = 12.12 g

$Ni(NO_3)_3.6H2O$ = 2.18 g

$Zn(NO_3)_2.6H2O$ = 2.23 g

50% NaOH & Deionized (DI) water (150 ml).

The salts were taken in a small round-bottomed flask with three openings, one for adding DI water and NaOH solution, second for inserting the thermometer and the other for inserting the pH meter. After adding the salts into the flask, 150 mL of DI water was poured into the same. This flask was now placed in a water bath. From then onwards, the flask was stirred magnetically at all times. The water bath was maintained at 70 ^{o}C. After ensuring that the temperature was constant at 70 ^{o}C, the pH meter's probe was inserted into the round-bottomed flask. Next, NaOH solution was added drop wise till the pH reached a value of 11. Now, the mixture was allowed to stir magnetically for 1 hour. After an hour, the flask was taken out of the water bath. The ferrite nanoparticles were separated from the NaOH solution using centrifugation The centrifuge used was an Eppendorf Centrifuge 5810 machine with interchangeable swing-bucket and high-speed

fixed-angle rotors for spinning micro centrifuge tubes. The speed used was 6000 rpm and the time for centrifugation was 5 minutes. The separated ferrite nanoparticles were re-dispersed in DI water.

Junyeon Hwang, who performs research for Professor Darryl P Butt at the department of Materials Science and Engineering, University of Florida, characterized these nanoparticles.

The primary purpose of characterization was to obtain the particle size distribution of the nanoparticles. However, the microstructure of these nanoparticles was also examined using Scanning Electron Microscopy and X-Ray Diffraction. Figures 5.2 through 5.4 show the results obtained. It seen from these figures that the particles have a size distribution ranging from 0.05μ to 1μ. The mean particle size was found to be 200 nm. XRD showed that the nanoparticles had a crystal lattice parameter of 8.3688 Å. The SEM image also shows that the particles are small in size and have a particle size distribution. Visual inspection revealed that these nanoparticles were brown in color. So, it was expected that the nanocomposites to have a brown tinge associated with them.

5.4 Processing of nanocomposites

Several papers on composites of ferrites with polymers have been published. Most of them report solution based processing techniques [173-175]. Mohammed et al. reported a melt processing technique for preparing natural rubber-ferrite composites using a brabender [176]. The nanocomposites for this research were prepared by melt compounding using a 30 mm APV co-rotating twin crew extruder, with 8-zone temperature settings. The temperature range used was 230 °C (feed zone) to 255 °C (die zone).

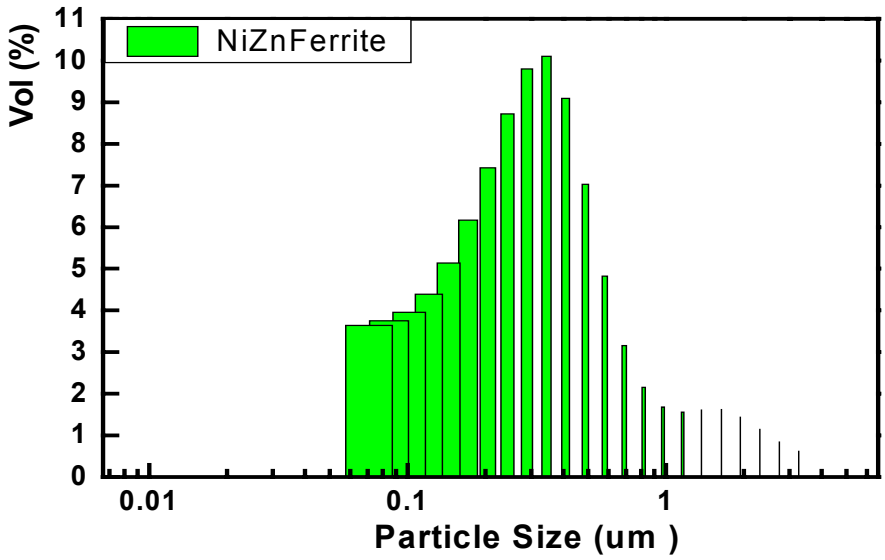

Figure 5.2. Results of particle size distribution of as-synthesized by particle size analyzer (UPA). It is measured after high power (650 W) ultrasonication for 10 min.

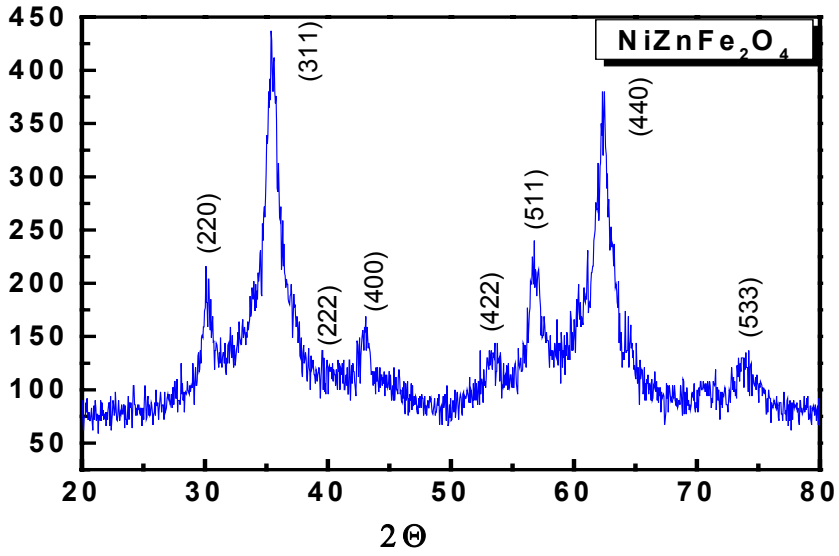

Figure 5.3. XRD patterns of $NiZnFe_2O_4$ after drying at 60 ^oC for 3 hours in oven. Lattice parameter, a = 8.368 Å.

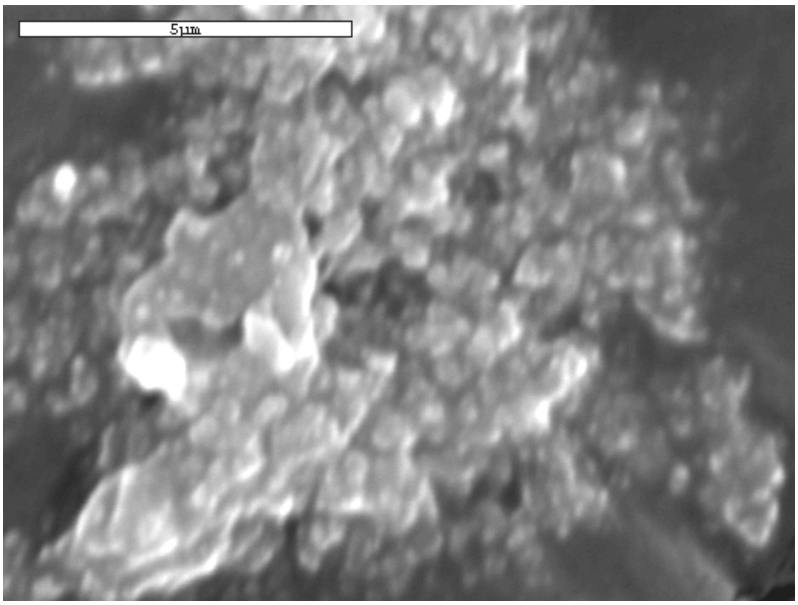

Figure 5.4. SEM image of Ni-Zn Ferrite after$_3$ drying at 60 ℃ for 3 hours in oven.

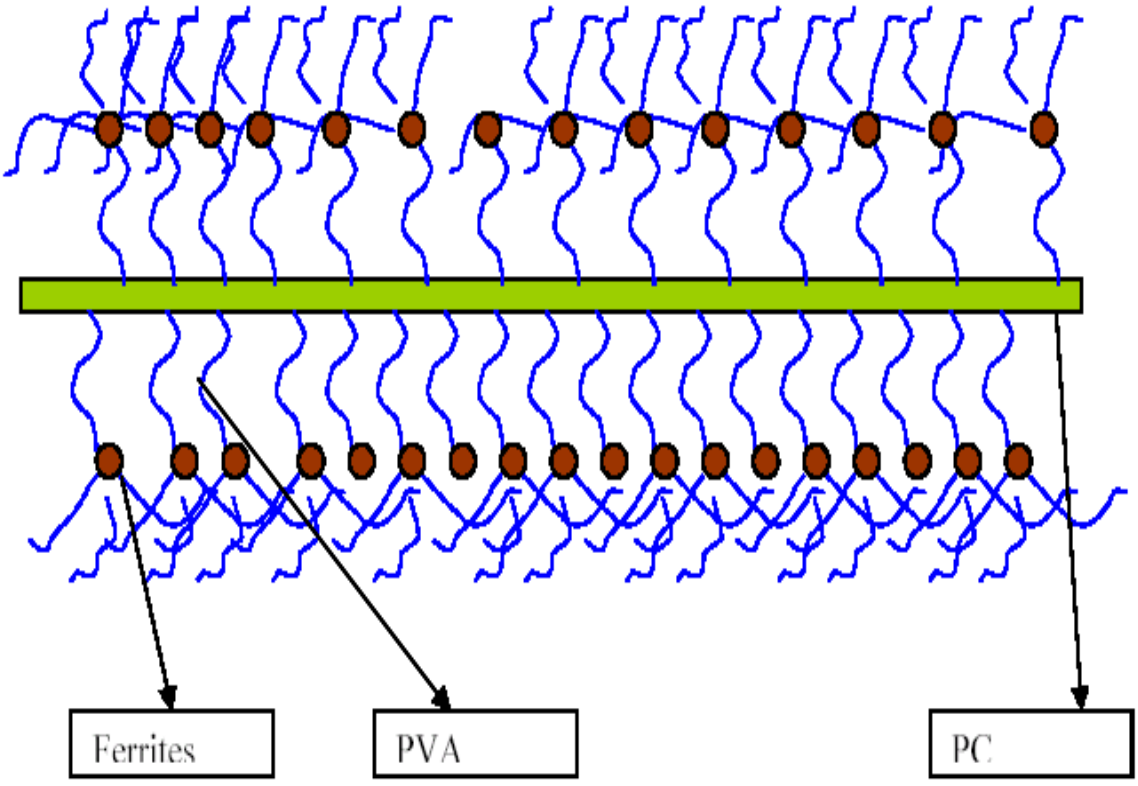

Figure 5.5. Proposed role of PVA in the formation of PC/ferrite nanocomposites.

The screw L/D was 40.The PC pellets were dried in an air-circulating oven for 24 hrs. at 85 ^{o}C prior to melt compounding. Table 5.2 shows the temperature settings in each zone. Figure 5.6 shows the operation in the form of a block diagram.

Table 5.2. Temperature settings in temperature zones of the twin-screw extruder.

Zone	Temperature (^{o}C)
Zone 1 (Feed Zone)	230
Zone 2	235
Zone 3	237
Zone 4	240
Zone 5	245
Zone 6	247
Zone 7	250
Zone 8 (Die Zone)	255

5 c.c (equivalent to 5 grams of the nanoparticles) of the ferrite nanoparticles dispersion was taken in a measuring cylinder. This was added to an aqueous solution containing 15 g of PVA (Poly Vinyl Alcohol). The dispersion was magnetically stirred for 1 hour. For melt compounding of PC with the PVA coated ferrite nanoparticles, the mass feed rate of PC used was 42 grams/min. About 500 grams of PC was used. The ferrite/PVA dispersion was introduced at the feed zone of the extruder. The screw rpm was 125. The extruded strands were pelletized and dried in an air-circulating oven for 24 hours at 75 ^{o}C. Pure PC was also run through the extruder under the same processing conditions to ensure uniform thermal history for all materials.

5.5 Characterization

In this section, the examination of mechanical behavior, thermal behavior, microstructure and extent of dispersion of ferrite nanoparticles is discussed. The following techniques were employed to investigate the same:

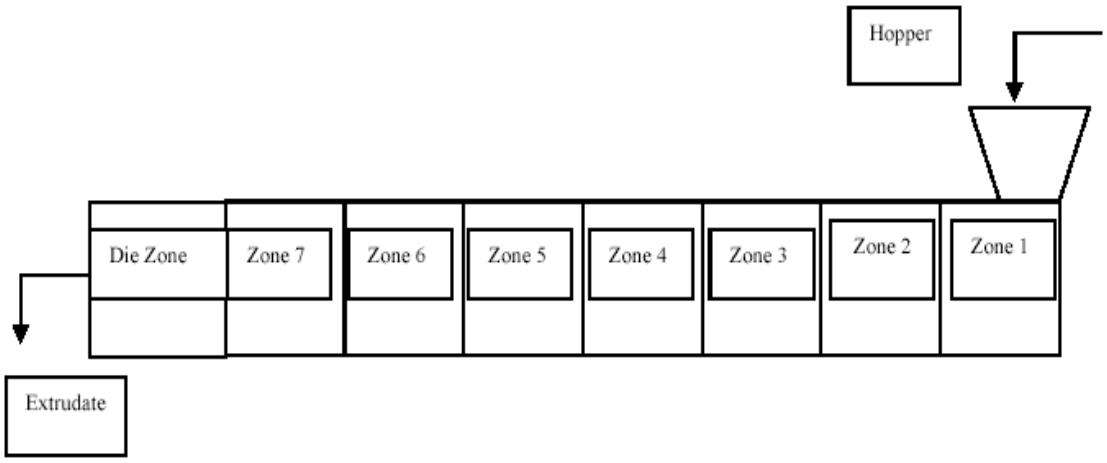

Figure 5.6. Block diagram for the processing of PC/Ferrite nanocomposites.

- Tensile testing
- X-Ray Diffraction
- Differential Scanning Calorimetry
- Transmission electron microscopy
- SQUID magnetometer

5.5.1 Specimen preparation

Specimens were prepared using compression molding. Compression molding is a process in which a polymer is made to take the shape of a mold by pressing it between two heated plates. The heat melts the polymer (if semi-crystalline) or takes the polymer chains well above the glass transition temperature (if amorphous). The press used for compression molding was a Carver, model C-81000-141 press.

In order to prepare the specimens, the press was first heated to 450 ^{o}F. The mold used was square in shape, with dimensions of 70 mm X 70 mm X 0.8 mm. The mold was placed on a metal plate covered with Teflon® coated aluminum foil. The mold was then filled with dried pellets. This plate with mold and the pellets was placed on the bottom plate of the press. Another Teflon® coated aluminum foil covered metal plate was placed on top of the mold bearing plate, to give a sandwiched assembly. The bottom plate of the

press was raised until the assembly just touched the top plate of the press. The pellets were then allowed to convert into a liquid state by heat transfer from the press. This took about 5-6 minutes. After that the pressure of the system was raised to 10, 000 psi. Initially, due to resistance offered by the liquid polymer as well relatively incomplete conversion to liquid, the pressure dropped below 10,000 psi. Under these circumstances, it was necessary again to raise the pressure to 10,000 psi. This was repeated until the pressure attained a steady value of 10,000 psi. The pressure could be measured using a gauge attached to the press. A pressure of 10, 000 psi. on the gauge corresponded to 9302 psi. on the sample. This was calculated using the formula:

$$Ps \times As = Pg \times Ag \qquad \text{(Equation 5.1)}$$

Where, Ps = Pressure on the sample

As = Cross sectional area of the sample

Pg = Gauge pressure

Ag = Cross sectional area of the piston of the press.

As $= 4900\ mm^2$

Ag $= 3.14. (3^2)/4$

Pg = 10, 000 psi.

After the gauge pressure became steady at 10, 000 psi., the mold was allowed to rest at the abovementioned temperature and pressure for 10 minutes. After that, the heat supply to the press was turned off. The mold was allowed to cool to ambient temperature. The mold containing the solidified sheet was taken out.

These sheets served as specimens for all the characterization techniques.

5.5.2 Tensile Testing

Tensile testing enables us to evaluate the mechanical response of the materials to a known strain or deformation rate. This gives us a plot of stress versus strain from which we can obtain a wealth of information such as the brittle or ductile behavior, tensile modulus or an indication of stiffness of the material, tensile strength etc. Tensile testing was carried out using an EnduraTEC ELF 3200 series machine. It consisted of the following components:

6. The linear motor assembly: Had a patented high-bandwidth, low-distortion actuator from Bose Corporation.

7. Testing Chamber: Had facilities for introducing hot air, for increasing temperature as well as introducing liquid nitrogen. A bulb for viewing the test in case liquid nitrogen made the chamber cloudy was also provided. The door had a transparent section for viewing testing while under progress. There were two sets of grips. The bottom grip was stationary and was connected to the load cell. The upper grip was mobile and its motion was regulated by the Wintest® software, and ultimately, the linear motor.

8. Temperature Controller: With the help of the software, temperature could be varied between –50 ^{o}C to 150 ^{o}C.

9. Controller box, which acted as an interface between the computer and the machine itself.

The deformation rate used was 0.05 mm/sec., and the testing temperature was 30 ^{o}C. Figure. 5.7 and Table 5.3 show the results obtained from tensile testing.

Table 5.3. Tensile modulus of PC and PC/Ferrite nanocomposite.

MATERIAL	MODULUS (N/mm^2)
PURE PC	1604.4
PC/FERRITES/PVA	1742.8
PC/FERRITES	2100

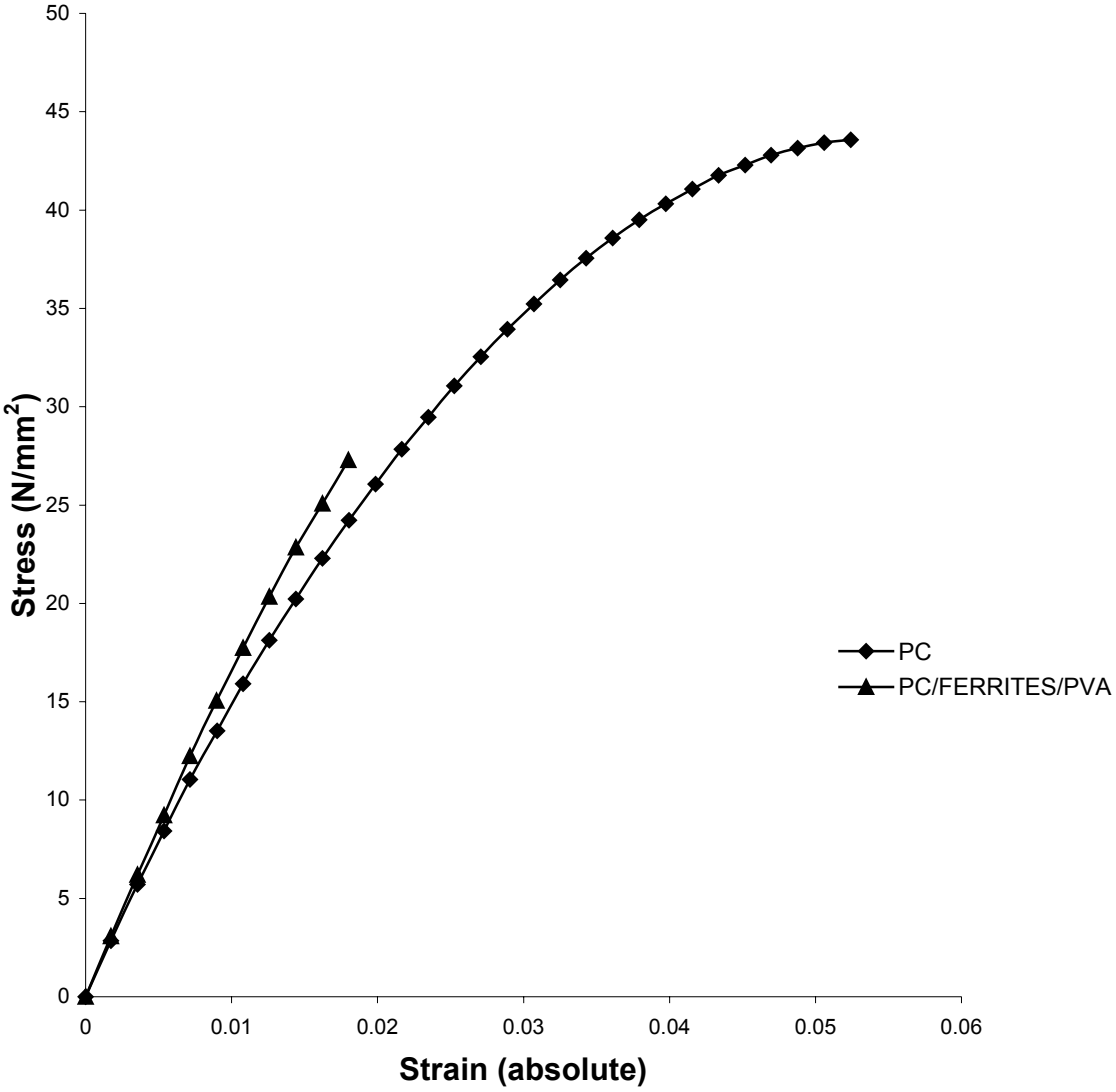

Figure 5.7. Tensile test comparisons at 0.05 mm/sec., 30 ^{o}C. All samples tested showed failure.

5.5.3 X-Ray Diffraction

XRD was performed using a Philips APD 3720 instrument. The objective was to investigate shifts in peaks associated with ferrite nanoparticles, giving an indication of interactions between PVA, ferrites and PC. The range of angles swept was 0-75 degrees. Reflective mode was used and the temperature was 15 ^{o}C. Figure 5.7 shows the results obtained.

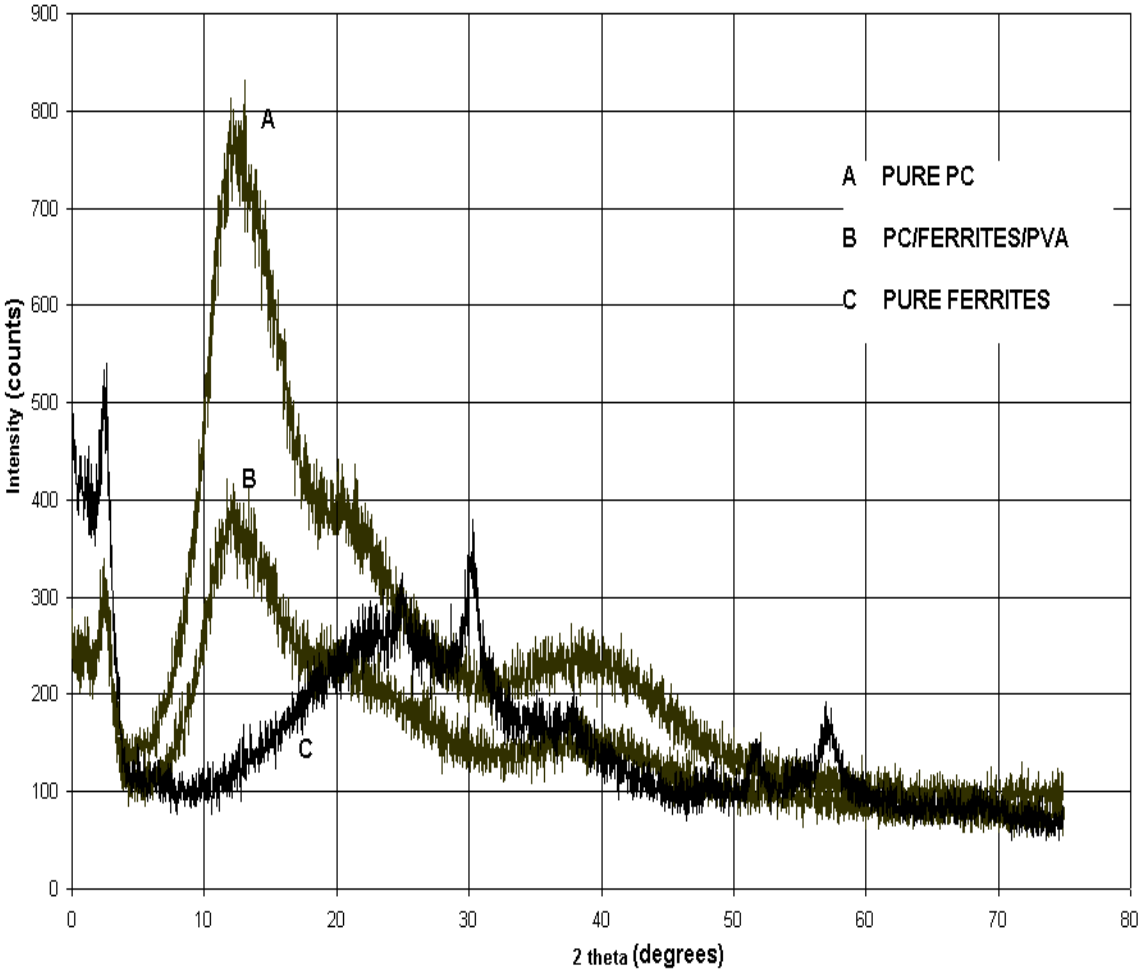

Figure 5.8. XRD patterns for PC and PC/Ferrite nanocomposite using reflective mode at 15 ^{o}C.

5.5.4 Differential Scanning Calorimetry (DSC)

DSC describes the behavior of a material when subjected to heat at a controlled rate. This enables us to determine different transitions associated with the polymer such as glass transition, melting transition, besides crystallization behavior etc. DSC on the samples was performed using a ThermoHaake DSC 220 C model instrument. Heating rate used was 10 ^{o}C/minute, while cooling rate was 50 ^{o}C/min. Two sweeps of this thermal treatment were performed. The output of the instrument is a plot between heat supplied in microwatts versus temperature. The heat supplied is directly proportional to

the specific heat of the material being tested. Figure 5.9 shows the results obtained from DSC. It is noteworthy that in this case, obtaining cooling thermograms was not necessary, because PC is an amorphous polymer, and therefore, does not crystallize.

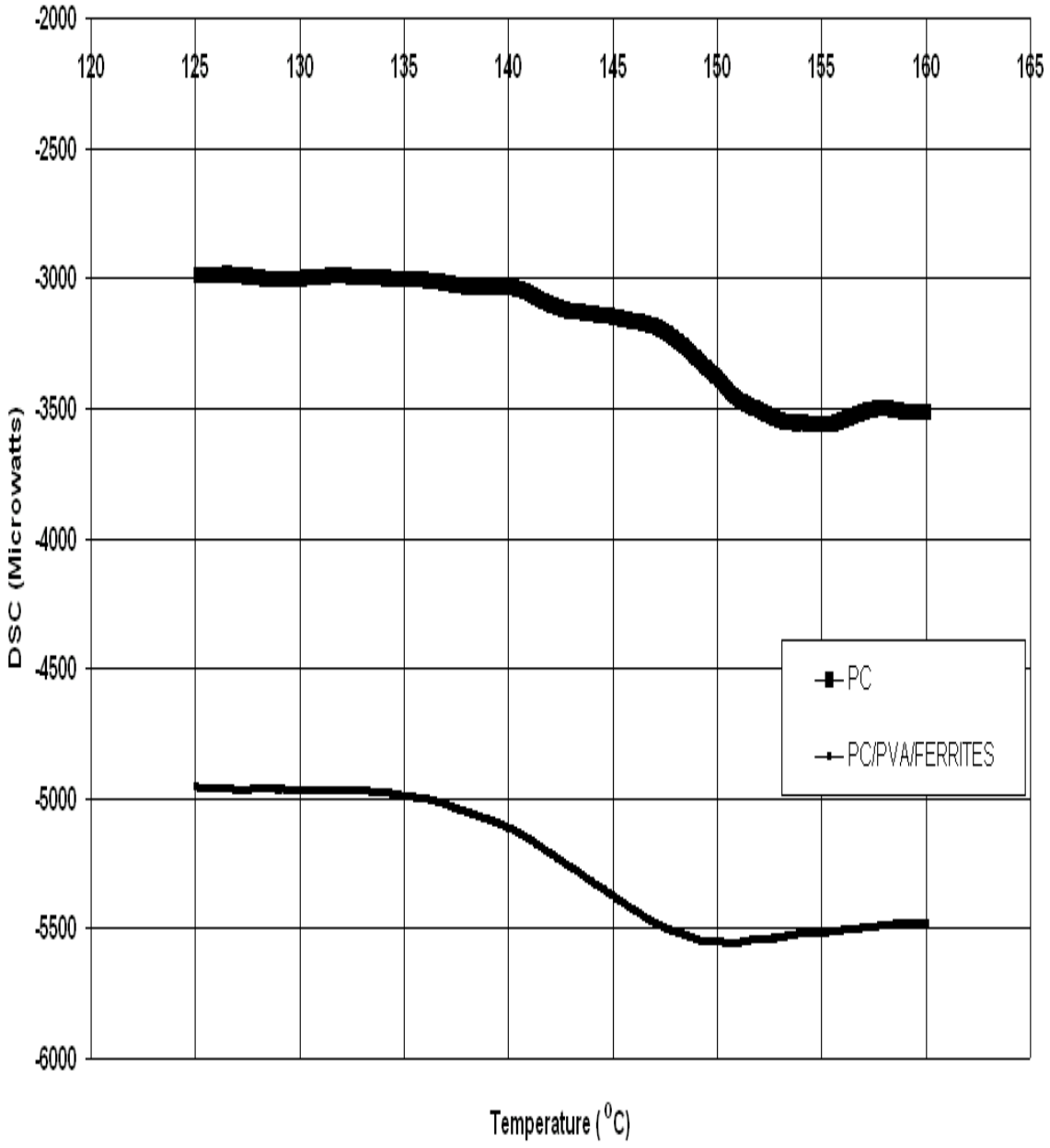

Figure 5.9. DSC thermograms for PC and PC/PVA/ferrite nanocomposite. Heating rate =10 ^{o}C/min., cooling rate = 50 ^{o}C/min.

5.5.5 Transmission Electron Microscopy (TEM)

Transmission electron microscopy was performed on the nanocomposites using a JEOL 200 CX TEM instrument. It had a tungsten based thermionic gun. TEM images usually complement XRD data and also enable us to view details on a nanometer scale.

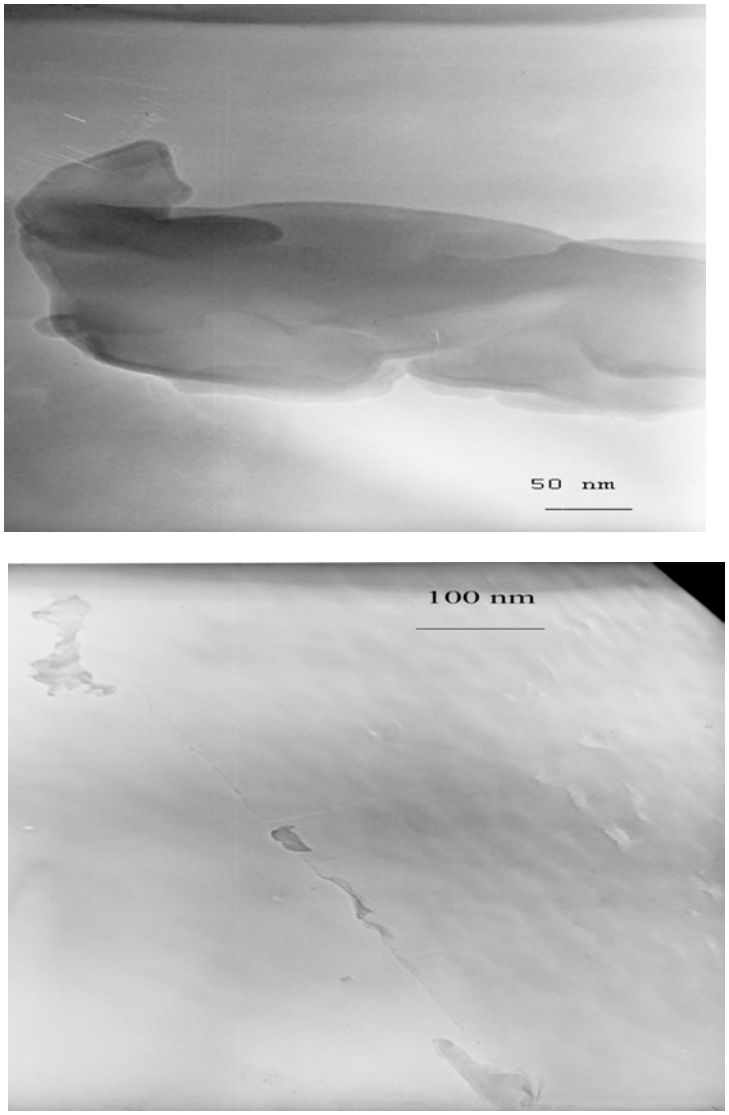

Figure 5.10. TEM images of PC/PVA/Ferrite nanocomposite.

Figure 5.10 shows the TEM images for PC/PVA/ferrites nanocomposite. We can actually *see* the polymer and the ferrite nanoparticles and therefore, obtain an idea of

dispersion and distribution of the nanoparticles. However, it should be noted that this technique gives image of a very small section of the material.

5.6 Discussion of Results

Having characterized the materials, it was attempted to interpret the results and study the phenomena that possibly occurred in these materials, on a macroscopic as well as microscopic level.

A few points were worth noting. The melt viscosity of PC/PVA/Ferrite nanocomposite was unusually low in comparison to pure PC. This was suspected to be due to degradation of PVA. So, it was thought that if this were the case, then the composite without any PVA would exhibit a melt viscosity similar to that of pure PC. Hence, another sample containing PC and ferrite nanoparticles, without PVA was prepared under identical conditions of processing, described earlier, and was designated as PC/ferrites. This product had a slightly lower viscosity than pure PC. This was speculated to be due to alignment of particles in the shear field. Such observations have been reported for polymer silicate nanocomposites [177]. Another sample with PC/PVA without any ferrites was also processed under identical conditions. It was found to be brown in color. Thus, our hypothesis was confirmed.

5.6.1 Tensile Testing

Figure 5.7 shows the tensile behavior of both materials, namely PC and PC/PVA/ferrite nanocomposite. From Table 5.3, we can infer that the nanocomposite has a slightly higher modulus and exhibits much brittle behavior in comparison to the pristine polymer, i.e. polycarbonate. This can be explained by the addition of two new phases, namely low molecular weight PVA and ferrites, both contributing to brittle behavior.

This would explain the increased modulus. However, PVA is expected to have poor mechanical properties in comparison to ferrites and PC. So, it can be inferred that if there were no PVA, then the composite should exhibit a higher modulus value and more brittle behavior than if PVA were present. Figure 5.11 shows the results of tensile tests, performed on PC/ferrites under identical conditions and is compared with other materials.

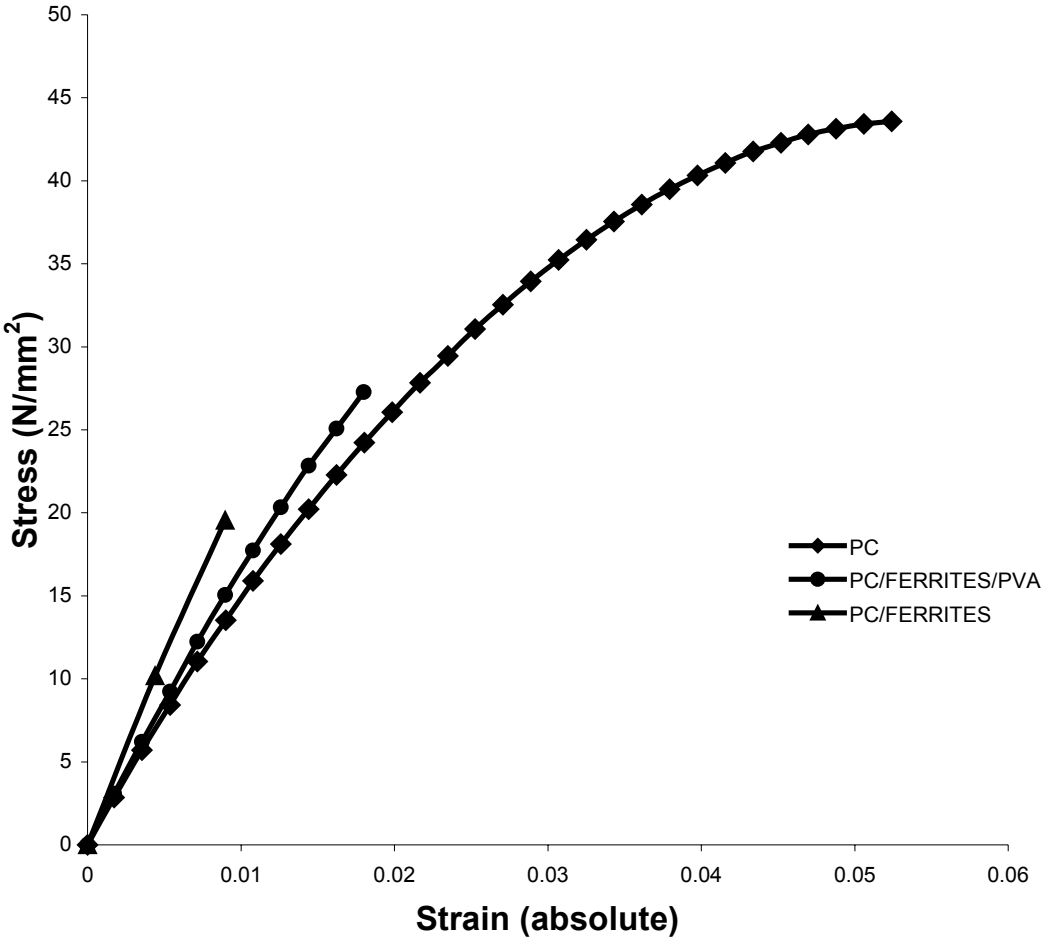

Figure 5.11. Stress strain comparisons for PC/Ferrites with and without PVA, at 0.05 mm/sec., 30 ^{o}C. All samples tested showed failure.

It shows that PC/ferrites had the greatest modulus and was most brittle. This again, confirmed our hypothesis. Table 5.3 also shows the modulus value for PC/ferrites, which is 30.8% greater than pure PC and 20.5% greater than PC/PVA/ferrites. This shows that

the addition of PVA serves to reduce the tensile modulus, or in other words it tends to make the tensile behavior more ductile. This is also indicated by the lower strain to failure for PC/ferrites in comparison to PC/PVA/ferrites.

5.6.2 XRD

XRD patterns (Figure 5.8) showed that the high angle peaks for pure ferrites, at ca 52 degrees and ca 58 degrees disappear in the nanocomposite. This indicates some interaction between the polymers and the nanoparticles, and possibly that significant dispersion of the nanoparticles has been achieved.

TEM images support this observation, and these are discussed in a later section. XRD analysis was also done for PC/Ferrites. Figures 5.12 and 5.13 present the results obtained.

It was observed from Figure 5.12 that the higher angle peaks disappear. But Figure 5.13 showed that the peak at ca 25 degrees has not disappeared completely in PC/Ferrites. On the other hand, in the nanocomposite containing PVA, this peak disappeared completely.

This indicated that the extent of interaction between the components is better in case of PC/PVA/ferrites. This could also possibly mean that the dispersion of ferrite nanoparticles is also better for PC/PVA/ferrites. This could also explain the fact that the physical appearance of PC/Ferrites was much darker than the nanocomposite containing PVA. TEM analysis was performed in order to confirm these findings further and the results are discussed in a later section.

5.6.3 DSC

From Figure 5.9, it was seen that Tg of the nanocomposite PC/PVA/ferrite was slightly lower than pure PC. One possibility is that two new phases have been added to

PC. First being the ferrite nanoparticles, which do not show any transitions within the given temperature range, and the second being the low molecular weight PVA.

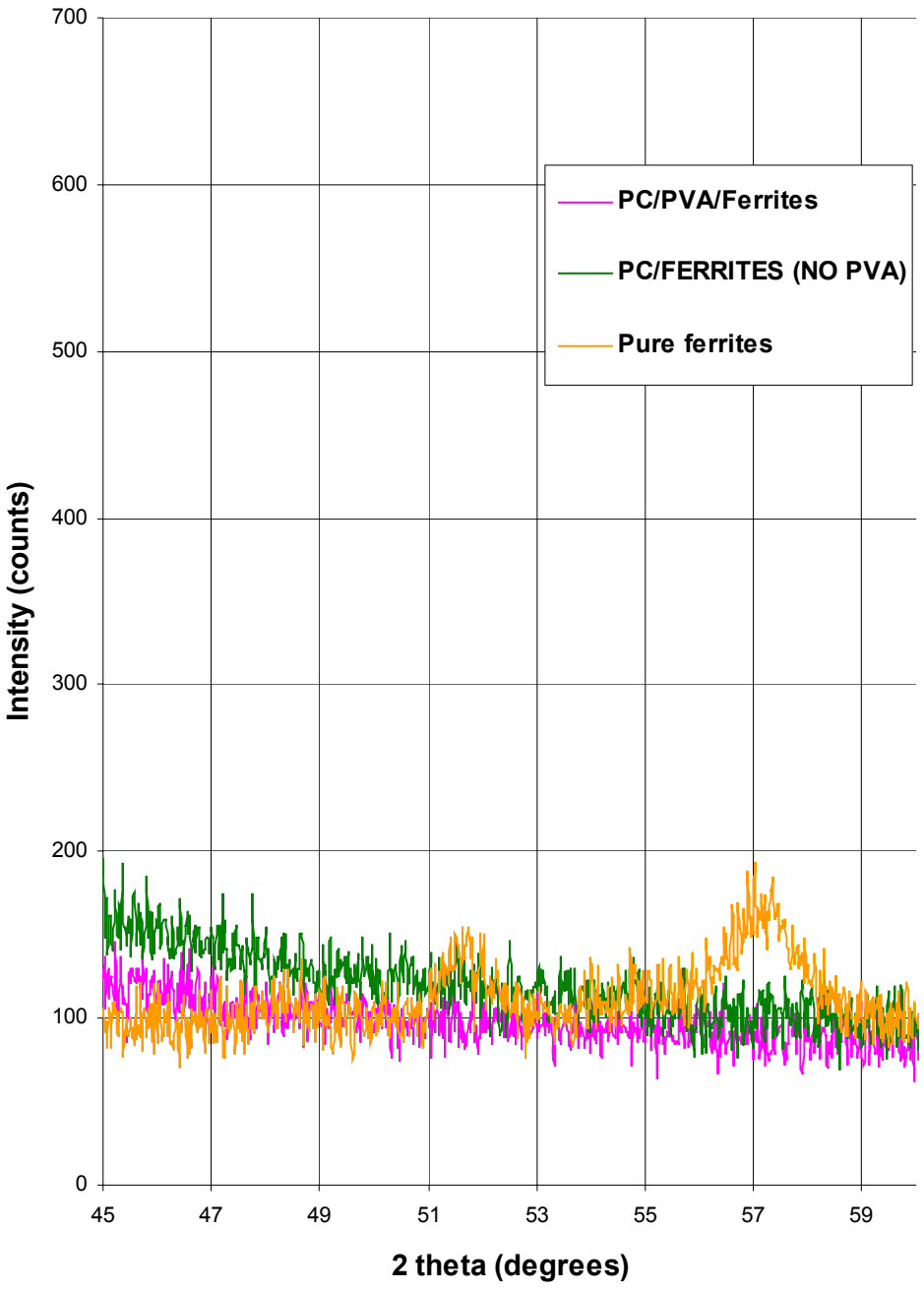

Figure 5.12 High angle XRD region for various nanocomposites using reflective mode at 15 ^{o}C.

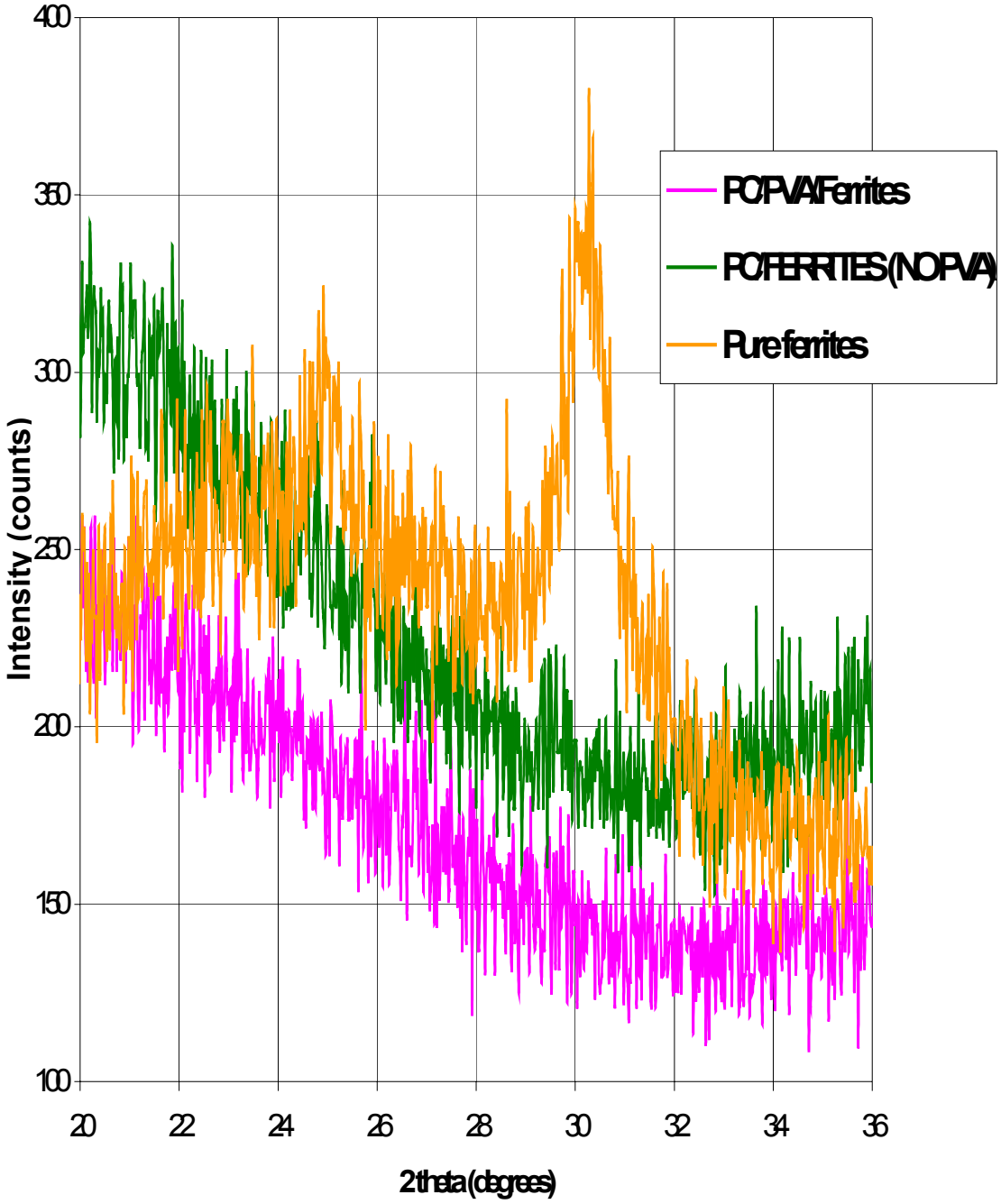

Figure 5.13. Lower angle region for various nanocomposites using reflective mode at 15 ^{o}C.

These chains are much easier to move than the bulky and stiff backbone chains of PC, and also have much higher free volume associated with them than PC, due to lower

molecular weight. This is because lower molecular weight translates into greater number of chain ends per unit volume. Also, degradation of PVA was suspected, leading to higher free volume due to creation of low molecular weight species. Thus, the Tg of the composite decreased.

However, the Tg of PC/ferrites was found to be almost same in comparison to PC/PVA/ferrites. It is seen that this decrease is approximately 5 degrees, as seen from the DSC thermograms (Figure 5.9).

No concrete explanation could be provided but Jiang et al. reported such a lowering in Tg for PC/potassium titanate whisker composites using different coupling agents by [178].

They suggested that such a lowering could occur due to lowering in the overall number average molecular weight. They also proposed that the whiskers and the coupling agent synergistically acted to degrade PC. But in their research, the filler content was much higher (about 10-15% by weight). In this case the amount of filler is quite low (1 % by weight).

Another observation was made regarding the heat required for transition (which is an indication of specific heat). The heat required for PC was highest among all the materials. This is expected because PC also has the highest specific heat.

However, the low molecular weight PVA and ferrites have a much lower value of specific heat. So it is possible that upon adding them, the heat required for transition for nanocomposites decreased. The observation that the heat requirement for PC/PVA/ferrites was higher than PC/ferrites could be possibly due to the presence of PVA, which could tie the ferrites and PC together.

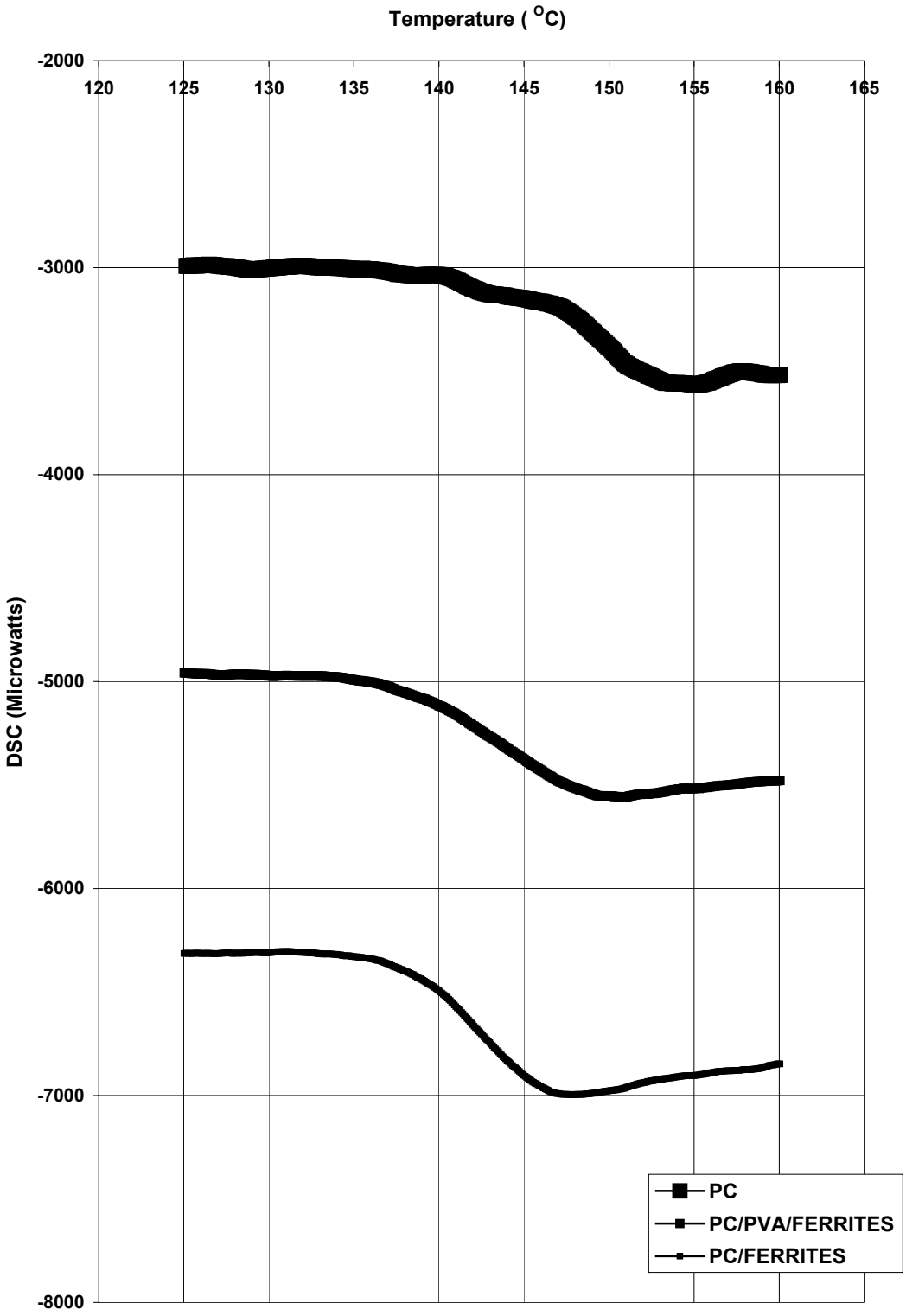

Figure 5.14. DSC Thermograms for PC and various nanocomposites. Heating rate = 10 ^{o}C/min., cooling rate = 50 ^{o}C/min.

5.6.4 TEM

TEM images shown in Figure 5.10 indicate that the particles are well dispersed and the domains are quite small in size. At many places they are certainly smaller than 100 nm (Figure 5.10 (b)), whereas at some other regions, they can get as big as 200 nm (Figure 5.10 (a)). After the interesting observation was made regarding the melt viscosity of PC/PVA/Ferrites, the material labeled PC/Ferrites was prepared and characterized for different properties. TEM analysis was also performed on the same. Figures 5.15 and 5.16 show the images.

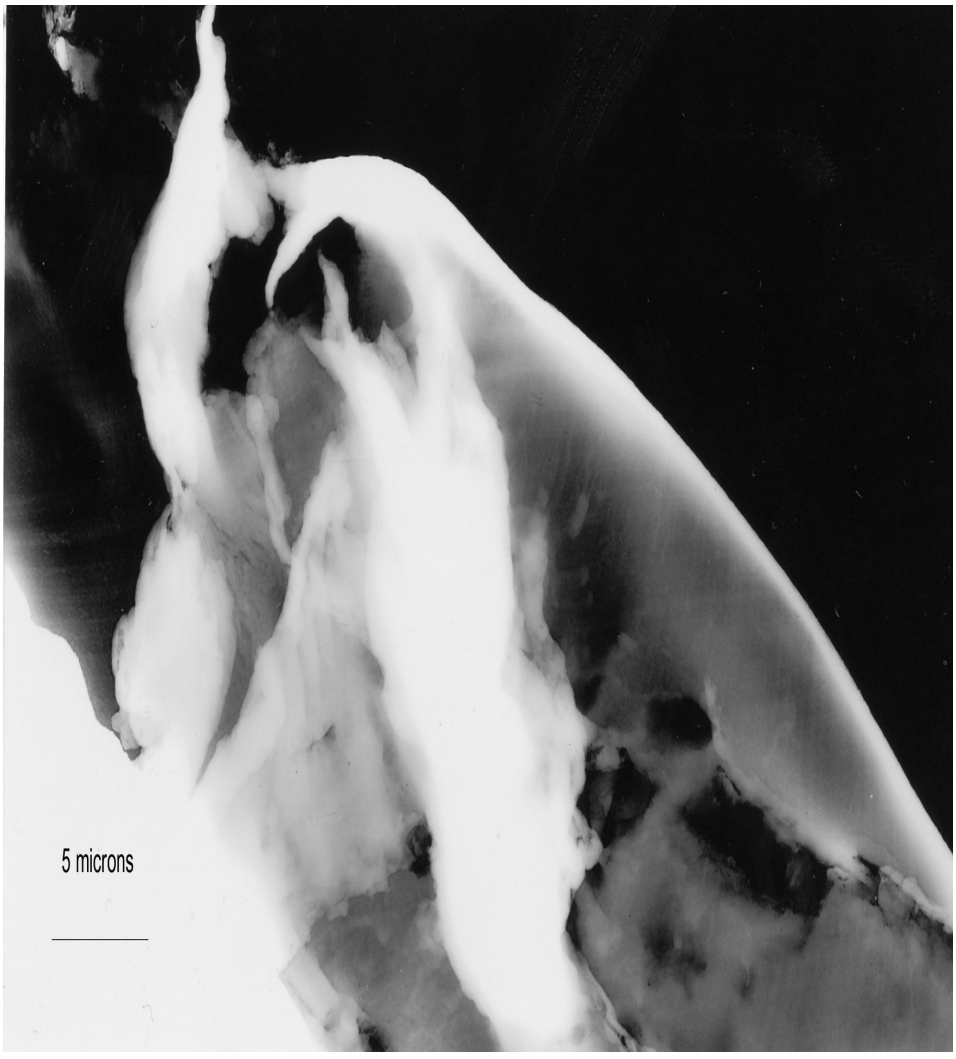

Figure 5.15. Dark Field TEM micrographs of PC/Ferrites, without PVA

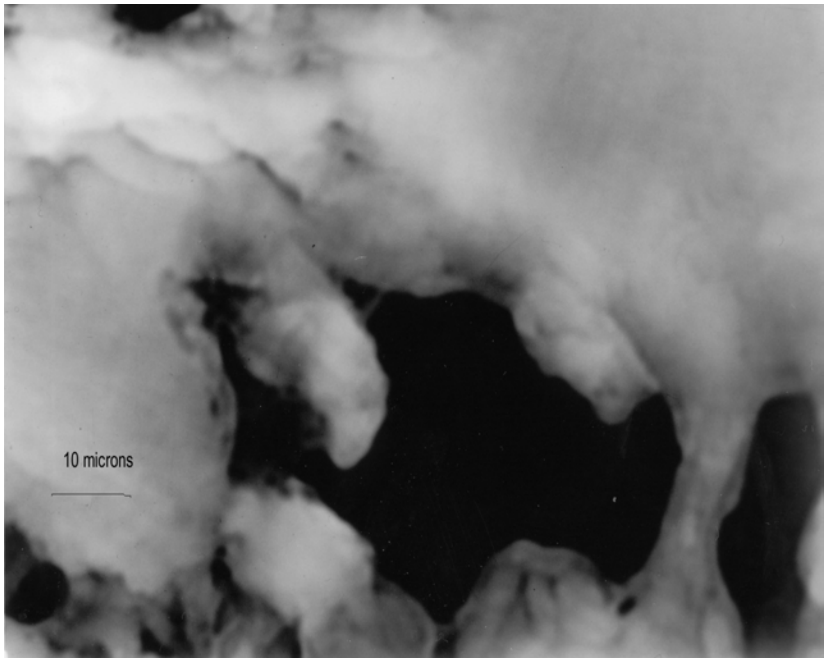

Figure 5.16. Dark Field TEM micrographs of PC/Ferrites, without PVA at a lower magnification.

It should be noted that these images are dark field TEM images. This means that here, instead of direct beam, the diffracted beam is imaged. Thus, the nanoparticles, due to crystalline morphology, appear bright whereas PC being amorphous appears dark.

From Figures 5.15 and 5.16, it can be said that the domain sizes are bigger in case of PC/Ferrites than in PC/PVA/Ferrites. Hence, even though addition of PVA has a deleterious effect on the mechanical properties of the nanocomposite, it is still necessary to obtain good dispersion and distribution.

5.6.5 SQUID Magnetometer

The materials, namely PC, PC/PVA/Ferrites, and PC/Ferrites were characterized with a SQUID magnetometer at Physics Department, University of Florida. Professor Mark Meisel and J. H Park performed the characterization. The results showed that both

PC/PVA/Ferrites and PC/Ferrites were magnetic in nature [Park, J.H., Meisel, M., 2003. Private unpublished communication].

5.7 Conclusions

From the research performed on PC/ferrite nanocomposites, the following can be concluded.

- Magnetic nanocomposites with optical clarity comparable to that of pure PC were prepared.
- A species that interacts with both ferrites and PC is necessary in order to prevent agglomeration of ferrite nanoparticles that leads to the formation of large domains. Such a molecule used for this research was PVA.
- Such a molecule may tie the filler and the matrix together. A similar theory has been proposed for the role of PVA, but it hasn't been confirmed.
- Different characterization techniques were performed on the nanocomposites and an insight into their microstructure was obtained. It was found that the nanocomposites exhibited more brittle behavior than pure PC.
- SQUID magnetometer studies showed that the resulting nanocomposites were magnetic in nature.

CHAPTER 6
FUTURE RESEARCH

6.1 Introduction

This chapter outlines the plans for various experiments and strategies for acquiring a better insight into existing studies as well as exploring novel avenues for the application of polymer nanocomposites. Also included are short notes on recycling ground fiberglass and impact modified fibers. These ideas were inspired from some of the strategies employed in previous research. As far as clay nanocomposites are concerned, prime focus would be on PP/clay nanocomposites. This is because PP is a commercial plastic used over a wide range of applications. It is quite inexpensive as well.

6.2 Polypropylene/Clay Nanocomposites

The following studies would help elucidating the structure-property relationships in PP/clay nanocomposites:

1. To study the effect of processing parameters such as temperature, screw speed etc.
2. To study the effect of molecular weight of compatibilizer.
3. To study the effect of extent of maleic anhydride grafting on the morphology and properties of nanocomposites.
4. To compare PP backbone chains modified with functional groups through reactive extrusion with blends of PP and maleic anhydride modified PP as matrix materials for PP/clay nanocomposites.
5. To study the effect of different surface modifications on clay surface on the properties and structure of nanocomposites.

6.3 Impact Modification of Nanocomposites

Prime focus would be on designing novel processing protocols for improving the impact properties of polymer/clay nanocomposites. For example, in the previous research (Chapter 3), the low molecular weight, end functionalized elastomer was added to Epolene. A modification would be to dissolve it in xylene and add it to the clay. This may result in intercalation of the oligomeric chains inside the clay galleries. This might eventually result in exfoliation of the clay platelets upon adding polymer and compatibilizer.

6.4 Polymer/Nanoclay Modified Cement

Cement is a fundamental construction material used for a variety of structural applications. It is known that cements have excellent compression strength. However, they do not have an excellent tensile strength. They exhibit a brittle behavior. It is proposed that by exfoliating montmorillonite clay with the help of a polymer, ductile cements may be prepared that may be possibly used for construction applications where resistance to high velocity projectiles or high seismic shocks is required.

However, cement is completely inorganic. Introducing organically modified clay might hinder the solubility of the components as well as alter hydration mechanisms. Hence, it is suggested that montmorillonite in its unmodified form should be used. As a result, the polymer selected for separating the clay platelets should also be polar in nature. PVA might be a good choice. This is suggested on the basis of earlier research performed with ferrite nanoparticles, where the nanoparticles were coated with PVA. Both were easily handled in water. PVA is easily soluble in water. Also, an organic ammonium salt (also soluble in water) could be used to enhance compatibility between the clay and polymer.

6.5 Impact Modified Glass Fibers

Some of the fundamental problems associated with glass fiber reinforced polymer composites are interfacial adhesion and formation of voids. Both lead to reduced impact properties. It is suggested on the basis of research on impact modification of PP/clay nanocomposites that an end functionalized oligomeric elastomer may be used with glass fibers for achieving enhanced impact properties. It is possible that one end of the elastomer would bond to the surface of the glass fiber and the other to the matrix resin. In order to enhance adhesion, a possibility that could be explored is the addition of a reactive monomer that would polymerize and bond to the elastomer and the matrix resin. Different parameters such as concentrations of different species, curing temperature etc. could be studied.

6.6 Recycling of Ground Fiberglass

Recycling is a subject that has always attracted considerable attention. Recycling of wastes is very important in order to maintain equilibrium in environment. Further, most of the industrial wastes are not biodegradable and therefore create imbalance in ecosystems.

One such material is fiberglass. A strategy is proposed here to recycle used fiberglass. The fiberglass could be ground and soaked in a reactive monomer and initiator. The resulting polymerization reaction could help bonding between the new polymer formed and the existing thermoset polymer on the fiberglass. These modified fibers could then be re-used with traditional thermosetting materials such as unsaturated polyester etc. The choice of the monomer should be such that the resulting composite should exhibit good mechanical properties. Different concentrations of the monomer and

initiator could be studied. This idea is proposed on the basis of earlier suggestion for obtaining high-impact glass fibers.

6.7 Characterization of Nanocomposites

Several characterization techniques need to be employed for understanding the microstructure of the polymer/clay nanocomposites better. Techniques such as FTIR would elucidate as to which species are bonded to which. SEM with EDS capability would help investigating the dispersion and distribution of clay platelets within the polymer matrix. Permeability measurements may explain the decreased permeation of gases and moisture through nanocomposite films due to a hindered and tortuous pathway offered by the clay platelets. Dynamical mechanical thermal analysis (DMTA) could be an effective tool in obtaining the response of the material to dynamic loading, as well as different transitions associated with the material. Dielectric relaxation techniques could complement DMTA results. Positron annihilation measurements could be performed for obtaining a free volume analysis on the nanocomposites.

Further insight into the microstructure of PMMA/Laponite nanocomposites could be obtained through DMTA. Permeability measurements could help in deciding the suitability of their application as coatings.

Regarding PC/ferrite nanocomposites, the possibility of PVA acting as a tethering agent between the ferrites and PC needs to be investigated. FTIR, NMR, SEM, DMTA could be used to investigate this. Also, detailed measurements on magnetometers for both A.C and D.C characteristics would elucidate the magnetic behavior of the nanocomposites.

6.8 Conclusions

It is seen that the concepts applicable to nanocomposites could possibly extend to other avenues as well, such as recycling of fiberglass and modification of glass fibers. Also, besides using nanocomposites for automotive applications, they may be also used for resistant coating as well as cellular phone housings. Nanocomposite cement seems to be an exciting possibility.

The research possibilities seem to be endless. However, one of the aims of this thesis is to outline certain ideas that could possibly develop into potential applications in a systematic way.

APPENDIX A
REPRESENTATIVE DATA FROM WINTEST® SOFTWARE

Table A.1 : Tensile testing data for pure polypropylene.

Displacement (mm)	Load (N)	Axial Command (mm)	Stress* (N/ mm^2)	Strain* (Absolute)
0	2.417	0	0	0
0.047	5.603	0.049	1.740603	0.001741
0.096	8.597	0.098	3.376311	0.003556
0.145	11.357	0.146	4.884178	0.00537
0.193	13.953	0.195	6.302448	0.007148
0.243	16.109	0.244	7.480332	0.009
0.292	18.265	0.293	8.658217	0.010815
0.34	19.989	0.342	9.600087	0.012593
0.389	21.664	0.391	10.51519	0.014407
0.438	23.251	0.439	11.38221	0.016222
0.487	24.541	0.488	12.08698	0.018037
0.536	25.688	0.537	12.71361	0.019852
0.585	26.698	0.586	13.26541	0.021667
0.633	27.762	0.635	13.8467	0.023444
0.682	28.6	0.684	14.30452	0.025259
0.731	29.554	0.732	14.82572	0.027074
0.78	30.296	0.781	15.2311	0.028889
0.829	30.996	0.83	15.61353	0.030704
0.877	31.848	0.879	16.079	0.032481
0.927	32.308	0.928	16.33031	0.034333
0.976	33.056	0.977	16.73896	0.036148
1.024	33.654	1.025	17.06567	0.037926
1.073	34.292	1.074	17.41423	0.039741
1.122	34.711	1.123	17.64314	0.041556
1.171	35.315	1.172	17.97312	0.04337
1.219	35.72	1.221	18.19438	0.045148
1.268	36.16	1.27	18.43477	0.046963
1.317	36.668	1.318	18.7123	0.048778
1.366	36.97	1.367	18.87729	0.050593
1.415	37.465	1.416	19.14773	0.052407
1.464	37.822	1.465	19.34277	0.054222
1.513	38.158	1.514	19.52633	0.056037
1.561	38.474	1.562	19.69897	0.057815
1.61	38.79	1.611	19.87161	0.05963
1.659	39.058	1.66	20.01803	0.061444
1.708	39.312	1.709	20.1568	0.063259
1.757	39.648	1.758	20.34036	0.065074
1.805	39.806	1.807	20.42668	0.066852
1.854	40.129	1.855	20.60315	0.068667
1.903	40.252	1.904	20.67035	0.070481
1.952	40.493	1.953	20.80201	0.072296
2.001	40.74	2.002	20.93695	0.074111
2.049	40.884	2.051	21.01563	0.075889

2.098	41.111	2.1	21.13964	0.077704
2.147	41.269	2.148	21.22596	0.079519
2.196	41.42	2.197	21.30846	0.081333
2.245	41.488	2.246	21.34561	0.083148
2.294	41.784	2.295	21.50732	0.084963
2.343	41.804	2.344	21.51825	0.086778
2.391	41.887	2.393	21.56359	0.088556
2.44	42.134	2.441	21.69854	0.09037
2.489	42.196	2.49	21.73241	0.092185
2.538	42.34	2.539	21.81108	0.094
2.587	42.415	2.588	21.85205	0.095815
2.636	42.546	2.637	21.92362	0.09763
2.684	42.546	2.686	21.92362	0.099407
2.733	42.649	2.734	21.9799	0.101222
2.782	42.8	2.783	22.06239	0.103037
2.831	42.793	2.832	22.05857	0.104852
2.88	42.917	2.881	22.12631	0.106667
2.929	42.965	2.93	22.15253	0.108481
2.977	43.075	2.979	22.21263	0.110259
3.026	43.102	3.027	22.22738	0.112074
3.075	43.123	3.076	22.23885	0.113889
3.124	43.233	3.125	22.29895	0.115704
3.173	43.191	3.174	22.27601	0.117519
3.222	43.349	3.223	22.36233	0.119333
3.27	43.342	3.272	22.3585	0.121111
3.319	43.432	3.32	22.40767	0.122926
3.368	43.363	3.369	22.36997	0.124741
3.417	43.459	3.418	22.42242	0.126556
3.466	43.459	3.467	22.42242	0.12837
3.514	43.432	3.516	22.40767	0.130148
3.563	43.5	3.565	22.44482	0.131963
3.612	43.487	3.613	22.43772	0.133778
3.661	43.576	3.662	22.48634	0.135593
3.71	43.507	3.711	22.44865	0.137407
3.759	43.466	3.76	22.42625	0.139222
3.807	43.596	3.809	22.49727	0.141
3.856	43.466	3.858	22.42625	0.142815
3.905	43.645	3.906	22.52404	0.14463
3.954	43.542	3.955	22.46777	0.146444
4.003	43.61	4.004	22.50492	0.148259
4.052	43.507	4.053	22.44865	0.150074
4.1	43.583	4.102	22.49017	0.151852
4.149	43.521	4.151	22.45629	0.153667
4.198	43.466	4.199	22.42625	0.155481
4.246	43.576	4.248	22.48634	0.157259
4.295	43.452	4.297	22.4186	0.159074
4.345	43.493	4.346	22.441	0.160926
4.394	43.425	4.394	22.40385	0.162741
4.442	43.418	4.443	22.40002	0.164519
4.491	43.439	4.492	22.41149	0.166333
4.54	43.322	4.541	22.34757	0.168148
4.589	43.308	4.59	22.33993	0.169963
4.637	43.26	4.639	22.3137	0.171741
4.686	43.315	4.687	22.34375	0.173556
4.735	43.349	4.736	22.36233	0.17537
4.784	43.315	4.785	22.34375	0.177185

4.833	43.315	4.834	22.34375	0.179
4.881	43.068	4.883	22.20881	0.180778
4.93	43.171	4.932	22.26508	0.182593
4.978	43.033	4.98	22.18969	0.18437
5.028	43.006	5.029	22.17493	0.186222
5.077	42.999	5.078	22.17111	0.188037
5.125	42.862	5.127	22.09626	0.189815
5.174	42.862	5.176	22.09626	0.19163
5.224	42.759	5.225	22.03999	0.193481
5.272	42.807	5.273	22.06622	0.195259
5.321	42.759	5.322	22.03999	0.197074
5.37	42.553	5.371	21.92745	0.198889
5.418	42.443	5.42	21.86735	0.200667
5.467	42.608	5.469	21.9575	0.202481
5.516	42.649	5.518	21.9799	0.204296
5.565	42.388	5.566	21.8373	0.206111
5.614	42.23	5.615	21.75098	0.207926
5.662	42.168	5.664	21.71711	0.209704
5.711	42.168	5.713	21.71711	0.211519
5.76	42.175	5.762	21.72094	0.213333
5.809	41.9	5.811	21.57069	0.215148
5.858	41.88	5.859	21.55977	0.216963
5.906	41.77	5.908	21.49967	0.218741
5.955	41.591	5.957	21.40188	0.220556
6.004	41.742	6.006	21.48438	0.22237
6.053	41.475	6.055	21.33851	0.224185
6.102	41.468	6.104	21.33468	0.226
6.151	41.303	6.152	21.24454	0.227815
6.199	41.227	6.201	21.20302	0.229593
6.249	40.953	6.25	21.05332	0.231444
6.297	40.884	6.299	21.01563	0.233222
6.345	40.685	6.348	20.90691	0.235
6.395	40.575	6.397	20.84681	0.236852
6.443	40.397	6.445	20.74956	0.23863
6.492	40.149	6.494	20.61407	0.240444
-0.752	-0.137	4.633	-1.39532	-0.02785
-0.319	-0.295	0.373	-1.48164	-0.01181

APPENDIX B
REPRESENTATIVE DATA FROM DSC SOFTWARE

Table B.1 : DSC data for pure polypropylene.

Time (X 0.1 sec.)	Temperature (^{o}C)	DSC (μW)	DDSC (μW/min.)
36590	-9.93558	-3002.01	113.566
36595	-9.85018	-3004.29	136.74
36600	-9.76277	-3004.34	140.007
36605	-9.67569	-3006.38	168.615
36610	-9.59319	-3007.81	178.21
36615	-9.50938	-3008.92	173.35
36620	-9.42523	-3010.51	168.337
36625	-9.33843	-3011.93	193.74
36630	-9.25329	-3013.32	193.465
36635	-9.16815	-3015.94	200.268
36640	-9.08334	-3016.45	231.861
36645	-8.99919	-3018.32	245.941
36650	-8.91504	-3020.48	268.799
36655	-8.83023	-3022.5	304.676
36660	-8.74509	-3024.5	320.739
36665	-8.66094	-3028.24	369.108
36670	-8.57514	-3031.01	405.636
36675	-8.49066	-3034.33	446.256
36680	-8.40518	-3038.71	489.252
36685	-8.32037	-3042.67	536.892
36690	-8.23523	-3047.21	572.271
36695	-8.1491	-3052.13	625.128
36700	-8.06395	-3057.67	680.496
36705	-7.97914	-3063.27	712.131
36710	-7.89433	-3069.24	766.318
36715	-7.80853	-3075.93	844.608
36720	-7.72405	-3083.1	893.64
36725	-7.63891	-3091.04	925.585
36730	-7.5541	-3098.06	1010.28
36735	-7.46929	-3106.53	1036.68
36740	-7.38348	-3117.59	1083.74
36745	-7.29768	-3126.6	1153.88
36750	-7.21254	-3134.8	1174.96
36755	-7.12839	-3147.46	1223.95
36760	-7.04258	-3155.63	1300.49
36765	-6.95711	-3166.24	1298.95
36770	-6.87197	-3179.26	1361.23
36775	-6.78848	-3188.95	1381.28
36780	-6.70434	-3200.05	1369.97
36785	-6.60329	-3214.91	1406.05
36790	-6.51881	-3225.84	1451.18
36795	-6.43467	-3240.03	1406.9
36800	-6.34986	-3249.91	1452.02

36805	-6.26438	-3261.63	1450.91
36810	-6.18123	-3272.8	1431.74
36815	-6.09741	-3287.17	1450.67
36820	-6.01393	-3296.5	1451.48
36825	-5.93077	-3309.95	1515.17
36830	-5.84795	-3320.96	1610.64
36835	-5.7638	-3334.22	1658.34
36840	-5.68032	-3346.73	1708.18
36845	-5.59716	-3360.99	1893.76
36850	-5.51533	-3376.17	2021.28
36855	-5.43252	-3395.85	2134.43
36860	-5.3479	-3410.99	2389.12
36865	-5.26361	-3429.52	2614.44
36870	-5.17932	-3454.31	2822.53
36875	-5.09503	-3478.39	3056.73
36880	-5.00975	-3498.83	3327.62
36885	-4.9248	-3533.31	3603.43
36890	-4.84117	-3564.6	3762.24
36895	-4.75688	-3596.2	4039.54
36900	-4.67127	-3630.9	4147.27
36905	-4.58665	-3673.15	4406.98
36910	-4.50203	-3711.28	4487.52
36915	-4.41807	-3743.04	4627.68
36920	-4.33444	-3790.94	4765.68
36925	-4.24982	-3824	4974.48
36930	-4.16421	-3866.08	4999.32
36935	-4.08025	-3907.27	4976.16
36940	-3.99563	-3950.24	5245.32
36945	-3.91134	-3993.34	5227.92
36950	-3.82705	-4045.44	5259.96
36955	-3.7421	-4089.76	5301.36
36960	-3.65814	-4125.96	5460.96
36965	-3.57319	-4180.15	5393.4
36970	-3.4889	-4226.6	5527.92
36975	-3.40428	-4262.33	5318.04
36980	-3.31999	-4307.86	5430.36
36985	-3.23603	-4362.35	5501.76
36990	-3.15241	-4399.69	5267.53
36995	-3.06812	-4454	5220.12
37000	-2.98184	-4488.61	5365.32
37005	-2.89656	-4542.29	5196.01
37010	-2.81095	-4584.44	5096.4
37015	-2.72666	-4619.11	4985.04
37020	-2.64171	-4661.61	4758.48
37025	-2.55577	-4709.44	4762.32
37030	-2.47115	-4740.86	4523.16
37035	-2.38653	-4787.05	4410.72
37040	-2.30092	-4815.11	4364.75
37045	-2.21498	-4850.54	4169.04
37050	-2.13102	-4885.47	3938.16
37055	-2.04739	-4919.22	3960.23
37060	-1.96376	-4952	3631.92
37065	-1.8798	-4982.84	3651.96
37070	-1.79254	-5009.03	3476.4
37075	-1.70726	-5037.62	3315.84
37080	-1.62231	-5070.88	3097.21

37085	-1.53669	-5089.71	2939.04
37090	-1.45042	-5119.44	2719.21
37095	-1.36481	-5140.24	2622.12
37100	-1.27986	-5161.79	2452.8
37105	-1.19458	-5177.32	2163.6
37110	-1.10996	-5196.92	2091.96
37115	-1.02369	-5209.44	1812.6
37120	-0.9394	-5227.54	1636.56
37125	-0.85478	-5242.02	1439.64
37130	-0.77016	-5251.18	1307.4
37135	-0.68521	-5264.04	1112.64
37140	-0.60059	-5270.49	980.039
37145	-0.51597	-5276.62	767.883
37150	-0.43036	-5281.76	561.604
37155	-0.34474	-5286.27	389.285
37160	-0.25814	-5289.64	193.441
37165	-0.17154	-5291.11	66
37170	-0.08659	-5291.53	-126
37175	-0.00197	-5288.82	-262.676
37180	0.083314	-5283.62	-453.357
37185	0.169587	-5280.16	-638.754
37190	0.254207	-5275.99	-783.246
37195	0.338827	-5266.12	-961.922
37200	0.423116	-5259.87	-1164.36
37205	0.507736	-5248.49	-1274.4
37210	0.592025	-5236.41	-1449.6
37215	0.675654	-5225.84	-1567.8
37220	0.759943	-5211.37	-1737.84
37225	0.844563	-5191.79	-1896
37230	0.930175	-5177.42	-2078.77
37235	1.01513	-5159.36	-2283.84
37240	1.09908	-5145.34	-2424.12
37245	1.20188	-5121.3	-2493.12
37250	1.28584	-5101.87	-2616.96
37255	1.37212	-5075.26	-2755.68
37260	1.45806	-5046.09	-2846.04
37265	1.54268	-5023.83	-3006.84
37270	1.6273	-5003.61	-2954.28
37275	1.71126	-4973.71	-3060.6
37280	1.79488	-4947.78	-3069.84
37285	1.87818	-4922.19	-3056.88
37290	1.9628	-4894.77	-3216.24
37295	2.0461	-4875.11	-3327.24
37300	2.13105	-4846.82	-3250.44
37305	2.21501	-4819.44	-3291.72
37310	2.29864	-4791.35	-3463.2
37315	2.38326	-4755.81	-3437.04
37320	2.46887	-4726.34	-3674.99
37325	2.55679	-4702.84	-3705.73
37330	2.64241	-4673.47	-3699.36
37335	2.72934	-4633.59	-3756.6
37340	2.81495	-4608.35	-3816.72
37345	2.90089	-4568.86	-3757.2
37350	2.9875	-4538.01	-3875.16
37355	3.07288	-4511.16	-3936
37360	3.15745	-4478.3	-3962.4

37365	3.24203	-4437.75	-3967.2
37370	3.32725	-4413.24	-3906.25
37375	3.41019	-4379.91	-4062.47
37380	3.49477	-4345.47	-4073.28
37385	3.57934	-4303.39	-4177.56
37390	3.66424	-4277.75	-4009.08
37395	3.74816	-4243.34	-4136.16
37400	3.83306	-4199.47	-4239.84
37405	3.91731	-4171.72	-4162.92
37410	4.00188	-4130.17	-4064.64
37415	4.08743	-4103.66	-4253.88
37420	4.17233	-4068.56	-4263.48
37425	4.25756	-4026.59	-4031.04
37430	4.34246	-3998.56	-4092.36
37435	4.42638	-3964.67	-4083.36
37440	4.51194	-3923.26	-4187.28
37445	4.59814	-3888.05	-4093.56
37450	4.68174	-3863.55	-4066.02
37455	4.765	-3830.69	-4133.29
37460	4.8499	-3789.89	-4042.22
37465	4.93317	-3754.72	-4007.65
37470	5.01644	-3727.43	-3971.26
37475	5.10003	-3687.75	-4038.2
37480	5.1833	-3654.12	-4040.16
37485	5.26787	-3627.82	-3940.34
37490	5.35179	-3589.29	-3981.7
37495	5.43539	-3557.11	-3924.84
37500	5.51931	-3527.03	-3846.72
37505	5.60486	-3494.01	-3888.37
37510	5.68944	-3461.53	-3862.34
37515	5.77434	-3422.91	-3870.85
37520	5.85858	-3400.36	-3770.99
37525	5.94348	-3367.19	-3840
37530	6.02838	-3330.09	-3727.85
37535	6.11296	-3305.96	-3757.42
37540	6.1972	-3266.72	-3570.79
37545	6.2821	-3242.86	-3753.29
37550	6.36635	-3207.03	-3692.53
37555	6.45092	-3183.36	-3589.42
37560	6.53517	-3148.41	-3555.88
37565	6.61909	-3125.35	-3418.29
37570	6.70367	-3087.59	-3518.38
37575	6.78693	-3059.48	-3357.02
37580	6.87183	-3030.97	-3367.86
37585	6.95641	-3009.63	-3341.99
37590	7.04	-2981.86	-3361.1
37595	7.12359	-2949.66	-3143.2
37600	7.20947	-2927.28	-3101.07
37605	7.29437	-2902.7	-3110.77
37610	7.37927	-2869.91	-3095.29
37615	7.46352	-2845.25	-3040.18
37620	7.54712	-2825.65	-2936.35
37625	7.633	-2801.06	-2950.92
37630	7.7179	-2771.74	-2921.89
37635	7.82043	-2751.69	-2853.72
37640	7.90631	-2728.51	-2780.63

37645	7.99251	-2704.97	-2857.25
37650	8.07774	-2681.37	-2824.21
37655	8.16362	-2659.21	-2679.14
37660	8.24819	-2632.1	-2714.53
37665	8.33244	-2613.54	-2633.52
37670	8.41702	-2587.55	-2583.76
37675	8.50028	-2565.71	-2584.02
37680	8.58322	-2548.48	-2537.24
37685	8.66551	-2525.48	-2356.13
37690	8.74845	-2509.05	-2352.47
37695	8.84837	-2489.66	-2305.34
37700	8.93131	-2466.04	-2197.98
37705	9.01426	-2447.77	-2198.65
37710	9.09818	-2435.76	-2146.14
37715	9.1834	-2417.5	-2182.88
37720	9.26863	-2395.44	-2094.33
37725	9.35157	-2382.54	-2043.32
37730	9.43549	-2365.26	-1962.86
37735	9.51811	-2346.64	-2086.31
37740	9.60268	-2327.15	-2030.41
37745	9.68595	-2315.13	-1904.75
37750	9.76889	-2295.76	-1932.83
37755	9.85183	-2284.2	-1889.88
37760	9.93412	-2261.9	-1828.37
37765	10.0158	-2248.3	-1791.01

APPENDIX C
REPRESENTATIVE DATA FROM XRD SOFTWARE

Table C.1 : XRD data for PP/COMP/F-OLIG/CLAY (90:4.75:0.25:5)

Counts	2θ*
400	0.02
372	0.04
365	0.06
365	0.08
324	0.1
384	0.12
365	0.14
400	0.16
350	0.18
384	0.2
384	0.22
376	0.24
376	0.26
384	0.28
342	0.3
357	0.32
342	0.34
357	0.36
350	0.38
365	0.4
350	0.42
331	0.44
369	0.46
372	0.48
346	0.5
369	0.52
346	0.54
365	0.56
353	0.58
353	0.6
342	0.62
396	0.64
396	0.66
369	0.68
392	0.7
369	0.72
376	0.74
396	0.76
392	0.78
400	0.8
416	0.82
380	0.84
380	0.86
384	0.88

396	0.9
404	0.92
404	0.94
404	0.96
412	0.98
412	1
396	1.02
396	1.04
420	1.06
441	1.08
437	1.1
384	1.12
424	1.14
428	1.16
408	1.18
392	1.2
437	1.22
404	1.24
437	1.26
388	1.28
396	1.3
441	1.32
433	1.34
384	1.36
420	1.38
445	1.4
380	1.42
353	1.44
396	1.46
380	1.48
404	1.5
392	1.52
350	1.54
353	1.56
365	1.58
306	1.6
376	1.62
331	1.64
328	1.66
346	1.68
365	1.7
335	1.72
313	1.74
303	1.76
324	1.78
296	1.8
313	1.82
282	1.84
276	1.86
317	1.88
286	1.9
331	1.92
276	1.94
253	1.96
276	1.98
279	2

253	2.02
296	2.04
292	2.06
276	2.08
279	2.1
320	2.12
282	2.14
246	2.16
292	2.18
266	2.2
296	2.22
296	2.24
256	2.26
266	2.28
292	2.3
282	2.32
296	2.34
296	2.36
269	2.38
313	2.4
279	2.42
317	2.44
296	2.46
269	2.48
259	2.5
299	2.52
310	2.54
272	2.56
296	2.58
289	2.6
276	2.62
296	2.64
299	2.66
266	2.68
272	2.7
259	2.72
269	2.74
228	2.76
259	2.78
240	2.8
246	2.82
250	2.84
228	2.86
219	2.88
243	2.9
246	2.92
213	2.94
225	2.96
202	2.98
219	3
231	3.02
180	3.04
196	3.06
210	3.08
180	3.1
185	3.12

182	3.14
169	3.16
169	3.18
149	3.2
139	3.22
154	3.24
174	3.26
161	3.28
142	3.3
154	3.32
137	3.34
172	3.36
156	3.38
125	3.4
144	3.42
144	3.44
121	3.46
154	3.48
139	3.5
119	3.52
117	3.54
128	3.56
119	3.58
98	3.6
112	3.62
119	3.64
112	3.66
94	3.68
110	3.7
110	3.72
108	3.74
96	3.76
92	3.78
98	3.8
94	3.82
100	3.84
102	3.86
110	3.88
94	3.9
121	3.92
85	3.94
98	3.96
88	3.98
98	4
88	4.02
94	4.04
90	4.06
92	4.08
85	4.1
108	4.12
98	4.14
106	4.16
90	4.18
96	4.2
106	4.22
90	4.24

67	4.26
104	4.28
110	4.3
94	4.32
98	4.34
102	4.36
102	4.38
94	4.4
108	4.42
112	4.44
108	4.46
86	4.48
112	4.5
96	4.52
106	4.54
121	4.56
112	4.58
90	4.6
86	4.62
100	4.64
96	4.66
106	4.68
85	4.7
94	4.72
98	4.74
94	4.76
112	4.78
92	4.8
100	4.82
88	4.84
110	4.86
90	4.88
114	4.9
104	4.92
96	4.94
98	4.96
104	4.98
100	5
108	5.02
98	5.04
123	5.06
90	5.08
104	5.1
102	5.12
94	5.14
108	5.16
98	5.18
98	5.2
117	5.22
114	5.24
104	5.26
102	5.28
94	5.3
106	5.32
112	5.34
114	5.36

112	5.38
94	5.4
106	5.42
102	5.44
130	5.46
94	5.48
104	5.5
114	5.52
90	5.54
119	5.56
112	5.58
98	5.6
108	5.62
117	5.64
112	5.66
117	5.68
96	5.7
92	5.72
83	5.74
119	5.76
119	5.78
100	5.8
106	5.82
102	5.84
117	5.86
117	5.88
96	5.9
110	5.92
114	5.94
102	5.96
108	5.98
112	6
123	6.02
117	6.04
121	6.06
112	6.08
132	6.1
108	6.12
96	6.14
130	6.16
123	6.18
121	6.2
139	6.22
130	6.24
110	6.26
112	6.28
130	6.3
132	6.32
112	6.34
128	6.36
112	6.38
117	6.4
130	6.42
121	6.44
114	6.46
135	6.48

123	6.5
114	6.52
146	6.54
123	6.56
125	6.58
117	6.6
125	6.62
110	6.64
123	6.66
130	6.68
130	6.7
132	6.72
139	6.74
123	6.76
137	6.78
137	6.8
137	6.82
137	6.84
128	6.86
151	6.88
144	6.9
149	6.92
132	6.94
114	6.96
128	6.98
154	7
137	7.02
132	7.04
139	7.06
137	7.08
142	7.1
154	7.12
139	7.14
154	7.16
137	7.18
161	7.2
159	7.22
177	7.24
174	7.26
159	7.28
154	7.3
164	7.32
177	7.34
130	7.36
164	7.38
174	7.4
130	7.42
169	7.44
166	7.46
169	7.48
156	7.5
154	7.52
154	7.54
190	7.56
169	7.58
185	7.6

156	7.62
196	7.64
177	7.66
182	7.68
144	7.7
199	7.72
182	7.74
177	7.76
190	7.78
202	7.8
188	7.82
193	7.84
188	7.86
182	7.88
204	7.9
188	7.92
188	7.94
182	7.96
177	7.98
213	8
219	8.02
216	8.04
216	8.06
188	8.08
225	8.1
243	8.12
228	8.14
210	8.16
193	8.18
237	8.2
207	8.22
231	8.24
246	8.26
256	8.28
222	8.3
250	8.32
262	8.34
250	8.36
299	8.38
262	8.4
292	8.42
276	8.44
292	8.46
320	8.48
292	8.5
342	8.52
346	8.54
365	8.56
342	8.58
376	8.6
380	8.62
408	8.64
445	8.66
408	8.68
458	8.7
524	8.72

534	8.74
538	8.76
562	8.78
595	8.8
615	8.82
660	8.84
660	8.86
655	8.88
740	8.9
778	8.92
795	8.94
894	8.96
900	8.98
936	9
924	9.02
924	9.04
1024	9.06
1056	9.08
1096	9.1
1116	9.12
1197	9.14
1183	9.16
1183	9.18
1303	9.2
1303	9.22
1282	9.24
1274	9.26
1332	9.28
1246	9.3
1218	9.32
1225	9.34
1183	9.36
1129	9.38
961	9.4
1050	9.42
930	9.44
829	9.46
773	9.48
784	9.5
692	9.52
713	9.54
625	9.56
566	9.58
538	9.6
497	9.62
497	9.64
467	9.66
408	9.68
433	9.7
380	9.72
396	9.74
412	9.76
353	9.78
372	9.8
384	9.82
372	9.84

306	9.86
328	9.88
384	9.9
328	9.92
303	9.94
350	9.96
331	9.98
357	10
353	10.02
339	10.04
320	10.06
320	10.08
328	10.1
317	10.12
324	10.14
320	10.16
342	10.18
335	10.2
339	10.22
289	10.24
289	10.26
303	10.28
303	10.3
328	10.32
303	10.34
292	10.36
335	10.38
303	10.4
313	10.42
282	10.44
331	10.46
310	10.48
342	10.5
286	10.52
296	10.54
320	10.56
292	10.58
269	10.6
310	10.62
279	10.64
286	10.66
313	10.68
289	10.7
320	10.72
296	10.74
299	10.76
296	10.78
303	10.8
317	10.82
299	10.84
320	10.86
331	10.88
335	10.9
342	10.92
320	10.94
324	10.96

342	10.98
328	11
376	11.02
346	11.04
372	11.06
357	11.08
372	11.1
353	11.12
369	11.14
380	11.16
369	11.18
384	11.2
392	11.22
392	11.24
357	11.26
380	11.28
369	11.3
400	11.32
384	11.34
384	11.36
392	11.38
400	11.4
400	11.42
428	11.44
396	11.46
412	11.48
441	11.5
428	11.52
475	11.54
493	11.56
484	11.58
566	11.6
520	11.62
576	11.64
566	11.66
610	11.68
645	11.7
702	11.72
708	11.74
713	11.76
812	11.78
807	11.8
847	11.82
942	11.84
961	11.86
949	11.88
1018	11.9
1076	11.92
1082	11.94
1129	11.96
1218	11.98
1218	12
1282	12.02
1218	12.04
1260	12.06
1267	12.08

1183	12.1
1089	12.12
1163	12.14
1109	12.16
1024	12.18
1011	12.2
930	12.22
961	12.24
870	12.26
784	12.28
724	12.3
681	12.32
600	12.34
600	12.36
562	12.38
538	12.4
520	12.42
497	12.44
493	12.46
416	12.48
416	12.5
392	12.52
424	12.54
396	12.56
396	12.58
369	12.6
372	12.62
380	12.64
388	12.66
376	12.68
396	12.7
372	12.72
346	12.74
380	12.76
400	12.78
404	12.8
388	12.82
361	12.84
404	12.86
420	12.88
380	12.9
404	12.92
396	12.94
441	12.96
412	12.98
412	13
412	13.02
437	13.04
412	13.06
449	13.08
467	13.1
445	13.12
449	13.14
449	13.16
471	13.18
506	13.2

529	13.22
529	13.24
543	13.26
566	13.28
562	13.3
586	13.32
586	13.34
660	13.36
692	13.38
650	13.4
676	13.42
697	13.44
718	13.46
718	13.48
756	13.5
790	13.52
824	13.54
858	13.56
841	13.58
829	13.6
906	13.62
918	13.64
912	13.66
841	13.68
888	13.7
870	13.72
930	13.74
888	13.76
888	13.78
790	13.8
801	13.82
807	13.84
807	13.86
778	13.88
729	13.9
708	13.92
671	13.94
666	13.96
650	13.98
640	14
615	14.02
600	14.04
571	14.06
595	14.08
538	14.1
524	14.12
529	14.14
506	14.16
543	14.18
502	14.2
502	14.22
488	14.24
488	14.26
454	14.28
471	14.3
441	14.32

428	14.34
424	14.36
458	14.38
462	14.4
424	14.42
449	14.44
404	14.46
445	14.48
475	14.5
408	14.52
384	14.54
449	14.56
433	14.58
408	14.6
428	14.62
384	14.64
380	14.66
428	14.68
396	14.7
369	14.72
445	14.74
416	14.76
369	14.78
428	14.8
392	14.82
400	14.84
404	14.86
437	14.88
408	14.9
412	14.92
400	14.94
404	14.96
376	14.98
372	15
388	15.02
412	15.04
416	15.06
392	15.08
384	15.1
376	15.12
400	15.14
353	15.16
376	15.18
400	15.2
396	15.22
396	15.24
404	15.26
376	15.28
357	15.3
396	15.32
396	15.34
376	15.36
384	15.38
353	15.4
400	15.42
380	15.44

384	15.46
361	15.48
412	15.5
437	15.52
404	15.54
404	15.56
424	15.58
428	15.6
445	15.62
400	15.64
437	15.66
384	15.68
488	15.7
437	15.72
471	15.74
458	15.76
484	15.78
520	15.8
524	15.82
571	15.84
557	15.86
557	15.88
576	15.9
566	15.92
692	15.94
666	15.96
610	15.98
650	16
686	16.02
692	16.04
767	16.06
762	16.08
745	16.1
762	16.12
773	16.14
790	16.16
829	16.18
853	16.2
858	16.22
853	16.24
858	16.26
888	16.28
858	16.3
876	16.32
853	16.34
882	16.36
818	16.38
912	16.4
858	16.42
847	16.44
824	16.46
835	16.48
853	16.5
824	16.52
900	16.54
853	16.56

858	16.58
870	16.6
894	16.62
853	16.64
841	16.66
876	16.68
870	16.7
918	16.72
912	16.74
942	16.76
967	16.78
942	16.8
1005	16.82
980	16.84
1037	16.86
1063	16.88
1024	16.9
1005	16.92
1030	16.94
1063	16.96
1037	16.98
986	17
1050	17.02
1056	17.04
1024	17.06
1030	17.08
973	17.1
980	17.12
912	17.14
961	17.16
888	17.18
894	17.2
829	17.22
790	17.24
767	17.26
740	17.28
740	17.3
635	17.32
645	17.34
625	17.36
586	17.38
534	17.4
548	17.42
529	17.44
480	17.46
449	17.48
437	17.5
449	17.52
424	17.54
380	17.56
433	17.58
365	17.6
357	17.62
357	17.64
310	17.66
369	17.68

342	17.7
320	17.72
292	17.74
299	17.76
320	17.78
313	17.8
279	17.82
289	17.84
250	17.86
289	17.88
266	17.9
292	17.92
266	17.94
282	17.96
269	17.98
253	18
266	18.02
262	18.04
266	18.06
282	18.08
272	18.1
234	18.12
266	18.14
234	18.16
262	18.18
272	18.2
240	18.22
250	18.24
266	18.26
276	18.28
256	18.3
246	18.32
246	18.34
243	18.36
256	18.38
237	18.4
250	18.42
279	18.44
234	18.46
243	18.48
269	18.5
222	18.52
262	18.54
243	18.56
243	18.58
231	18.6
225	18.62
269	18.64
266	18.66
219	18.68
282	18.7
237	18.72
237	18.74
240	18.76
219	18.78
219	18.8

228	18.82
216	18.84
250	18.86
210	18.88
259	18.9
231	18.92
240	18.94
237	18.96
240	18.98
228	19
240	19.02
237	19.04
286	19.06
246	19.08
269	19.1
237	19.12
266	19.14
228	19.16
250	19.18
282	19.2
262	19.22
240	19.24
276	19.26
269	19.28
272	19.3
240	19.32
272	19.34
256	19.36
262	19.38
262	19.4
289	19.42
269	19.44
250	19.46
256	19.48
266	19.5
276	19.52
276	19.54
286	19.56
243	19.58
286	19.6
262	19.62
276	19.64
269	19.66
279	19.68
276	19.7
282	19.72
276	19.74
272	19.76
276	19.78
259	19.8
259	19.82
286	19.84
256	19.86
269	19.88
262	19.9
286	19.92

289	19.94
266	19.96
262	19.98
269	20
262	20.02
269	20.04
289	20.06
317	20.08
269	20.1
282	20.12
317	20.14
313	20.16
310	20.18
324	20.2
313	20.22
331	20.24
320	20.26
335	20.28
331	20.3
353	20.32

LIST OF REFERENCES

1. LeBaron, P.C., Wang, Z., Pinnavaia, T.J., 1999. Polymer-layered silicate nanocomposites: An overview. Appl. Clay Sci. 15, 11-29.

2. Brune, D.A., Bicerano, J., 2002. Micromechanics of nanocomposites: Comparison of tensile and compressive elastic moduli, and prediction of effects of incomplete exfoliation and imperfect alignment on modulus. Polymer 43, 369-387.

3. Nyden, A.R., Gilman, J.W., 1997. Molecular dynamics simulations of the thermal degradation of nano-confined polypropylene. Comp. Theo. Poly. Sci. 7 [3], 191-198.

4. Hay, N.J., Shaw, S.J., 2000. A review of nanocomposites. J. Mater. Res. 7, 962-988.

5. Gloaguen, J.M, Lefebvre, J.M, 2001. Plastic deformation behavior of thermoplastic clay nanocomposites. Polymer 41, 5841-5847.

6. Alexandre, M., Dubois, P., 2000. Polymer-layered silicate nanocomposites: Preparation, properties and uses of a new class of materials. Mat. Sci. and Engg. 28, 1-63.

7. Usuki, A., Kawasumi, M., Kojima, Y., Okada, A., 1993. Swelling behavior of montmorillonite cation exchanged ω-amino acids by ε-caprolactam. J. Mater. Res. 8, 1174-1178.

8. Usuki, A., Kawasumi, M., Kojima, Y., Okada, A., Fukushima, Y., Kurauchi, T., Kamigato, O., 1993. Synthesis of nylon 6-clay hybrid. J. Mater. Res. 8, 1179-1184.

9. Kojima, Y., Usuki, A., Kawasumi, M., Okada, A., Fukushima, Y., Kurauchi, T., Kamigato, O., 1993. Mechanical properties of nylon 6-clay hybrid. J. Mater. Res. 8, 1185-1189.

10. Kojima, Y., Usuki, A., Kawasumi, M., Okada, A., Y., Kurauchi, T., Kamigato, O., 1993. Sorption of water in nylon 6-clay hybrid. J. Appl. Polym. Sci. 49, 1259-1264.

11. Gilman, J.W., Kashiwagi, T., Lichtenhan, J.D., 1997. Nanocomposites: A revolutionary new flame retardant approach. SAMPE J. 33, 40–46.

12. Cho, J.W, Paul, D.R., 2001. Nylon 6 nanocomposites by melt compounding. Polymer 42, 1083-1094.

13. Fornes, T.D, Yoon, P.J, Hunter, D.L., Keskkula, H., Paul, D.R., 2002. Effect of organoclays structure on nylon 6 nanocomposite morphology and properties. Polymer 43, 5916-5933.

14. Fornes, T.D, Yoon, P.J, Hunter, D.L., Keskkula, H., Paul, D.R., 2001. Nylon 6 nanocomposites: The effect of matrix molecular weight. Polymer, 42, 9929-9940.

15. Wu, S.H., Wang, Y.H., Chen, C.M., Chang, W.C., Kuo, T.C., Kuan, C.H., Chen, J.W., 2001. Mechanical, thermal and morphological properties of glass fiber and carbon fiber reinforced polyamide-6 and polyamide-6/clay nanocomposites. Mater. Lett. 49, 327-333.

16. Liu, X., Wu, Q., Berglund, L., Fan, J., Qui, Z., 2001. Polyamide 6-clay nanocomposites/polypropylene-grafted-maleic anhydride alloys. Polymer 42, 8235-8239.

17. Lincoln, D.M, Pinnavaia, R.A., Wang, G.Z., Hsiao, B.S., Krishnamoorti, R., 2001.Temperature dependence of polymer crystalline morphology in nylon 6/montmorillonite nanocomposites. Polymer 42, 9975-9985.

18. Lan, T., Pinnavaia, T.J., 1994. Clay-reinforced epoxy nanocomposites. Chem. Mater. 6, 2216-2219.

19. Messersmith, P.B., Gianellis, E.P., 1994. Synthesis and characterization of layered silicate-epoxy nanocomposites. Chem. Mater. 6, 1719-1725

20. Massam, J., Pinnavaia, T.J., 1998. Clay nanolayer reinforcement of a glassy epoxy polymer. Mater. Res. Soc. Sym. Proc. 520, 223-232.

21. Wang, Z., Pinnavaia, T.J., 1998b. Hybrid organic inorganic nanocomposites: Exfoliation of magadiite nanolayers in an Elastomeric epoxy polymer. Chem. Mater. 10, 1820-1826.

22. Yasmin, A., Abot, L.J., Daniel, I.M., 2003. Processing of clay/epoxy nanocomposites by shear mixing. Scripta Mater. 49, 81-86.

23. Gu, A., Liang, G., 2003. Thermal degradation behavior and kinetic analysis of epoxy/montmorillonite nanocomposites. Polym. Degrad. Stabil. 80, 383-391.

24. Triantafillidis, C.S., Lebaron, P.C., Pinnavaia., 2002. Thermoset epoxy-clay nanocomposites: The dual role of α, ω-diamines as surface modifiers and polymer curing agents. J. Solid State Chemistry 167, 354-362.

25. Park, S., Seo, D., Lee, J., 2002. Surface modification of montmorillonite on surface acid-base characteristics and thermal stability of epoxy/clay nanocomposites. J. Colloid Interface Sci. 251, 160-165.

26. Chin, I., Albrecht, T., Kim, H., Russell, T.P., Wang, J., 2001. On exfoliation of montmorillonite in epoxy. Polymer 42, 5947-5952.

27. Kornmann, X., Lindberg, H., Berglund, L.A., 2001. Synthesis of epoxy clay nanocomposites: Influence of nature of clay surface on structure. Polymer 42, 1303-1310.

28. Kornmann, X., Lindberg, H., Berglund, L.A., 2001. Synthesis of epoxy clay nanocomposites: Influence of nature of clay surface on structure. Polymer 42, 4493-4499.

29. Lan, T., Kaviratna, P.D., Pinnavaia, T.J., 1996. Epoxy self polymerization in smectite clays. J. Phys. Chem. Solids. 57 [6-8], 1005-1010.

30. Wang. Z., Pinnavaia., T.J., 1998a. Nanolayer reinforcement of Elastomeric polyurethane. Chem. Mater. 10, 3769-3771.

31. Kim, B.K., Seo, J.W., Jeong, M.H., 2003. Morphology and properties of waterborne polyurethane/clay nanocomposites. Eur. Polym. J. 39, 85-91.

32. Yao, K.J., Song, M., Hourston, D.J., Luo, D.Z., 2002. Polymer/layered nanocomposites: 2. polyurethane nanocomposites. Polymer 43, 1017-1020.

33. Tortora, M., Gorrasi, G., Vittoria V., Galli, G., Ritrovati, S., Chiellini, E., 2002. Structural characterization and transport properties of organically modified montmorillonite/polyurethane nanocomposites. Polymer 43, 6147-6157.

34. Chen, T.K., Tien, Y.I., Wei, K.H., 2000. Synthesis and characterization of novel segmented polyurethane nanocomposites. Polymer 41, 1345-1353.

35. Xinmin, Z., Rongjing, X., Zenggang, W., Chixing, Z., 2003. The synthesis and characterization of polyurethane/clay nanocomposites. Polym. Int. 52, 790-794.

36. Devaux, E., Maryline, R., Serge, B., 2002. Polyurethane/Clay and Polyurethane/POSS Nanocomposites as Flame Retarded Coating for Polyester and Cotton Fabrics. Fire Mater. 26, 149-154.

37. Ma, J., Zhang, S., Qi, Z., 2001. Synthesis and characterization of elastomeric polyurethane/clay nanocomposites. J. Appl. Polym. Sci. 82, 1444-1448.

38. Chen, T.K., Tien, Y.I., Wei, K.H., 1999. Synthesis and characterization of novel segmented polyurethane/clay nanocomposites via poly (ε-caprolactone)/clay. J. Appl. Polym. Sci. Part A: Polym. Chem. 37, 2225-2233.

39. Kaempfer, D., Thomann, R., Mülhaupt, R., 2002. Melt compounding of syndiotactic polypropylene clay nanocomposites containing organophilic layered silicates and in-situ formed core/shell nanoparticles. Polymer 43, 2909-2916.

40. Nam. P.H., Maiti. P., Okamoto, M., Kotaka, T., Hasegawa, N., Usuki, A., 2001. A hierarchical structure and properties of intercalated polypropylene/clay nanocomposites. Polymer 42, 9633-9640.

41. Liu, X., Wu, Q., 2001. PP/clay nanocomposites prepared by grafting-melt intercalation. Polymer 42, 10013-10019.

42. Kodgire, P., Kalgaonkar, R., Hambir, S., Bulakh, N., Jog, J.P., 2001. PP/Clay Nanocomposites: Effect of Clay Treatment on Morphology and Dynamic Mechanical Properties. J. Appl. Polym. Sci. 81, 1786-1792.

43. Ma, J., Qi, Z., Hu, Y., 2001. Synthesis and Characterization of Polypropylene/Clay Nanocomposites. J. Appl. Poolym. Sci. 82,3611-3617.

44. Xu, W. Ge, M., He, P., 2002. Nonisothermal Crystallization Kinetics of Polypropylene/Montmorillonite Nanocomposites. J. Polym. Sci. Part B: Polym. Phys. 40, 408-414.

45. Hambir, S., Bulakh, N., Kodgire, P., Kalagaonkar, R., Jog, J.P., 2001. PP/Clay Nanocomposites: A Study of Crystallization and Dynamic Mechanical Behavior . J. Polym. Sci. Part B: Polym. Phys. 39, 446-450.

46. Hasegawa, N., Okamoto, H., Kato, M., Usuki, A., 2000. Preparation and Mechanical Properties of Polypropylene–Clay Hybrids Based on Modified Polypropylene and Organophilic Clay. J. Appl. Polym. Sci. 78, 1918-1922.

47. Svoboda, P., Zeng, C., Wang, H., Lee, J.j Tomasko, D.L, Morphology and mechanical properties of polypropylene/organoclays nanocomposites. J. Appl. Polym. Sci. 85, 1562-1570.

48. Boucard, S., Duchet, J., Gérard, J.F., Prele, P., Gonzalez, S., 2003. Processing of polypropylene-clay hybrids. Macromol. Symp. 194, 241-246.

49. Wagenknecht, U., Kretzschmar, B., Reinhardt, G., 2003. Investigations of fire retardant properties of polypropylene-clay-nanocomposites. Macromol. Symp. 194, 207-212.

50. Sun, T., Gracés, M., 2002. High performance polypropylene clay nanocomposites by in-situ polymerization with metallocene/clay catalysts. Adv. Mater. 14 [2], 128-130.

51. Hasegawa, N.,Kawasumi, M., Kato, M., Usuki, A., Okada, A., 1998. Preparation and mechanical properties of polypropylene clay nanocomposites using maleic-anhydride-grafted oligomer. J. Appl. Polym. Sci. 67, 87-92.

52. Gorrasi, G., Tortora, M., Vittora, V., Kaempfer, D., Thomann, R., Mülhaupt, R., 2003. Transport properties of organic vapors in nanocomposites of layered silicate and syndiotactic polypropylene. Polymer 43, 3679-3675.

53. Morgan, A.B., Harris, D.J., 2003. Effect of Organoclay soxhlet extraction on mechanical properties, flammability properties and organoclays dispersion of polypropylene clay nanocomposites. Polymer 44, 2313-2320.

54. Xu, W., Liang, G., Zhai H., Tang, S., Hang, G., Pan, W., 2003. Preparation and crystallization behavior of PP/PP-g-MAH/Org-MMT nanocomposite. Eur. Polym. J. 39, 1467-1474.

55. Zhang, Q., Wang, Y., Fu, Q., 2003. Shear induced change of exfoliation and orientation in polypropylene/montmorillonite nanocomposites. . J. Polym. Sci. Part B: Polym. Phys. 41, 1-10.

56. Zhang, Q., Fu, Q., Jiang, L., Lei, Y., 2000. Preparation and properties of polypropylene montmorillonite layered nanocomposites. Polym. Int. 49, 1561-1564.

57. Ma, J., Zhang, S., Qi, Z., Li, G., Hu, Y., 2001. Crystallization behaviors of polypropylene/montmorillonite nanocomposites. J. Appl. Polym. Sci, 83, 1978-1985.

58. Xu, W., Ge, M., He, P., 2002. Nonisothermal crystallization kinetics of polypropylene/montmorillonite nanocomposites. J. Polym. Sci. Part B: Polym. Phys. 40, 408-414.

59. Garcia-López, D., Picazo, O., Merino, J.C., Pastor, J.M., 2003. Polypropylene clay nanocomposites: Effect of compatibilizing agents on clay dispersion. Eur. Polym. J. 39, 945-950.

60. Rong, M.Z., Zhang, M.Q., Zheng, X.Y., Zeng, M.H., Walter, R., Friedrich, K., 2001. Structure-property relationships of irradiation grafted nano-inorganic particle filled polypropylene composites. Polymer 42, 167-183.

61. Kato, M., Usuki, A., Okada, A., 1997. Synthesis of polypropylene oligomer-clay intercalation compounds. J. Appl. Polym. Sci. 66, 1781-1785.

62. Li, J., Zhou, C., Gang, W., 2003. Study on nonisothermal crystallization of maleic anhydride polypropylene/montmorillonite nanocomposite. Polym. Test. 22, 217-223.

63. Gorrasi, G., Tortora, M., Vittora, V., Pollet, E., Lepoittevin, B., Alexandre, M., Dubois, P., 2003. Vapor barrier properties of polycaprolactone montmorillonite nanocomposites: Effect of clay dispersion. Polymer 44, 2271-2279.

64. Lepoittevin, B., Pantoustier, N., Devalckenaere, M., Alexandre, M., Calberg, C., Jéróme, R., Henrist, C., Rulmont, A., Dubois, P., 2003. Polymer/layered silicate nanocomposites by combined intercalative polymerization and melt intercalation: A masterbatch process. Polymer 43, 2033-2040.

65. Bharadwaj, R.K., Mehrabi, A.R., Hamilton, C., Trujillo C., Murga, M., Fan, R., Chavira, A., Thompson, A.K., 2002. Structure-property relationships in cross-linked polyester-clay nanocomposites. Polymer 43, 3699-3705.

66. Lee, S., Park, H., Lim, H., Kang, T., Li, X., Cho, W., Ha, C., 2002. Microstructure, tensile properties and biodegradability of aliphatic polyester/clay nanocomposites. Polymer 43, 2495-2500.

67. Wang, J., Du, J., Zhu, J., Wilkie, C.A., 2002. An XPS study on thermal degradation an flame retardation mechanism of polystyrene-clay nanocomposites. Polym. Degrad. Stabil. 77, 249-252.

68. Park, C.I., Park, O.O., Lin, J.G., Kim, H.J., 2001. Nanocomposites of syndiotactic polystyrene and organophilic clay. Additives for Polymers Dec. 2001, 10-11.

69. Tseng, C., Wu, J., Lee, H., Chang, F., 2001. Preparation and crystallization behavior of syndiotactic polystyrene-clay nanocomposites. Polymer 42, 10063-10070.

70. Park, C., Park, O.O., Lim, G.J., Kim, H.J., 2001. The fabrication of syndiotactic polystyrene/organophilic clay nanocomposites and their properties. Polymer 42, 7465-7475.

71. Fu, X., Qutubuddin, S., 2001. Polymer–clay nanocomposites: Exfoliation of organophilicmontmorillonite nanolayers in polystyrene. Polymer 42, 807-813.

72. Okamoto, M., Morita, S., Taguchi, H., Kim, Y.H., Kotaka, T., Tateyama, H., 2000. Synthesis and structure of smectic clay/poly(methyl methacrylate) and clay/polystyrene nanocomposites via in situ intercalative polymerization. Polymer 41, 3887-3890.

73. Fu, X., Qutubuddin, S., 2000. Synthesis of polystyrene-clay nanocomposites. Mater. Lett. 42, 12-15.

74. Wu, T., Hsu, S., Wu, J., 2003. Effect of the premelting temperature and sample thickness on the polymorphic behavior of syndiotactic polystyrene/ Clay Nanocomposites. J. Polym. Sci. Part B: Polym. Phys. 41, 1730-1738.

75. Su, S., Wilkie, C.A., 2003. Exfoliated poly(methyl methacrylate) and polystyrene nanocomposites occur when the clay cation contains a vinyl monomer. J. Polym. Sci. Part A: Polym. Chem. 41, 1124-1135.

76. Morgan, A.B., Harris, R.H., Kashiwagi, T., Chyall, L.J., Gilman, J.W., 2002. Flammability of polystyrene layered silicate (clay) nanocomposites: Carbonaceous char formation. Fire Mater. 26, 247-253.

77. Tseng, C., Wu, J., Lee, H., Chang, F., 2002. Preparation and characterization of polystyrene–clay nanocomposites by free-radical polymerization. J. Appl. Polym. Sci. 87, 1370-1375.

78. Wu, T., Hsu, S., Wu, J., 2002. Polymorphic behavior in syndiotactic polystyrene/clay nanocomposites. J. Polym. Sci. Part B: Polym. Phys. 40, 736-746.

79. Fan, J., Liu, S., Chen, G., Qi, Z., 2002. SEM study of a polystyrene/clay nanocomposite. J. Appl. Polym. Sci. 83, 66-69.

80. Tseng, C., Lee, H., Chang, F., 2001. Crystallization kinetics and crystallization behavior of syndiotactic polystyrene/clay nanocomposites. J. Polym. Sci. Part B: Polym. Phys. 39, 2097-2107.

81. Zhu, J., Wilkie, C.A., 2000. Thermal and fire studies on polystyrene-clay nanocomposites. Polym. Int. 49, 1158-1163.

82. Bafna, A., Beucage, G., Mirabella, F., Mehta, S., 2003. 3D hierarchical orientation in polymer-clay nanocomposite films. Polymer 44, 1103-1115.

83. Arroyo, M., López-Manchado, M.A., Herrero, B., 2003. Organo-montmorillonite as substitute for carbon black in natural rubber compounds. Polymer 44, 2447-2453.

84. Usuki, A., Tugikase, A., Kato, M., 2002. Preparation and properties of EPDM-clay hybrids. Polymer 43, 2185-2189.

85. Dai, J.C., Huang, J.T., 1999. Surface modification of clay and clay-rubber composite. Appl. Clay. Sci. 15, 51-65.

86. Akelah, A., El-Deen, S.N., Hiltmer, A., Baer, E., Moet, A., 1995.Organophilic rubber-montmorillonite nanocomposites. Mater. Lett. 22, 97-102.

87. Nah, C., Ryu, H.J., Kim, W.D., Choi, S., 2002. Barrier property of clay/Acrylonitrile butadiene copolymer nanocomposite. Polym. Adv. Technol. 13, 649-652.

88. Mark, J.E., 1996. Ceramic-reinforced polymers and polymer-modified ceramics. Polym. Eng. Sci. 36, 2905–2920.

89. Chang, J., Seo, B., Hwang, D., 2002. On exfoliation of organoclays in thermotropic liquid crystalline polyester nanocomposites. Polymer 43, 2969-2974.

90. Carter, N., MacDonald, W.A., Pitman, D., Ryan, T.G., 1999. High temperature non dispersion polymerization of aromatic main chain liquid crystal polymers using organo-clay stabilization. Polymer 40, 7233-7241.

91. Kawasumi, M., Hasegawa, N., Usuki, A., Okada, A., 1999. Liquid crystal / clay mineral composites. Appl. Clay Sci. 15, 93-108.

92. Kawasumi, M., Hasegawa, N., Usuki, A., Okada, A., 1998. Nematic liquid crystal / clay mineral composites. Mater. Sci. Engg. C 6, 135-143.

93. Giannelis, E.P., 1996. Polymer layered silicate nanocomposites. Adv. Mater. 8 [1], 29-35.

94. Garcés, J.M., Moll, D.J., Bicerano, J., Fibiger, R., McLeod, D.G., 2000. Polymeric nanocomposites for automotive applications. Adv. Mater. 12 [23], 1835-1839.

95. Moore, E.P., 1996. Polypropylene handbook. Munich: Hanser publishers.

96. Karger-Kocsis, J., 1995. Polypropylene: Structures, blends and composites. London: Chapman and Hall publishers.

97. Kawasumi, M., Hasegawa, N., Kato, M., Usuki, A., Okada, A., 1997. Preparation and mechanical properties of polypropylene-clay hybrids. Macromolecules 30, 6333-6338.

98. Usuki, A., Kato, M., Okada, A., Kurauchi, T., 1997. Synthesis of polypropylene-clay hybrid. J. Appl. Polym. Sci. 63 [1], 137-138.

99. Reichert, P., Nitz, H., Klinke, S., Bransch, R., Thomann, R., Mülhaupt, R., 2000. Poly(propylene)/organoclays nanocomposite formation: Influence of compatibilizer functionality and organoclays modification. Macromol. Mater. Eng. 275, 8-17.

100. Kurokawa, Y., Yasuda, H., Kashiwagi, M., Oyo, A., 1997. Preparation of a nanocomposite of polypropylene and smectite. J. Mater. Sci. Lett. 16, 1670-1675.

101. Kurokawa, Y., Y., Yasuda, H., Oyo, A., 1996. Structure and properties of a montmorillonite/polypropylene nanocomposite. J. Mater. Sci. Lett. 15, 1481-1488.

102. Nanocor Inc., 2003. Nylon nanocomposites using Nanomer® I.34 TCN. Available from URL: http://www.nanocor.com/tech_sheets/N605.pdf. Site last visited June 2003.

103. Michalovic, M., 1995. Differential Scanning Calorimetry. Available from URL: http://www.psrc.usm.edu/macrog/dsc.htm. Site last visited June 2003.

104. Kim, G.M., Lee, D.H., Hoffman, B., Kressler, J., Stopplemann, G., 2001. Influence of nanofillers on the deformation process in layered silicate/polyamide-12 nanocomposites. Polymer 42, 1095-1100.

105. Pozgay, A., Fráter, T., Papp, L., Sajó, I., Pukánzsky, B., 2002. Nucleating effect of montmorillonite nanoparticles in polypropylene. J. Macromol. Sci. Phys. B41 [4-6], 1249-1265.

106. Kim, G.M., Michler, G.H., Reichert, P., Kresseler, J., Mülhaupt, R., 1998. Micromechanical deformation processes in PA12-layered silicate nanocomposite. Polym. Mater. Sci. Engg. 79, 178-179.

107. Lepoittevin, B., Devalckenaere, M., Pantoustier, N., Alexandre, M., Kubies, D., Calberg, C., Jéróme, R., Dubois, P., 2002. Poly(ε-caprolactone)/clay nanocomposites prepared by melt intercalation: Mechanical, thermal and rheological properties. Polymer 43, 4017-4023.

108. Bucknell, C.B., Clayton, D., 1972. Rubber toughening of plastics. I) Creep mechanisms in HIPS. J. Mater. Sci. 79 [2], 202-210.

109. Scott, J.M., Phillips, D.C., 1975. Carbon fiber composites with rubber toughened matrices. J. Mater. Sci. 10 [4], 551-562.

110. Gee, G., 1966. The present status of the theory of rubber elasticity. Polymer 7 [8], 373-385 .

111. Kambour, R.P., Russell, R.R., 1971. Electron microscopy of crazes in polystyrene and rubber modified polystyrene: Use of iodine-sulphur eutectic as a craze reinforcing impregnant. Polymer 12 [4], 237-246 .

112. Keskkula, H., Turley, S.G. and Boyer, R.F, 1971. The significance of the rubber damping peak in rubber modified polymers. J. Appl. Polym. Sci. 15 [2], 351.

113. Wetton, R.E., Moore J.D., Ingram,P., 1973. Transition magnitudes and impact improvement in rubber-modified plastics. Polymer 14 [4], 161-166 .

114. Scott, G., Tahan, M., 1977. The photo-oxidation of PVC and impact modified PVC: Physical and mechanical changes. Eur. Polym. J. 13 [12], 997-1005 .

115. Mogensen, O.E., Jacobsen, F., Pethrick, R.A., 1979. Posistron annihilation in a rubber modified epoxy resin. Polymer 20, 1034-1036 .

116. Ashurov, N.R., Vylegzhanina, K.A., Kusakova, I.Y., Lishanskii, I.S., Manusevich, Y.Y., Martynov, M.A., Panov N.Y., Frenkel, S.Y., 1980. Relation between morphology and mechanical characteristics of polystyrene modified by siloxane rubber, Polym. Sci. U.S.S.R. 22, 1539-1543 .

117. Daly, J.H., Pethrick, R.A., 1982. Rubber-modified epoxy resins: 3. Influence of filler on the dielectric relaxation properties. Polymer 23, 1619-1621 .

118. Zebarjad, S.M., Lazzeri, A., Bagheri, R., Reihani, S.M.S., Frounchi, M., 2003. Fracture mechanism under dynamic loading of elastomer-modified polypropylene. Mater. Lett. 57 [18], 2733-2741.

119. Laura, D.C., Keskkula, H., Barlow, J.W., Paul, D.R., 2003. Effect of rubber particle size and rubber type on the mechanical properties of glass fiber reinforced, rubber-toughened nylon 6. Polymer 44, 3347-3361.

120. Arias, M.L., Frontini, P.M., Williams, R.J.J., 2003. Analysis of the damage zone around the crack tip for two rubber-modified epoxy matrices exhibiting different toughenability. Polymer 44, 1537-1546 .

121. Imanaka, M., Nakamura, Y., Nishimura, A., Iida, T., 2003. Fracture toughness of rubber-modified epoxy adhesives: Effect of plastic deformability of the matrix phase, Compos. Sci. Technol. 63 [1], 41-51 .

122. Kaynak, C., Arikan, A., Tincer, T., 2003. Flexibility improvement of short glass fiber reinforced epoxy by using a liquid elastomer. Polymer 44, 2433-2439 .

123. Gensler, R., Plummer, C.J.G., Grein,C., Kausch, H.H., 2000. Influence of the loading rate on the fracture resistance of isotactic polypropylene and impact modified isotactic polypropylene. Polymer 41, 3809-3819.

124. Zhou, X., Dai, G., Lin, Q., 2002. Improvement in impact property of continuous glass mat reinforced PP composites. J. Appl. Polym. Sci. 83 [12], 2680-2688.

125. Du, J., Zhu, J., Wilkie, C.A., Wang, J., 2002. An XPS investigation of thermal degradation and charring on PMMA clay nanocomposites. J. Polym. Degrad. Stab. 77, 377-381 .

126. Okamoto, M., Morita, S., Taguchi, H., Kim, Y.H., Kotaka, T., Tateyama, H., 2000. Synthesis and structure of smectic clay/poly(methyl methacrylate) and clay/polystyrene nanocomposites via in situ intercalative polymerization. Polymer 41, 3887-3890 .

127. Tabtiang, A., Lumlong, S., Venables, R.A., 2000.The influence of preparation method upon the structure and relaxation characteristics of poly(methyl methacrylate)/clay composites. Eur. Polym. J. 36, .2559-2568.

128. Hwu, J.M., Jiang, G.J., Gao, Z.M., Xie, W., Pan, W.P., 2002. The characterization of organic modified clay and clay-filled PMMA nanocomposite. J. Appl. Polym. Sci. 83 [8], 1702-1710.

129. Lee, D.C., Jang, W.L., 1996. Preparation and characterization of PMMA-Clay hybrid composite by emulsion polymerization. J. Appl. Polym. Sci. 61 [7], 1117-1122.

130. Hao, Z., Zhu, H.Y., Lu, G.Q., 2003. Zr-Laponite pillared clay-based nickel catalysts for methane reforming with carbon dioxide. Appl. Catal. A-Gen. 242 [2], 275-286 .

131. Stacey, M.H., 1988. Alumina-pillared clays and their adsorptive properties. Catal. Today 2 [5], 621-631 .

132. Chevalier, Y., Coche-Guérente, L., Labbé, P., 2002. Small angle neutron scattering studies and kinetic analysis of laponite–enzyme hydrogels in view of biosensors construction. Mater. Sci. Engg. C 21 [1-2], 81-89 .

133. Besombes, J.L., Cosnier, S., Labbé, P., 1997. Improvement of poly(amphiphilic pyrrole) enzyme electrodes via the incorporation of synthetic laponite-clay-nanoparticles. Talanta 44 [12], 2209-2215 .

134. Labbé, P., Brahimi, B., Reverdy, G., Mousty, C., Blankespoor, R., Gautier, A., Degrand, C., 1994. Possible analytical application of laponite clay modified electrodes. J. Electroanal. Chem. 379 [1-2], 103-110.

135. Zebrowski, J., Prasad, V., Zhang, W., Walker, L.M., Weitz, D.A., 2003. Shake-gels: Shear-induced gelation of laponite–PEO mixtures. Colloid. Surface. A 213 [2-3], 189-197 .

136. Wang, H.K., Choi, H.M., Koo, C.M., Xu, M., Chung, I.J., Jang, M.C., Choi, W., Song, H.H., 2002. Morphology and physical properties of polyethylene/silicate nanocomposite prepared by melt intercalation. J. Polym. Sci. Part B: Polym. Phys. 40 [14], 1454-1463.

137. Mitchell, C.A., Krishnamoorti, R., 2002. Rheological properties of diblock copolymer/layered-silicate nanocomposites. J. Polym. Sci. Part B: Polym. Phys. 40, 1434-1443.

138. Senillou, A., Jaffrezic, N., Martelet, C., Cosnier, S., 1999. A laponite clay-poly(pyrrole–pyridinium) matrix for the fabrication of conductimetric microbiosensors. Anal. Chim. Acta 401[1-2], 117-124 .

139. Coche-Guérente, L., Desprez, V., Labbé, P., 1998. Characterization of organosilasesquioxane-intercalated-laponite-clay modified electrodes and (bio)electrochemical applications. J. Electroanal. Chem. 458 [1-2], 73-86 .

140. Southern Clay Products Inc., 2003. Manufacture, structure and chemistry. Available at URL: http://www.laponite.com. Site last visited June 2003.

141. Beake, B.D., Leggett, G.J., 2002. Nanoindentation and nanoscratch testing of uniaxially and biaxially drawn poly(ethylene terephthalate) film. Polymer 43, 319-327.

142. Rar, A., Zhou, J.N., Liu, W.J., Barnard, J.A., Bennett, A., Street, S.C., 2001. Dendrimer-mediated growth of very flat ultrathin Au films. Appl. Surf. Sci. 175-176, 134-139.

143. Lee, Y., Lee, E.H., Mansur, L.K., 1992. Hardness and wear properties of boron-implanted poly(ether-ether-ketone) and poly-ether-imide. Surf. Coat. Tech. 51 [1-3], 267-272 .

144. Rao, G.R., Blau, P.J., Lee, E.H., 1995. Friction microprobe studies of ion implanted polymer surfaces. Wear 184, 213-222 .

145. Li, M., Palacio, M.L., Carter, C.B., Gerberich, W.W., 2002. Indentation deformation and fracture of thin polystyrene films. Thin Solid Films 416, 174-183.

146. Karapanagiotis, I., Evans, D.F., Gerberich, W.W., 2002. Dewetting dynamics of thin polystyrene films from sputtered silicon and gold surfaces. Colloid. Surf. A 207, 59-67.

147. Rangel, E.C., Cruz, N.C., Lepienski, C.M., 2002. Effect of helium implantation on the properties of plasma polymer films. Nucl. Instrum. Meth. B 191, 704-707.

148. Gao, S., Mäder, E., 2002. Characterisation of interphase nanoscale property variations in glass fibre reinforced polypropylene and epoxy resin composites, Composites A 33, 559-576.

149. Karapanagiotis, I., Evans, D.F., Gerberich, W.W., 2002. Dynamics of the leveling process of nanoindentation induced defects on thin polystyrene films. Polymer 43, 1343-1348.

150. Poilane, C., Delobelle, P., Lexcellent, C., Hayashi, S., Tobushi, H., 2000. Analysis of the mechanical behavior of shape memory polymer membranes by nanoindentation, bulging and point membrane deflection tests. Thin Solid Films 379, 156-165 .

151. Benítez, F., Martínez, E., Galán, M., Serrat, J., Esteve, J., 2000. Mechanical properties of plasma deposited polymer coatings. Surf. Coat. Tech. 125, 383-387 .

152. Serruys, Y., Marin, N., 1997. Metallic impurities diffusion in a polymer film (Kapton) under and out of irradiation. Nucl. Instrum. Meth. B 131, 109-120 .

153. Bhattacharjee, B., Ganguli, D., Chaudhuri, S., Pal, A.K., 2003. Synthesis and optical characterization of sol–gel derived zinc sulphide nanoparticles confined in amorphous silica thin films. Mater. Chem. Phys. 78 [2], 372-379.

154. Chen, D., He, X., 2001. Synthesis of nickel ferrite nanoparticles by sol-gel method, Mater. Res. Bull. 36, 1369-1377.

155. Yang, Q., Wang, F., Tang, F., Wang, C., Chen, Z., Qian, Y., 2003. The formation of fractal Ag nanocrystallites via γ-irradiation route in isopropyl alcohol, Pages 495-500. Mater. Chem. Phys. 78 [2], 495-500.

156. Sankaranarayanan, V.K., Sreekumar, C., 2003. Precursor synthesis and microwave processing of nickel ferrite nanoparticles. Curr. Appl. Phys. 3 [2-3], 205-208.

157. Green, D.L., Jayasundara., S., Lam, Y., Harris, M.T., 2003. $Bi_4Ti_3O_{12}$ nanoparticles prepared by hydrothermal synthesis. J. Eur. Cer. Soc. 23, Pages 161-166.

158. Upadhyay, C., Mishra, D., Verma, H.C., Anand, S., Das, R.P., 2003. Effect of preparation conditions on formation of nanophase Ni–Zn ferrites through hydrothermal technique. J. Magn. Magn. Mater. 260, 188-194.

159. Kundu, A., Upadhyay, C., Verma, H.C., 2003. Magnetic properties of a partially inverted zinc ferrite synthesized by a new coprecipitation technique using urea. Phys. Lett. A 311, 410-415 .

160. Chen, D., Chen,Y., 2002. Synthesis of strontium ferrite nanoparticles by coprecipitation in the presence of polyacrylic acid. Mater. Res. Bull. 37, 801-810 .

161. Chen, Q., Rondinone, A.J., Chakoumakos, B.J., Zhang, Z.J., 1999. Synthesis of superparamagnetic $MgFe_2O_4$ nanoparticles by coprecipitation. J. Magn. Magn. Mater. 194, 1-7.

162. González-Carreño, T., Morales, M.P., Serna, C.J., 2000. Barium ferrite nanoparticles prepared directly by aerosol pyrolysis. Mater. Lett. 43, 97-101 .

163. Hamdeh, H.H., Barghout, K., Ho, J.C., Willey, R.J., O'Shea, M.J., Chaudhuri, J., 2000. Structural and magnetic characterization of aerogel-produced $Ge_{0.5}Fe_{2.5}O_y$ nanoparticles. J. Magn. Magn. Mater. 212, 112-120.

164. Shi, Y., Ding, J., Yin, H., 2000. $CoFe_2O_4$ nanoparticles prepared by the mechanochemical method. J. Alloy. Compd. 308, Pages 290-295 .

165. Goya, G.F., Rechenberg, H.R., 1999. Magnetic properties of $ZnFe_2O_4$ synthesized by ball milling. J. Magn. Magn. Mater. 203, 141-142.

166. Satyanarayana, L., Reddy, K.M., Manorama, S.V., 2003. Synthesis of nanocrystalline $Ni_{1-x}Co_xMn_xFe_{2-x}O_4$: A material for liquefied petroleum gas sensing. Sensor. Actuator. B: Chem. 89, 62-67.

167. Li, X., Kuta, C., 2003. Synthesis and characterization of superparamagnetic $Co_xFe_{3-x}O_4$ nanoparticles. J. Alloy. Compd., 349, 264-268.

168. Sileo, E.E., Rotelo, R., Jacobo, S.E., 2002. Nickel zinc ferrites prepared by the citrate precursor method. Physica B 320, 257-260.

169. Liu, J., He, H., Jin, X., Hao, Z., Hu, Z., 2001. Synthesis of nanosized nickel ferrites by shock waves and their magnetic properties. Mater. Res. Bull. 36, 2357-2363.

170. Sena, D., Deb, P., Mazumder, S., Basumallick, A., 2000. Microstructural investigations of ferrite nanoparticles prepared by nonaqueous precipitation route. Mater. Res. Bull. 35, 1243-1250.

171. Pillai, V., Kumar, P., Multani, M.S., Shah, D.O., 1993. Structure and magnetic properties of nanoparticles of barium ferrite synthesized using microemulsion processing. Colloid. Surface. A 80, 69-75.

172. Mathur, R., Sharma, D.R., Vadera, S.R., Gupta, S.R., Sharma, B.B., Kumar, N., 1999. .Room temperature synthesis of nanocomposites of Mn-Zn ferrites in a polymer matrix. Nanostruct. Mater. 11, 677-686.

173. Kim, H.S., Sohn, B.H., Lee, W., Lee, J.K., Choi, S.J., Kwon, S.J., 2002. Multifunctional layer-by-layer self-assembly of conducting polymers and magnetic nanoparticles. Thin Solid Films 419 [1-2], 173-177.

174. Verma, A., Saxena, A.K., Dube, D.C., 2003. Microwave permittivity and permeability of ferrite–polymer thick films. J. Magn. Magn. Mater. 263 [1-2], 228-234.

175. Sharma, D.R., Mathur, R., Vadera, D.R., Kumar, N., Kutty, T.R.N., 2003. Synthesis of nanocomposites of Ni–Zn ferrite in aniline formaldehyde copolymer and studies on their pyrolysis products. J. Alloy. Compound. , In Press.

176. Mohammed, E.M., Malini, K.A., Kurian, P., Anantharaman, M.R., 2002. Modification of dielectric and mechanical properties of rubber ferrite composites containing manganese zinc ferrite, Mater. Res. Bull. 37 [4], 753-768.

177. Krishnamoorti, R., Yurekli, K., 2001. Rheology of polymer silicate layered nanocomposites. Curr. Opin. Coloid. In. 6, 464-470.

178. Jiang, W., Tjong, S.C., 1999. Thermal stability of polycarbonate composites reinforced with potassium titanate whiskers: Effect of coupling agent addition. Polym. Degrad. Stab. 66, 241-246.

BIOGRAPHICAL SKETCH

The author was born in Tiruvallur, a small district near Chennai in Tamil Nadu, India. He obtained his high school diploma from Kendriya Vidyalaya, IFFCO, Gandhidham, Gujrat, India. He then pursued a Bachelor of Engineering degree in chemical engineering at Sardar Vallabhbhai Regional College of Engineering and Technology, Surat, Gujrat, India. He then attended University of Florida for pursuing a Master of Science degree in materials science and engineering. He worked with Professor Charles Beatty as a research assistant and performed research on polymeric nanocomposites.